THE INFLUENCE OF V-TYPE H^+-ATPASES ON VESICLE FUSION PROCESSES

DISSERTATION

in partial fulfillment of the requirements for the degree

'Doctor rerum naturalium (Dr. rer. nat.)'

submitted to the Faculty of Mathematics and Natural Sciences

at the Christian Albrechts University of Kiel

submitted by

SANDRA KISSING

Kiel, March 2016

Referee:	Prof. Dr. Paul Saftig
Co-referee:	Prof. Dr. Axel Scheidig
Date of oral presentation:	25th April 2016
Approved for publication:	25th April 2016

Prof. Dr. Wolfgang J. Duschl
(The decan)

TABLE OF CONTENTS

List of abbreviations

AA	Amino acids
ATG	Autophagy-related
ATP6AP2	V-ATPase accessory protein 2
BSA	Bovine serum albumin
cDNA	Complementary DNA
cKO	Conditional knockout
CLEAR	Coordinated lysosomal expression and regulation
CORVET	Class C core vacuole/ endosome tethering
CTF	C-terminal fragment
DAPI	4-,6-diamidino-2-phenylindole
DIC	Differential interference contrast
DMEM	Dulbecco´s Modified Eagle Medium
DMSO	Dimethyl sulfoxide
E. coli	*Escherichia coli*
EBSS	Earle´s Balanced Salt Solution
EDTA	Ethylenediaminetetraacetic acid
EEA1	Early endosomal antigen 1
EGF	Epidermal growth factor
EYFP	Enhanced yellow fluorescent protein
FACS	Fluorescence-activated cell sorting
FBS	Fetal bovine serum
FcγRIIa	Fcγ receptor IIa
fl	Full length

fwd	Forward
GAP	GTPase activating protein
GAPDH	Glyceraldehyde 3-phosphate dehydrogenase
GM130	Golgin subfamily A member 2/ 130 kDa cis Golgi matrix protein
H&E staining	Hematoxylin and eosin staining
HOPS	Homotypic fusion and protein sorting
IgG	Immunglobulin G
LAMP-2	Lysosomal associated membrane protein 2
LB	Lysogeny broth
LC3	Microtubule-associated protein 1A/ 1B-light chain 3
MEF	Mouse embryonic fibroblasts
MOI	Multiplicity of infection
mTORC1	Mechanistic target of rapamycin complex 1
MVB	Multi-vesicular body
NSF	N-ethylmaleimide-sensitive-factor
NTF	N-terminal fragment
p70S6K	70 kDa ribosomal S6 kinase 1
PAGE	Polyacrylamide gel electrophoresis
PBS	Phosphate-buffered saline
PCR	Polymerase chain reaction
PEI	Polyethylenimine
PFA	Paraformaldehyde
PI3K	Phosphatidylinositol-3-kinase
poly (I:C)	Polyinosinic:polycytidylic acid
PRAS40	Proline-rich Akt1 substrate 1

PRR	(Pro-)renin receptor
qPCR	Quantitative real-time PCR
Rab5	Ras-like protein from rat brain 5/ Ras-related protein Rab-5
Rab7	Ras-related protein Rab-7a
Rag GTPase	Ras-related GTP-binding protein
RAS	Renin angiotensin system
RAVE	Regulator of the H^+-ATPase of vacuolar and endosomal membranes
rev	Reverse
Rheb	Ras homologue enriched in brain
SDS	Sodium dodecyl sulfate
SLC38A9	Solute carrier family 38, member 9
SNAP	Soluble NSF attachment protein
SNARE	NSF attachment receptor
SREBP	Sterol regulatory element-binding protein
SV40	Simian virus 40
TAE	Tris-acetate-EDTA
TBS	Tris-buffered saline
TFEB	Transcription factor EB
TSC	Tuberous sclerosis complex
ULK	Uncoordinated-51 (unc)-like kinase
V-ATPase	V-type H^+-ATPase
Vph1p	Vacuolar pH 1
Vps	Vacuolar protein sorting
Wnt	Wingless/ in

SUMMARY

The proton pumping activity of the V-type H^+-ATPase (V-ATPase) complex is essential to maintain the luminal acidification of defined cellular compartments. A broad range of physiological functions, *e.g.* the proteolytic degradation within lysosomes, intracellular protein sorting and signalling by the mTORC1 (mechanistic target of rapamycin complex 1) depend on functional V-ATPase complexes. In addition, there is an ongoing debate about a role for the V-ATPase V_0 sector in promoting membrane fusion processes.

The present work addresses the influence of the V-ATPase complex on vesicle fusion events in genetically defined mouse models, lacking either the V-ATPase V_0 subunit a3 or the V-ATPase accessory subunit 2 (ATP6AP2), a chaperone for V-ATPase V_0 sector assembly.

In fibroblasts, a detailed characterisation of endosome and phagosome maturation revealed functional vesicle fusion upon knockout of the V-ATPase V_0 subunit a3. Similarly, phagosome maturation proceeded in ATP6AP2-deficient macrophages with significantly decreased V-ATPase V_0 subunit levels. Even the pharmacological reduction of accessible, free V_0 sectors or pharmacologically inhibited vesicle acidification did not disturb the acquisition of lysosomal markers to phagosomes. In summary, neither the presence nor the activity of the V-ATPase complex were required for endocytic and phagosomal fusion processes. Therefore, a general fusion promoting influence of V-ATPases is not supported by the data obtained in this study.

Despite of the V-ATPase-independent progression of vesicle fusion in fibroblasts and macrophages, the liver-specific depletion of ATP6AP2 led to a massive accumulation of endocytic and autophagic vacuoles. This vacuolisation was not caused by a major block in lysosomal protein degradation or impaired vesicle fusion along the endocytic and autophagic pathways. The V-ATPase complex inhibits the formation of autophagosomes through the stimulation of mTORC1. Unexpectedly, mTORC1 signalling was increased in liver lacking ATP6AP2. Although the presence of the V-ATPase was required for the activation of mTORC1 by amino acids, other stimulatory pathways, *e.g.* PI3K/ Akt signalling, contributed to the increased mTORC1 activity in the absence of ATP6AP2. It can be concluded that the regulation of autophagy is based on multiple pathways, such as the PI3K/ Akt signalling, in addition to the V-ATPase-mediated stimulation of mTORC1.

ZUSAMMENFASSUNG

Die vesikuläre H^+-ATP□se (V-ATP□se) vermittelt □ls Protonenpumpe die Ansäuerung definierter Komp□rtimente der Zelle. Auf diese Weise ermöglicht die V-ATP□se eine Vielz□hl physiologischer Funktionen, beispielsweise die lysosom□le Proteindegr□dierung, die intr□zelluläre Sortierung von Proteinen und den mTORC1 (*mechanistic target of rapamycin complex 1*) Sign□lweg. D□rüber hin□us wird eine mögliche Beteiligung des V_0 Komplexes der V-ATP□se □n der Fusion biologischer Membr□nen diskutiert.

In der vorliegenden Arbeit wurde □nh□nd von M□usmodellen untersucht, inwieweit sich die genomische Deletion der V_0 Untereinheit □3 bzw. des V-ATP□se □kzessorischen Proteins 2 (ATP6AP2), eines Assemblierungshelfers des V_0 Komplexes, □uf die Fusion von Vesikeln □uswirkt.

Die det□illierte An□lyse der Endosomen- und Ph□gosomenreifung in Fibrobl□sten demonstrierte □uch in Abwesenheit der V_0 Untereinheit □3 eine funktion□le Vesikelfusion. Ebenso h□tten der *Knockout* von ATP6AP2 und die d□r□us resultierende, verminderte Expression von V_0 Komplex Untereinheiten keinen Einfluss □uf die Ph□gosomenreifung in M□kroph□gen. Selbst die ph□rm□kologische Reduktion frei zugänglicher V_0 Komplexe oder der induzierte Anstieg des vesikulären pH-Wertes konnten den Tr□nsfer lysosom□ler M□rkerproteine □uf Ph□gosomen nicht beeinträchtigen. Zus□mmenf□ssend w□r weder die Präsenz der V-ATP□se noch ihre Aktivität für den Abl□uf der □n□lysierten Fusionsprozesse notwendig. Dementsprechend k□nn ein fusionsfördernder Einfluss des Komplexes mit den Ergebnissen dieser Arbeit nicht bestätigt werden.

Obwohl die Vesikelfusion in Fibrobl□sten und M□kroph□gen von der V-ATP□se un□bhängig □blief, führte der Leber-spezifische Verlust von ATP6AP2 zu einer vermehrten Akkumul□tion von endosom□len und □utoph□gosom□len Strukturen. Als Urs□che dieser Vesikel□ns□mmlung konnte sowohl eine Block□de des lysosom□len Protein□bb□us, □ls □uch eine □usbleibende Vesikelfusion zwischen endosom□len und □utoph□gosom□len Org□nellen □usgeschlossen werden. Durch die Stimul□tion von mTORC1 inhibiert die V-ATP□se indirekt die Bildung von Autoph□gosomen. Überr□schenderweise zeigte sich in ATP6AP2-depletierter Leber trotz □usgeprägter Autoph□gie ein erhöhtes M□ß □n mTORC1 Aktivität. Zw□r w□r die Präsenz der V-ATP□se für die Aminosäure-□bhängige Aktivierung von mTORC1 essentiell, jedoch vermittelte d□rüber hin□us die Stimul□tion des PI3K/ Akt Sign□lweges eine gesteigerte Aktivierung von

mTORC1 in Abwesenheit von ATP6AP2. Daraus lässt sich ableiten, dass neben der Stimulation von mTORC1 durch die V-ATPase eine Vielzahl von zusätzlichen Faktoren, z. B. der PI3K/ Akt Signalweg, zur Regulation der Autophagie beitragen.

1. INTRODUCTION

1.1. Vesicle fusion in biological systems

As the smallest autonomously living unit, a cell consists of various compartments that are separated by biological membranes and designated to distinct cellular functions. This compartmentalization is not constrained to a rigid state, but rather relies on transport processes and interactions to create a functional meshwork. Direct contact and the fission of vesicles from a donor compartment to subsequent fusion with an acceptor compartment are, among others, means of oriented transmission. These vesicle fission and fusion processes are important in many cellular aspects, *e.g.* the distribution of newly synthesised proteins or the sorting of endocytic cargo (summarised in Huotari and Helenius, 2011). Neuronal transmission at the synapse is also highly dependent on fusion of secretory vesicles with the presynaptic membrane and illustrates the variety of applications that are accomplished by regulated alterations in the cell´s compartmentalization state (Sudhof and Rizo, 2011). Next to these intracellular events, fusion can occur between two or more cells and thereby plays an important role in tissue and organ development.

Due to a high degree of conservation, current models of the mechanism behind fusion processes have gained a considerable amount of knowledge from studies conducted within the yeast *Saccharomyces cerevisiae* (summarised in Gautreau *et al.*, 2014). This conservation is reflected by the fact that the proteins required for yeast vacuole fusion mostly exhibit orthologous gene products in mammalian cells. Based on initial findings in yeast, *in vitro* fusion assays and the complete reconstitution of single fusion events fostered the understanding of the mammalian fusion process and of the molecules that are involved in it. In the course of vesicle fusion, compartments designated to fuse with each other undergo three distinct phases: a tethering phase, followed by vesicle docking and finally, organelle fusion upon formation of a fusion pore.

1.1.1. Vesicle tethering

An initial, loose contact between two vesicles is established during the phase of tethering and it bridges distances of more than 25 nm (Pfeffer, 1999). In the endocytic pathway, tethering is mediated by different classes of tethering factors (summarised in Gautreau *et al.*, 2014).

The early endosomal antigen 1 (EEA1) and rabenosyn-5 are two long coiled-coil proteins that belong to one class of tethering molecules (Simonsen *et al.*, 1998; Christoforidis *et al.*, 1999; Nielsen *et al.*, 2000). They form dimers and bind to the small GTPase Rab5 (Ras-like protein from rat brain 5) and phosphatidyl-inositol-3-phosphate on the endosomal membrane.

The second class of tethering factors interacts with these long coiled-coil proteins and consists of the two complexes 'homotypic fusion and protein sorting', shortened HOPS and 'class C core vacuole/ endosome tethering', also named CORVET. Both complexes were first discovered in yeast and appear to be conserved across species (Seals *et al.*, 2000; Kim *et al.*, 2001; Richardson *et al.*, 2004). Yeast HOPS and CORVET share a common core of the four C class vacuolar protein sorting (Vps) proteins Vps11p, Vps16p, Vps18p and Vps33p and bear tethering as well as fusion promoting properties (Hickey and Wickner, 2010; Balderhaar *et al.*, 2013; Zick and Wickner, 2013). Additional subunits of each complex specify their ability to bind different Rab proteins. The better characterised HOPS complex binds to the protein 'yeast protein transport 7' (Ypt7p), the homologue of the mammalian late endosomal membrane protein Rab7, whereas the CORVET complex interacts with the yeast homologue of the early endosomal Rab5 (Wurmser *et al.*, 2000; Peplowska *et al.*, 2007; Plemel *et al.*, 2011; Cabrera *et al.*, 2013). By implication, mammalian HOPS-like proteins are thought to be involved in the tethering of Rab7-decorated late endosomes and lysosomes, while the same is assumed for the tethering of two Rab5-positive early endosomes by CORVET analogues (Pryor *et al.*, 2004; Pols *et al.*, 2013). However, mammalian HOPS complexes cannot directly attach to Rab7, but rather bind to the Rab7 interacting lysosomal protein/ RILP (van der Kant *et al.*, 2013; Lin *et al.*, 2014). Other fusion processes, like fusion of secretory vesicles with the plasma membrane at the synapse rely on a similar tethering phase and tethering factors (reviewed in Onel *et al.*, 2014).

1.1.2. SNARE-mediated docking

Tethering proteins can further act as adaptor molecules for upcoming fusion steps. Beside the function as a tethering complex, HOPS subunits were shown to interact with vesicular *s*oluble N-ethylmaleimide-sensitive-factor (NSF) attachment receptor (SNARE) proteins in yeast and mammals. These SNARE proteins are required to initiate the next step of vesicle fusion, the docking phase (Collins *et al.*, 2005; Kramer and Ungermann, 2011; Lobingier and Merz, 2012).

During vesicle docking, the distance between the two lipid bilayers is reduced to less than five to ten nm upon formation of *trans*-SNARE complexes (Pfeffer, 1999). Such a complex is assembled from a total of four intertwined parallel α-helices consisting of one R-SNARE and one of each of the three Q-SNARE subclasses Q_a, Q_b, Q_c (Fasshauer *et al.*, 1998; Bock *et al.*, 2001). While the R-SNARE is localised on one of the vesicles, the Q-SNAREs belong to its fusion partner. The mammalian *trans*-SNARE complexes involved in homotypic late endosome fusion as well as heterotypic fusion between late endosomes and lysosomes were largely analysed in inhibitor studies and rely on the same set of Q-SNAREs, namely syntaxin 7 (Q_a), Vti1b (Q_b) and syntaxin 8 (Q_c). The R-SNAREs Vamp8 and Vamp7 distinguish between homotypic and heterotypic fusion events, respectively (Antonin *et al.*, 2000; Mullock *et al.*, 2000; Ward *et al.*, 2000; Pryor *et al.*, 2004).

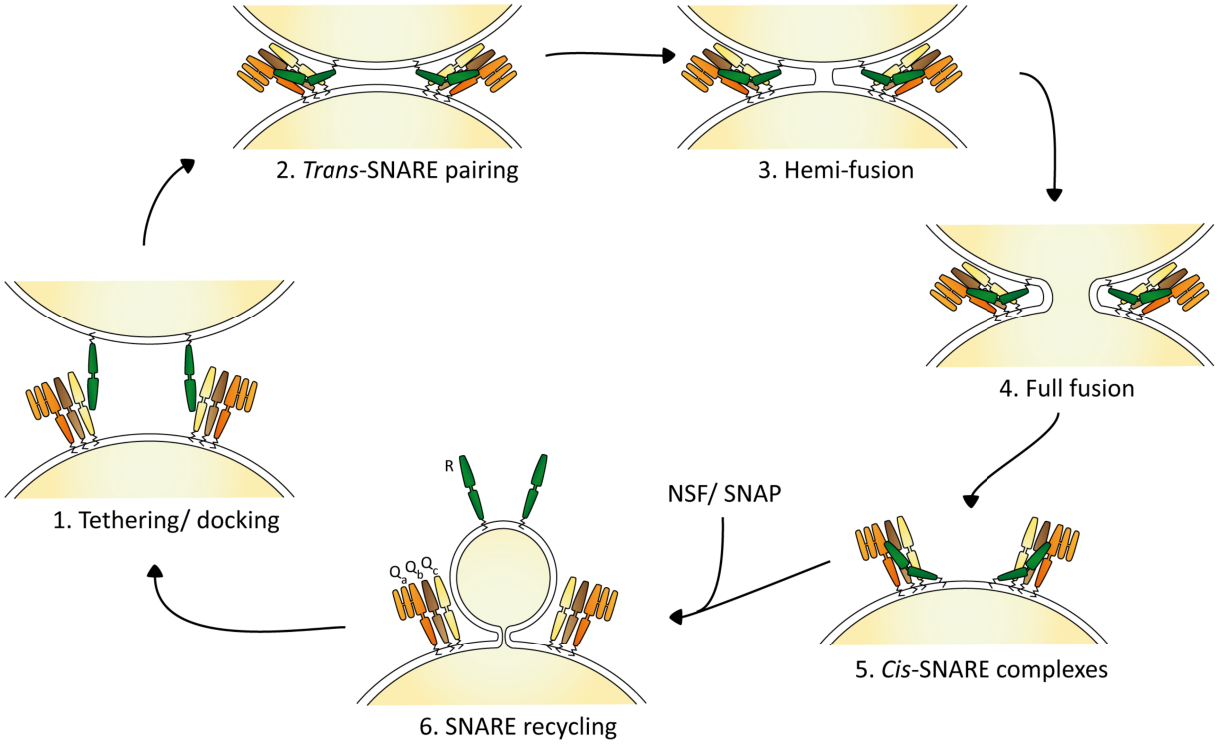

Figure 1.1: SNARE proteins in vesicle fusion.

In the course of vesicle fusion, SNARE proteins pass through distinct pairing and recycling processes. (1, 2) During the transition from vesicle tethering to vesicle docking, SNARE proteins from adjacent membranes entangle in *trans*-SNARE complexes. These complexes consist of three Q-SNAREs (Q_a – Q_c) and one R-SNARE (R). (3) *Trans*-SNARE complexes reduce the distance between two membranes and can initiate the mixing of the outer membrane leaflets to a hemi-fusion state. (4) Additional mixing of the inner membrane leaflets results in full membrane fusion. (5) Following this process, SNARE complexes are conferred into a *cis*-conformation and have to be disassembled by NSF and SNAPs. (6) The individual SNARE proteins are then recycled to appropriate membranes and can enter a new cycle of membrane fusion after a priming step. Modelled according to (Sudhof and Rizo, 2011).

In yeast homotypic vacuole fusion, *trans*-SNARE complex formation furthermore depends on an acidic vesicle lumen that is generated by the vacuolar H^+-ATPase (V-ATPase) complex (Ungermann *et al.*, 1999). Once formed, *trans*-SNARE complexes display an exceptional stability and feature fusogenic characteristics that could be explained by a destabilisation of the lipid bilayers through the introduction of mechanical forces (Jahn and Scheller, 2006). Thereby, SNARE proteins could help to overcome the energy barrier of vesicle fusion. Upon fusion, SNARE complexes convert from the *trans* to a *cis*-conformation and need to be re-transferred into an active state as well as recycled to their donor compartments to allow the progress of new fusion reactions (Fig. 1.1). The disassembly of low energy *cis*-SNARE complexes is mediated by NSF and its cofactors the soluble NSF attachment proteins (SNAPs), which utilise the hydrolysis of ATP to provide the required energy (Sollner *et al.*, 1993; Mayer *et al.*, 1996). For subsequent re-sorting, SNARE proteins bind to clathrin adaptors and are transported from the newly formed hybrid organelle independently of cargo sorting (Miller *et al.*, 2007).

1.1.3. Formation of a fusion pore

The fusion promoting steps that follow SNARE pairing and lead to the final mixing of two lipid bilayers are not yet completely understood. It could be shown that the local release of Ca^{2+} acts in these late stages, as fast acting Ca^{2+} chelators like 1,2-bis(o-aminophenoxy)ethane-N,N,N',N'-tetraacetic acid (BAPTA) and Ca^{2+} depletion of vesicles are capable of blocking membrane fusion (Peters and Mayer, 1998; Holroyd *et al.*, 1999; Pryor *et al.*, 2000). In yeast and mammals, this Ca^{2+}-mediated signalling occurs after the docking and formation of *trans*-SNARE complexes and likely requires the Ca^{2+} sensor calmodulin. A requirement for Ca^{2+} was further shown for vesicle fusion in the Golgi apparatus and during regulated exocytosis at the synapse (reviewed in Luzio *et al.*, 2003).

How the Ca^{2+} release is aiding the late stages of fusion mechanistically remains elusive. A link from Ca^{2+}/ calmodulin to the V-ATPase complex has been proposed in different species and there is growing evidence for the importance of the V-ATPase in the completion of membrane fusion (Peters *et al.*, 2001; Bayer *et al.*, 2003; Hiesinger *et al.*, 2005; Liegeois *et al.*, 2006; Sun-Wada *et al.*, 2006; Peri and Nusslein-Volhard, 2008; Zhang *et al.*, 2008; Di Giovanni *et al.*, 2010; Strasser *et al.*, 2011; Poea-Guyon *et al.*, 2013; Wang *et al.*, 2014). The membrane integral V_0 sector of the V-ATPase complex and *trans*-SNARE pairings as described in section 1.1.2

therefore provide the basis for two models of a fusion pore, the last intermediate before completion of the fusion process.

SNARE proteins are part of the stalk hypothesis in which these partially stiff proteins induce curvature of membranes until the formation of a proteinous fusion pore is energetically favoured (Jahn and Scheller, 2006). Between three and 15 *trans*-SNARE complexes have been implied in one single fusion event (Montecucco *et al.*, 2005). The pore formation begins with the mixing of the outer membrane leaflets to form the hemifusion intermediate at which fusion can be arrested (Giraudo *et al.*, 2005; Reese *et al.*, 2005; Xu *et al.*, 2005). Upon mixing of the inner membrane leaflets, the fusion pore opens and vesicle fusion can progress (Fig. 1.1).

A second model describes a fusion pore that is initiated with the aid of the V-ATPase V_0 sector. This membrane-integral part of the H^+-ATPase complex is built around a highly hydrophobic, hexameric proteolipid cylinder consisting of the V_0 subunits vacuolar membrane ATPase 3 (Vma3p), Vma11p and Vma16p in yeast or its homologous subunits c, c' and c'' in higher eukaryotes (Hirata *et al.*, 1997; Forgac, 1999; Wilkens *et al.*, 1999) (see also chapter 1.2). Since the initial discovery of a fusogenic role for the V-ATPase in yeast, the associated model has developed from a described requirement of the V-ATPase V_0 sector in the membrane of both fusion partners to the sufficiency of V_0 sectors in just one of the two membranes (Peters *et al.*, 2001; Strasser *et al.*, 2011). In contrast to the importance of acidification for *trans*-SNARE pairing, the role of the V-ATPase is limited to its physical presence and therefore independent of the proton pumping activity of the whole V-ATPase complex in these models. The current view suggests that acyl chains from the lipid bilayer might invade a gap in the V_0 sector, which is formed upon conformational changes (Clare *et al.*, 2006; Strasser *et al.*, 2011). This invasion will influence the orientation and curvature of the lipid bilayer to allow the formation of a lipidic fusion pore (Fig. 1.2). Like the SNARE-mediated fusion pore, it reflects the last stage of vesicle fusion. The SNARE proteins have furthermore been suggested as the initiator of the conformational change in the yeast V_0 sector (Strasser *et al.*, 2011; Vavassori and Mayer, 2014).

Moreover, the yeast subunit vacuolar pH 1 (Vph1p) has also been linked to vacuole fusion (Bayer *et al.*, 2003) and both, its homologous a subunits and the proteolipid subunit c, emerged repeatedly in independent studies of membrane fusion in higher eukaryotes. The rat V_0 subunit c was shown to interact with the SNARE synaptobrevin and thereby modulate neurotransmitter release by exocytosis (Di Giovanni *et al.*, 2010). Similarly, studies in *Drosophila melanogaster*

could demonstrate that the fly homologue of the V_0 subunit a1 regulates synaptic vesicle release in association with SNARE complexes (Hiesinger *et al.*, 2005; Wang *et al.*, 2014). Using chromaffin cells and photoinactivation of the V_0 subunit a1 in mouse and cow, the V_0 sector of the V-ATPase was identified as a sensor for intra-granular pH that regulates exocytosis pH-dependently (Poea-Guyon *et al.*, 2013). Interestingly, the depletion of the same subunit in zebrafish interferes with phagosomal fusion in microglial cells (Peri and Nusslein-Volhard, 2008). In addition, mutations of the V_0 a subunit are correlated with defective secretion of Hedgehog-related proteins in *Caenorhabditis elegans* (Liegeois *et al.*, 2006) and deletion of the V_0 subunit a3 leads to impaired secretion of insulin from mouse pancreatic islets cells (Sun-Wada *et al.*, 2006).

Taken together, different isoforms of the V_0 subunit a were found depending on the analysed tissue. This further suggests a tissue-specific contribution of distinct V-ATPase complexes to membrane fusion.

The common feature of all these descriptions, the proton pumping-independent role of V-ATPases in membrane fusion, was challenged by recent observations in yeast, where impaired vacuole fusion was attributed to a lack of V-ATPase-mediated vesicle acidification (Coonrod *et al.*, 2013). Therefore the nature of the linkage between V-ATPases and membrane fusion is still the topic of an ongoing debate.

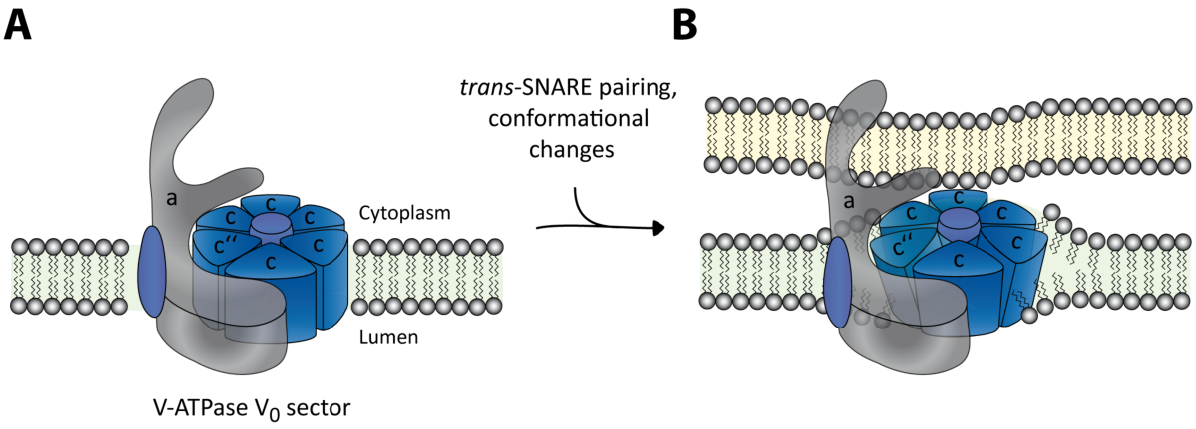

Figure 1.2: Fusogenic properties of V-ATPase V_0 sectors.

Model of how the membrane-integral V_0 sector of V-ATPases could aid the mixing of two lipid bilayers in vesicle fusion. (**A**) Upon dissociation of V-ATPases into individual V_1 and V_0 sectors, sector V_0 is available for conformational changes. (**B**) This rearrangement is thought to be induced by an interaction with *trans*-SNARE complexes and could expose hydrophobic residues of the hexameric subunit c subcomplex. Membrane lipids are prone to invade the newly formed gaps and thereby might undergo a reorientation that will stimulate membrane fusion. The figure was modelled according to (Strasser *et al.*, 2011).

1.1.4. Meet and greet – the kiss and run hypothesis

The fusion reactions between distinct vesicles can be of either terminal or transient nature. Terminal, so-called full fusion results in the complete blend of individual compartments. Full fusion therefore acts reverse to vesicle fission, which describes the budding of a new compartment up to its final dissection. To achieve a terminal fusion, the newly formed fusion pore has to expand at the end of membrane fusion as it is described for full-collapse synaptic vesicle exocytosis (Heuser and Reese, 1973).

Transient fusion, on the other hand, allows only limited mixing of luminal and membrane contents, and it is followed by recurrent vesicle separation – a process termed kiss and run (Fesce *et al.*, 1994; Desjardins, 1995; Storrie and Desjardins, 1996). The first evidences for this phenomenon originate from studies of vesicle exocytosis *e.g.* at neuromuscular junctions (Ceccarelli *et al.*, 1973) and in mast cells (Fernandez *et al.*, 1984; Alvarez de Toledo *et al.*, 1993). But also the biogenesis of both, phagosomes and lysosomes involves such restricted fusion steps (Desjardins, 1995; Storrie and Desjardins, 1996). During a kiss and run event, the fusion pore will be closed after an undefined amount of time. Platch-clamp experiments with mast cells revealed a vesicle-size correlated increase in the opening time of the pore lasting between milliseconds up to two seconds (Alvarez de Toledo *et al.*, 1993). In macrophages, Rab5 was suggested as a regulator of fusion pore opening duration (Duclos *et al.*, 2000).

A re-closable fusion pore could mimic the function of a channel for small solutes and molecules. In this respect, the kiss and run hypothesis provides an explanation for the observed, sequential delivery of small and large endocytic cargo into phagosomes and lysosomes, where smaller molecules were the first to reach their destination (Wang and Goren, 1987; Berthiaume *et al.*, 1995; Desjardins *et al.*, 1997). Due to its fluctuate nature, studies of a fusion pore in events other than vesicle exocytosis have relied on rigid snapshots for a long period of time. With the further development of high resolution imaging techniques, studies in living cells could demonstrate that indeed, in endocytosis and autophagy, a mixture of kiss and run and fusion with subsequent fission co-exist and simultaneously contribute to content exchange between compartments (Bright *et al.*, 2005; Jahreiss *et al.*, 2008).

1.2. The vesicular H^+-ATPase complex

Apart from the afore mentioned function in membrane fusion, the vesicular H^+-ATPase or shortened V-ATPase complex is an ubiquitously encountered mediator of essential cellular processes. V-ATPases are the major proton pumps in eukaryotic membranes and responsible for luminal acidification. In this respect they facilitate intracellular transport and proteolytic processing, but also the entrance of various pathogens such as the influenza virus (Guinea and Carrasco, 1995; Marjuki *et al.*, 2011). In specialised cells that harbour plasma membranous V-ATPases, these complexes enable *e.g.* bone resorption and acid secretion (Nelson *et al.*, 1992; Scimeca *et al.*, 2000). The upcoming sections will focus on these functions and the regulation of the V-ATPase complex.

1.2.1. Structure and mechanism of V-ATPases

The V-ATPases are multiprotein complexes belonging to a family of ATP-dependent proton pumps. They consist of 14 different subunits that are arranged in two main sectors – the peripheral V_1 sector containing eight and the membrane-integral V_0 sector containing six different subunits (Fig. 1.3) (Toei *et al.*, 2010; Cotter *et al.*, 2015). A functional complex is made of varying combinations of existing isoforms and even splice variants of the individual subunits (Table 1.1).

Table 1.1: Functions and isoforms of V-ATPase subunits
Modified from (Toei *et al.*, 2010).

Sector	Subunit	Molecular Mass	Isoforms	Function
V_1	A	70 kDa	-	ATP hydrolysis, regulatory subunit
	B	60 kDa	B1 B2	ATP hydrolysis, actin binding
	C	40 kDa	C1 C2	Stator and regulatory subunit, actin and RAVE binding
	D	34 kDa	-	Rotary subunit
	E	33 kDa	E1 E2	Stator subunit, RAVE binding
	F	14 kDa	-	Rotary subunit
	G	13 kDa	G1 G2 G3	Stator subunit, RAVE binding
	H	50 kDa	-	Stator and regulatory subunit

Sector	Subunit	Molecular Mass	Isoforms	Function
V_0	a	100 kDa	a1	Stator subunit, H^+ transport, complex targeting
			a2	
			a3	
			a4	
	d	38 kDa	d1	Rotary subunit, coupling
			d2	
	e	9 kDa	-	unknown
	c	17 kDa	-	Rotary subunit, H^+ transport
	c'	17 kDa	-	No mammalian subunit, H^+ transport, assembly
	c''	21 kDa	-	Rotary subunit, H^+ transport

The V-ATPase V_0 subunit a is the only known subunit that is expressed in four isoforms in mammalian cells. Interestingly, it is also the only subunit with more than one gene in yeast. The yeast a subunit isoforms Vph1p and Stv1p (similar to Vph1p 1) show distinct cellular localisations. While Vph1p is located in the vacuolar membrane, Stv1p-containing V-ATPases are found at the Golgi apparatus (Manolson *et al.*, 1994; Kawasaki-Nishi *et al.*, 2001a). The respective targeting information is encoded in their N-terminal domain and this differential V-ATPase composition affects the efficiencies of the proton pumps (Kawasaki-Nishi *et al.*, 2001a; Kawasaki-Nishi *et al.*, 2001c). Therefore it might explain differences in the acidification that is achieved in both compartments of which the Golgi apparatus is the less acidic.

There is no strict compartmentalisation of the mammalian V_0 a1 to a4 subunits, but they are also expressed with distinct tissue preferences. The V_0 subunit a1 is the predominant isoform in neuronal cell and especially found on synaptic vesicles (Morel *et al.*, 2003; Hiesinger *et al.*, 2005; Peri and Nusslein-Volhard, 2008; Zhang *et al.*, 2008). Among others, isoform 2 of subunit a was found in apical endosomes in kidney proximal tubule cells (Hurtado-Lorenzo *et al.*, 2006). The V_0 subunit a4 is also expressed in kidney, where it is located in the apical membrane of renal intercalated cells and mediates urinary acid secretion (Smith *et al.*, 2000; Oka *et al.*, 2001). Subunit a3, on the other hand, is present in various tissues. It is indispensable for bone resorption, because it targets the V-ATPase to the ruffled border of the resorption lacuna to obtain optimal pH conditions for enzymatic matrix degradation (Scimeca *et al.*, 2000; Toyomura *et al.*, 2003). V-ATPase V_0 subunit a3 further mediates secretion of insulin from pancreatic islet

cells and it is also the most prominent a isoform on lysosomes and lysosome-related organelles (Sun-Wada *et al.*, 2006; Tabata *et al.*, 2008; Sun-Wada *et al.*, 2009).

Similar to F-type and A-type ATPases, a rotary mechanism serves to couple the hydrolysis of ATP within sector V_1 to the transport of protons across a membrane that is mediated by the sector V_0. A hexameric ring of the nucleotide-binding subunits A and B (A_3B_3) builds up the catalytic centre of the V-ATPase in sector V_1. The connection between this catalytic unit and the site of proton translocation in sector V_0 is achieved by two types of stalks that include subunits of both sectors each (summarised in Cotter *et al.*, 2015).

The central stalk, which consists of the V_1 subunits D and F as well as the V_0 subunit d, provides the rotary connection between both sectors and conveys the energy gained by the processing of ATP into complex movement (Imamura *et al.*, 2003; Zhao *et al.*, 2015). The V_0 subunit d functions as a linker, which is localised on top of the V_0 proteolipid cylinder built of the different c subunits (Iwata *et al.*, 2004). Buried within these c subunits are conserved, glutamic acid residues that can be assessed through the V_0 subunit a (Noumi *et al.*, 1991; Hirata *et al.*, 1997). Therefore, subunit a is composed of eight transmembrane domains in its C-terminal region that form a cytoplasmic (TM7 and TM8) and a luminal hemichannel (TM3, TM4, TM7) (Toei *et al.*, 2011). A critical arginine residue stabilises the deprotonated glutamic acid of subunit c, so that protons can be captured within the cytoplasmic hemichannel. Rotation of the proteolipid cylinder then delivers the glutamic acid-bound proton across the membrane and to the luminal hemichannel of subunit a, in which it will be released (Fig. 1.3) (Kawasaki-Nishi *et al.*, 2001b, 2003; Wang *et al.*, 2004). Therefore, proton transport is always directed from the cytoplasm to the luminal space.

The V_0 subunit a is also part of the peripheral stalk that connects the V_0 and V_1 sectors by interaction with the V_1 subunits C and H. Subunits C and H in turn bind to heterodimers of the V_1 subunits E and G that exist in triplicates in mammalian V-ATPase complexes (Fethiere *et al.*, 2004; Inoue and Forgac, 2005; Benlekbir *et al.*, 2012). The peripheral stalk acts as a stator and has to withstand the torque that develops during ATP hydrolysis and central stalk rotation.

An important feature of V-ATPases is their ability of reversible V_0-V_1 dissociation as a regulatory measure. During this dissociation all contact sites between the two sectors have to be dissolved and the ATPase activity of free V_1 sectors must be inhibited. It is assumed that the V_1 subunit H plays a significant role in ATP hydrolysis inhibition by binding to subunit F in free V_1 sectors and

thereby preventing the movement of the rotary central stalk (Parra *et al.*, 2000; Jefferies and Forgac, 2008; Diab *et al.*, 2009).

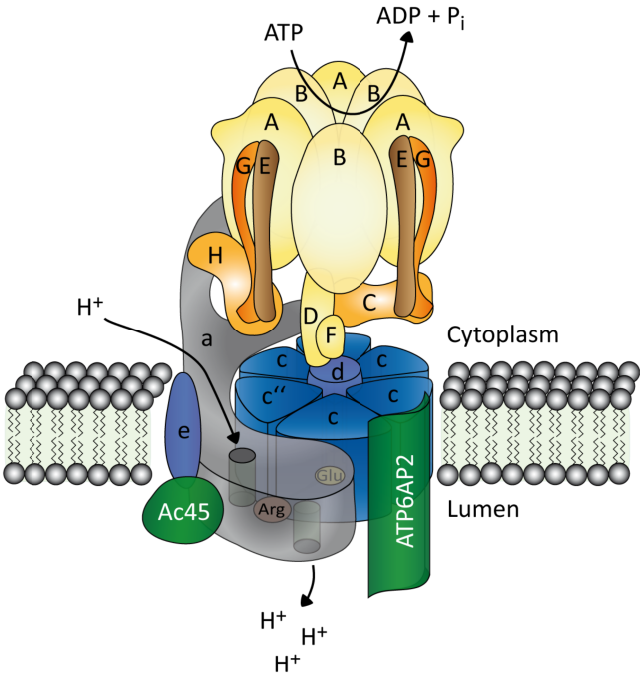

Figure 1.3: V-ATPase structure and function.

Schematic representation of a functionally assembled V-ATPase complex in mammalian cells. Upper case letters and yellow to brown colouring identifies V_1 sector members. Lower case letters and grey to blue colouring desribes V_0 sector affiliation. Accessory subunits are depicted in green. Energy is provided by ATP hydrolysis in sector V_1 and transferred into a rotational force onto sector V_0. Cytoplasmic protons that are localised within the subunit a hemichannel are captured by glutamic acid residues of subunit c. Rotation of the c subunits drives the transport to the second hemichannel of subunit a and leads to the release of the proton into the luminal space. Modified from (Forgac, 2007).

1.2.2. The V-ATPase accessory subunits

To complement the structure of V-ATPases, two accessory subunits exist in mammalian complexes that are attached to the V_0 sector: the V-ATPase accessory protein 1/ Ac45 and the V-ATPase accessory protein 2/ ATP6AP2, which is also known as the (pro-)renin receptor. In the last years, both proteins have entered the focus of attention as their necessity for V-ATPase assembly and function was elaborated.

The type I transmembrane protein Ac45 was initially identified in bovine chromaffin granules (Supek *et al.*, 1994; Getlawi *et al.*, 1996). It actively regulates V-ATPase trafficking and function in the course of vesicle secretion (Jansen *et al.*, 2008; Jansen *et al.*, 2010). To do so, the full length Ac45 has to undergo cleavage into a small N-terminal and a large C-terminal fragment,

where the latter represents the active form of the protein (Holthuis *et al.*, 1999; Schoonderwoert *et al.*, 2002). The exact mechanism by with Ac45 influences V-ATPases is not fully understood, yet. Targeted disruption of Ac45 expression in mice is lethal at an early embryonic stage following blastocyst injection (Schoonderwoert and Martens, 2002). A similar phenotype was observed upon deletion of the V-ATPase V_0 subunit c and it was associated with the loss of vesicle acidification (Sun-Wada *et al.*, 2000). This implies a tight link between Ac45 and the V-ATPase in developmental functions. By regulation of granular acidification, cleaved Ac45 modulates pro-hormone processing (Jansen *et al.*, 2010). Comparable to the V-ATPase V_0 subunit a3, Ac45 is further required to mediate the plasma membrane transport of V-ATPase complexes and thus for bone resorption during osteoclast differentiation (Feng *et al.*, 2008; Yang *et al.*, 2012).

Like Ac45, ATP6AP2 is also a type I transmembrane protein that consists of 350 amino acids and contains a large extracellular N-terminal as well as a short cytosolic C-terminal domain. ATP6AP2 can be processed by the proteases furin or ADAM19 (Cousin *et al.*, 2009; Yoshikawa *et al.*, 2011). Cleavage of the full length protein results in a soluble N-terminal fragment and a membrane-bound C-terminal fragment termed M8-9 (Fig. 1.4). This small C-terminal fragment was purified in 1998 by Ludwig and colleagues as an accessory protein of the V-ATPase complex, hence the name ATP6AP2 (Ludwig *et al.*, 1998).

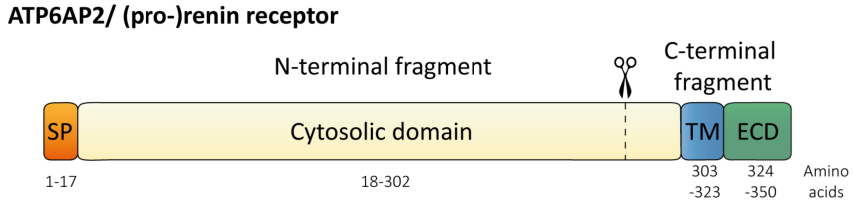

Figure 1.4: ATP6AP2 domain structure.

The type I transmembrane protein ATP6AP2 features a short signal peptide (SP) in its N-terminus that is followed by a long cytosolic domain and a distal transmembranous region (TM). An extracellular domain (ECD) completes the protein sequence. ATP6AP2 can be processed by either furin or ADAM19 within its cytosolic domain (dashed line) yielding an N-terminal and a C-terminal fragment as cleavage products.

The full length ATP6AP2, also called the (pro-)renin receptor (PRR) was identified in 2002, representing a new member of the renin angiotensin system (RAS) (Nguyen *et al.*, 2002). Its discovery filled a long existing gap in the understanding of the RAS, which mediates hormonal blood pressure regulation. Before the PRR, there was no known receptor for the

inactive renin precursor prorenin that circulates within the bloodstream in significant concentrations (reviewed in Krop *et al.*, 2013). The PRR binds both, the cleaved, enzymatically active renin and the inactive prorenin (Nguyen *et al.*, 2002). Binding of renin to the PRR elevates its catalytic activity, whereas binding of prorenin to the PRR induces conformational changes that allow enzymatic activity without further proteolytic processing (Krop *et al.*, 2013). In both cases, increased action of the RAS is triggered. The affiliation of the PRR to the V-ATPase complex became clear several years later, because its knockout in mouse resulted in early lethality, a phenotype that was quite uncommon for other members of the RAS (Methot and Reudelhuber, 2001; Burckle and Bader, 2006). Furthermore the PRR showed a clear co-localisation with the V_1 B1/2 subunit of the V-ATPase in kidney (Advani *et al.*, 2009). Thus, to allow thorough phenotypic analyses, tissue-specific PRR knockout mice were designed.

The deletion of *Atp6ap2* in podocytes and cardiomyocytes gave rise to cell mortality caused by the accumulation of vesicles that were filled with non-degraded material (Kinouchi *et al.*, 2010; Oshima *et al.*, 2011; Riediger *et al.*, 2011). This alteration was clearly associated with a loss of V-ATPase V_0 sectors and subsequent impairment in V-ATPase activity and proteolytic degradation. In mouse embryonic fibroblasts lacking ATP6AP2, the V-ATPase V_0 subunits as well as vesicle acidification were similarly absent (Kinouchi *et al.*, 2010). These findings imply a chaperone function of ATP6AP2 for the V-ATPase V_0 sector assembly and make ATP6AP2 an attractive target for the generation of V-ATPase knockdown mice.

Together with the V-ATPase complex, ATP6AP2 has further been brought in connection with the canonical wingless/ in (Wnt) signalling pathway (Cruciat *et al.*, 2010; Hermle *et al.*, 2010; Bernhard *et al.*, 2012). There it was proposed to act as an adapter between the V-ATPase and the complex consisting of Wnt3a, frizzled and the low-density lipoprotein receptor-related protein 6 (LRP6). The resulting acidification of the signalling endosome is a prerequisite for proper pathway stimulation and subsequent transcription of Wnt responsive genes.

1.2.3. Regulation of V-ATPase activity and functional implications

The intracellular and intracompartmental pH underlies constant changes in response to various stimuli. To control the activity of V-ATPases is an important measure to regulate the magnitude of proton enrichment. Since the subunit composition of V-ATPases influences their efficiency, differential targeting of distinct V-ATPase complexes can regulate the intracellular pH (Kawasaki-Nishi *et al.*, 2001a; Kawasaki-Nishi *et al.*, 2001c). The targeted delivery of individual V-ATPases

in the course of vesicle fusion events provides an example for this. But there are also other means to influence the V-ATPase´s activity, one major mechanism being its reversible dissociation into separate and inactive V_1 and V_0 sectors.

In yeast, V-ATPase complex dissociation occurs upon glucose depletion (Kane, 1995; Parra and Kane, 1998). This dissociation requires the microtubular network, while the reversion, V-ATPase association, relies on a protein complex termed regulator of the H^+-ATPase of vacuolar and endosomal membranes, shortly RAVE (Seol *et al.*, 2001; Xu and Forgac, 2001). The heterotrimeric RAVE complex aids to stabilise free V_1 complexes during V-ATPase dissociation as well as during its biosynthetic assembly by binding to the V_1 subunits E, G and C (Smardon *et al.*, 2002; Smardon and Kane, 2007). The switch between association and dissociation of V_1 and V_0 sectors in response to glucose is controlled by the Ras/ cAMP/ protein kinase A signalling pathway and helps to couple nutrient availability to ATP consumption (Bond and Forgac, 2008).

Reversible V-ATPase dissociation is also present in higher eukaryotes. The protein kinase A and phosphatidylinositol-3-kinase (PI3K) steer V-ATPase assembly in insect and renal cells, respectively (Sautin *et al.*, 2005; Voss *et al.*, 2007). Furthermore, during activation of dendritic cells V-ATPase assembly is also triggered in a PI3K-dependent manner to generate the acidic compartments necessary for antigen processing (Trombetta *et al.*, 2003; Liberman *et al.*, 2014).

This versatile regulatory network accounts for the broad functional range of V-ATPase complexes. The proton motive force that is built up by V-ATPase complexes can be utilised to transport small molecules and ions across the membrane to ultimately generate luminal acidification. Thereby intracellular V-ATPases provide the optimal pH for enzyme function in proteolytically active compartments, *e.g.* late endosomes, phagosomes and lysosomes. The plasma membranous V-ATPases exploit similar functional features to procure processes like urine acidification in the kidney and matrix resorption within bones (Karet *et al.*, 1999; Scimeca *et al.*, 2000; Smith *et al.*, 2000; Toyomura *et al.*, 2003).

Low vesicular pH values generated by intracellular V-ATPases trigger the dissociation of receptor ligand complexes, which is important upon receptor-mediated endocytosis and in receptor-guided delivery of newly synthesised proteins to their target compartment (Forgac, 2007). The latter includes protein transport via the mannose-6-phosphate receptor as well as the transport of β-glucocerebrosidase by the lysosomal integral membrane protein type 2 (LIMP-2) (Zachos *et al.*, 2012).

Another important feature of an acidic luminal pH with respect to transport processes is the evoked binding of ADP-ribosylation factor 1 (Arf1) to the endosomal membrane (Gu and Gruenberg, 2000). Arf1 acts as an adaptor for the coat protein complex that is required for the budding of endosomal carrier vesicles and subsequent (re-)distribution of endosome-resident constituents.

In addition, the gradual acidification of newly formed endosomes is important in the afore mentioned Wnt and the Notch pathway, which both depend on functional V-ATPase complexes (Yan *et al.*, 2009; Cruciat *et al.*, 2010; Hermle *et al.*, 2010; Vaccari *et al.*, 2010; Bernhard *et al.*, 2012; Kobia *et al.*, 2014).

The V_1 subunits B and C were shown to interact with filamentous actin and might be involved in actin bundling (Lee *et al.*, 1999; Vitavska *et al.*, 2005). In epididymal clear cells and osteoclasts, this contact was negatively correlated to PI3K activity and partially pH-dependent (Chen *et al.*, 2004; Beaulieu *et al.*, 2005). However the role of the V-ATPase-actin interplay will have to be addressed in detail in follow-up studies.

On the downside, various pathogens take advantage of the gradual pH decrease along the endocytic axis and express for example pH-activated fusion-promoting surface proteins such as the influenza hemagglutinin (Han *et al.*, 2001). By fusion of the viral and endosomal membrane, the pathogen escapes the ensued proteolytic degradation. Moreover, V-ATPases at the plasma membrane can be misused under pathogenic conditions. Explicitly, the metastasis of tumour cells relies on the degradation of the extracellular matrix to escape the primary place of tumour development and gain access to the blood stream (Martinez-Zaguilan *et al.*, 1993; Capecci and Forgac, 2013).

As already described for the formation of a fusion pore in membrane fusion (chapter 1.1.3), there are also proposed proton pumping-independent functions of the V-ATPase complex. A novel connection was established between V-ATPases and the mechanistic target of rapamycin (mTOR) complex 1/ mTORC1. This so called master regulator of metabolic function requires the V-ATPase for amino acid sensing at the lysosome and subsequent activation of the complex (Zoncu *et al.*, 2011; Zhang *et al.*, 2014; Jewell *et al.*, 2015; Wang *et al.*, 2015). Once active, mTORC1 promotes cell growth, while it directly inhibits autophagy and lysosomal biogenesis. The meshwork of mTORC1 function and regulation will be explained in more detail in section 1.4.

Overall, V-ATPases participate in many of the most crucial processes for cellular life, and this yields severe phenotypes, *e.g.* embryonic lethality and accumulation of autophagic vesicles in V-ATPase knockout models. Therefore studies on single mechanistic aspects prove difficult, since they have to distinguish between directly related and potentially superordinate effects due to a defective vesicle acidification.

1.3. Lysosomal processing in the endocytic and autophagic pathways

The compartment lysosome is a highly dynamic organelle that was initially discovered as a source for acid phosphatase activity (Duve *et al.*, 1955; Bainton, 1981). A broad range of acid hydrolases is enriched in the lysosomal lumen and the membrane contains a high density of associated (LAMPs) and integral membrane proteins (LIMPs). Additional lysosomal membrane components, *e.g.* V-ATPase complexes and small molecule transporters are localised to lysosomes and generate an acidic luminal pH or help to redistribute various degradation products, respectively (Eskelinen *et al.*, 2003; Lubke *et al.*, 2009).

Because the low lysosomal pH (4.8 – 5.2) provides optimal conditions for hydrolase activity, many lysosomal membrane proteins are protected from proteolytic cleavage by dense glycosylation (Ohkuma and Poole, 1978; Fukuda, 1991; Schwake *et al.*, 2013). In distinction from late endosomes, lysosomes lack the mannose-6-phosphate receptor within their membrane.

Lysosomes provide the tools for the enzymatic degradation of extracellular proteins or nutrients. Upon endocytic uptake of these compounds, the newly formed endosomes acquire an acidic, proteolytically active milieu through fusion with the storage organelles. A similar delivery of proteases and microbicidal components represents the basis for the digestion of phagocytosed pathogens during phagosome maturation or helps to reassimilate the cell´s own constituents in the course of autophagy. Thereby lysosomes occupy the centre of all these pathways and have to be reformed constantly (Fig. 1.5).

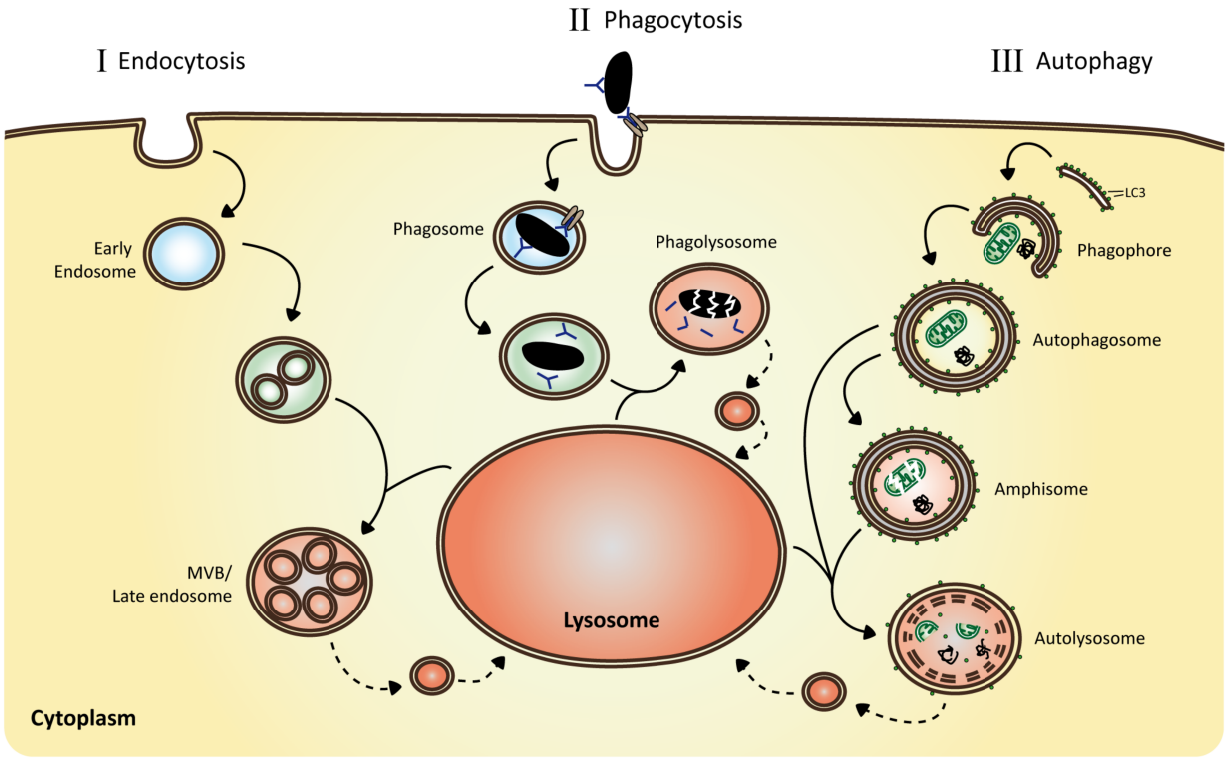

Figure 1.5: Incoming pathways that feed the lysosome.

The lysosome is the central element in providing degradative properties to vesicular compartments within the cell. (I) Endocytosis starts at the plasma membrane by formation of an endocytic vesicle that will mature into a multi-vesicular body (MVB) and dissect small particles of the extracellular fluid. (II) In a similar pathway, pathogens are engulfed in phagosomes at the plasma membrane. These phagosomes will develop into phagolysosomes, in which pathogen degradation can take place. (III) Intracellular constituents will be fed into the autophagy pathway upon inclusion into an autophagsome. Autophagosome formation starts with a limiting membrane in the cytosol and these compartments fuse with endosomes to produce amphisomes or with lysosomes to generate proteolytically active autolysosomes. Lysosomal components have to be recaptured from the late compartments of all pathways by lysosome reformation as indicated by dashed arrows.

1.3.1. The different routes of endocytosis

Endocytosis describes the uptake of extracellular particles through invagination of the plasma membrane and subsequent segmentation of an endocytic vesicle. Thereby it serves to incorporate extracellular nutrients as well as fluids and to internalise plasma membrane components like receptor-ligand complexes or lipids. There are various means of endocytic uptake that differ in the size of the developing endocytic vesicle or the involved coat proteins. Three commonly known types are clathrin-mediated endocytosis, calveolin-/ flotillin-mediated endocytosis and macropinocytosis (summarised in Hansen and Nichols, 2009). While clathrin- and calveolin-1-/ flotillin-coated endocytic vesicles are smaller (60 – 110 nm in diameter) and

rely on the action of dynamin to pinch off, macropinosome formation depends on the actin cytoskeleton and results in larger vesicles (up to 5 µm in diameter) (Swanson and Watts, 1995; Hansen and Nichols, 2009). Whether these endocytosis modes differ in the upcoming maturation of their respective endocytic vesicles is not clarified, yet.

The best characterised of these processes is clathrin-mediated endocytosis. Following formation of the clathrin-coated vesicles, they deliver their endocytosed cargo to early endosomes in the cell periphery, where sorting for either recycling or degradation takes place. The weakly acidic character of endosomes (pH 5.9 – 6.8) allows receptor-ligand dissociation and subsequent reuse of the receptors upon re-transfer to the plasma membrane (reviewed in Huotari and Helenius, 2011). On the other hand, proteins that are marked for degradation, *e.g.* by ubiquitylation, are packed into intraluminal vesicles with the aid of the endosomal sorting complexes required for transport, the ESCRT (Henne *et al.*, 2013). This morphological change is part of the endosome maturation process into late endosomes/ multi-vesicular bodies and is accompanied by the movement of the endosomes into the perinuclear area. The pH drops to 4.9 – 6.0 and more than 30 intraluminal vesicles can be accumulated (Maxfield and Yamashiro, 1987; Huotari and Helenius, 2011). Late endosomes pass through multiple fusion processes with other late endosomes, lysosomes and endosome-lysosome hybrid organelles. Over time, early endosome marker proteins, *e.g.* EEA1 and Rab5, which are required for fusion with early compartments, are exchanged for late markers, *e.g.* Rab7, and enable fusion with other late compartments like lysosomes (Huotari and Helenius, 2011; Gautreau *et al.*, 2014). Upon acquisition of acid hydrolases from the lysosome, the endocytosed cargo can be dissected into usable segments such as monosaccharides and amino acids. In this way, endocytic degradation provides the access to valuable extracellular resources.

1.3.2. Phagocytic pathogen clearance

The endocytic route is not restricted to fluids and non-viable particles. Furthermore it enables the entry of pathogens in a process termed phagocytosis. To allow the uptake of such pathogenic organisms into so-called phagosomes, the microbes have to be recognised by appropriate receptors that are expressed on the plasma membrane of and within specialised phagocytes and bind to conserved antigenic structures (reviewed in Brubaker *et al.*, 2015; Bryant *et al.*, 2015). Protruding molecules like the bacterial sugar mannose, bacterial of fungal lipoproteins or the fungal polysaccharide glucan are recognised ligands for plasma membranous

pattern-recognition receptors. In addition, microbes that are decorated with opsonins can bind to opsonin-specific receptors. IgG- or IgE-decorated pathogens, for example, form complexes with receptors for the constant fragment (Fc) of the respective antibody class (Unkeless *et al.*, 1988; van de Winkel and Anderson, 1991; Sutton and Gould, 1993).

Upon engulfment of the pathogenic particles into phagosomes, these compartments have to mature and gain microbicidal properties in a process comparable to the development of late endosomes. In the beginning of phagosome maturation, the vesicles will preferentially fuse with early endosomes and receptor molecules can be recycled back to the plasma membrane (Mayorga *et al.*, 1991). Upon fusion of early phagosomes with late endosomes, they acquire membrane proteins that allow further fusion with lysosomes as well as decrease their luminal pH by increasing the presence and activity of V-ATPases. Phagosome maturation terminates in the delivery of lysosomal content or even full fusion with lysosomes to form a phagolysosome (Desjardins *et al.*, 1994; Desjardins *et al.*, 1997). Degradation of the pathogens is then achieved with the aid of hydrolases, specific microbicidal peptides and the generation of reactive oxygen species.

Through the neutralisation of pathogens, professional phagocytes, *e.g.* macrophages and dendritic cells are a major part of the innate immune system. They further help to induce a more specific, adaptive immune response by presenting antigenic peptides on their cell surface that are derived of the degraded pathogens and can subsequently activate T and B cells.

1.3.3. Autophagy and nutrient recycling

Apart from the uptake of extracellular particles, cells recycle intracellular components in a process called macroautophagy (hereafter referred to as autophagy) to meet their demand for essential nutrients. In this process, cellular constituents are segregated into individual compartments, the autophagosomes that will mature and obtain degradative qualities upon fusion with lysosomes. Hence, engulfed particles can be broken down into reusable elements (summarised in McEwan and Dikic, 2011). Autophagy can have either a selectively or a non-selective mode of operation. While selective autophagy is a propagated measure of protein quality control, the non-selective autophagy randomly processes cellular contents to provide a sufficient amount of nutrients during periods of amino acid deprivation.

The formation of an isolation membrane represents the first step of autophagy. The generation of this lipid bilayer is tightly coupled to the activity of an initiation complex surrounding the

uncoordinated-51 (unc)-like kinase 1 or 2 (ULK1/ 2 complex) and to the recruitment of the PI3K class-III (PI3KC3) complex that is triggered upon ULK-mediated phosphorylation. Attracted by newly generated phosphatidylinositol-3-phosphate, autophagy-related (Atg) proteins arrive at the site of the isolation membrane and contribute to its elongation (summarised in Tanida, 2011; Wirawan *et al.*, 2012). During growth of the newly formed phagophore a cleaved form of the microtubule-associated protein 1A/ 1B-light chain 3 (LC3), LC3-I is conjugated to phosphatidylethanolamine to form LC3-II and incorporated into the autophagosomal membrane (Kabeya *et al.*, 2000; Kabeya *et al.*, 2004). Once the autophagosome is completed, LC3-II is actively removed from the outer membrane, while LC3-II located at the inner membrane will be degraded in the course of autophagosome maturation. The conversion of LC3-I to LC3-II and subsequent LC3-II proteolysis are often used as markers for autophagic flux.

Early autophagosomes will encouter endocytic vesicles in various fusion and kiss and run processes (Jahreiss *et al.*, 2008; Tong *et al.*, 2010). The combination of autophagosomes with early and late endosomes yields an amphisome that features a decreased luminal pH and late endocytic marker proteins. Amphisomes then fuse with lysosomes and aquire acid hydrolases to degrade the autophagic cargo. However, amphisome formation is not a prerequisite for fusion with lysosomes, since autophagosomes can also directly merge with the storage organelles (Liou *et al.*, 1997).

Since high rates of autophagy (*i.e.* more than protein synthesis and organelle biogenesis) would lead to the destruction of a cell, the process is strictly regulated in multiple instances. The switch between cell growth and the supply with nutrients by cellular degradation processes is among others controlled by the afore mentioned mTOR complex 1.

1.4. Mechanistic target of rapamycin complex 1

Environmental and intracellular signals are integrated by the mechanistic target of rapamycin complex 1 (mTORC1) to balance anabolic and catabolic processes within the cell and modulate cell growth. The conserved serine-threonine kinase mTOR was named according to its initial discovery as an effector of the immunosuppressive macrolide rapamycin and represents the heart of the two independently formed complexes mTORC1 and mTORC2 (Brown *et al.*, 1994; Sabatini *et al.*, 1994; Sabers *et al.*, 1995). Although both complexes contribute to proliferation and cell growth, mTORC1 exerts the major function in metabolic control.

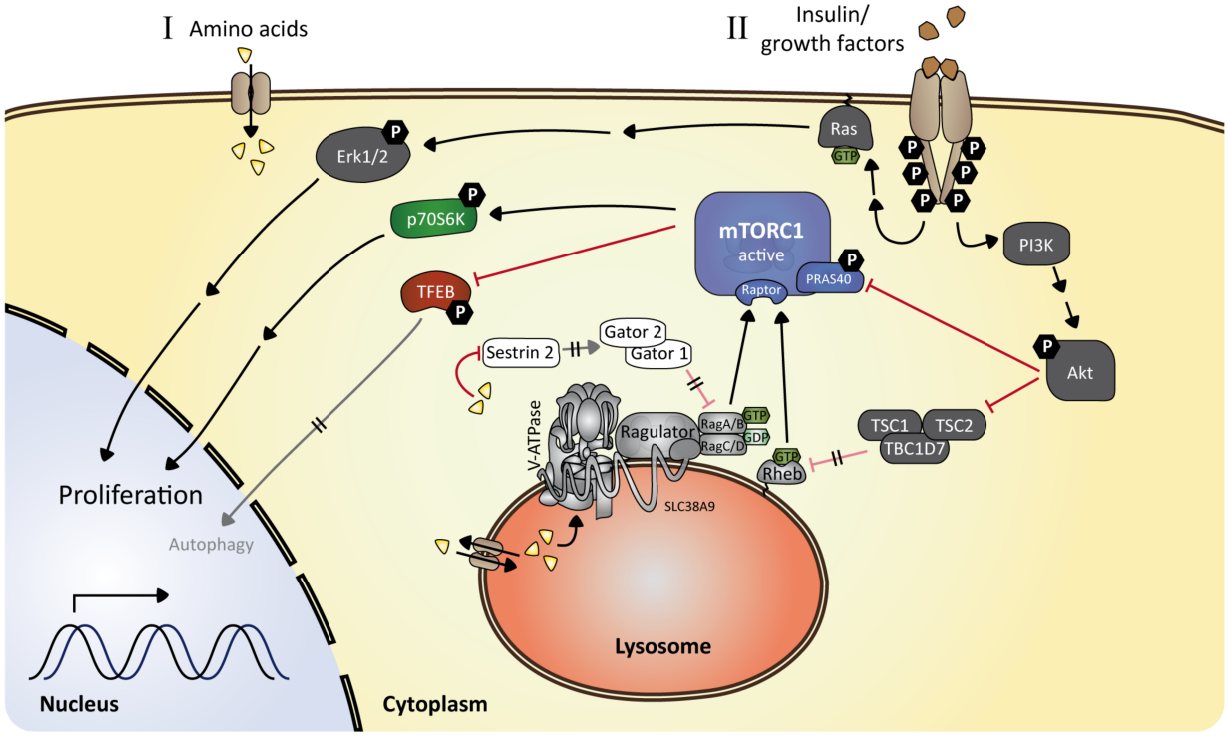

Figure 1.6: Influence of amino acids and growth factors on mTORC1 signalling.

(I) The mTOR complex 1 can be activated by nutrients, *e.g.* amino acids that are taken up into the cell or produced upon intracellular protein degradation. Amino acids act on the V-ATPase complex and the transporter SLC38A9 from within the lysosome, which leads to mTORC1 recruitment involving the Ragulator complex and the Rags. Furthermore, cytosolic amino acids inhibit sestrin 2, thereby releasing the inhibitory effect of the Gator supercomplexes on the Rags. Once recruited to the lysosome, mTORC1 can be stimulated by the small G-protein Rheb. (II) Extracellular growth factors and insulin trigger mTORC1 activity via the PI3K and the protein kinase B/ Akt. Akt inactivates the mTORC1 inhibitory component PRAS40 and silences the TSC1/2/TBC1D7 complex via phosphorylation. Thereby, it liberates Rheb at the lysosomal surface from the negative influence of TSC1 and 2. Erk1/2 activation is also triggered by growth factors and insulin via Ras-GTP and directly promotes cell proliferation. Active mTORC1 accomplishes both, cell proliferation and concomitant inhibition of autophagy, through phosphorylation of p70S6K and TFEB. Inhibitory actions are depicted using red lines, stimulatory actions are represented by black arrows. Pathways that are not active are shown with diminished colouring. Two consecutive arrows indicate indirect influences involving additional mediators that are not included in the scheme. Modelled on (Dibble and Manning, 2013; Wolfson *et al.*, 2015).

Both, mTORC1 and mTORC2 share common and complex-specific subunits (Laplante and Sabatini, 2012). Belonging specifically to mTORC1 are the kinase inhibitor proline-rich Akt1 substrate 1 (PRAS40) as well as the regulatory-associated protein of mTOR (Raptor) that influences mTORC1 localisation and substrate binding. Since mTORC1 is the modulator of multiple cellular processes, the complex and its effectors are quite thoroughly controlled and

the regulatory mesh is entangled in various cross-connections. Still, mTORC1 is also associated with various pathological situations, *e.g.* type-2 diabetes, cancer, and neurodegeneration. The upcoming sections aim to give an overview on the activation of mTORC1 and its function (Fig. 1.6).

1.4.1. Modes of mTORC1 activation

Activity of mTORC1 can be triggered by either intracellular amino acid pools or extracellularly initiated signalling of growth factors and peptide hormones. Depending on the stimulus, distinct routes lead from the source of input to the activation mTORC1.

The presence of essential amino acids is sensed either in the cytoplasm or the lumen of lysosomes. It is suggested that different amino acids have distinct sensors within the cell. Recognition of arginine and glutamine takes place in the lysosome and requires the member 9 of the solute carrier family 38 (SLC38A9) as an amino acid transporter and/ or the V-ATPase complex (Zoncu *et al.*, 2011; Jewell *et al.*, 2015; Jung *et al.*, 2015; Rebsamen *et al.*, 2015; Wang *et al.*, 2015). Mechanistically still not fully clarified, lysosomal amino acids are proposed to activate mTORC1 by inducing the lysosome-associated Ragulator complex and the Ras-related GTP-binding (Rag) proteins RagA to RagD. This machinery in turn recruits mTORC1 to the lysosomal surface, a process that is mediated by specific interactions between the mTORC1 component Raptor and the Rags (summarised in Bar-Peled and Sabatini, 2014). The V-ATPase/ Ragulator axis is also implied in controlling the AMP-activated kinase activity, which represents another master regulator of metabolic pathways (Zhang *et al.*, 2014).

The translocation of mTORC1 to the lysosome is necessary for subsequent activation of the kinase mTOR by the lysosome-resident Ras homologue enriched in brain (Rheb) (Saucedo *et al.*, 2003; Stocker *et al.*, 2003; Long *et al.*, 2005). Both the V-ATPase and SLC38A9 are directly involved in this signalling cascade. Overexpression studies using HEK 293T cells demonstrated a direct and amino acid-dependent interaction between the V-ATPase and the mTORC1 recruiting Ragulator subunits p14 and p18 (Zoncu *et al.*, 2011). Knockdown of the V-ATPase V_0 subunit c furthermore decreased the response of mTORC1 to amino acid stimulation (Zoncu *et al.*, 2011; Jewell *et al.*, 2015). Similarly, depletion of SLC38A9 renders mTORC1 insensitive to activation by distinct amino acids, *e.g.* arginine (Jung *et al.*, 2015; Rebsamen *et al.*, 2015; Wang *et al.*, 2015). Additional immunoprecipitation experiments using overexpressed SLC38A9 demonstrated a physical connection between the amino acid transporter and V_1 and V_0 subunits of the V-ATPase

(Wang *et al.*, 2015). However, whether both components act synergistically or in parallel means has to be further elucidated.

In addition, sensing of leucine also takes place within the cytoplasm and by the mTORC1 inhibiting protein sestrin 2 that belongs to another branch of mTORC1 regulation (Chantranupong *et al.*, 2014; Wolfson *et al.*, 2015). Sestrin 2 exerts its function via the Gator supercomplex that acts as a GTPase activating protein (GAP) for the Rags A and B and therefore influences mTORC1 translocation to the lysosome. Following the binding of leucine, sestrin 2 is inhibited and the Gator supercomplex releases RagA and B for upcoming mTORC1 induction.

The presence of intracellular amino acids further provides the basis for mTORC1 signalling triggered by extracellular stimuli. Upon elucidation by growth factors, *e.g.* the epidermal growth factor (EGF), receptor tyrosine kinases initiate canonical kinase cascades that trigger the activation of PI3K. Phosphatidylinositol (3,4,5)-trisphosphate produced by PI3K then recruits the protein kinase B/ Akt and is also involved in its excitation (Laplante and Sabatini, 2012). Originating from Akt, mTORC1 is influenced by both, direct and indirect routes. The mTORC1 component PRAS40 is directly phosphorylated by the kinase Akt, which diminishes the PRAS40-inhibitory effect and allows subsequent mTORC1 activation (Sancak *et al.*, 2007; Vander Haar *et al.*, 2007; Wang *et al.*, 2007). Furthermore Akt silences the tuberous sclerosis complex (TSC) consisting of TSC1, TSC2 and TBC1D7 (Dibble *et al.*, 2012). This TSC works as a GAP for the small GTPase Rheb that interacts with mTORC1 at the lysosome (Inoki *et al.*, 2002; Inoki *et al.*, 2003; Tee *et al.*, 2003). Hence, by blocking TSC, Akt triggers a second, indirect stimulation of mTORC1 and therefore occupies a dual role in mTORC1 activation. In addition, growth factors and peptide hormones exert a positive effect on proliferation via the Ras-induced mitogen-activated protein (MAP) kinase cascade (reviewed in Meister *et al.*, 2013).

1.4.2. Physiological relevance of mTORC1

Under nutrient-rich conditions, active mTORC1 promotes cell proliferation, energy metabolism and the biosynthesis of proteins as well as lipids. Simultaneously, mTORC1 inhibits the cellular recycling by interference with autophagy and excessive lysosomal degradation. This is achieved through the phosphorylation of distinct mTORC1 downstream targets, among them a multitude of transcription factors.

The mTOR complex 1 conveys a broad influence on the processes involved in protein synthesis (summarised in Tee and Blenis, 2005; Magnuson *et al.*, 2012). A major mTORC1 substrate is the eukaryotic initiation factor 4E (eIF4E)-binding protein 1 (4E-BP1) that, upon phosphorylation by mTORC1, releases the eIF4E to trigger cap-dependent mRNA translation (Brunn *et al.*, 1997; Hara *et al.*, 1997; Burnett *et al.*, 1998). A second mTORC1 effector, the 70 kDa ribosomal S6 kinase 1 (p70S6K), positively influences mRNA transcription as well as translation, when activated by phosphorylation (Brown *et al.*, 1995; Burnett *et al.*, 1998). To mediate these functions, the p70S6K itself has several downstream targets that include the ribosomal S6 protein and the eukaryotic elongation factor 2 kinase (eEF2K). Additionally, biogenesis of ribosomal and transfer RNA is induced upon mTORC1 stimulation through phosphorylation of the tripartite motif-containing protein 24 (TIF-1A) and the RNA polymerase III repressor Maf1, respectively (Mayer *et al.*, 2004; Kantidakis *et al.*, 2010; Shor *et al.*, 2010).

To promote cell growth, mTORC1 further provides the required material for the construction of membranes and their enlargement. The transcription factors sterol regulatory element-binding proteins 1 and 2 (SREBP1/ 2) regulate the expression of important genes for fatty acids and cholesterol synthesis and can be activated by mTORC1 in several ways (Porstmann *et al.*, 2008; Duvel *et al.*, 2010; Li *et al.*, 2010). SREBP1/ 2 processing that is needed for efficient nuclear entry of the transcription factors is supported by the p70S6K in a yet elusive manner. Within the nucleus, SREBPs are inhibited by Lipin-1, another direct target of mTORC1. Upon phosphorylation of Lipin-1, this negative regulator is excluded from the nucleus and SREBP1/ 2 are released to mediate lipid synthesis (Peterson *et al.*, 2011). Uptake and esterification of fatty acids is furthermore promoted by mTORC1-dependent regulation of the peroxisome proliferator-activated receptor γ (Kim and Chen, 2004; Zhang *et al.*, 2009).

Since proliferation consumes a considerable amount of cellular energy resources, mTORC1 is also linked to glucose metabolism and mitochondrial biogenesis. The hypoxia-inducible factor 1 α (HIF1α) elevates the mRNA abundance for proteins involved in glucose transport and glycolysis. Therefore, increased HIF1α mRNA translation mediated by mTORC1 promotes ATP production (Laughner *et al.*, 2001; Hudson *et al.*, 2002; Brugarolas *et al.*, 2003; Duvel *et al.*, 2010). Next to that, mTORC1 activation is associated with increased amounts of mitochondrial DNA and genes that are involved in cellular respiration, and thus again supplies energy in the form of ATP (Cunningham *et al.*, 2007; Koyanagi *et al.*, 2011). Hence, the balance between energy-supplying and energy-consuming processes is controlled by active mTORC1.

At the same time, parallel mTORC1 actions compromise the initiation of autophagy and proteolytic cleavage within lysosomes. The autophagy-initiating ULK complex is directly phosphorylated and thereby inactivated by mTORC1 (Ganley *et al.*, 2009; Hosokawa *et al.*, 2009; Jung *et al.*, 2009). In addition, other autophagy-regulating proteins, *e.g.* the death-associated protein 1, are influenced by mTOR phosphorylation (Koren *et al.*, 2010). The expression of many autophagic as well as lysosomal genes is also steered by mTORC1. The transcription factor EB (TFEB), a helix-loop-helix leucine zipper, binds to coordinated lysosomal expression and regulation (CLEAR) motifs in such genes to drive their transcription (Sardiello *et al.*, 2009; Palmieri *et al.*, 2011; Settembre *et al.*, 2011). However, cytosolic TFEB is phosphorylated by mTORC1, which facilitates binding of 14-3-3 proteins to the transcription factor and prevents its nuclear translocation (Settembre *et al.*, 2011; Martina *et al.*, 2012; Roczniak-Ferguson *et al.*, 2012; Settembre *et al.*, 2012). Thereby, mTORC1 interferes with TFEB function and the progression of autophagy and lysosomal biogenesis whenever nutrients are available.

1.5. Aim of this dissertation

Although the connection between V-ATPases and membrane fusion was revealed more than ten years ago, the nature of this involvement remains part of an ongoing debate. Past data include a variety of species but mostly lack mammalian representatives. The present thesis aims to clarify the requirement for V-ATPases in the late steps of membrane fusion in the mouse model and relate it to either the proton pumping activity or the sole presence of the protein complex.

In two independent genetic approaches, one specific subunit of the V-ATPase, the V_0 subunit a3, or a chaperone for V-ATPase assembly, the V-ATPase accessory protein 2, should be analysed for their contribution to membrane fusion upon knockout in mice. Both attempts appeal to alter the physical presence of the V-ATPase complex by either changing its composition or reduce its overall assembly rate. Impairments in the fusion between lysosomes and endocytic organelles resulting from these alterations should be characterized using *in cellulo* experimental analyses. In addition, the importance of the V-ATPase´s proton pumping function should be addressed in distinct pharmacological advances by utilization of established pH modulators.

By unravelling the significance of V-ATPases in vesicle transport and thereby membrane fusion, this thesis aims to strengthen one of the sites in the ongoing discussion and help the current understanding of vesicle merger.

In an extended analysis of intracellular transport routes that were reported to rely on the V-ATPase complex, the flow of autophagy should be studied in the V-ATPase knockdown animals. This autophagic flux is furthermore bound to V-ATPases through the regulation of the mTORC1. Hence, the activity of mTORC1 should be assessed and related to the expression level of V-ATPase complexes and the rate of autophagic clearance. In this respect, the conducted work might imply *in vivo* functions of the V-ATPase in autophagy and mTORC1 signalling.

2. MATERIAL AND METHODS

2.1. Material

2.1.1. Laboratory chemicals

Unless stated otherwise, all chemicals were purchased with the purity grade *pro analysi* (*p.a.*) and from Sigma-Aldrich, Carl Roth, AppliChem or Merck.

2.1.2. Bacteria

Amplification of plasmid DNA was conducted using *Escherichia coli* XL1-blue (Agilent Technologies).

Genotype: *recA1 endA1 gyrA96 thi-1 hsdR17 supE44 relA1 lac* [F´ *proAB lacI*^{q}*ZΔM15* Tn*10* (Tet^{r})]

2.1.3. Cell lines

Table 2.1: List of cell lines

Cell line	Description	Reference
Tcirg1$^{+/+}$ #9 (wild-type)	Mouse embryonic fibroblasts, SV40 Large T antigen-immortalised	Prof. Dr. Uwe Kornak (Charité Berlin)
Tcirg1$^{oc/oc}$ #7 (*a3*$^{-/-}$)		
Tcirg1$^{+/+}$ FcγRII #9/1-8 (wild-type)	Mouse embryonic fibroblasts, SV40 Large T antigen-immortalised, stably FcγRII-myc expressing (FcγRII-myc/ pcDNA4™/TO)	Generated in the course of this thesis
Tcirg1$^{oc/oc}$ FcγRII #7/1-2 (*a3*$^{-/-}$)		
Atp6ap2$^{+/Y}$ #7A (wild-type)	Mouse embryonic fibroblasts, SV40 Large T antigen-immortalised, stably Cre recombinase expressing (pCAG-Cre:GFP/ pGK-hyg)	
Atp6ap2$^{flox/flox}$ #6A (*Atp6ap2* knockout)		
CathepsinD$^{-/-}$	Mouse embryonic fibroblasts, SV40 Large T antigen-immortalised	(Saftig *et al.*, 1995)
CathepsinL$^{-/-}$		(Roth *et al.*, 2000)

2.1.4. Transgenic mouse lines

Table 2.2: Transgenic mouse lines

Mouse strain	Mouse strain (full name)	Source	Reference
Atp6ap2 flox	B6-Atp6ap2^{tm1Aich}	Dr. Atsuhiro Ichihara (Tokyo Women´s Medical University)	(Kinouchi *et al.*, 2010)
Mx1-Cre	B6.Cg-Tg(Mx1-cre)1Cgn/J	The Jackson Laboratory	(Kuhn *et al.*, 1995)

Mouse strain	Mouse strain (full name)	Source	Reference
LysM-Cre	B6.129P2-*Lyz2*$^{tm1(cre)Ifo}$/J	Prof. Dr. Börn Rabe (University Kiel)	(Clausen *et al.*, 1999)
Rosa26-EYFP	B6.129X1-*Gt(ROSA)26Sor*$^{tm1(EYFP)Cos}$/J	Prof. Dr. Radislav Sedlacek (Academy of Science of the Czech Republic)	(Srinivas *et al.*, 2001)

2.1.5. Cell culture media, additives and fluorescence probes

Bafilomycin A1	Calbiochem
Bovine serum albumin (BSA)	Roth
BSA-gold	CMC Utrecht
Collagen type VII from rat tail	Sigma-Aldrich
Dextran-FITC	Life Technologies
Dextran-Oregon Green® 514	Life Technologies
Dextran-Texas Red®	Life Technologies
DQ™ Red-BSA	Life Technologies
Dulbecco´s Modified Eagle Medium (DMEM)	Life Technologies
DMEM with stable L-glutamine	Sigma-Aldrich
Earle´s Balanced Salt Solution (EBSS)	Sigma-Aldrich
Fetal bovine serum (FBS)	Biochrom
Hygromycin B Gold™	InvivoGen
LysoTracker® Red DND-99	Life Technologies
Nigericin	AppliChem
Penicillin-Streptomycin	Life Technologies
Polyethylenimin Max MW 40,000 (PEI)	Polysciences
Polystyrene latex beads (d = 1.1 µm)	Sigma-Aldrich
Trypsin/EDTA	Sigma-Aldrich
Zeocin™	InvivoGen

2.1.6. Antibodies

Table 2.3: Primary antibodies

Antigen	Clonality	Host	Relevant dilution	Reference
β-actin	polyclonal	Rabbit	1:2000 (WB)	Sigma-Aldrich #A2066
ATP6AP2	polyclonal	Rabbit	1:500 (WB)	Pineda Antibody Service (Kissing *et al.*, 2015)
Cathepsin D	polyclonal	Rabbit	1:500 (WB) 1:100 (IF)	*Prof. Dr. Stefan Höning (University Cologne)* #sII10
Cathepsin L	polyclonal	Goat	1:500 (WB)	R&D Systems #AF1515
EEA1	monoclonal	Rabbit	1:100 (IF)	Cell Signaling Technology #3288
F4/80	monoclonal	Rat	1:200 (F)	Ebioscience #17-4801
GAPDH	polyclonal	Rabbit	1:5000 (WB)	Santa Cruz Biotechnology #sc-25778
GM130	monoclonal	Mouse	1:100 (IF)	BD Biosciences #610823
KDEL	monoclonal	Mouse	1:300 (IF)	Enzo Life Sciences #ADI-SPA-827
LAMP-1	monoclonal	Rat	1:250 (IF)	DSHB #1D4B
LAMP-2	monoclonal	Rat	1:1000 (WB) 1:50 (IF)	DSHB #Abl93
LC3	polyclonal	Rabbit	1:1000 (WB) 1:500 (IF)	MBL #PM036
mTOR	monoclonal	Rabbit	1:2000 (WB) 1:200 (IF)	Cell Signaling Technology #2983
Myc-tag	monoclonal	Mouse	1:5000 (WB)	Cell Signaling Technology #2276
p14	monoclonal	Rabbit	1:1000 (WB)	Cell Signaling Technology #8145
p18	monoclonal	Rabbit	1:1000 (WB)	Cell Signaling Technology #8975
p62	polyclonal	Rabbit	1:2000 (WB+IF)	Enzo Life Sciences #BHL-PW-9860
p70S6K	polyclonal	Rabbit	1:500 (WB)	Cell Signaling Technology #9202
Phospho-p70S6K (Thr389)	polyclonal	Rabbit	1:2000 (WB)	Cell Signaling Technology #9205
PRAS40	monoclonal	Rabbit	1:2000 (WB)	Cell Signaling Technology #2691
Phospho-PRAS40 (Thr246)	monoclonal	Rabbit	1:2000 (WB)	Cell Signaling Technology #2997
Rab5	monoclonal	Mouse	1:30 (IF)	Synaptic Systems #621.3
RagA	monoclonal	Rabbit	1:1000 (WB)	Cell Signaling Technology #4357
RagC	monoclonal	Rabbit	1:2000 (WB)	Cell Signaling Technology #5466
Tubulin	monoclonal	Mouse	1:5000 (WB)	DSHB #E7
V-ATPase V_0 a1	polyclonal	Rabbit	1:500 (WB)	*Prof. Dr. Beth S. Lee (The Ohio State University College of Medicine)* (Manolson *et al.*, 2003)

Antigen	Clonality	Host	Relevant dilution	Reference
V-ATPase V_0 a2	polyclonal	Rabbit	1:2000 (WB)	Abcam #ab96803
V-ATPase V_0 a3	polyclonal	Guinea pig	1:500 (WB) 1:100 (IF)	*Prof. Dr. Thomas Jentsch (MDC/FMP Berlin)* (Lange *et al.*, 2006)
V-ATPase V_0 c	polyclonal	Rabbit	1:2000 (WB)	Pineda Antibody Service (Kissing *et al.*, 2015)
V-ATPase V_0 d1	polyclonal	Rabbit	1:2000 (WB)	Proteintech Group #18274-1-AP
V-ATPase V_0 B2	monoclonal	Rabbit	1:2000 (WB)	Cell Signaling Technology #14617

Dilution factors are presented for Western blotting (WB), flow cytometry (F) or immunofluorescene (IF)

Purified human IgG (#I4506) and IgG from mouse serum (#5381) for unspecific latex bead opsonisation were purchased from Sigma-Aldrich.

Table 2.4: Secondary antibodies

Antibody	Coupled to	Host	Relevant dilution	Reference
Anti-goat	Horseradish-Peroxidase	Rabbit	1:15,000	Dianova #305-035-003
Anti-guinea pig		Donkey		Dianova #706-035-148
Anti-mouse		Sheep		Dianova #515-035-062
Anti-rabbit		Goat		Dianova #111-035-144
Anti-rat		Goat		Dianova #112-035-143
Anti-rabbit	IRDye® 800CW	Donkey	1:10,000	LI-COR® #926-32213
Anti-goat	AlexaFluor® 488, 594, 647, 680	Donkey	1:300 – 1:500	Cell Signaling Technology
Anti-guinea pig		Goat		
Anti-human		Goat		
Anti-mouse		Goat/ donkey		
Anti-rabbit		Goat/ donkey		
Anti-rat		Goat		

2.1.7. Enzymes

DreamTaq™ DNA Polymerase	Thermo Fisher Scientific
Proteinase K	Roche

2.1.8. Oligonucleotides

Table 2.5: List of oligonucleotides used for genotyping

Oligonucleotide name	Sequence 5'- 3'
Tcirg1^{oc} forward 1	GCC TTC CAG AGA CGC TTC GTG
Tcirg1^{oc} forward 2	TGT TTA GAA GCA GCC GCT CTG
Tcirg1^{oc} reverse	GTT TAT CTC CTC ACT CAC ATC
Atp6ap2^{flox} forward	GGG GGG TAA ATT GTT GAT GAG TCT TGG AGC ATA GC
Atp6ap2^{flox} reverse	GAA GCC CAT GGA CAG TGC AGC TAC GTC TGG GAT TCG A
Sry forward	TGG GAC TGG TGA CAA TTG TC
Sry reverse	GAG TAC AGG TGT GCA GCT CT
Cre recomb. forward	GCA TAA CCA GTG AAA CAG CAT TG
Cre recomb. reverse	GAC ATG TTC AGG GAT CGC CAG G
Rosa26-EYFP forward wt	GGA GCG GGA GAA ATG GAT ATG
Rosa26-EYFP forward insert	AAG ACC GCG AAG AGT TTG TC
Rosa26-EYFP reverse	AAA GTC GCT CTG AGT TGT TAT

Table 2.6: List of oligonucleotides and hydrolysis probes (UPL, Roche) used for qPCR

Gene			Oligonucleotide sequence 5'- 3'	UPL #
Actb	NM_007393.3	Left	CTA AGG CCA ACC GTG AAA AG	64
		Right	ACC AGA GGC ATA CAG GGA CA	
Atg10	NM_025770.3	Left	TGG GAA GGT GTT CAT GAG TG	1
		Right	GCC CAA GTA TTG GAT GTT CC	
Atg9a	NM_001003917.3	Left	CGA GGC TGG TAA CTG GAA TC	105
		Right	GCC CTG GTT GGA CAG TTG	
Atp6v0a1	NM_001243050.1 NM_001243051.1 NM_001243049.1 NM_016920.3	Left	ACC GTG GCT ATC CTG CTG	69
		Right	CCC AGT GTA GAA TTT GTT CTG GA	
Atp6v0a2	NM_011596.4	Left	TCC CGC CTT AGA GAA CGA C	33
		Right	CTG AAT CAG GCC AGA AAC G	
Atp6v0a4	NM_080467.3	Left	GAT GCT GAG ACC CCT CTC C	80
		Right	TGC AGC TCT CCT TCC AAC TT	

Gene			Oligonucleotide sequence 5'- 3'	UPL #
Atp6v0c	NM_009729.3	Left	GTC CGC CAT GGT CTT CAG	46
		Right	CAG CTC TGG CCT CAT GAC T	
Atp6v0d1	NM_013477.3	Left	CAA TGC CAT TCT GGT GGA C	15
		Right	TTT CGG ATT ATC TCG ATG TTC A	
Atp6v0d2	NM_175406.3	Left	AAG CCT TTG TTT GAC GCT GT	47
		Right	GCC AGC ACA TTC ATC TGT ACC	
Atp6v1a	NM_007508.5	Left	CCA TTA TCC GGG AGC ACA T	25
		Right	CTC GCC ATC TTT CAC TGG AT	
Atp6v1b1	NM_134157.2	Left	CAT TGA CAA AGG ACC TGC TG	53
		Right	GGT CAT GGG GAT TGA TTG G	
Atp6v1b2	NM_007509.3	Left	ACA TGA GCT CCT ACG CTG AAG	103
		Right	TCA TAG ATT GTG GCT AAG TCG GTA	
Bnip3	NM_009760.4	Left	CCT GTC GCA GTT GGG TTC	52
		Right	GAA GTG CAG TTC TAC CCA GGA G	
Clcn7	NM_011930.3	Left	CCT GTG GTG GAG GAT GTA GG	20
		Right	ATA AGC TGG GAA CGC AGG AT	
Fbxo32	NM_026346.3	Left	AGT GAG GAC CGG CTA CTG TG	53
		Right	GAT CAA ACG CTT GCG AAT CT	
GluI	X16314.1 AY044241.1	Left	CTC GCT CTC CTG ACC TGT TC	31
		Right	TTC AAG TGG GAA CTT GCT GA	
HexA	NM_010421.4	Left	ACC TGG GAG GGG ATG AAG T	11
		Right	ATG AAG GCC TGG ATG TTG G	
Hprt1	J00423.1	Left	CCT CCT CAG ACC GCT TTT T	95
		Right	AAC CTG GTT CAT CAT CGC TAA	
LAMP-1	NM_010684.2	Left	CCT ACG AGA CTG CGA ATG GT	110
		Right	CCA CAA GAA CTG CCA TTT TTC	
Sdha	NM_023281.1	Left	TGT TCA GTT CCA CCC CAC A	71
		Right	TCT CCA CGA CAC CCT TCT G	
Sqstm1	NM_011018.2	Left	AGA CCC CTC ACA GGA AGG AC	41
		Right	CAT CTG GGA GAG GGA CTC AA	

Gene			Oligonucleotide sequence 5'- 3'	UPL #
Tcirg1 +E2	NM_016921.3 NM_001136091.2 NM_001167784.1	Left	CCT CGT GGA GTT CAG AGA CCT	50
		Right	CCG GAC GTC TAC CAC GAA	
Tcirg1 -E2	NM_016921.3 NM_001136091.2 NM_001167784.1	Left	CCA TAT CCC TTT GGC ATT GA	97
		Right	GAG AAA GCT CAG GTG GTT CG	
Tuba1a	NM_011653.2	Left	CTG GAA CCC ACG GTC ATC	88
		Right	GTG GCC ACG AGC ATA GTT ATT	

2.1.9. Expression constructs and plasmids

The expression construct for Fcγ receptor IIa-myc was kindly provided by *Prof. Dr. Sergio Grinstein (University of Toronto)* (Downey *et al.*, 1999).

Table 2.7: Utilised plasmids

Plasmid	Resistance	Reference
pCAG-Cre:GFP	Ampicillin/ G418	(Kinouchi *et al.*, 2010)
pcDNA4™/TO	Ampicillin/ zeocin™	(Kuhn *et al.*, 1995)
pGK-hyg	Ampicillin/ hygromycin	(Clausen *et al.*, 1999)
pMSSVLT	Ampicillin/ G418	(Srinivas *et al.*, 2001)

2.1.10. Protein and DNA standards

PageRuler™ Plus Prestained Protein Ladder	Thermo Fisher Scientific
GeneRuler 100 bp Plus DNA Ladder	Thermo Fisher Scientific

2.1.11. Ready-made reagent collections and kits

PureYield™ Plasmid Midiprep System	Promega
NucleoSpin® RNA Plus Kit	Macherey Nagel
RevertAid First Strand cDNA Synthesis Kit	Thermo Fisher Scientific
Pierce™ BCA Protein Assay Kit	Thermo Fisher Scientific
ECL Advance™ Western Blotting Detection Kit	GE Healthcare

2.1.12. Frequently used buffers and aqueous solutions

LB medium	1 % (w/v)	Trypton/ Pepton
	0.5 % (w/v)	Yeast extract
	1 % (w/v)	NaCl
		pH 7.0
LB agar	1.5 % (w/v)	Agar-agar
	in	LB medium
Phosphate buffer (0.1 M)	84 mM	Na_2HPO_4
	16 mM	KH_2PO_4
		pH 7.2 – 7.4
Phosphate-buffered saline (PBS) (10x)	100 mM	Na_2HPO_4
	18 mM	KH_2PO_4
	1,37 M	NaCl
	27 mM	KCl
		pH 6.8
Mounting medium	1x	PBS pH 7.4
	17 % (w/v)	Mowiol 4-88
	33 % (v/v)	Glycerol
	20 mg/ml	1,4-diaza-bicyclo-[2,2,2]-octane (DABCO)

2.2. Molecular biological methods

2.2.1. Generation of electro-competent *Escherichia coli*

The internalisation of plasmid DNA by *Escherichia coli (E. coli)* can be stimulated using electric impulses. Therefore, the bacteria have to be prepared in a solution with low ion conductivity. XL1-blue cells were separated on an LB agar plate containing 20 mg/ml tetracyclin using the 13-line procedure. Fifty ml LB media (20 mg/ml tetracyclin) were inoculated with a single colony

and incubated overnight at 37 °C under continuous shaking. The next day, 20 ml pre-culture were transferred to 1 l LB media containing 20 mg/ml tetracyclin and cultivated until the exponential growth phase was reached (OD_{600} = 0.5 – 0.6). Bacteria were collected by 15 minutes centrifugation at 31,000 x *g* and 4 °C. The sediment was washed twice in 250 ml of ice-cold double-distilled water followed by a third washing step in 100 ml 10 % (v/v) glycerol. Bacteria were subjected to centrifugation at 2,210 x *g* for 20 minutes and 4 °C and finally resuspended in 4 ml 10 % (v/v) glycerol. Aliquots of 50 µl cell suspension were stored at -80 °C until usage.

2.2.2. Transformation of electro-competent *Escherichia coli*

For transformation of plasmid DNA into *E. coli*, electro-competent bacteria (see 2.2.1) were thawed on ice before the addition of 0.5 µg DNA (max. 2 µl). In a pre-cooled cuvette, the bacterial cell membrane was permeabilised at 2.5 kV utilising an electroporator (C = 25 µF and R = 400 Ω). Following electroporation, the cell suspsension was immediately transferred to 1 ml pre-warmed LB medium and incubation at 37 °C for 30 minutes. One fifth of the cultivated bacteria was plated on LB agar plates containing the appropriate selection antibiotic (50 µg/ml ampicillin).

2.2.3. Purification of plasmid DNA

XL1-blue *E. coli* were transformed as described in 2.2.2 to amplify plasmid DNA and obtain suitable amounts for the transfection of mammalian cells. Single clones were picked from LB agar plates and used to inoculated 200 ml LB medium containing the respective selection antibiotic (50 µg/ml ampicillin) and the suspension incubated at 37 °C overnight under continuous shaking. Purification of the plasmid DNA was conducted using the PureYield™ Plasmid Midiprep System according to the manufacturer´s protocol.

2.2.4. Determination of nucleid acid concentration

The concentration of DNA and RNA was measured photometrically in a Synergy HT (BioTek) microplate reader using the absorption maximum of nucleid acids at 260 nm. An absorbance of 1.0 reflects a concentration of 50 ng/µl double stranded DNA or 40 ng/µl RNA, respectively. In addition, absorbance at 280 nm was used to determine the purity of the nucleid acid preparation with respect to protein contaminations. The ratio A_{260}/A_{280} should reside between 1.7 and 2.0.

2.2.5. Total RNA extraction

Total RNA was isolated with the aid of the Nucleospin® RNA Plus kit according to the manufacturer´s instructions. Cell samples were lysed directly in their respective culture dishes. For homogenisation of liver samples, small pieces of the organ were supplied with 350 µl of the kit´s lysis buffer and disrupted using a Precellys® homogenizer (Peqlab) at 6,000 rpm for two times 30 seconds. A small portion of isolated total RNA was subjected to agarose gel electrophoresis (see section 2.2.8) for quality control.

2.2.6. cDNA synthesis

Synthesis of complementary DNA (cDNA) was achieved with the RevertAid First Strand cDNA Synthesis Kit following the manufacturer´s protocol. Transcription was conducted using 0.2 – 2 µg total RNA (2.2.5) in combination with random hexamer primers (Thermo Fisher Scientific).

2.2.7. Quantitative real-time PCR (qPCR)

The expression levels of distinct mRNAs were assessed using quantitative real-time PCR (qPCR) with the Universal ProbeLibrary (UPL) System Technology (Roche). Small hydrolysis probes containing the reporter fluorescein at their 5' and a dark quencher dye at their 3' end hybridise with their target sequence and will be cleaved by the polymerase during amplification. The resulting dequenching of the reporter yields increasing fluorescence signals during PCR-based sequence amplification and can be used for quantification. Specific assays for each target were created with the UPL Assay Design Center (table 2.6). Complementary DNA (0.5 µl, see chapter 2.2.6) was supplied with 0.1 µM hydrolysis probe, 0.3 µM of each, left and right oligonucleotide and 1x LightCycler® 480 Probes Master (Roche) containing a FastStart™ Taq DNA Polymerase, reaction buffer, a mixture of dNTPs and $MgCl_2$. Duplicates were analysed using a LightCycler® 480 Instrument II (Roche). Resulting C_P values were normalized to the logarithmic average C_P of the most stable house keeping genes (*Actb*, *Tuba1a*, *Hprt1* and *Sdha*) to obtain ΔC_P describing relative mRNA expression levels. The comparison of ΔC_P values between genotypes was used in statistical analyses. Furthermore, serial cDNA dilutions were analysed in each assay to determine the primer efficiency ($E = 10^{-1/slope}$). Bar charts visualising relative mRNA expression levels result from $E^{(-\Delta CP)}$.

2.2.8. Agarose gel electrophoresis

50x Tris-acetate-EDTA (TAE) buffer	2 M	Tris/ HCl pH 8.0
	5.5 % (v/v)	Acetic acid
	50 mM	EDTA

Agarose gel electrophoresis was utilised to separate DNA and RNA samples according to their length. For preparation, nucleid acid samples were supplemented with 6x DNA gel loading dye (Thermo Fisher Scientific) to adjust the sample density and visualise its migration during gel electrophoresis. Agarose gels were casts in 1x TAE buffer with a final concentration of 1.5 – 2.0 % (w/v) agarose and 500 ng/ml ethidium bromide. Separation was performed by applying a voltage of 120 V. The length of the separated products determines their migration through the gel, which was compared to a standard DNA ladder. Detection was performed using UV light (λ = 312 nm) and documented with a Gel Jet Imager (Intas®).

2.3. Cell biological methods

2.3.1. Maintenance of cell lines

All murine cells were kept at 37 °C in a humidified 7.5 % (v/v) CO_2 atmosphere. Sterile handling and treatment of cells was performed under a laminar flow clean bench. Mouse embryonic fibroblast (MEF) lines were cultivated in DMEM containing 4 mM L-glutamine and 4.5 g/l D-glucose with the addition of 10 % (v/v) FBS. For maintenance, MEF lines were passaged twice a week at 100 % confluence by trypsin digest. Therefore, cells were rinsed once with PBS and covered with trypsin/ EDTA (0.5 mg/ml / 0.22 mg/ml in PBS) until they detached easily. Subsequently, cells were recovered in growth medium and seeded onto new culture dishes in a 1:25 dilution. For cultivation of primary cells, the growth medium was supplemented with 100 U/ml penicillin and 100 µg/ml streptomycin to avoid bacterial contaminations. Cultures of primary macrophages were furthermore kept with a FBS concentration of 20 % (v/v).

2.3.2. Isolation of peritoneal macrophages

Primary mouse macrophages were isolated from the peritoneal cavity of mice. Therefore, the peritoneum of euthanised animals (section 2.6.7) was flushed with 10 ml ice-cold PBS for 5 minutes using a 20 G needle attached to a syringe. Peritoneal cells were collected in a falcon

tube and centrifuged at 210 x *g* and 4 °C for 10 minutes. The cell pellet was resuspended in 5 ml pre-warmed culture medium and cell count determined from a 1:10 dilution containing trypan blue in a Neubauer improved counting chamber (C-Chip, Biochrom). Between 1 x 10^5 (Imaging Dish) to 5 x 10^6 (6 cm culture dish) cells were seeded for experimental analyses the next day. After three hours, the culture medium was replaced to remove non-adherent cells and obtain a highly pure macrophage culture. The yield of peritoneal macrophages was increased by pretreatment of the mice with a 4 % (w/v) thioglycolate solution (see 2.6.6).

2.3.3. Preparation of primary hepatocytes

10x Stock buffer	16 mM	Na_2HPO_4
	4 mM	KH_2PO_4
	1.4 M	NaCl
	50 mM	KCl
	8 mM	$MgCl_2$
Perfusion buffer	1x	Stock buffer pH 7.4
	25 mM	$NaHCO_3$
	2.55 mM	EDTA
	16.5 mM	D-Glucose
	7.5 mM	Lactate
	0.25 mM	Pyruvate

Murine hepatocytes were prepared by EDTA dissociation (Meredith, 1988). Therefore, Ketamine/ Rompun®-anaesthetised mice (2.6.7) were subjected to hepatic arterial perfusion with oxygenated perfusion buffer for 45 to 60 minutes at a flow rate of 5 – 8 ml/min. Single cells were obtained following disruption of the liver in culture medium and subsequent filtration through a 70 µm nylon cell strainer. The resulting suspension was spun down at 28 x *g* and room temperature for 4 minutes and the pellet dissolved in 8 ml culture medium. Hepatocytes were then separated in a self-generating Percoll gradient by addition of 13.9 ml Percoll (Amersham) and 2.1 ml Stock buffer and centrifugation at 855 x *g* for 6 minutes. The pellet was dissolved in culture medium and hepatocytes maintained on collagen type VII-coated culture dishes or cover slips. After one hour, the culture medium was replaced. Experiments were conducted at the day of isolation but not before cells became adherent for at least two hours.

2.3.4. Isolation of mouse embryonic fibroblasts (MEFs)

To isolate mouse embryonic fibroblasts, pregnant female mice were sacrificed (see 2.6.7) at day 13.5 *post coitum*. Both uterine horns were prepared and placed in a Petri dish containing sterile PBS. From then on, further processing was carried out under the clean bench and with sterile instruments. Each embryo was separated from its placenta and amniotic sac and transferred to a fresh Petri dish with PBS. Embryo heads were removed and utilised for genotype determination using the DirectPCR® Lysis Reagent Tail (Peqlab) and proteinase K digest (see sections 2.6.3, 2.6.4). Furthermore, all red organs were dissected. In a 3.5 cm culture dish containing 2 ml of trypsin/ EDTA (0.5 mg/ml / 0.22 mg/ml in PBS) the remaining tissue was minced using a razor blade and incubated for 15 minutes at 37 °C. Single cells were collected in culture medium and the suspension spun down at 300 x *g* and room temperature for 5 minutes. The pellets containing the fibroblasts were resuspended in 10 ml culture medium and added to one 10 cm culture dish per embryo.

2.3.5. Cryo-preservation of cell lines

MEF lines were preserved as cryo-cultures over liquid nitrogen. For freezing of cells, these were detached with trypsin (see 2.3.1) from a 10 cm culture dish grown to confluence and collected in a falcon tube by centrifugation at 600 x *g* and room temperature for 10 minutes. The cell pellet was dissolved in a small volume of DMEM containing 20 % (v/v) FBS and 10 % (v/v) DMSO and frozen at-80 °C as 1 – 2 cryo-cultures. For long-term storage, cryo-cultures were transferred to the gas phase of a liquid nitrogen tank.

Cryo-cultures were reactivated by thawing at 37 °C and addition of nine parts prewarmed culture medium. To support cell growth and minimise the concentration of DMSO, cells were spun down in a falcon tube at 600 x *g* and room temperature for 10 minutes and the pellet resuspended in fresh culture medium before seeding. Stably transfected cell lines were kept for 24 hours before the selection antibiotic was added to the culture medium.

2.3.6. Generation of stable expression cell lines

Plasmid DNA was incorporated into mouse embryonic fibroblasts by transfection using polyethylenimine (PEI). In a first step, primary cells were immortalised by transfection with the SV40 Large T antigen. The plasmid encoding SV40 Large T and all other expression plasmids used within this work contained a sequence that conveys G418 resistance (2.1.9). Therefore,

transfections following immortalisation were conducted with the addition of empty vectors bearing suitable resistance genes in a 10:1 ratio to allow subsequent selection. Per 10 cm culture dish, 7 µg DNA and a 2.5-fold excess of PEI were incubated in 0.6 ml DMEM for 20 minutes at room temperature and added to the cells. After three hours, the medium was replaced by fresh culture medium and the fibroblasts kept for 24 hours. To induce stable integration of the plasmid DNA into the cell genome, a selection antibiotic was added permanently to the transfected cells after this incubation period (400 µg/ml hygromycin B gold or 250 µg/ml zeocin™). Colonies of successfully recombined cells were separated onto 24 well plates and stable expression of the protein of interest was validated by immunoblot analysis (see 2.4.5).

2.3.7. Visualisation of acidic compartments by LysoTracker® Red

Organelles with a low luminal pH were stained with LysoTracker® Red DND-99. The acidotrophic dye is membrane permeant at neutral pH and specifically accumulates in acidic organelles. To evaluate luminal acidification, cells were incubated in the presence of 333 nM LysoTracker® Red in DMEM for 20 minutes, rinsed three times in PBS and directly analysed by live cell fluorescence imaging using an Olympus FV1000 confocal laser scanning microscope. Alternatively, samples were rinsed five times in PBS and fixed in 4 % (w/v) paraformaldehyde (PFA) in PBS for 20 minutes at room temperature. Following three washing steps in PBS, the cover slips were embedded in mounting medium containing 5 µg/ml DAPI (4-,6-diamidino-2-phenylindole) before image acquisition.

2.3.8. Ratiometric determination of late endosomal/lysosomal pH

pH calibration solution	20 mM	Acetate/ Mes/ HEPES (pH 4.0 – 5.5/ 5.5 – 6.5/ 7.0)
	145 mM	KCl
	10 mM	D-Glucose
	1 mM	$MgCl_2$

A quantitative determination of the luminal vesicle pH was achieved with the aid of the pH-sensitive dye Oregon Green® 514 that was coupled to dextran (70,000 MW). High molecular weight dextran conjugates can be internalised by cells using macropinocytosis. Thus, the compound can be applied to track organelles of the endocytic pathway. In this respect, cells

were seeded onto imaging dishes (145 µm glass bottom, PAA) and incubated in the presence of 0.5 mg/ml dextran-Oregon Green® 514 in DMEM with stable L-glutamine containing 1 mg/ml BSA overnight. To ensure labelling of late compartments only, excessive dextran-Oregon Green® 514 was washed away with PBS and samples kept in DMEM containing stable L-glutamine in the absence of further dextran for additional two hours. For ratiometric pH determination, Oregon Green® 514 was excited alternately at 440 and 488 nm in live cell analyses. Emission of the pH-sensitive fluorophore was captured at 535 ± 20 nm using an Olympus FV1000 confocal laser scanning microscope equipped with a U Plan S Apo 100x oil immersion objective (NA = 1.40) and the Olympus FluoView™ Software. An *in situ* calibration was performed at the end of each experiment by sequentially incubating the cells with K^+-rich pH calibration solutions ranging from pH 4.0 to 7.0 and containing 10 µg/ml of the ionophore nigericin. For each genotype, the obtained fluorescence intensity ratios (488/440) were used to generate a calibration curve according to the Boltzmann equation. Late endosomal/ lysosomal pH was then interpolated from the experimental data. As a control for assay functionality, the lysosomal pH gradient was collapsed in selected samples by addition of 100 – 200 nM bafilomycin A1 or 10 µg/ml nigericin 15 minutes prior to live cell imaging.

2.3.9. Dextran endocytosis assay

Dextran derivatives were used to visualise the lysosomal delivery of endocytic cargo molecules. For end-point determination, semi-confluent cultures of cells grown on cover slips were supplied with 0.5 mg/ml dextran-Texas Red® (70,000 MW) in DMEM containing 1 mg/ml BSA and incubated for 30 minutes. Samples were washed thrice in PBS and cultivated in the absence of further dextran for additional three hours before they were processed for immunofluorescence staining (see 2.3.12).

In a kinetic approach, cells were pre-loaded with 0.25 mg/ml dextran-FITC (10,000 MW) in DMEM containing 1 mg/ml BSA overnight and the compound cleared of early compartments during a three hours chase period as described above. Dextran-Texas Red® (0.5 mg/ml) was then added for distinct time periods between 10 and 60 minutes, samples were rinsed three times and subsequently fixed in 4 % (w/v) PFA in PBS for 20 minutes at room temperature. Samples were analysed by confocal laser scanning microscopy on an Olympus FV1000 following the embedding in mounting medium containing 5 µg/ml DAPI.

2.3.10. Latex bead phagocytosis assay

Latex beads were applied to track phagosome maturation and indirectly, phagosome-lysosome fusion. To allow Fcγ receptor (FcγR)-mediated phagocytosis by primary mouse macrophages or hFcγRII-expressing MEFs, latex beads of 1.1 µm diameter have been opsonised with murine or human IgG molecules, respectively. Therefore, 30 µl bead suspension were supplemented with 15 µl of 2 mg/ml IgG and 405 µl sterile PBS and incubated with rotation overnight at 4 °C. Opsonised latex beads were spun down at 16,000 x *g* and 4 °C for 1 minute and washed three times in PBS. The final latex bead stock solution was made in 1 ml PBS and used within one day. In parallel, cells were grown to semi-confluence on cover slips. At the point of latex bead administration (MOI = 8), the medium was replaced by serum-free DMEM. A synchronised latex bead phagocytosis was achieved by brief centrifugation at 300 x *g* and room temperature for 1 minute, before cells were incubated for 15 minutes at 37 °C. Then, excessive latex beads were washed away with PBS and phagosome maturation was allowed at 37 °C for time periods up to three hours as indicated. At the end of this chase period, extracellular latex beads were labelled with anti-IgG antibodies coupled to AlexaFluor® 594 for 1 minute and the samples processed for immunofluorescence staining as described in 2.3.12. Whenever phagosome maturation should be assessed under conditions of increased vesicle pH, 200 nM bafilomycin A1 or 10 µg/ml nigericin were applied during the 15 minutes latex bead uptake period and the treatment continued until sample fixation.

2.3.11. Visualisation of lysosomal protease activity

A qualitative determination of lysosomal protease activity was conducted using DQ™ Red-BSA. The self-quenched fluorochrome is internalised by cells via endocytosis and becomes fluorescent following its degradation along the endocytic route. MEFs were labelled overnight with 100 µg/ml DQ™ Red-BSA in DMEM containing 1 mg/ml BSA. Primary macrophages and hepatocytes received a 30 minutes treatment with a DQ™ Red-BSA concentration of 0.5 mg/ml. In any case, cells were rinsed thrice in PBS and incubated for further three hours in DMEM containing 1 mg/ml BSA. At the end of the experiment, all samples were processed for immunofluorescence labelling (see 2.3.12).

2.3.12. Indirect immunofluorescence labelling of cells

Quenching solution	1x	PBS pH 7.4
	0.2 % (w/v)	Saponin
	0.12 % (w/v)	Glycine
Blocking solution	1x	PBS pH 7.4
	0.2 % (w/v)	Saponin
	10 % (v/v)	FBS

Intracellular compartments were detected by antibodies targeting organelle-specific marker proteins. Therefore, semi-confluent cells grown on cover slips were fixed in 4 % (w/v) PFA in PBS for 20 minutes at room temperature and rinsed thrice in PBS. For permeabilisation, 0.2 % (w/v) saponin in PBS were added to the cells for 5 minutes at room temperature. The fixative was then quenched with quenching solution for 10 minutes and samples rinsed once in 0.2 % (w/v) saponin in PBS. To interfere with unspecific antibody binding, a saturation step was conducted for at least one hour using blocking solution. Thereafter, samples were incubated with primary antibodies (table 2.3) diluted in blocking solution overnight at 4 °C. The cover slips were washed five times in 0.2 % (v/v) saponin in PBS and transferred to blocking solution containing diluted AlexaFluor® dye-conjugated secondary antibodies (1:300, see table 2.4) for one hour at room temperature. Following a final wash, five times in 0.2 % (v/v) saponin and two times in water, the cover slips were mounted on microscope slides using mounting medium supplemented with 5 µg/ml DAPI. Images were acquired on an FV1000 confocal laser scanning microscope using a U Plan S Apo 100x oil immersion objective (NA = 1.40) and the Olympus FluoView™ Software.

2.3.13. Labelling of surface molecules for flow cytometry

FACS sample buffer	1x	PBS pH 7.4
	2.0 % (v/v)	FBS
	0.2 mM	EDTA
	0.1 %	NaN_3

Splenic mouse macrophages were characterised by flow cytometry. Therefore, the spleen was prepared from euthanised animals (2.6.7), dissected and passed through a 100 µm nylon cell strainer in 10 ml FACS sample buffer. A 1:20 dilution of splenic cells stained with trypan blue

was counted using a Neubauer improved counting chamber (C-Chip, Biochrom). Samples including 6 x 10^5 viable cells were collected in 96 well round bottom tissue culture plates by centrifugation at 210 x *g* and 4 °C for 5 minutes and washed twice in FACS sample buffer. Surface molecules were labelled by 45 minutes incubation at 4 °C using specific antibodies coupled to allophycocyanin (see table 2.3) that were diluted 1:200 in FACS sample buffer, respectively. Intracellular EYFP fluorescence was visible without the conduction of a permeabilisation and additional antibody staining. Samples were rinsed once, followed by a brief incubation with 500 ng/ml propidium iodide in FACS sample buffer and a final washing step. For measurement, the cells were suspended in 200 µl FACS sample buffer per well and analysed on a FACSCanto™ II using the FACSDiva™ software. For each sample, an unstained specimen and a specimen stained with an antibody isotype control were included in the analysis. Furthermore, a compensation of spectral overlap was calculated for the utilised dyes before every experiment.

2.3.14. Labelling of endocytic compartments with BSA-gold

To trace the endocytic route at an ultra-structural level, BSA-gold was utilised in endocytosis assays followed by electron microscopic analysis. In this respect, primary hepatocytes grown on cover slips were cultivated in the presence of BSA coupled to colloidal gold (10 nm diameter, OD_{600} = 5) in DMEM containing 1 mg/ml BSA for one hour. The cells were rinsed and supplied with fresh culture medium for further two hours, in which the internalised BSA-gold was subjected to vesicular transport. Thereafter, cover slips were transferred to 2 % (v/v) glutaraldehyde in 0.2 M HEPES pH 7.4 for two hours at room temperature. Samples were stored in 0.2. M HEPES pH 7.4 without fixative at 4 °C until further processing (see 2.3.15).

2.3.15. Analysis of cell morphology by electron microscopy

Endocytic compartments of hepatocytes prelabelled with BSA-gold (10 nm) were analysed by electron microscopy. Fixed samples (2.3.14) were processed and examined by *Prof. Dr. Eeva-Liisa Eskelinen (University Helsinki)*. Following post-fixation in 1 % (w/v) OsO_4, flat embedding was performed in TAAB resin. Ultra-thin sections were cut on an EM UC6 ultramicrotome (Leica Microsystems) and collected on Formvar-coated copper grids. A staining with 2 % (w/v) uranyl acetate and 0.3 % (w/v) lead citrate was performed as described before (Yla-Anttila *et al.*, 2009) and sections analysed on a 1400EX transmission electron microscope (Jeol).

For ultra-structural analysis of fibroblast morphology, MEFs were grown to confluence on 3.5 cm culture dished. The culture medium was removed by washing thrice in PBS and subsequently replaced with 3 % (v/v) glutaraldehyde in 0.1 M phosphate buffer. Further processing was performed by *Dagmar Niemeier* and *Prof. Dr. Renate Lüllmann-Rauch (University Kiel)*. Samples were post-fixed in 2 % (w/v) OsO_4 and subjected to flat embedding. Ultra-thin sections were cut as described above. Images of sections stained according to standard protocols were acquired on an EM900 transmission electron microscope (Zeiss).

2.3.16. Modulation of mTORC1 activity

The activation state of the mTOR complex 1 was modulated in fibroblasts by regulating nutrient availability. To silence mTORC1 signalling, MEFs were grown to 80 % confluence, rinsed once in PBS and cultivated for one hour in EBSS, thereby mimicking the absence of nutrients and growth factors. For subsequent reactivation of the complex, cells were washed with PBS and transferred to DMEM without additives for 30, 60 or 120 minutes. The amino acid content of DMEM should be sufficient to trigger mTORC1 activity in response to this stimulus. Application of 250 nM torin 1 (Cayman Chemicals) during the reactivation procedure was used to inhibit mTOR kinase activity even in the presense of nutrients. Samples were lysed as described in 2.4.1 and used to subsequently assess the influence of nutrient availability on mTORC1 signalling by immunoblot analysis (see 2.4.4, 2.4.5).

2.4. Protein biochemical methods

2.4.1. Generation of cell lysates for protein extraction

Lysis buffer	1x	PBS pH 7.4
	1 % (v/v)	Triton X-100
	1x	cOmplete Protease Inhibitor Cocktail (Roche)
Lysis buffer with phosphokinase/ phosphatase inhibitors	20 mM	NaF
	4 mM	Na_3VO_4
	120 nM	β-Glycerophosphate
	in	lysis buffer

For the generation of cell lysates, cells grown on culture dishes were washed with PBS, supplied with 0.5 ml 1x PBS containing 1x cOmplete Protease Inhibitor Cocktail (Roche) and harvested using a cell scraper. Resulting suspensions were centrifuged for 10 minutes at 900 x *g* and 4 °C. The sedimented cells were lysed on ice for 30 minutes in an appropriate volume of lysis buffer or lysis buffer including phosphokinase/ phosphatase inhibitors, whenever phosphate modifications were assessed. In addition, samples were sonicated for 30 seconds at 4 °C using a Branson Sonifier 450 (level 7 in a cup horn, Emerson Industrial Automation) before cell debris was separated by centrifugation at 16,000 x *g* and 4 °C for 10 minutes. The supernatants containing the extracted proteins were transferred to new reaction tubes and protein concentrations determined (see 2.4.3).

2.4.2. Preparation of tissue homogenates

RIPA lysis buffer

50 mM	HEPES/ NaOH pH 7.4
150 mM	NaCl
1 mM	EDTA
0.5 mM	Sodium deoxycholate
1 % (v/v)	Nonidet™ P-40

Protein extraction from mouse tissue was achieved by homogenisation in RIPA lysis buffer. Small pieces of tissue were supplemented with an appropriate volume of RIPA lysis buffer and ceramic beads of 1.4 mm diameter (Peqlab) (refer to table 2.8). Then, the tissues were disrupted using a Precellys® homogenizer (Peqlab) at 6,000 rpm for two times 30 seconds interrupted by a 30 seconds break.

Table 2.8: Number of ceramic beads used for tissue homogenisation

Tissue	Added ceramic beads
Heart, liver	4
Spleen	3
Brain, lung, thymus	2
Lymph nodes	0

Homogenates were incubated for 10 minutes on ice before debris was removed by centrifugation at 16,000 x *g* and 4 °C for 10 minutes. The protein content of the supernatants was determined as described in 2.4.3 and samples subjected to SDS-PAGE and immunoblot analysis (see 2.4.4, 2.4.5).

2.4.3. Determination of protein concentration

Protein concentrations were measured using the Pierce™ BCA Protein Assay Kit according to the manufacturer´s instructions. This assay is based on the biuret reaction and subsequent chelation of Cu^{1+} by bicinchoninic acid (BCA) to a complex with strong linear absorption at 562 nm. Diluted samples were incubated with the assay mixture at 37 °C for 20 minutes and measured photometrically with a Synergy HT (BioTek) microplate reader. Sample absorption values were related to a calibration curve based on albumin standard concentrations ranging from 0 to 2.0 mg/ml to determine their protein content.

2.4.4. SDS polyacrylamide gel electrophoresis (SDS-PAGE)

Sample buffer (5x)	625 mM	Tris/ HCl pH 6.8
	50 % (v/v)	Glycerol
	5 % (w/v)	SDS
	100 mM	DTT
	traces of	Bromophenol blue
Separating gel buffer	1.5 M	Tris/ HCl pH 8.8
	0.4 % (w/v)	SDS
Stacking gel buffer	0.5 M	Tris/ HCl pH 6.8
	0.4 % (w/v)	SDS
10x SDS gel electrophoresis running buffer	0.25 M	Tris
	2 M	Glycine
	1 % (w/v)	SDS

Analytic separation of protein preparations was achieved using a discontinuous sodium dodecyl sulfate polyacrylamide gel electrophoresis (SDS-PAGE) according to Laemmli (Laemmli, 1970). The samples were supplemented with 5x sample buffer and heated to 95 °C for 5 minutes. The anionic SDS attaches to the heat-denatured proteins, which yields a negative complex netto charge according to the protein surface. Thereby, sample migration in the electric field becomes size-dependent. The analysed proteins were segregated using 8 – 15 % separating gels combined with a 4.5 stacking gel (see table 2.9). Gel electrophoresis was performed using

a Tris/ glycine buffer system with constant voltages of 80 V (stacking gel) to 120 V (separation gel). A protein ladder was included in the sample setup to allow a comparison of the migration behaviour to known molecular weight standards.

Table 2.9: Composition of SDS polyacrylamide gels

		8 % Separating gel	12.5 % Separating gel	15 % Separating gel	4.5 % Stacking gel
Separating/ stacking gel buffer	[ml]		2.6		1.35
30 % (w/v) Acrylamide/ bisacrylamide Rotiphorese® Gel 30 (37,5:1)	[ml]	2.7	4.2	5	1.75
Water	[ml]	4.6	3.1	2.3	3.1
10 % (w/v) Ammoniumpersulfate	[µl]		60		
TEMED	[µl]		30		

2.4.5. Western blotting and immunodetection

10x Transfer buffer	250 mM	Tris
	2 M	Glycine
	add 20 % (v/v)	MeOH to 1x diluted
10x Tris-buffered saline (TBS)	200 mM	Tris/ HCl pH 7.0
	1.5 M	NaCl
TBS-T	1x	TBS
	0.1 % (v/v)	Tween® 20
Detection solution A	0.1 M	Tris/ HCl pH 8.6
	0.025 % (w/v)	Luminol
Detection solution B	0.11 % (w/v)	p-Coumaric acid
	in	DMSO

For the specific, immunological detection of proteins, preparations separated on an SDS polyacrylamide gel (chapter 2.4.4) were transferred to a nitrocellulose membrane using the semi-dry Western blot method. Therefore, two sheets of Whatman® blotting paper, a nitrocellulose membrane, the SDS polyacrylamide gel and additional two sheets of Whatman® blotting paper – all equilibrated in transfer buffer – were mounted on a transfer chamber, beginning at the anode and sealed with the cathode. The transfer was performed at a constant current of 1.5 mA per cm^2 of nitrocellulose membrane for 90 – 120 minutes.

For detection using horseradish peroxidase-coupled secondary antibodies, unspecific interaction sites on the blotting membranes were saturated with 5 % (w/v) dry milk in TBS-T for one hour at room temperature. Primary antibodies (table 2.3) were then diluted in 5 % (w/v) dry milk in TBS-T or 5 % BSA (w/v) in TBS-T according to the manufacturer´s instruction and incubated with the blotting membranes overnight at 4 °C in gentle agitation. Thereafter, the membranes were washed thrice in TBS-T for 5 minutes and incubated for one hour at room temperature with the appropriate secondary antibody (see table 2.4), diluted 1:15,000 in 5 % (w/v) dry milk in TBS-T. Following further washing for three times 15 minutes in TBS-T, horseradish peroxidase activity was determined using an ImageQuant™ LAS 4000 (GE Healthcare). Therefore, the membranes were covered with a mixture of the ECL Advance™ Western Blotting Detection Kit (50 µl of each) diluted in 1 ml detection solution A and 100 µl detection solution B and supplemented with 4 µl H_2O_2. Signal intensities were quantified using the ImageJ software.

Nitrocellulose membranes used for the detection of phosphorylated and total p70S6K and PRAS40 were analysed using an Odyssey® Fc Dual-Mode Imaging System (LI-COR®). Therefore, the membranes were dried for one hour between Whatman® blotting paper following the transfer procedure. Dried membranes were then equilibrated in TBS and subjected to a one hour blocking step in 1:2 diluted Odyssey® blocking buffer (LI-COR®) in TBS. Binding of primary antibodies was performed as described above. The membranes were rinsed three times in TBS-T and incubated for one hour at room temperature with IRDye® 800CW-coupled secondary antibodies (see table 2.4) diluted 1:10,000 in a 1:2 mixture of Odyssey® blocking buffer (LI-COR®) and TBS containing 0.1 % (v/v) Tween® 20. Subsequently, the membranes were washed thrice in TBS-T and once in TBS, each step 10 minutes. Detection and signal quantification was carried out with the Odyssey® Fc Dual-Mode Imaging System (LI-COR®).

2.4.6. Reprobing of Western blots

Stripping buffer	62.5 mM	Tris/ HCl pH 6.8
	2 % (w/v)	SDS
	0.83 % (v/v)	2-Mercaptoethanol

To allow the successive analyses utilising distinct primary antibodies on one Western blot membrane, existing antibodies signals have to be decreased before re-detection. In this

respect, membranes were incubated in stripping buffer for 30 minutes at 80 °C. After residual 2-mercaptoethanol was washed away with TBS-T, these membranes were ready for reprobing with new primary and secondary antibodies as described in section 2.4.5.

2.4.7. *In vitro* measurement of lysosomal hydrolase activity

Assay buffer	0.2 M	Trisodium citrate pH 4.6
	0.4 % (w/v)	BSA
	0.08 % (w/v)	NaN_3

The activities of lysosomal β-hexosaminidase and β-glucocerebrosidase were determined using whole cell lysates (2.4.1) and the artificial, chromogenic substrates 4-nitrophenyl-N-acetyl-β-D-glucosaminide and 4-nitrophenyl-β-D-glucopyranoside, respectively. The enzyme-mediated hydrolysis of the chromogenic substrates leads to the generation of 4-nitrophenol. Further deprotonation at an alkaline pH yields the 4-nitrophenolate anion, which displays strong absorption at 405 nm and allows photometric quantification.

The measurements were conducted in duplicates by incubation of 10 µl protein lysate in the presence of 10 mM substrate in 100 µl assay buffer at 37 °C. After 30 minutes to six hours, hydrolysis was stopped by addition of 500 µl 0.4 M glycine pH 10.4 and non-soluble aggregates were segregated by centrifugation at 16,000 x *g* and room temperature for 10 minutes. The supernatants were used for photometric determination of A_{405} in a Synergy HT (BioTek) microplate reader. Each measurement included a sample control consisting of lysate in assay buffer without substrate. An additional assay control was performed for each experiment and contained a mixture of substrate solution and assay buffer without the addition of lysate. The formulations 2.1 were used to calculate the specific enzyme activities. A set of 8 – 9 experiments was conducted for every analysed genotype to obtain mean specific enzyme activities.

$$Activity\left[\frac{mU}{ml}\right]=\frac{\left(A_{Sample}-A_{Sample\,Ctrl}\right)*10^{6}}{\varepsilon_{405}\left[\frac{l}{mol\,cm}\right]*d\left[cm\right]*t\left[min\right]}*\frac{V_{Total}}{V_{Sample}}$$

$$Specific\ Activity\left[\frac{mU}{mg}\right]=\frac{Activity\left[\frac{mU}{ml}\right]}{c_{Sample}\left[\frac{mg}{ml}\right]}$$

Formulations 2.1: Specific enzyme activity

A = absorption at 405 nm; ε_{405} = 18,500 M^{-1} cm^{-1}; d = cell thickness (1 cm)

2.4.8. Purification of tritosomes

For the analysis of lysosomes, these organelles were enriched with an artificially increased lipid proportion as so-called tritosomes and isolated by differential density centrifugation in a sucrose gradient according to Wattiaux and Leighton (Wattiaux *et al.*, 1963; Leighton *et al.*, 1968). For this purpose, mice were treated with tyloxapol (Triton WR-1339, see 2.6.6), which induces an increase in low density lipoprotein (LDL) plasma levels and elevated rates of LDL particle uptake within the liver (Hayashi *et al.*, 1982). The lysosomal delivery and subsequent dissection of LDL then leads to lipid accumulations in hepatic lysosomes. Pre-treated animals were sacrificed (2.6.7) and their livers prepared. For homogenisation, the dissected liver was subjected to five strokes in a dounce homogeniser in 5 ml 0.25 M sucrose and subsequently centrifuged at 1140 x *g* and 4 °C for 10 minutes. The resulting pellet was dissolved in 3.5 ml 0.25 M sucrose and subjected to another centrifugation step at 1140 x *g* and 4 °C for 10 minutes. The supernatants of both centrifugation steps were combined, the volume adjusted to 9 ml and contained organelles sedimented at 56.500 x *g* and 4 °C for 7 minutes. The pellet consisting of light mitochondria and lysosomes was washed in 8.5 ml 0.25 M sucrose and recovered by centrifugation. Thereafter, the sediment was resuspended in 1 ml ρ = 1.21 sucrose and overlaid by a discontinuous sucrose gradient of 2.5 ml ρ = 1.15 sucrose, 2.5 ml ρ = 1.14 sucrose and 2 ml ρ = 1.06 sucrose (Fig. 2.1). After separation at 110,000 x *g* at 4 °C for 150 minutes, the protein content of fraction 2 (Fig. 2.1) was determined (see chapter 2.4.3) and this fraction was used for analysis by immunoblotting (2.4.4, 2.4.5).

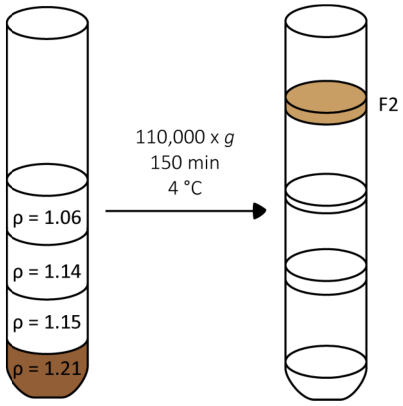

Figure 2.1: Separation of tritosomes by differential density centrifugation.

A discontinuous sucrose density gradient is built up on the suspension containing light mitochondria and lysosomes (ρ = 1.21). Following separation by centrifugation, tyloxapol-ladden lysosomes are enriched in fraction 2 (F2).

2.5. Histological methods

2.5.1. Preparation of semi-thin cryosections

For cryosectioning, small pieces of tissue were fixed in 4 % (w/v) PFA in 0.1 M phosphate buffer at room temperature for 20 minutes and subsequently at 4 °C overnight. Then, the fixative was replaced by 30 % sucrose in 0.1 M phosphate buffer and the tissue incubated for another 24 hours. Semi-thin sections (35 µm) were cut on a Leica SM 2000 R sliding microtome (Leica Microsystems) with dry-ice cooling and stored in 0.1 M phosphate buffer containing 0.02 % (w/v) sodium azide.

2.5.2. Hematoxylin and eosin staining of semi-thin cryosections

Hematoxylin and eosin (H&E) staining was performed with free floating semi-thin cryosections (2.5.1) according to standard protocols. The sections were collected on mounting slides, rinsed with water and stained with Mayer´s hemalaun solution for 7 minutes. Thereafter the mounting slides were purged using tap water for 10 to 15 minutes. A counterstaining was performed in 0.1 % (w/v) eosine/ 0.5 % (v/v) glacial acetic acid for 5 minutes and sections were rinsed twice with water. An ascending alcohol series to 100 % was followed by clearing of the sections in Roti®-Histol for 10 minutes and final mounting on cover glass using Eukitt® mounting medium.

2.5.3. Immunofluorescence staining of semi-thin cryosections

Blocking buffer	0.1 M	Phosphate buffer pH 7.4
	4 % (v/v)	Normalised goat serum
	0.5 % (v/v)	Triton-X-100
Wash buffer	0.1 M	Phosphate buffer pH 7.4
	0.25 % (v/v)	Triton-X-100

Specific protein labelling on semi-thin cryosections was performed by indirect immunofluorescence staining. Sections as prepared in 2.5.1 were rinsed thrice in 0.1 M phosphate buffer to remove residual sodium azide. Unspecific binding sites were saturated by incubation in blocking buffer for two hours at room temperature and gentle agitation. Thereafter, the sections were washed three times in 0.1 M phosphate buffer and incubated

with appropriate dilutions of the respective primary antibody (see table 2.3) in blocking buffer overnight at 4 °C. The labelling was followed by three times washing in wash buffer and incubation with 1:300 diluted AlexaFluor®-coupled secondary antibodies (table 2.4) for two hours at room temperature and gentle shaking. Subsequently, sections were rinsed once in wash buffer and nuclei stained in the presence of 5 µg/ml DAPI in wash buffer. After a final washing step, embedding was performed using mounting medium.

2.5.4. Electron microscopy of ultra-thin plastic sections

Electron microscopy was used to evaluate the morphology of selected tissues at an ultra-structural level. In this respect, mice were anaesthetised with Ketamine/ Rompun® (refer to section 2.6.7) and perfused transcardially with 6 % (v/v) glutaraldehyde in 0.1 M phosphate buffer. Tissue samples were post-fixed in 2 % (w/v) OsO_4 before their dehydration and subsequent embedding in Araldite® M/ dodecenylsuccinic anhydride. An EM UC6 ultramicrotome (Leica Microsystems) was utilised to cut ultra-thin section that were collected on Formvar-coated copper grids and stained with uranyl acetate and lead citrate according to standard protocols. Electron micrographs were acquired with an EM900 transmission electron microscope (Zeiss).

2.6. Animal experimentation

2.6.1. Animal housing

All animals were housed in individually ventilated cages (IVC) to generate a specific pathogen free environment. The room temperature was maintained at 19 – 22 °C with a humidity of 45 – 60 % and light conditions of 12 hours lighting followed by 12 hours darkness were applied in turns. Access to water and standard laboratory animal food (pellets by Ssniff Spezialdiäten) was granted *ad libitum*. Animal handling and care were performed in agreement with the German animal welfare law according to the guidelines of the Christian Albrechts University of Kiel. Experiments involving animals were approved by the Ministry of Energy, Agriculture, the Environment and Rural Areas Schleswig-Holstein under the reference number V312-72241.121-3.

2.6.2. Breeding strategies

Breeding of mice was achieved by appointing animals of at least nine weeks of age in one-to-one matings. To obtain offspring bearing the desired genotype, the breeding strategies depicted within figures 2.2 and 2.3 were applied. The progeny was weaned three weeks after birth and subjected to tail biopsy to allow subsequent genotyping (see chapters 2.6.3, 2.6.4).

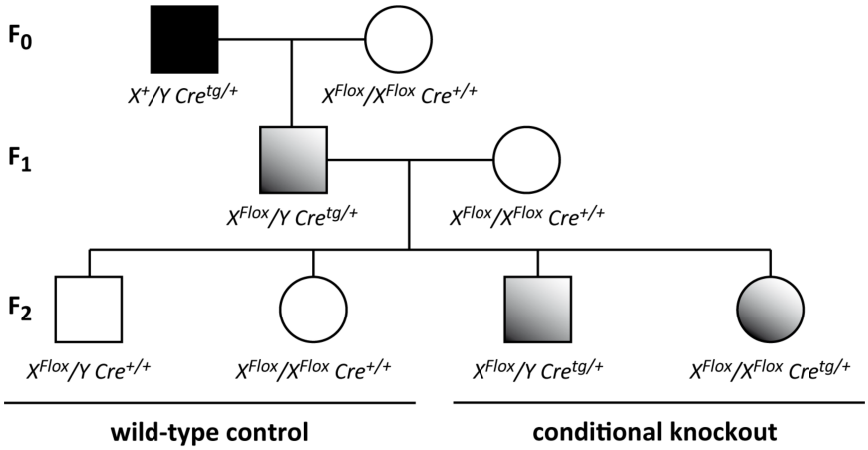

Figure 2.2: Breeding schematic to obtain Atp6ap2^{flox} *control and conditional knockout animals.*

Representative mating pattern used for breeding of *Atp6ap2 Mx1-Cre* and *Atp6ap2 LysM-Cre* conditional knockout mice. All genotypes appearing in F_2 were used in experimental setups as either wild-type control or conditional knockout animals as indicated.

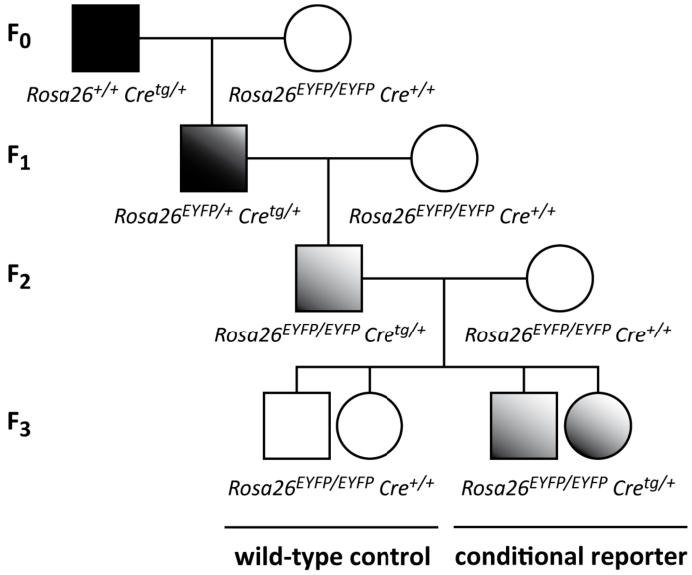

Figure 2.3: Breeding schematic for the generation of Rosa26-EYFP *conditional reporter animals.*

Mating pattern used to obtain *Rosa26-EYFP Mx1-Cre* double transgenic mice and *Cre* allele negative control animals as emerging in F_3.

2.6.3. Tail biopsy and isolation of genomic DNA

To gain access to genomic mouse DNA suitable for genotype determination, a tail biopsy was collected from three to four weeks old animals. The tissue was digested in DirectPCR® Lysis Reagent Tail (Peqlab) containing 0.3 mg/ml proteinase K at 55 °C and vigorous shaking overnight. Thereafter, proteinase K was inactivated by incubation at 85 °C for 45 minutes and debris sedimented at 16,000 x *g* and room temperature for two minutes. The lysate was directly employed for genotyping (2.6.4) without intermediate DNA precipitation. Genomic DNA of mouse embryos or mouse embryonic fibroblasts was isolated similarly but with a reduced incubation time of approximately six hours for proteinase K digest.

2.6.4. Genotyping by Polymerase chain reaction (PCR)

The genotype of the experimental animals and derived cell lines was analysed by polymerase chain reaction (PCR). This *in vitro* assay allows the exponential amplification of specific DNA template sequences by application of distinct oligonucleotides (primers, see table 2.5) and a heat-stable DNA polymerase. The following PCRs (tables 2.10, 2.11) were used to assess the mouse alleles with respect to the deletion mutation in *Tcirg1*, insertion of *loxP* sites into exon 2 of *Atp6ap2*, the presence of *Sry*, the gene coding for the Cre recombinase (locus-independent) or the insertion of the *EYFP-Stop* construct into the locus *Rosa26*.

Table 2.10: Pipetting scheme for PCR-based genotype determination

Tcirg1/Atp6ap2/ Sry*	*[µl]*	*Cre recombinase*	*[µl]*	*Rosa26*	*[µl]*
Primer forward	1	Primer forward	1	Primer forward wt	1
Primer reverse	1	Primer reverse	1	Primer forward insert	1
				Primer reverse	1
dNTP Mix (2 mM each)	5	dNTP Mix (10 mM each)	0.4	dNTP Mix (10 mM each)	0.4
10x DreamTaq™ buffer	5	10x DreamTaq™ buffer	2	10x DreamTaq™ buffer	2
DMSO	2.5	DMSO	1	DMSO	0
Template DNA	3	Template DNA	1	Template DNA	1
DreamTaq™ Pol. (5 U/µl)	0.5	DreamTaq™ Pol. (5 U/µl)	0.3	DreamTaq™ Pol. (5 U/µl)	0.3
H_2O *ad* 50 µl	32	H_2O *ad* 20 µl	13.3	H_2O *ad* 20 µl	13.3

**Tcirg1* PCR was performed in separate assays with either primers *Tcirg1*^{oc} forward 1 and reverse or *Tcirg1*^{oc} forward 2 and reverse

Table 2.11: PCR conditions applied for genotyping

Tcirg1			
Step	*ϑ [°C]*	*t [s]*	
Initiation	95	180	
Cycle	95	30	39x
	57	30	
	72	60	
Elongation	72	300	
Hold	10	∞	

Atp6ap2			
Step	*ϑ [°C]*	*t [s]*	
Initiation	95	120	
Cycle	95	10	5x
	74	180	
Cycle	95	10	5x
	72	180	
Cycle	95	10	5x
	70	180	
Cycle	95	10	15x
	68	180	
Elongation	68	420	
Hold	10	∞	

Cre recombinase/ Rosa26/ Sry			
Step	*ϑ [°C]*	*t [s]*	
Initiation	95	180	
Cycle	95	45	30x
	51	60	
	72	60	
Elongation	72	480	
Hold	10	∞	

The amplification products were separated and analysed using agarose gel electrophoresis (see Fig. 2.4 and section 2.2.8).

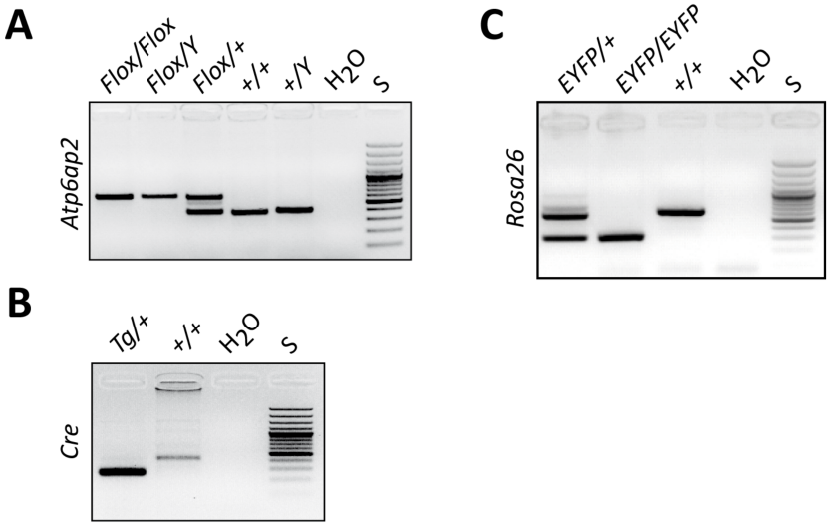

Figure 2.4: Agarose gel electrophoretic analysis of mouse genotypes assessed by PCR.

(A) Different amplification products of wild-type and floxed exon 2 of *Atp6ap2*. (B) Positive detection of Cre transgene insertion. (C) Differentiation between wild-type and *EYFP-Stop*-modified *Rosa26*. S, DNA standard ladder

2.6.5. Activation of the *Mx1* promotor by poly (I:C) administration

The *Mx1* promotor was activated in *Mx1-Cre* conditional and control animals by application of polyinosinic:polycytidylic acid (poly (I:C)). Therefore, poly (I:C) potassium salt was dissolved in 0.9 % (w/v) NaCl solution to a stock concentration of 5 mg/ml and passed through a 0.2 µm sterile filter. To obtain a dosage of 250 µg per application, working dilutions of 500 µg/ml were prepared in sterile 0.9 % (w/v) NaCl and 500 µl aliquots taken for intra-peritoneal injection using 27 ½ G needles. Control and conditional knockout animals received three injections within five days beginning at the age of seven weeks. Mice were sacrificed five to ten days after the last application of poly (I:C) (2.6.7).

2.6.6. Enrichment of peritoneal macrophages and treatment for tritosome isolation

In addition to *Mx1* promotor activation by poly (I:C) (section 2.6.5), the experimental animals were subjected to two other forms of treatment to either increase the number of peritoneal macrophages or allow the purification of liver tritosomes.

To elucidate macrophage infiltration into the peritoneal cavity, animals were treated with sterile thioglycollate broth. In this respect 4 % (w/v) thioglycollate broth was dissolved in water and autoclaved for sterilisation. The mice received one intra-peritoneal injection of 0.5 to 1 ml thioglycollate broth three days prior to euthanasia (see 2.6.7) and cell harvest.

For isolation of tritosomes from mouse liver, animals were treated with 17 % (v/v) triton WR-1339 (tyloxapol) in 0.9 % (w/v) NaCl three days prior to euthanasia and subsequent tritosome purification (chapter 2.4.8). Four µl tyloxapol solution were injected intra-peritoneally per g body weight.

2.6.7. Euthanasia of mice

Experimental animals were sacrificed for organ harvesting by cervical dislocation. If necessary, mice were anaesthetised by intra-peritoneal injection of 10 mg/ml Ketamine and 6 mg/ml Rompun® in 0.9 % (w/v) NaCl solution. Therefore, animals received a dosage of 10 µl narcotic agent per g body weight.

3. RESULTS

3.1. Deficiency of V-ATPase V_0 subunit a3 in mouse embryonic fibroblasts

The presence of the V-ATPase V_0 subunit a has been reported to be a prerequisite for vesicle fusion at different stages of the endocytic and exocytic pathways (Hiesinger *et al.*, 2005; Liegeois *et al.*, 2006; Sun-Wada *et al.*, 2006; Peri and Nusslein-Volhard, 2008; Di Giovanni *et al.*, 2010). This function seems conserved over a variety of species, ranging from yeast to mammals. Yet, there is no data available on the necessity of the V-ATPase a subunits for vesicle fusion in mice. There are four murine a subunit isoforms, of which isoform 3 is most prominently localised to lysosomes and directly recruited to nascent phagosomes during phagosome maturation (Toyomura *et al.*, 2003; Sun-Wada *et al.*, 2009). Thus, to elucidate the contribution of the murine V-ATPases to the merger of vesicles, a knockout mouse model for V-ATPase V_0 subunit a3 was analysed.

3.1.1. Generation of a3-deficient mouse embryonic fibroblasts

To achieve a knockout of V-ATPase V_0 subunit a3, we took advantage of a natural occurring osteosclerotic mutation (*oc*) in the gene for this subunit, the murine locus *Tcirg1*. This mutation consists of a 1.6 kB deletion, which eliminates exon 2 of *Tcirg1* and its translation initiation site encoded therein (Scimeca *et al.*, 2000). Mice homozygous for the *Tcirg1*^{oc} allele suffer from severe osteopetrosis and usually die within three weeks of age. For this reason, rather than using primary cells from adult mice, mouse embryonic fibroblast (MEF) lines were generated prior to this work in the group of *Prof. Dr. Uwe Kornak (Institute for Medical Genetics and Human Genetics, Charité – Universitätsmedizin Berlin)* at day E13.5 from breeding pairs yielding wild-type as well as *Tcirg1*$^{oc/oc}$ and heterozygous offspring. To identify MEFs carrying the *Tcirg1*^{oc} mutation, genomic DNA was prepared from each MEF line and subjected to PCR to distinguish between the mutant and wild-type alleles (Fig. 3.1). Amplification with a primer pair surrounding the mutation site (fwd-1 and rev) produced a large PCR amplicon from MEF line #9 and a 1.6 kB smaller amplification product from MEF line #7. This indicated that MEF line #9 possessed two wild-type *Tcirg1* alleles, while MEF line #7 was homozygous for the *Tcirg1*^{oc} allele. In agreement with these findings, a PCR using a forward primer binding within exon2 (fwd-2), resulted in the absence of a PCR product in samples of MEF line #7, only. According to

the PCR-based genotyping results, MEF line #9 will be referred to as wild-type and MEF line #7 as *a3*$^{-/-}$ or a3 knockout MEFs.

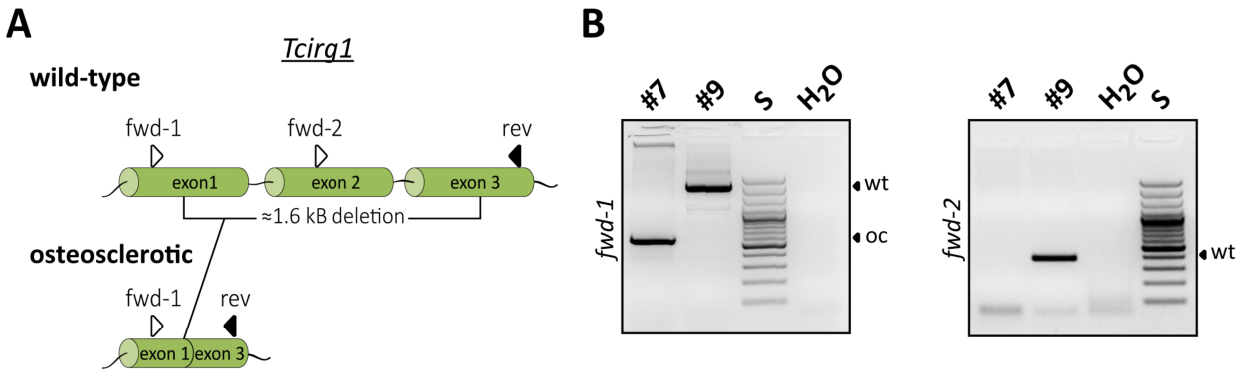

Figure 3.1: PCR-based distinction between wild-type and mutant Tcirg1*.*

(A) Schematic illustration of wild-type and mutated, osteosclerotic *Tcirg1* alleles. A 1.6 kB deletion disrupts the translation initiation site located on exon 2. Arrowheads highlight the annealing sites for primers forward 1 (fwd-1), forward 2 (fwd-2) and reverse (rev) as utilised for genotyping. (B) Agarose gel electrophoresis separating the PCR products obtained from genomic DNA of MEF lines #7 and #9 upon application of primers forward 1 and reverse (fwd-1, left panel) or forward 2 and reverse (fwd-2, right panel). The signals expected for wild-type (wt) and osteoclerotic (oc) *Tcirg1* are indicated. A water-based amplification (H_2O) served as negative control and the length of the amplification products was estimated with the aid of a standard ladder (S).

3.1.2. The V-ATPase V_0 subunit a1 is up-regulated in *a3*$^{-/-}$ MEFs

The impact of the genetic alteration on gene transcription in *a3*$^{-/-}$ MEFs was then analysed by qPCR (Fig. 3.2A). Consistent with the genotyping data, mRNA for V-ATPase subunit a3 was not detectable in *a3*$^{-/-}$ MEFs, if the amplified region resided within the excised exon 2. However, a sequence of the *Tcirg1* mRNA that was not targeted by the deletion could be amplified to a similar extent from MEFs of both genotypes, implying that a truncated *Tcirg1* was still transcribed in the *a3*$^{-/-}$ line. Despite the comparable amount of mRNA coding for V_0 subunit a3, the level of V_0 subunit a1 mRNA was significantly elevated in *a3*-deficient cells when compared to wild-type MEFs. This might reflect a possible compensatory role of the a isoform 1. A similar, but weaker tendency was found for the subunit a2 mRNA. In contrast, the levels of mRNA coding for V_0 subunit a4 were comparable in wild-type and *a3*$^{-/-}$ MEFs, but showed an at least 100-fold lower overall mRNA abundance than the other three isoforms. The low rate of V_0 subunit a4 mRNA was in agreement with the described kidney-specific expression pattern of this particular subunit (Smith *et al.*, 2000; Oka *et al.*, 2001).

To gain insight into the actual protein amount of the highly expressed isoforms a1 to a3, immunoblotting was performed using isoform specific antibodies (Fig. 3.2B). Corresponding to V_0 subunit a3, a prominent signal of 116 kDa could be seen with the anti-a3 antibody in wild-type MEF lysates. Although a3 mRNA expression was detectable in *a3*$^{-/-}$ MEFs, the protein signal for subunit a3 was absent in lysates from these cells, thereby verifying the loss of the translation start sequence within exon 2. Comparable to the results from the qPCR, lysates from *a3*$^{-/-}$ MEFs contained almost four times more V_0 subunit a1 than wild-type lysates, while no change was observed for subunit a2. Further probing for V-ATPase V_0 subunits d1 and c and V_1 subunit B2 revealed comparable protein levels for all analysed subunits in wild-type and *a3*$^{-/-}$ MEFs.

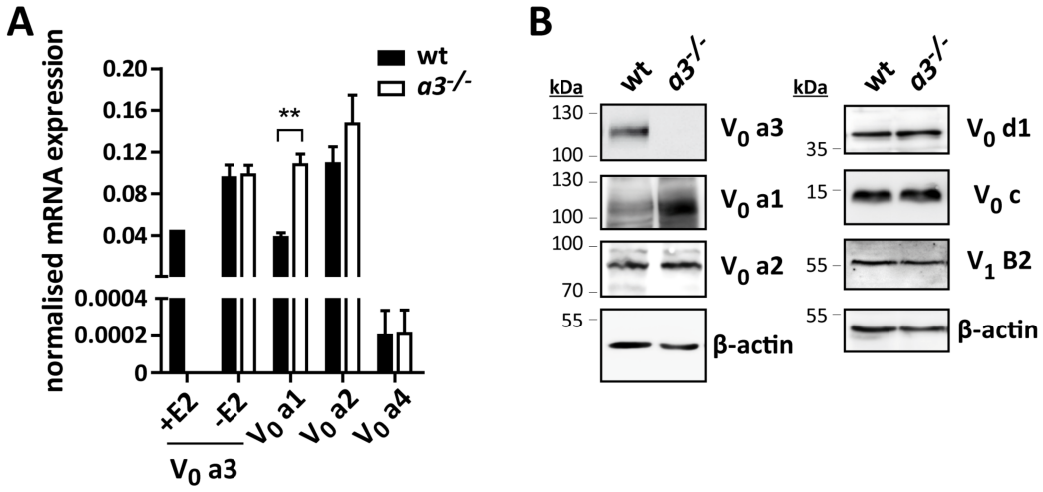

Figure 3.2: Deficit of V-ATPase V_0 subunit a3 in a3$^{-/-}$ *MEFs albeit continued mRNA expression.*

(A) Expression of mRNA coding for the V-ATPase subunits V_0 a1 to V_0 a4 was analysed by qPCR in wild-type (wt) and *a3*$^{-/-}$ MEFs and correlated to the expression of the housekeeping genes *Tuba1a*, *Hprt1* and *Sdha*. The abundance of mRNA coding for the V_0 subunit a3 was assessed at the site of exon 2 (+E2) or at the border between exons 13 and 14 (-E2). Shown are mean normalised mRNA levels ± standard error from three independent experiments (**, $P < 0.01$ according to an unpaired, two-tailed Student´s t test). (B) Immunoblot analysis of total lysates generated from wild-type and *a3*$^{-/-}$ MEFs showing the protein expression of the V-ATPase subunits V_0 a1 to V_0 a3, V_0 d1 and V_0 c as well as V_1 B2. Probing for β-actin was used to control for an equal protein load.

Since V_0 subunit a3 was reported to exhibit a lysosomal localisation, an indirect immunofluorescence staining was conducted to clarify the subcellular V_0 a3 distribution in wild-type and a3-deficient MEFs (Fig. 3.3). Lysosomes were visualised with antibodies directed against the lysosomal membrane protein LAMP-2. In wild-type MEFs, the signals received for V_0 subunit a3 showed a 78 % overlap (Pearson´s correlation coefficient = 0.74) with the LAMP-2 staining, proving the co-localisation of both proteins. Consistent with the findings in the

Western blot analysis, V_0 a3-levels were reduced to background noise in *a3*$^{-/-}$ MEFs (Pearson´s correlation coefficient = 0.09) while LAMP-2 staining appeared unchanged in comparison to wild-type MEFs.

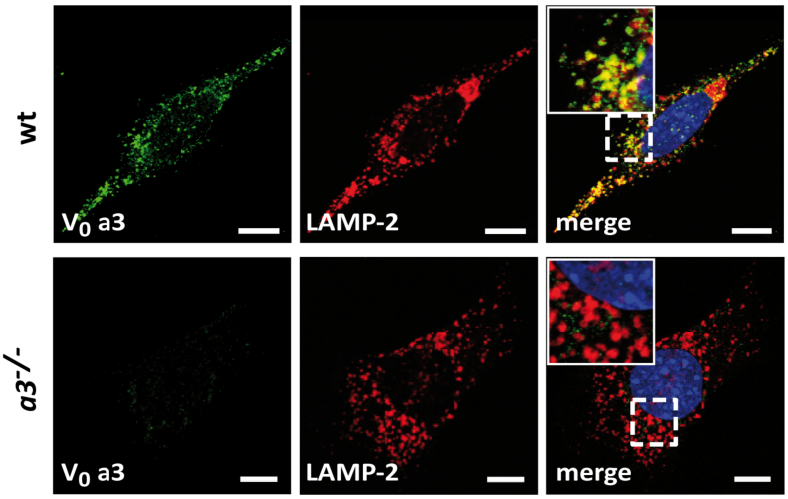

Figure 3.3: Lysosomal localisation of the V-ATPase V_0 subunit a3 in wild-type MEFs.

Immunofluorescence analysis of the V-ATPase V_0 subunit a3 distribution in PFA-fixed wild-type (wt) and *a3*$^{-/-}$ MEFs. A LAMP-2 staining was conducted to assess the intracellular localisation of lysosomes, nuclei were visualised by DAPI incorporation. Indicated regions of interest are magnified in the respective inset. Scale bars = 10 µm.

Taken together, the analyses on V-ATPase expression showed that a3-deficient MEFs harboured a specific knockout of the lysosomal V_0 subunit a3, while V_0 subunit a1 was up-regulated in comparison to wild-type MEFs. The other subunits of the V-ATPase seemed to be unaffected by the depletion of V_0 a3.

3.1.3. Unaltered lysosome function albeit deletion of V_0 subunit a3

To examine, whether the loss of one of the V_0 subunit a isoforms blocks the proton pumping activity of the V-ATPase complex and thereby interferes with multiple cellular functions, lysosome acidification was assessed in wild-type and *a3*$^{-/-}$ MEFs (Fig. 3.4). For ratiometric measurement of the lysosomal pH, the endocytic system of MEFs was labelled with dextran-Oregon Green® 514 overnight with an additional two hours dye-free incubation period to clear early compartments. Cells were then subjected to live cell confocal fluorescence imaging (Fig. 3.4A). The acquired fluorescence intensity ratios were related to defined pH values by performing an *in situ* calibration (Fig. 3.4B). Treatment with bafilomycin A1 and nigericin increased the fluorescence intensity ratios above the ratio measured for pH 6.5, reflecting the

neutralising effect of these pharmaceuticals on the lysosomal pH. The calculated pH values for wild-type (4.78 ± 0.13) and *a3*$^{-/-}$ (4.90 ± 0.23) lysosomes indicated no apparent defect in lysosome acidification upon depletion of V_0 subunit a3 (Fig. 3.4C).

As a second read-out for lysosome function and as an indirect measure for lysosomal acidification, the processing and activity of different lysosomal enzymes was analysed in *a3*$^{-/-}$ MEFs and compared to wild-type cells. For this purpose, the specific activity of the acidic hydrolases β-hexosaminidase and β-glucocerebrosidase was measured from whole cell lysates using artificial, chromogenic substrates. This revealed no significant differences between both genotypes with specific β-hexosaminidase activities of 24.5 ± 3.5 mU/mg in wild-type and 25.7 ± 5.9 mU/mg in a3-deficient samples and specific β-glucocerebrosidase activities of 1.2 ± 1 mU/mg (wild-type) versus 1.1 ± 0.8 mU/mg (*a3*$^{-/-}$).

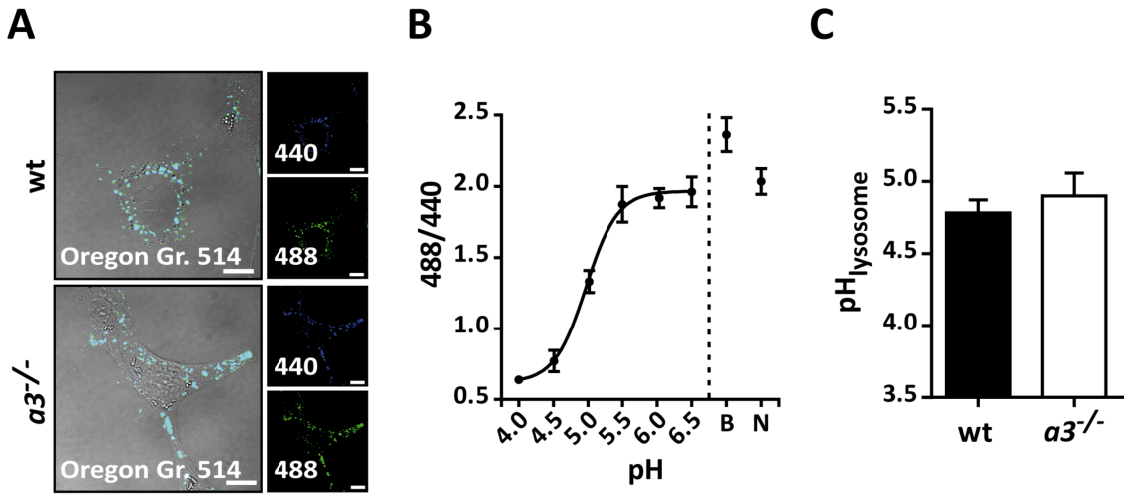

Figure 3.4: Lysosome pH is comparable between wild-type and a3-deficient MEFs.

(A) Live cell fluorescence imaging of dextran-Oregon Green® 514 (Oregon Gr. 514) taken up by wild-type and *a3*$^{-/-}$ MEFs overnight and cleared of early endocytic compartments during a two hours chase period. Oregon Green® 514 fluorescence was measured upon alternate excitation at 440 nm (blue) or 488 nm (green). Scale bars = 10 µm. (B) The ratio of fluorescence emission was calculated at defined lysosome pH values that were generated through K^+-rich buffer solutions containing 10 µg/ ml nigericin. Shown are mean intensity ratios 488/440 ± standard error of a representative wild-type calibration. Application of bafilomycin A1 (100 nM, B) or nigericin (10 µg/ml, N) was performed 15 minutes prior to live cell imaging as control for an increased lysosome pH. A calibration curve was extrapolated to the Boltzmann equation and used in (C) to calculated the basal lysosome pH for both genotypes. Shown are mean pH values ± standard error resultant from three independent experiments.

However, these assays did not distinguish between enzymes that are correctly targeted to the lysosome and enzymes that might be retained in the ER due to an impaired protein transport. Hence, the transport and processing of cathepsins was assessed in addition. During maturation,

cathepsin D is transported to acidic lysosomes, where it undergoes a final processing step, yielding its mature and active form (Gieselmann *et al.*, 1985). The localisation of cathepsin D was followed in wild-type and a3-deficient MEFs through indirect immunofluorescence including marker proteins for lysosomes (LAMP-2), the Golgi apparatus (GM130) and the ER (KDEL) (Fig. 3.5A). In both genotypes, the majority of cathepsin D co-localised with LAMP-2 at the lysosome, while only minor amounts resided in the Golgi apparatus or the ER, respectively. Overall this pointed to a comparable transport of cathepsin D to the lysosome in both genotypes.

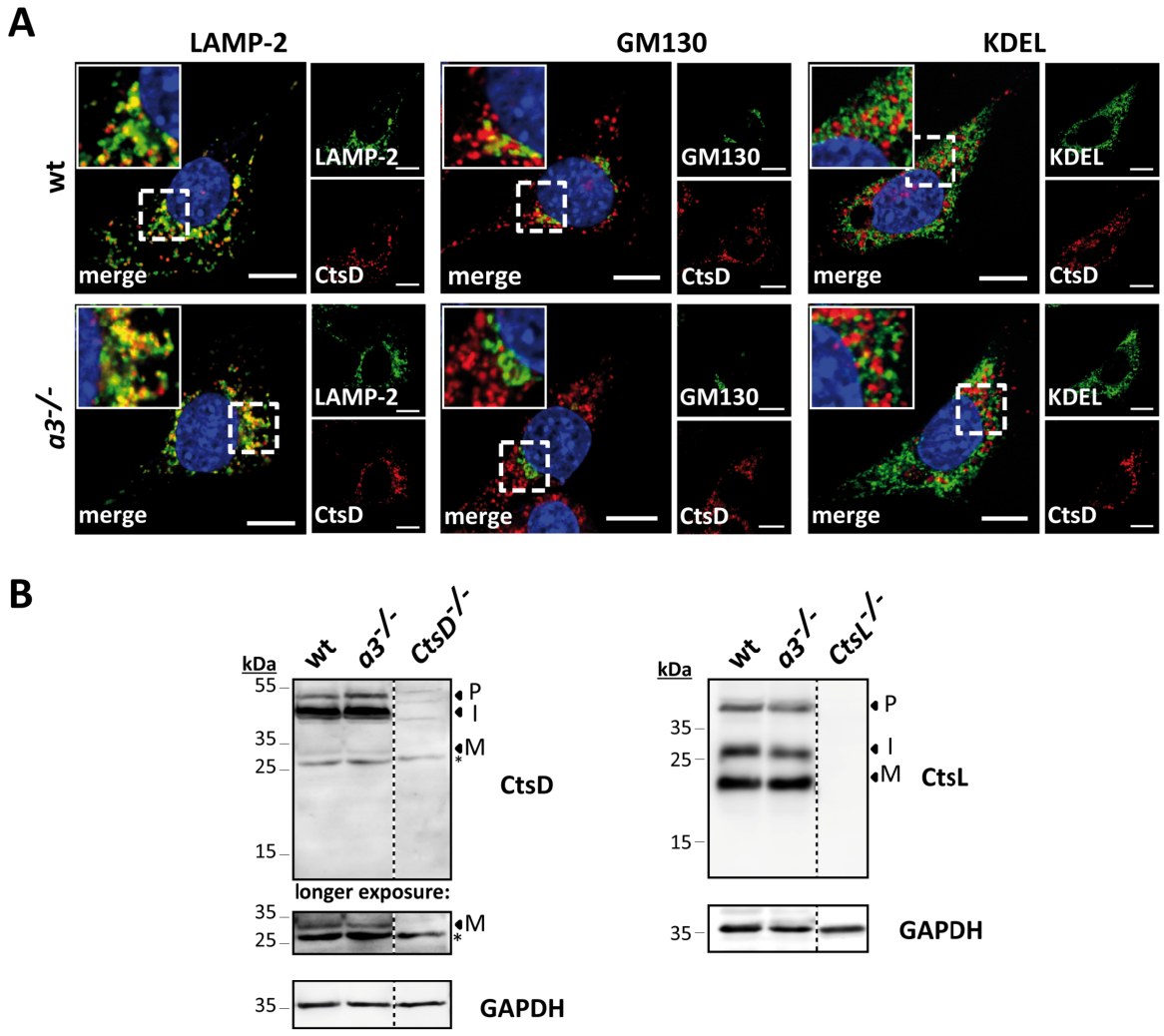

Figure 3.5: Unaltered cathepsin transport and processing in a3-deficient MEFs.

(A) Subcellular localisation of cathepsin D (CtsD) analysed by indirect immunofluorescence staining of wild-type (wt) and *a3*$^{-/-}$ cells. Insets include magnified regions of interest. A co-staining (from left to right) with LAMP-2, GM130 and KDEL was conducted to correlated cathepsin D-associated signals to specific compartments. Scale bars = 10 µm. (B) Immunoblot analysis of wild-type versus a3-deficient MEF lysates probed for cathepsin D (left panel) and cathepsin L (CtsL, right panel). MEF lysates lacking either cathepsin (*CtsD*$^{-/-}$ or *CtsL*$^{-/-}$) were used in control lanes, while GAPDH probing served to assure a comparable protein load. Proform (P), intermediate (I) and mature forms (M) are indicated by arrowheads. Unspecific antibody binding is highlighted with asterisks.

The processing of cathepsin D as well as cathepsin L was further examined by immunoblotting (Fig. 3.5B). Lysates from MEF lines lacking either cathepsin were used as controls. The cathepsin D immunoblot revealed signals of three distinct molecular weights, which correspond to the proform of 52 kDa, an intermediate of 48 kDa and the mature form of the protease with a molecular weight of 34 kDa (Zaidi *et al.*, 2008). When comparing cathepsin D processing in wild-type and *a3*$^{-/-}$ MEF, no obvious variations were detectable. Similar to the cathepsin D Western blot, probing for cathepsin L revealed signals of three specific molecular weights belonging to the proform, intermediate and mature cathepsin L (Ishidoh *et al.*, 1998) and featuring comparable intensities with or without V_0 subunit a3 expression.

The data concerning the functionality of lysosomes collectively implied that the knockout of V_0 subunit a3 did interfere with neither lysosomal acidification nor the activity of lysosomal enzymes. Furthermore, the correct transport of cathepsin D to the lysosome already indicated at least partially functional vesicle fusion in *a3*$^{-/-}$ MEFs.

3.1.4. Endocytic uptake is independent of the presence of V-ATPase V_0 a3

To further assess fusion processes in selected examples for the multiple subcellular transport routes, the uptake and fusion-dependent delivery of endocytic cargo to the lysosome was studied in the presence or absence of the V_0 subunit a3.

Therefore, dextran-Texas Red® (70 kDa), a target for macropinocytosis, was added to the culture medium of MEF cells for 30 minutes. Following this uptake period, the external supply of dextran-Texas Red® was removed by washing and fresh culture medium was added. The intracellular transport of the endocytosed polysaccharides was analysed by confocal fluorescence microscopy after three hours in the absence of further dextran-Texas Red® (Fig. 3.6A). The fluorescence signals of the fluorochrome co-localised with the LAMP2-staining as a marker for lysosomes in wild-type and a3-deficient cells. This suggested an efficient transport of the compound to the lysosome, regardless of the expression of V_0 subunit a3. Loss of V_0 subunit a3 in *a3*$^{-/-}$ MEFs was verified by staining with an anti-V_0 a3 antibody, which displayed prominent signals in wild-type MEFs that were absent in a3-deficient cells.

To further verify the correct uptake and delivery of BSA to lysosomes, wild-type and *a3*$^{-/-}$ MEFs were incubated with the self-quenched DQ™ Red-BSA. Upon degradation of BSA in the late endocytic system, *e.g.* late endosomes and lysosomes, the quenching effect is relieved and a fluorescence signal can be detected (Fig. 3.6B). Similar to the results obtained with

dextran-Texas Red®, DQ™ Red-BSA fluorescence was seen in both genotypes after 12 hours in the presence of the fluorochrome, hinting to efficient uptake, transport and degradation of BSA independent of the V-ATPase V_0 subunit a3.

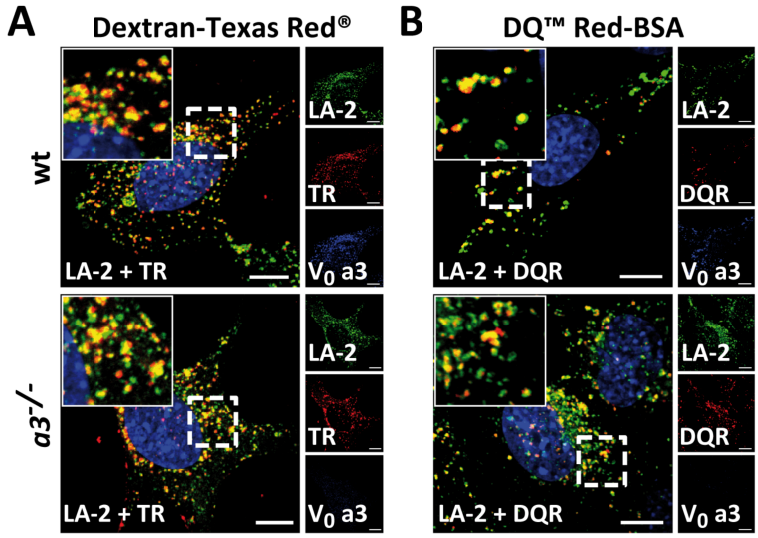

Figure 3.6: Endocytic uptake is comparable between wild-type and a3$^{-/-}$ *MEFs.*

(**A**) Uptake and intracellular delivery of dextran-Texas Red® (TR) was visualised in wild-type (wt) and *a3*$^{-/-}$ MEFs using confocal fluorescence microscopy and application of a co-staining for LAMP-2-containing lysosomes (LA-2). Cells were incubated with dextran-Texas Red® for 30 minutes and left to process the compound for additional three hours. The presence or absence of the V-ATPase V_0 subunit a3 was controlled by an additional staining, which is not included in the merge image. DAPI was used to assess nuclei. Insets display magnified regions of interest. (**B**) Endocytic digestion of DQ™ Red-BSA (DQR) similar to (A) but utilising the self-quenched DQ™ Red-BSA for 12 hours instead of dextran-Texas Red®. Scale bars = 10 µm.

3.1.5. Latex bead-containing phagosome maturation proceeds in the absence of the V_0 subunit a3

Since the V_0 subunit a3 was described to be localised to both, lysosomes and phagosomes (Sun-Wada *et al.*, 2009), further analyses focused on the fusion between these two compartments in regard to its dependence on the V-ATPase V_0 subunit a3.

During phagosome maturation, a newly developed phagosome has to acquire degradative activity through fusion processes with endosomes and lysosomes. To allow phagocytosis in MEFs, which are non-professional phagocytes, wild-type and a3-deficient cells were transfected with DNA coding for a C-terminally myc-tagged human Fcγ receptor IIa (FcγRIIa). This protein enables phagocytosis of IgG-opsonised particles by binding to the Fc part of the antibody (Tuijnman *et al.*, 1992). After transfection, cells were selected for stable FcγRIIa-myc expression and single clones analysed by immunoblotting (Fig. 3.7). Probing for the myc-tag of the fusion

protein revealed no FcγRIIa expression in the lysates from untransfected wild-type and *a3*$^{-/-}$ MEFs. However, a prominent myc signal appeared in the lanes of the transfected cell lines, wild-type #1-8 and *a3*$^{-/-}$ #1-2, corresponding to the expression of the FcγRIIa construct in these cells.

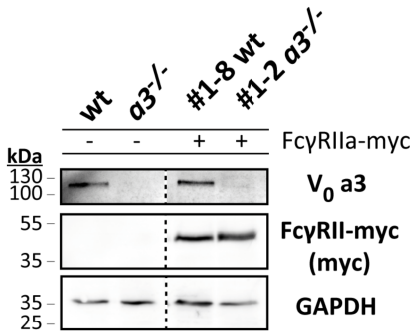

Figure 3.7: FcγRII-myc expression in wild-type and a3-deficient MEF lines.

Wild-type (wt) and *a3*$^{-/-}$ MEF lines were stably transfected with a human FcγRII-myc construct and expression of the protein assessed by immunoblotting against the myc-tag in lysates of untransfected (left panel) and transfected (right panel, clones #1-8 and #1-2) cells. Probing for the V_0 subunit a3 and GAPDH was used to verify the knockout of V_0 a3 and an equal loading, respectively.

The FcγRIIa-myc-positive MEF lines were then used to study the maturation of phagosomes containing human IgG-opsonised latex beads. Following a 15 minutes uptake of latex beads (MOI = 8), phagosome maturation was tracked for one hour by indirect immunofluorescence labelling including marker proteins for early endocytic (EEA1) and lysosomal (LAMP-2) compartments (Fig. 3.8A). External beads were visualised with an antibody directed against human IgG that was applied prior to permeabilisation of the samples. Directly after uptake of the latex beads into phagosomes, co-localisation of the beads and EEA1 was detectable in both, wild-type and a3-deficient MEFs. One hour later, most of the latex-beads co-localised with LAMP-2, hinting to efficient phagosome maturation in presence and absence of the V_0 subunit a3.

To get a quantitative measure of phagosome maturation and thereby of phagosome-lysosome fusion, the co-localisation rate of latex beads with either EEA1 or LAMP-2 signals was counted for distinct time points after bead uptake (Fig. 3.8B). During the one hour maturation, the co-localisation of the latex beads with EEA1 decreased from 65 % to 30 % in wild-type and from 69 % to 34 % in *a3*$^{-/-}$ MEFs, whereas the co-localisation with LAMP-2 increased from 17 % to 75 % (wild-type) or from 24 % to 78 % (a3-deficient), respectively. No kinetic disparities were

revealed in the departure of EEA1 from or the acquisition of LAMP-2 to the maturing phagosomes in wild-type and a3-deficient MEFs.

In conclusion, since phagosome maturation progressed normally regardless of the expression of the V-ATPase subunit a3, this subunit seemed to be dispensable in the process of phagosome-lysosome fusion.

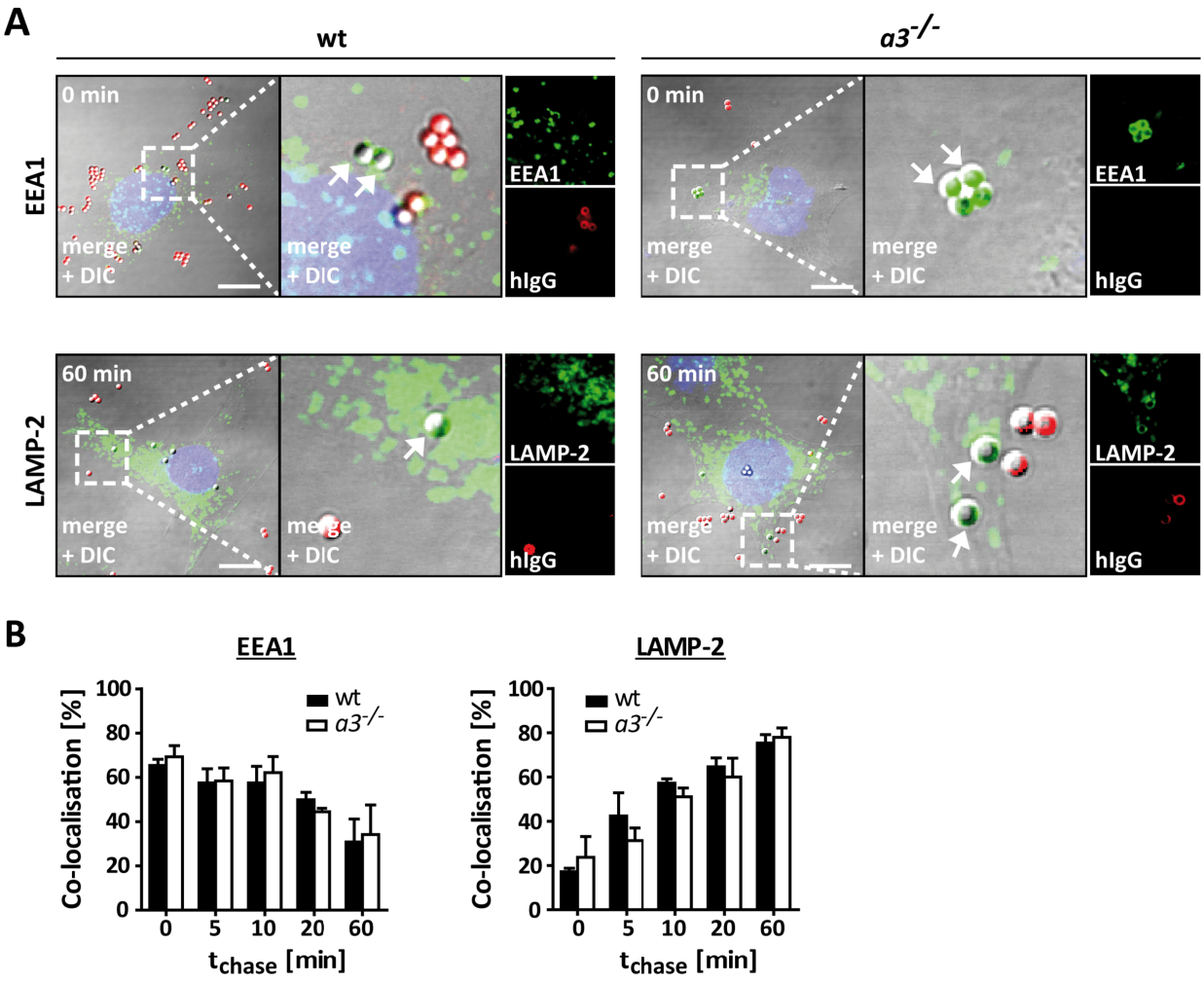

Figure 3.8: Knockout of V-ATPase V_0 subunit a3 does not interfere with the progression of phagosome maturation.

Latex bead phagocytosis was visualised in FcγRII-expressing wild-type (wt) and *a3*$^{-/-}$ MEFs that were incubated in the presence of human IgG-opsonised latex beads (MOI = 8) for 15 minutes and cultivated for up to 60 additional minutes to deliver the phagocytic cargo to phagolysosomes. (**A**) Immunofluorescene analysis of both MEF lines directly following uptake of the latex beads (0 min) or at the end of the maturation process (60 min). Extracellular beads (hIgG-positive) were stained prior to fixation and processing of the cells for immunostaining directed against EEA1 (upper panel) or LAMP-2 (lower panel). DAPI incorporation was used to dye nuclei. The DIC channel allows visualisation of internalised latex beads so that a signal overlap of these beads with the marker proteins is observable as indicated by arrowheads in the magnified regions of interest. Scale bars = 10 µm. (**B**) The number of latex beads co-localising with either EEA1 (left panel) or LAMP-2 (right panel) was counted for various time points and plotted as a fraction of internalised globules in total. Bars represent means ± standard error from three independent experiment with at least 100 counted beads per individual time point and experiment.

3.1.6. Maturation of latex bead-containing phagosomes under conditions of increased lysosome pH and altered V_0 sector availability

To this point, the physical participation of the V-ATPase in the mixing of two lipid bilayers could not be confirmed using V_0 a3-deficient cells. However, recent findings rather support a fusion promoting role for the low intraluminal pH generated by the complex (Coonrod *et al.*, 2013). Thus, the influence of an increased vesicular pH on phagosome maturation was analysed in wild-type and a3-deficient MEFs, hereafter.

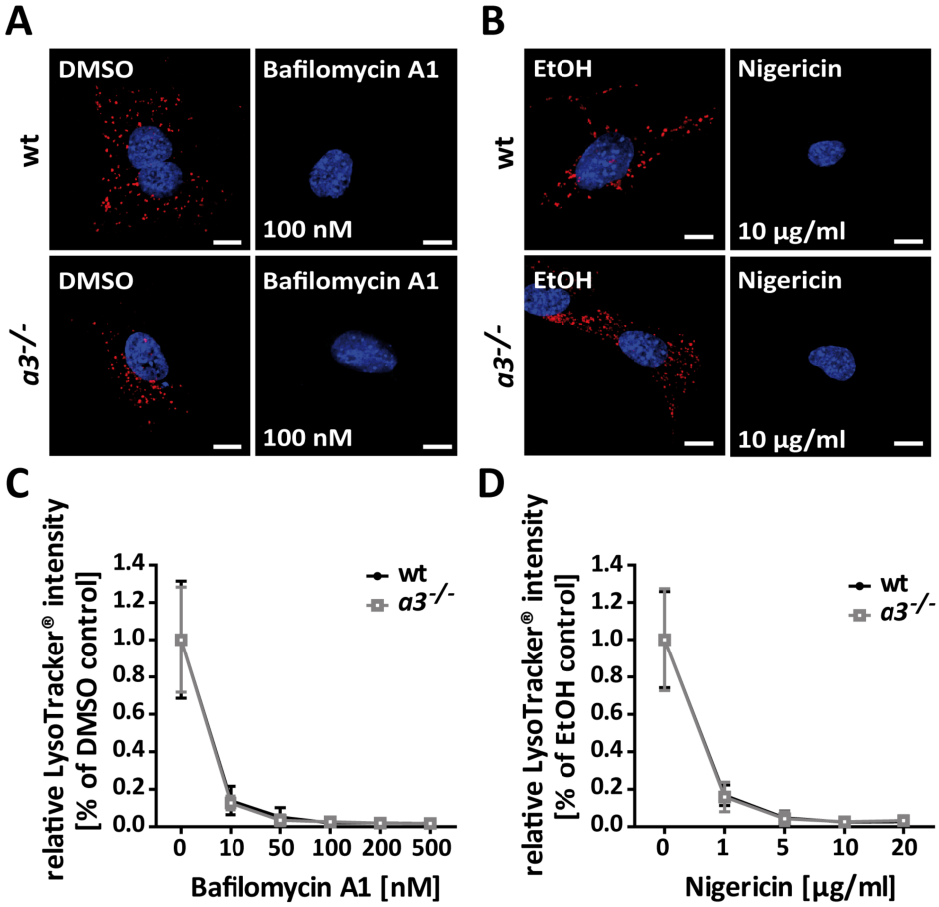

Figure 3.9: Dose-dependent influence of bafilomycin A1 and nigericin on lysosome pH.

(A-B) Acidic compartments of wild-type (wt) and *a3*$^{-/-}$ MEFs were visualised by LysoTracker® Red staining, and fixed and embedded cells were analysed by confocal fluorescence microscopy. Treatment with either bafilomycin A1 (A) or nigericin (B) at the indicated concentration was applied 15 minutes prior to and during LysoTracker® Red administration to alkalise lysosomes. Control cells were cultivated in the presence of the respective solvent. Scale bars = 10 µm. (C-D) LysoTracker® Red intensity were measured for ascending concentrations of bafilomycin A1 (C) or nigericin (D) and related to the solvent-treated control to generate a dose-response curve for both genotypes representing mean values ± standard error from three separate experiments.

Accordingly, fibroblasts of both genotypes were treated for 15 minutes with variable concentrations of bafilomycin A1 or nigericin and the raise of lysosome pH was verified by LysoTracker® Red staining under continued drug treatment (Fig. 3.9A, B). The fluorescence intensity of the acidotropic dye decreased in a dose-dependent manner when either of the pH modulators was applied, confirming their neutralising effect (Fig. 3.9C, D). Compared to the DMSO-treated fibroblasts, the lowest dose of bafilomycin A1 was able to reduce the LysoTracker® Red signal intensities to residual 13 – 14 %. When nigericin was administrated, the fluorescence diminished to 16 – 17 % of the intensity received from the ethanol-treated controls. Interestingly, wild-type and a3-deficient acidic compartments behaved similarly, implying that the loss of V_0 subunit a3 was not detrimental to the V-ATPase function *per se*.

Since no further reduction of LysoTracker® Red staining was observed for dosages above 200 nM bafilomycin A1 or 10 µg/ ml nigericin, respectively, these concentrations were chosen for the analysis of phagosome-lysosome fusion as in 3.1.5. The kinetics of EEA1 disappearance from the phagosomes of wild-type MEFs were unchanged by application of either bafilomycin A1 or nigericin 15 minutes prior to and during the one hour phagosome maturation (Fig. 3.10A). The same was observed for the kinetics of phagosomal LAMP-2 acquisition in the course of the maturation process (Fig. 3.10A), revealing no pH dependence of the fusion between phagosomes and lysosomes. Even when the pharmacologically impaired acidification was combined with the deficiency of V_0 subunit a3 by the application of bafilomycin A1 or nigericin to *a3*$^{-/-}$ MEFs, the distribution of the two marker proteins on the phagosomes appeared unaltered again (Fig. 3.10B), implying no impairment of phagosome maturation.

In addition to their negative impact on lysosome acidification, bafilomycin A1 and nigericin have distinct effects on the V_0-V_1 association state of the V-ATPase complex (Fig. 4.2). Bafilomycin A1 interacts with the V-ATPase V_0 sector, which interferes with binding of V_1 (Bowman *et al.*, 2006; Poea-Guyon *et al.*, 2013; Wang and Hiesinger, 2013; Morel and Poea-Guyon, 2015). Accordingly, the amount of available free V_0 sectors for membrane fusion is increased upon bafilomycin A1 treatment. Application of the ionophore nigericin consumes luminal protons to mediate a potassium influx. This induces compensatory activation of the V-ATPase and enhances V_0-V_1 interaction. As a consequence, the amount of free V_0 sectors is decreased (Poea-Guyon *et al.*, 2013; Wang and Hiesinger, 2013; Morel and Poea-Guyon, 2015). Since both pharmaceuticals showed no effect on the maturation of latex-bead containing phagosomes in fibroblasts, fusion along the phagocytic pathway was not influenced by the number of available free V_0 sectors.

Overall, the studies involving phagosome maturation in wild-type and a3-deficient MEF lines supported a role for neither the V-ATPase driven lysosome acidification nor the presence of the V-ATPase subunit a3. The accessibility of the membrane-integral V_0 subunits was no prerequisite for fusion along the phagocytic axis.

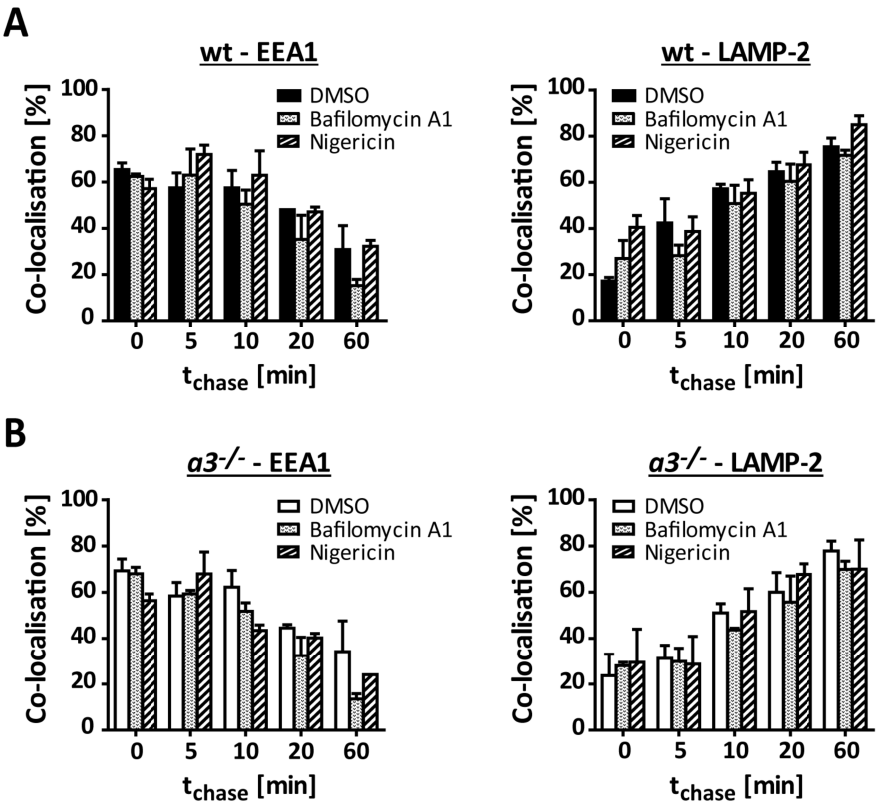

Figure 3.10: Efficient phagosome maturation under conditions of increased vesicular pH.

(A) Stably FcγRII-myc expressing wild-type MEFs were exposed to IgG-opsonised latex beads for 15 minutes and maturation of the latex-beads-containing phagosomes observed for further 60 minutes (0 – 60 min). Pretreatment with 200 nM bafilomycin A1 or 10 µg/ml nigericin was applied to alkalise vesicles and continued during the uptake of latex beads and subsequent phagosome maturation. Administration of DMSO served as solvent control. Phagocytosed beads that co-localised with fluorescently labelled EEA1 (left panel) or LAMP-2 (right panel) were counted from three independent experiments and compared to the total amount of at least 100 internalised latex beads per condition. Error bars display standard error. (B) Experiments in (A) were conducted using *a3*$^{-/-}$ MEFs that expressed the FcγRII-myc construct.

3.2. Vesicle fusion in ATP6AP2-deficient macrophages

The maintained vesicle fusion in a system that is based on the knockout of a single V-ATPase subunit could reflect the diversity of the V-ATPase complex with its multiple subunits and subunit isoforms. Overlapping functions of similar components could lead to compensation upon the deprivation of one specific subunit, which might have been the cause for the up-regulation of the V-ATPase V_0 subunit a1 in the *a3*$^{-/-}$ MEFs. Hence, a more thorough knockout

mouse model should be generated to continue with the study of the V-ATPase function in vesicle fusion. For this purpose, the V-ATPase accessory protein 2/ ATP6AP2 was chosen as target for a gene knockout, because it occupies a chaperone function for the assembly of the V-ATPase V_0 sector (Kinouchi *et al.*, 2010; Oshima *et al.*, 2011; Kinouchi *et al.*, 2013). The consequent disruption in V_0 sector formation should interfere with the function and stability of the whole V-ATPase complex.

3.2.1. The *Mx1-Cre* conditional knockout mouse model affects macrophages

Since a constitutive knockout of *Atp6ap2* is lethal at an early embryonic stage (Sihn *et al.*, 2010), a conditional knockout mouse line was established by application of the *Cre/ loxP* recombination system. To achieve a deletion resulting in a non-functional gene product, the presence of *loxP* sites flanking exon 2 of *Atp6ap2* (floxed) was combined with the expression of the Cre recombinase under the control of the inducible *Mx1* promotor. The *Mx1* promotor region is responsive to interferon α/ β receptor signalling, thereby targeting a multitude of immune cells (Kuhn *et al.*, 1995). Among these, macrophages are prone to the *Mx1* promotor activity and represent a suitable professional phagocyte cell line to analyse phagosome-lysosome fusion.

The breeding strategy (see section 2.6.2) aimed to obtain homo- and hemizygous floxed mice with 50 % offspring carrying one *Mx1-Cre* allele by breeding of female mice bearing *loxP* sites within *Atp6ap2* with mice that were heterozygous for the *Mx1-Cre* transgene. Animals possessing homo- or hemizygous floxed *Atp6ap2* but no *Mx1-Cre* allele were referred to as wild-type controls, whereas those with floxed *Atp6ap2* and positive for the *Mx1-Cre* transgene were named conditional knockout (cKO) animals.

In addition, the *Mx1-Cre* transgenic mice were bred with a *Rosa26-EYFP* reporter strain (Srinivas *et al.*, 2001) for a better evaluation of the *Mx1* promoter activity. These reporter mice feature a genomic insertion, which transcribes for the enhanced yellow fluorescent protein (EYFP), in the ubiquitously expressed locus *Rosa26*. The integrated sequence includes a *STOP* cassette flanked by *loxP* sites upstream of the EYFP coding region. Recombination mediated by the Cre recombinase can hence be visualised through an EYFP expression. Similar to the *Atp6ap2* floxed *Mx1-Cre* transgenic mice, animals homozygous for the $Rosa26^{EYFP}$ allele, but without *Mx1-Cre* insertion were used as wild-type controls, whereas $Rosa26^{EYFP/EYFP}$ and $Mx1\text{-}Cre^{tg/+}$ double

transgenic mice were referred to as *Mx1-Cre* reporter (for breeding scheme see section 2.6.2).

In both conditional mouse lines, the activation of the *Mx1* promotor was triggered by an interferon α and β release, which resulted from the administration of synthetic double stranded RNA to mimic a viral infection (Kuhn *et al.*, 1995) (Fig. 3.11A). Therefore, *Mx1-Cre* transgenic mice and wild-type controls were treated with three doses of polyinosinic:polycytidylic acid (poly (I:C)) within five days by intra-peritoneal injection and sacrificed ten days after the last application for experimental analysis (Fig. 3.11B).

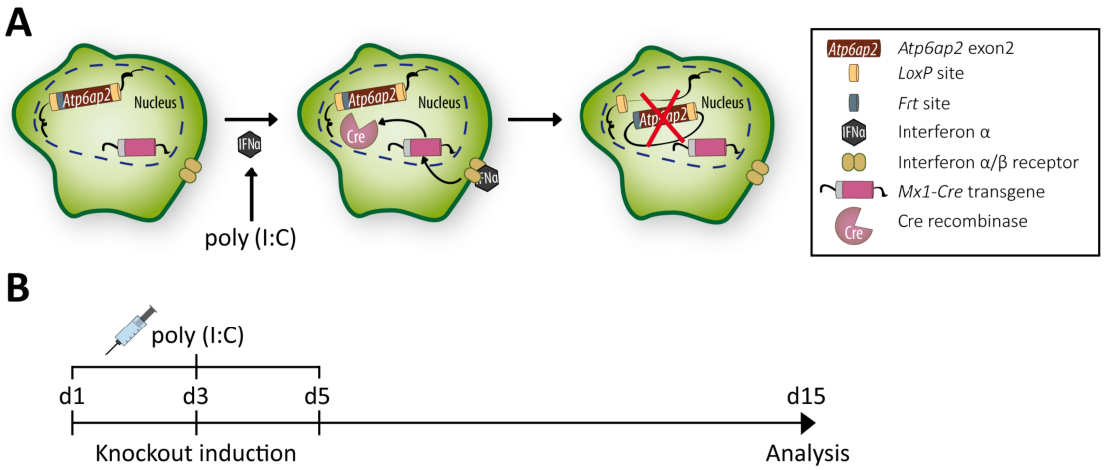

Figure 3.11: Mx1-Cre-*mediated deletion of* Atp6ap2 *exon 2 upon poly (I:C) induction.*

(A) Schematic illustration of interferon α (IFN α) induced deletion in *Atp6ap2*. Binding of interferon α to its receptor initiates a signalling cascade that drives the *Mx1*-controlled expression of the Cre recombinase. *LoxP* sites flanking exon 2 of *Atp6ap2* will be targeted by Cre-mediated recombination that leads to the excision of the internal region. The circular extract will be cleared by the cell´s degradation machinery. A similar result can be obtained with interferon β. (B) Time scale of *Mx1* induction in *Mx1-Cre* transgenic animals and the respective wild-type controls. Three doses of poly (I:C), 250 µg each, are applied by intra-peritoneal injection within five days and the animals kept for further ten days before experimental analysis.

The tissue specificity of the subsequent Cre-mediated recombination was assessed by immunoblotting (Fig. 3.12A). Selected tissue lysates from wild-type and *Atp6ap2* conditional knockout animals were probed for ATP6AP2 expression. This revealed a strong signal for the ATP6AP2 C-terminal fragments (CTF) at approximately 15 kDa as well as a weaker signal of 37 kDa corresponding to full length ATP6AP2 in brain samples of both genotypes. The high expression level in brain is in agreement with previous Northern blot results indicating a high abundance of *Atp6ap2* mRNA within this organ (Nguyen *et al.*, 2002).

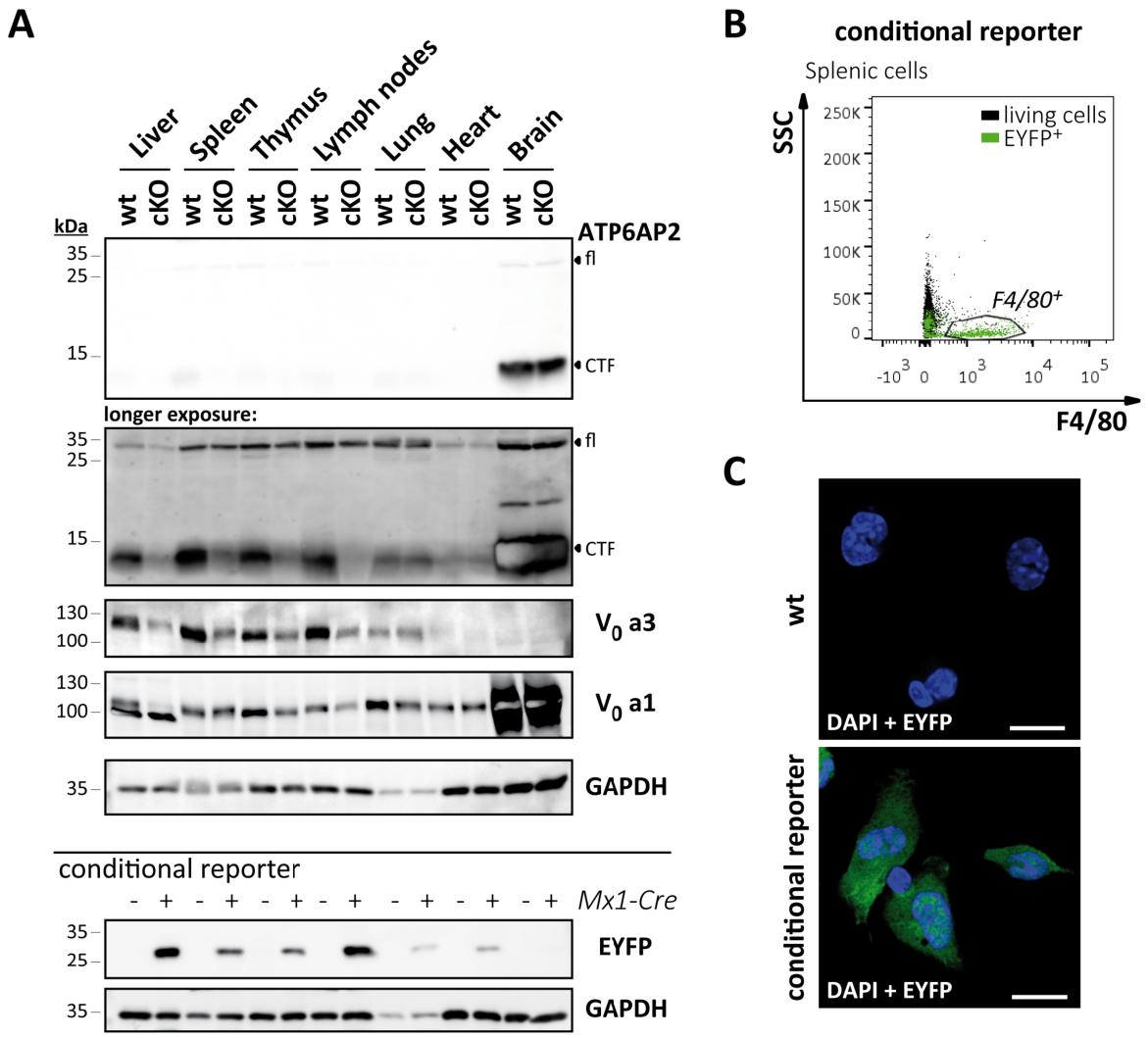

Figure 3.12: Poly (I:C) induces Mx1-Cre *activity in various tissues and in macrophages.*

(A) Conditional *Atp6ap2* knockout mice, *Mx1-Cre* reporter and the respective wild-type controls were treated three times with poly (I:C) to induce an activation of the *Mx1* promotor and sacrificed after additional ten days in housing. Indicated tissue lysates of *Atp6ap2* knockout (cKO) and wild-type (wt) mice were analysed via immunoblotting targeting ATP6AP2 and the V-ATPase subunits a1 and a3 (Upper panel). Full length (fl) and C-terminal fragments (CTF) of ATP6AP2 are indicated with arrowheads. Identical tissue lysates were generated from wild-type (-*Mx1-Cre*) and conditional *Mx1-Cre* reporter animals (+*Mx1-Cre*, lower panel) to assess EYFP expression. GAPDH served as loading control. (B) Splenic cells of *Mx1-Cre* reporter mice were probed for the macrophage marker F4/80 using fluorescence labelling and flow cytometry. Propidium iodid incorporation was applied to exclude necrotic and dead cell populations. In a sidewards scatter – F4/80 plot, living cells were gated as indicated to assess the percentages of EYFP-positive cells in the F4/80 expressing ($F4/80^+$) species. EYFP expression was assessed in the $F4/80^+$ populations of three animals per genotype. (C) Isolated peritoneal macrophages of wild-type and conditional reporter animals were fixed and embedded to visualise EYFP fluorescence in confocal laser scanning microscopy. Scale bars = 10 µm.

In contrast, the other examined tissues displayed a much weaker expression of full length ATP6AP2 and its CTF. While uncleaved ATP6AP2 was detectable at only slightly lower levels in knockout samples, the intensity of the CTF signal was significantly reduced in liver, spleen,

thymus and lymph nodes when compared to the respective wild-type tissue, indicating *Mx1* promotor activity in these organs. In agreement with these findings, the levels of the V-ATPase V_0 subunit a3 as well as partially the levels of V-ATPase V_0 subunit a1 were reduced in the identical samples. In addition, the knockout of *Atp6ap2* and a reduction of the V-ATPase V_0 a subunits was observed in bone marrow samples of conditional knockout animals (data not shown).

Using wild-type and conditional reporter mice in a comparable analysis, further immunoblotting was performed against EYFP. The *Mx1-Cre* activity, as visualised through EYFP expression, was confirmed to be mostly present in liver, spleen, thymus and lymph nodes but also to a minor extent in lung and heart lysates of the reporter animals (Fig. 3.12A). The brain, as an immune privileged organ, was not targeted by the interferon α and β secretion, which overall suited the previously reported distribution of a poly (I:C)-induced *Mx1-Cre* activation (Kuhn *et al.*, 1995).

The wide spread nature of the initiated recombination events reflected the variety of cells from different tissues that are involved in an immune response to viral infections. Flow cytometric analyses of spleen, thymus and bone marrow extracted from wild-type and *Mx1-Cre* reporter mice could not completely track the lineage of cells that are directly targeted by the activation of the *Mx1* promoter (data not shown). However, splenic macrophages showed the highest rate of cells positive for EYFP fluorescence with a percentage of 94.8 % (Fig. 3.12B). Since macrophages were also the desired cell type to continue the analysis of the role for the V-ATPase in vesicle fusion, peritoneal macrophages were further tested for EYFP expression in conditional reporter mice. EYFP fluorescence of isolated peritoneal macrophages was assessed via confocal microscopy (Fig. 3.12C). Macrophages extracted from wild-type mice showed no visible EYFP fluorescence, whereas EYFP signals were prominent in the phagocytes of conditional reporter animals. This verified that peritoneal macrophages were targeted in a *loxP Mx1-Cre* knockout system and the *Atp6ap2* conditional knockout mice could be used to study the dependence of vesicle fusion on the presence of the V-ATPase complex.

3.2.2. Deprivation of ATP6AP2 disrupts the V-ATPase V_0 sector assembly

In line with the characterisation of the *Mx1-Cre* reporter animals, an efficient deletion of ATP6AP2 should be demonstrated in peritoneal macrophages of *Atp6ap2* conditional knockout mice and evaluated with respect to its influence on the V-ATPase complex assembly. To obtain suitable amounts of these phagocytes from a peritoneal lavage, macrophages were enriched

inside the peritoneal cavity through a thioglycollate treatment three days prior to their isolation. Lysates of wild-type and *Atp6ap2* knockout macrophages were then subjected to immunoblot analysis directed against ATP6AP2 (Fig. 3.13A).

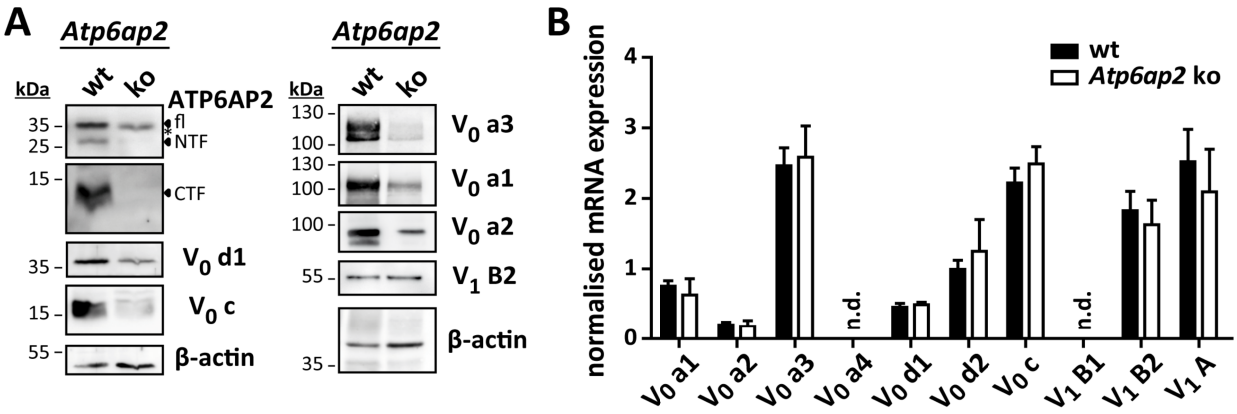

Figure 3.13: Deletion of Atp6ap2 *leads to a post-transcriptional disruption of the V-ATPase V_0 sector.*

(A) Immunoblot analysis of wild-type (wt) and *Atp6ap2* knockout (ko) macrophage lysates probing for ATP6AP2 and the indicated V-ATPase subunits. Full length, N-terminal (NTF) and C-terminal fragments (CTF) are highlighted by arrowheads. Unspecific binding is marked with an asterisk. To control for equal amounts of protein load, β-actin was detected in addition. (B) Expression of mRNA coding for the indicated V-ATPase subunits was assessed via qPCR using cDNA generated from total RNA extracts of wild-type and ATP6AP2-deficient macrophages. Mean expression rates are presented upon normalisation to the stable transcription of the housekeeping genes *Tuba1a*, *Hprt1* and *Sdha* including standard error from three independent experiments. Not detectable (n.d.) labels expression rates below the detection limit.

The loss of the full length ATP6AP2 as well as its N-terminal (NTF) and C-terminal fragments (CTF) was clearly visible in the *Atp6ap2* knockout samples when compared to wild-type macrophages, which verifies the successful disruption of *Atp6ap2*. Further probing for different V-ATPase subunits revealed a subsequent reduction of the V-ATPase V_0 subunit a3, which showed only 5 – 23 % of the wild-type signal intensity. The level of V_0 subunit a1 was reduced to 25 % in the *Atp6ap2* knockout macrophages, that of V_0 subunit d1 to 30 % and the level of V_0 subunit c down to 15 %. In contrast, the V_1 subunit B2 showed an equal signal strength in both genotypes, indicating that sector V_1 was not affected by the deletion in *Atp6ap2*. In summary, the impaired expression of the accessory subunit ATP6AP2 successfully induced a clear decrease in the subunits of the V-ATPase V_0 sector in peritoneal macrophages.

How this supplemental protein is aiding the assembly of the V-ATPase complex as well as the

actual assembly process is not understood completely, thus far. Previous analyses indicate that the expression of ATP6AP2 does not influence the protein stability of the V-ATPase V_0 subunits (Kinouchi *et al.*, 2013). However, ATP6AP2 might already affect the different V_0 subunits at the stage of mRNA expression. This aspect was assessed by performing qPCR utilising cDNA isolated from wild-type and *Atp6ap2* knockout peritoneal macrophages (Fig. 3.13B). The expression of the subunit a1 to a3 mRNA was comparable between both genotypes. As was already seen in wild-type and a3-deficient MEFs (3.1.2), the kidney-specific subunit a4 was not detectable at the mRNA level. A second kidney-specific isoform, V_1B1 (Nelson *et al.*, 1992; Miller *et al.*, 2005) was also not found in the mRNA pool of peritoneal macrophages. Interestingly, out of the a subunit isoforms, subunit a3 showed an over three times elevated expression level, probably highlighting its described role in phagocytosis in this cell type (Sun-Wada *et al.*, 2009). Messenger RNA coding for V_0 subunit d1/ 2 and V_0 subunit c was transcribed comparably in wild-type and *Atp6ap2* knockout macrophages, as was the mRNA belonging to the V_1 subunits B2 and A1. This data indicated that a disappearance of ATP6AP2 did not affect the transcription of the V-ATPase subunits but rather acted at a post-transcriptional level.

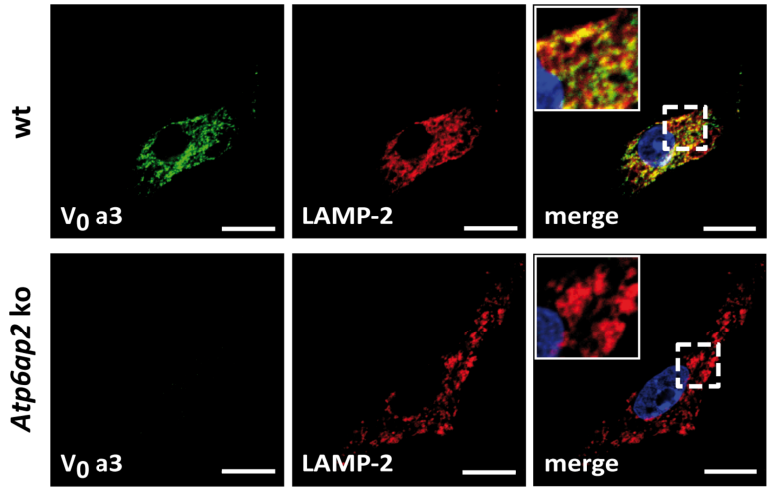

Figure 3.14: The lysosomal V_0 subunit a3 is lost in Atp6ap2 *knockout macrophages.*

Wild-type (wt) and *Atp6ap2* knockout (ko) macrophages were fixed with PFA and processed for immunostaining of the V-ATPase V_0 subunit a3. A LAMP-2 and DAPI labelling served to identify lysosomes and nuclei, respectively. Regions of interest are magnified within insets. Scale bars = 10 µm.

Because the V-ATPase V_0 subunit a3 showed the highest mRNA expression level of the analysed V_0 elements, this subunit was used to verify the deletion of *Atp6ap2* in indirect immunofluorescence analyses (Fig. 3.14). Fluorescence signals for V_0 subunit a3 were received in wild-type macrophages, in which they co-localised with a staining for LAMP-2, reflecting the

prominent lysosomal localisation. However, V_0 a3 fluorescence was completely lost in *Atp6ap2* knockout cells, again verifying the efficient knockdown of the V-ATPase complex.

3.2.3. *Atp6ap2* knockout macrophages harbour functional lysosomes

Due to the severely reduced presence of V-ATPase V_0 subunits, which presumably affected the activity of the whole V-ATPase complex, lysosome function should also be addressed in ATP6AP2-deficient macrophages. Consequently, the ability of the V-ATPase to drive lysosome acidification was measured using LysoTracker® Red staining in peritoneal macrophages of wild-type and *Atp6ap2* knockout origin (Fig. 3.15A).

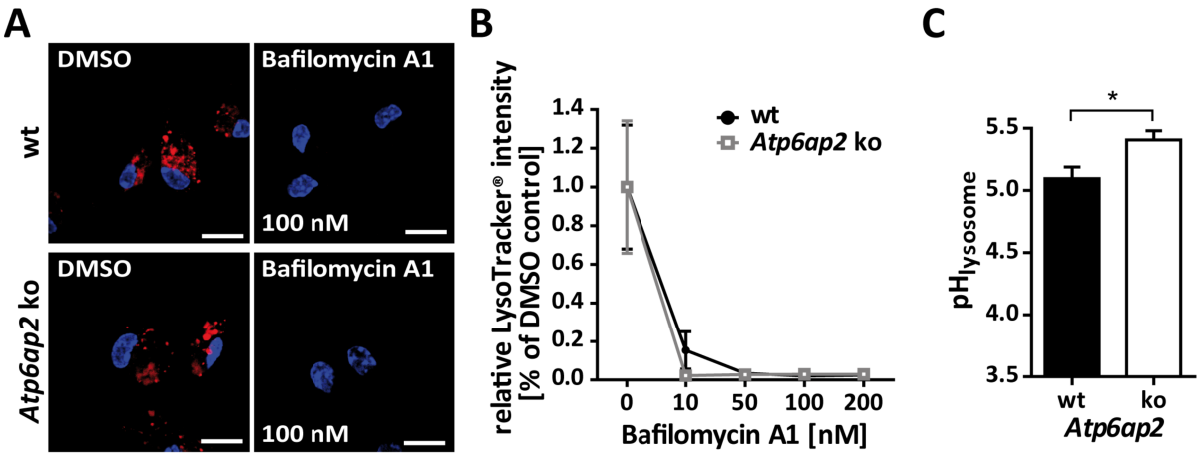

Figure 3.15: Reduced concentrations of V-ATPases affect the stability of lysosome acidification.

(A) LysoTracker® Red staining of acidic compartments in wild-type (wt) or *Atp6ap2* knockout (ko) macrophages. Cells were either pretreated with DMSO or 100 nM of the V-ATPase inhibitor bafilomycin A1 and the treatment continued during the staining procedure. Nuclei were identified by DAPI staining. Scale bars = 10 µm. (B) To assess the stability of lysosome acidification in both genotypes, LysoTracker® Red staining was conducted as in (A) while applying ascending concentrations of bafilomycin A1 as indicated. The intensity of LysoTracker® fluorescence was measured for each concentration in three independent experiments and mean values plotted as percentage of the DMSO-treated specimen ± standard error. (C) Ratiometric measurement of lysosome pH using dextran-Oregon Green™ 514 shown as mean lysosome pH ± standard error from four (wild-type) to six (*Atp6ap2* knockout) macrophage preparations (*, $P < 0.05$ according to unpaired, two-tailed Student´s t test).

Surprisingly, acid compartments could be found in both, wild-type and *Atp6ap2* knockout macrophages. In either case, the LysoTracker® Red signal was lost when 100 nM bafilomycin A1 were applied 15 minutes prior to and during the staining procedure, indicating that V-ATPases were indeed responsible for the measured lysosome acidification. The susceptibility of wild-type and ATP6AP2-deficient macrophages to bafilomycin A1 was further analysed as an

indication for the amount of functional V-ATPase complexes in the different genotypes (Fig. 3.15B). Therefore, the intensity of LysoTracker® Red was measured in the presence of varying concentrations of the agent and used to generate a dose-response curve. Reflecting the reduced amounts of the V-ATPase V_0 subunits proven in the immunoblot analysis, *Atp6ap2* knockout macrophages lost all LysoTracker® Red staining already when applying the lowest dose of bafilomycin A1 (10 nM). At the same concentration, 15 % of the signal intensity detected in DMSO-treated samples was still present in the wild-type cells. Since LysoTracker® Red cannot distinguish between different acidic pH values, the actual pH of the lysosomal lumen was measured in macrophages of both genotypes using ratiometric fluorescence analysis of dextran coupled to Oregon Green® 514 as in section 3.1.3 (Fig. 3.15C). It became apparent that lysosomes of macrophages deficient for ATP6AP2 were slightly less acidic (pH = 5.40 ± 0.16) than the respective wild-type compartments (pH = 5.09 ± 0.16), thereby confirming an alteration in the physiological function of the complex upon loss of ATP6AP2. However, the residual V-ATPases seemed *per se* sufficient to mediate a moderate lysosome acidification even in conditions of a reduced V-ATPase expression.

To determine whether the small disparity in the lysosome pH of wild-type and *Atp6ap2* knockout macrophages entailed an impairment in the function of lysosome-resident enzymes, these proteins were analysed for their activity and correct processing. The rate of hydrolysis of the artificial, chromogenic substrate 4-nitrophenyl-N-acetyl-ß-D-glucosaminide, performed by β-hexosaminidase was comparable in total lysates of wild-type (126 ± 24 mU/ mg) and *Atp6ap2* knockout macrophages (126 ± 33 mU/ mg).

Furthermore, the transport of cathepsin D from the ER to lysosomes was assessed via immunofluorescence microscopy using a co-staining of cathepsin D with the marker proteins KDEL (ER), GM130 (Golgi apparatus) and LAMP-2 (lysosomes, Fig. 3.16A). The highest rate of co-localisation was observed between the signals for cathepsin D and LAMP-2, indicating the lysosomal localisation of the protease in wild-type and ATP6AP2-deficient cells. Minor amounts of the signal for cathepsin D co-localised with KDEL and GM130 in both genotypes, reflecting the transport through these two compartments following protein synthesis. Overall, this data indicate a correct trafficking of cathepsin D to lysosomes, independent of the expression of ATP6AP2.

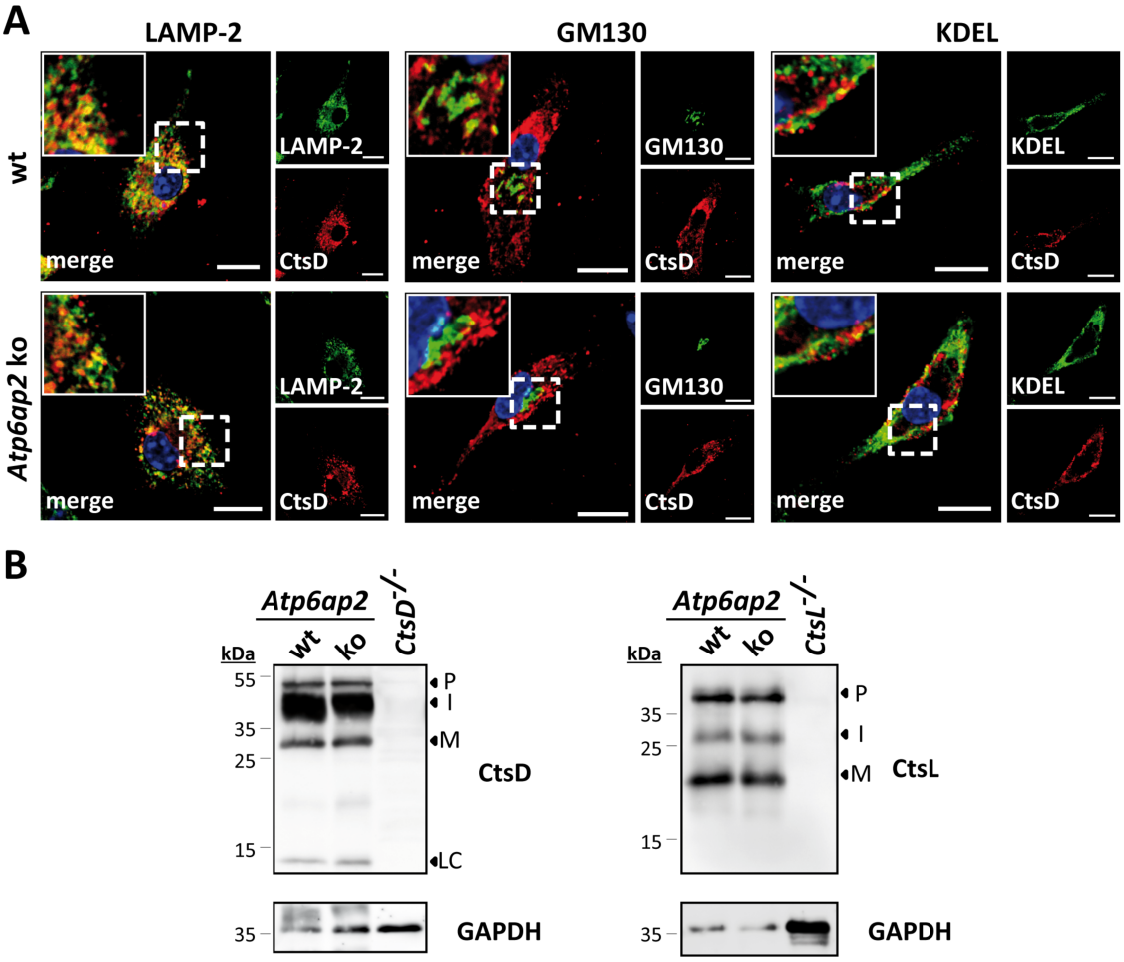

Figure 3.16: Correct cathepsin processing is independent of an ATP6AP2 expression.

(A) Indirect immunofluorescence analysis of the cathepsin D (CtsD) localisation using the marker proteins (from left to right) LAMP-2, GM130 and KDEL in wild-type (wt) and *Atp6ap2* knockout (ko) macrophages captured by confocal microscopy. DAPI staining is included within the merge channel. Insets contain magnified regions of interest. Scale bars = 10 µm. (B) Proteolytic processing of cathepsin D (left panel) and cathepsin L (CtsL, right panel) in wild-type and ATP6AP2-deficient macrophage lysates was assessed in immunoblot analyses directed against either cathepsin. Probing for GAPDH was included as loading control. Arrowheads indicate proform (P), intermediate (I) and mature (m) cathepsin as well as the cathepsin light chain (LC). *CtsD*$^{-/-}$ and *CtsL*$^{-/-}$ MEF lysates served as negative controls.

To obtain an additional read-out for cathepsin function, the processing of the cathepsins D and L was examined in total macrophage lysates through immunoblotting (Fig. 3.16B). Cell lysates of MEF lines lacking either cathepsin D or cathepsin L served as negative controls. Comparable to wild-type and *a3*$^{-/-}$ MEFs (chapter 3.1.3), probing for cathepsin D revealed a set of distinct protein signals belonging to a proform of 52 kDa, an intermediate form of 48 kDa and the mature cathepsin D of 34 kDa. Furthermore, the light chain of cathepsin D (14 kDa), which is

generated in the course of the final maturation step (Gieselmann *et al.*, 1985), was also detectable in the macrophages lysates. All forms of cathepsin D were observed with an equal intensity in wild-type and *Atp6ap2* knockout macrophages, hinting to a normal processing in both genotypes. The same, undisturbed proteolysis could be seen in western blot analyses regarding the maturation of cathepsin L.

Thus, although the lysosomes of ATP6AP2-deficient peritoneal macrophages were altogether more alkaline than their wild-type counterparts, this did apparently not affect their degradative capacity.

3.2.4. Continuous endocytic procressing in V-ATPase knockdown macrophages

Since lysosomes appeared overall functional in the *Atp6ap2* knockout macrophages, the influence of the generated V-ATPase knockdown on vesicle fusion within the endocytic system was addressed in these cells as in 3.1.4. Accordingly, wild-type and *Atp6ap2* knockout macrophages were incubated in the presence of dextran-Texas Red® (70 kDa, 0.5 mg/ ml) for 30 minutes and the fluorophore traced into lysosomes during a three hours dextran-Texas Red®-free chase period. Indirect immunofluorescence staining against LAMP-2, as a representative of lysosomes, revealed a co-localisation between LAMP-2 and Texas Red® following the pulse-chase labelling in both genotypes (Fig. 3.17A). The V-ATPase knockdown efficiency was assessed by further probing for the V-ATPase V_0 subunit a3, which showed a clear reduction in the ATP6AP2-deficient macrophages. These data indicated a proceeding endocytic flow independent of the presence of ATP6AP2.

Moreover, the ongoing delivery of the endocytic cargo to lysosomes was re-evaluated by examining the lysosomal dequenching of DQ™ Red-BSA (Fig. 3.17B). Pursuing a similar protocol as conducted for the endocytosis of dextran-Texas Red®, DQ™ Red fluorescence was observed in wild-type and *Atp6ap2* knockout macrophages after the three hours chase period. In both cases, this fluorescence co-localised with the signals of a LAMP-2 immunostaining, verifying the regular flow of the endocytic system in conditions of a V-ATPase knockdown and again demonstrating the ongoing degradation in lysosomes of ATP6AP2-deficient macrophages.

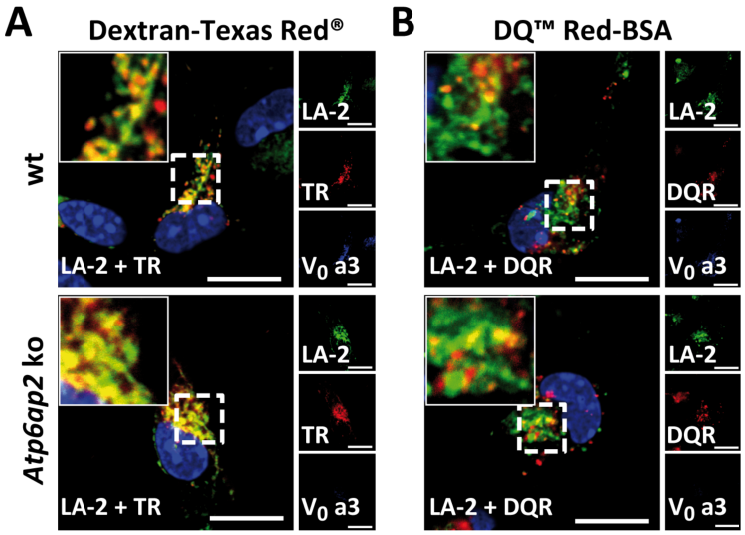

Figure 3.17: Continuous endocytic flux in macrophages lacking ATP6AP2.

(A) Endocytic delivery of dextran-Texas Red® (TR) to lysosomes of wild-type (wt) and *Atp6ap2* knockout (ko) macrophages upon 30 minutes labelling and an additional three hours incubation period in the absence of extracellular tracer molecules. Probing for LAMP-2 (LA-2) was performed to detect lysosomal structures, while DAPI incorporation was used to assess nuclei. Further immunostaining was directed against V_0 subunit a3 to prove the successful knockout of *Atp6ap2*. Insets display higher magnification of indicated regions of interest. (B) Uptake and intracellular proteolysis of the self-quenched DQ™ Red-BSA (DQR) similar as in (A). Scale bars = 10 µm

3.2.5. Depletion of ATP6AP2 does not impair phagosome maturation

On the basis of the continuous endocytic flux and the absence of an acidification-related distortion in the *Atp6ap2* knockout macrophages, further studies were able to evaluate the influence of the physical presence of the V-ATPase complex, only. In this respect, phagosome maturation, and therefore phagosome-lysosome fusion was examined in these cells. Being professional phagocytes, macrophages take up murine IgG-opsonised latex beads naturally and without the additional need for the transfection of an Fcγ receptor. Wild-type and *Atp6ap2* knockout macrophages were incubated with such modified latex beads (MOI = 8) for 15 minutes, and the newly generated latex bead-containing phagosomes were allowed to mature for one hour, during which the localisation of the beads was analysed by confocal microscopy (Fig. 3.18).

Following this procedure, a LAMP-2 positive halo could be found around the internalised latex beads by immunostaining in macrophages of both genotypes. This lysosomal localisation implied a completed phagosome maturation, which was unaffected by the significant drop in the concentration of V-ATPase complexes. The V-ATPase knockdown was again controlled by probing for the V_0 subunit a3.

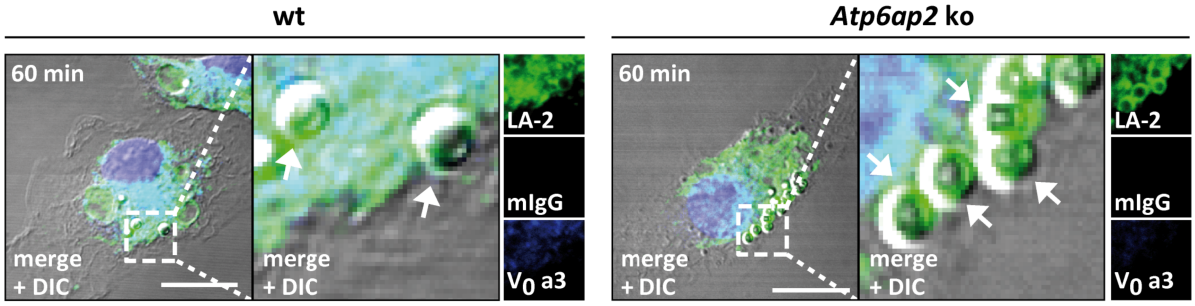

Figure 3.18: Knockout of Atp6ap2 *does not disturb phagosomal acquisition of LAMP-2.*

Wild-type (wt) and *Atp6ap2* knockout (ko) macrophages were cultivated in the presence of murine IgG-opsonised latex beads at an MOI of eight for 15 minutes and phagosome maturation allowed for further 60 minutes before the localisation of the internalised latex beads was assessed by confocal laser scanning microscopy. LAMP-2 staining (LA-2) served to prove constituents of lysosomal membranes on the mature phagosome. Arrows within magnified regions of interest point to LAMP-2 halos surrounding the internalised globules. Labelling of V_0 subunit a3 was used to control for reduced V-ATPase expression levels. Merge images include DAPI staining to visualise nuclei and the DIC channel. Extracellular latex beads were assessed with antibodies directed against murine IgG (mIgG) before fixation and the further staining procedure. Scale bars = 10 µm.

In a co-operation with the groups of *Prof. Dr. Albert Haas (Institute for Cell Biology, University of Bonn)* and *Prof. Dr. Gareth Griffiths (Department of Biosciences, University of Oslo)* the process of phagosome maturation was further defined by electron microscopy. In an experimental setup designed to determine the rate of phagosome-lysosome fusion, the delivery of lysosomal cargo to the developing phagosomes was analysed (refer to Fig. 4.3). To our surprise, macrophages lacking ATP6AP2 and consequently bearing reduced expression levels of the V-ATPase complex showed even more cargo delivery per phagosome than wild-type cells, possibly reflecting an increased rate of phagosome-lysosome fusion (presented in section 4.2.3 and (Kissing *et al.*, 2015)).

Overall these findings did not support a fusion promoting role for the V-ATPase complex in the merger of phagosomes with lysosomes.

3.2.6. *Atp6ap2* knockout macrophages show unaltered fusion kinetics

The elevated delivery of lysosomal cargo to the phagosomes of *Atp6ap2* knockout macrophages that was observed in electron microscopy particularly reflected an increase in small area deposits. This hints to the occurrence of the kiss and run phenomenon. Kiss and run terms an incomplete fusion event that is characterised by the transient mixing of two lipid bilayers and will ultimately result in separated vesicles (Desjardins *et al.*, 1994; Desjardins, 1995). During the

connection between the vesicles, a transient fusion pore is formed that allows the rapid transfer of small solutes but impedes the exchange of large cargo molecules (Wang and Goren, 1987; Storrie and Desjardins, 1996; Bright *et al.*, 2005). Dextran bearing a molecular weight of 70 kDa was reported to be delivered only in later stages of endosomes maturation (Wang and Goren, 1987). Hence, to further characterise fusion in the absence of ATP6AP2, the endocytic delivery of such dextran molecules was assessed with respect to its kinetics in wild-type and ATP6AP2-deficient macrophages.

Therefore, the endocytic compartments of macrophages were labelled overnight with dextran-fluorescein (-FITC, 0.25 mg/ ml) bearing a molecular mass of 10 kDa and this complex cleared of early compartments by a three hours incubation in DMEM only. Dextran-Texas Red® with a molecular weight of 70 kDa (0.5 mg/ ml) was then added for up to 60-minutes and the delivery of this compound to the pre-labelled late endocytic compartments was analysed by confocal microscopy (Fig. 3.19A).

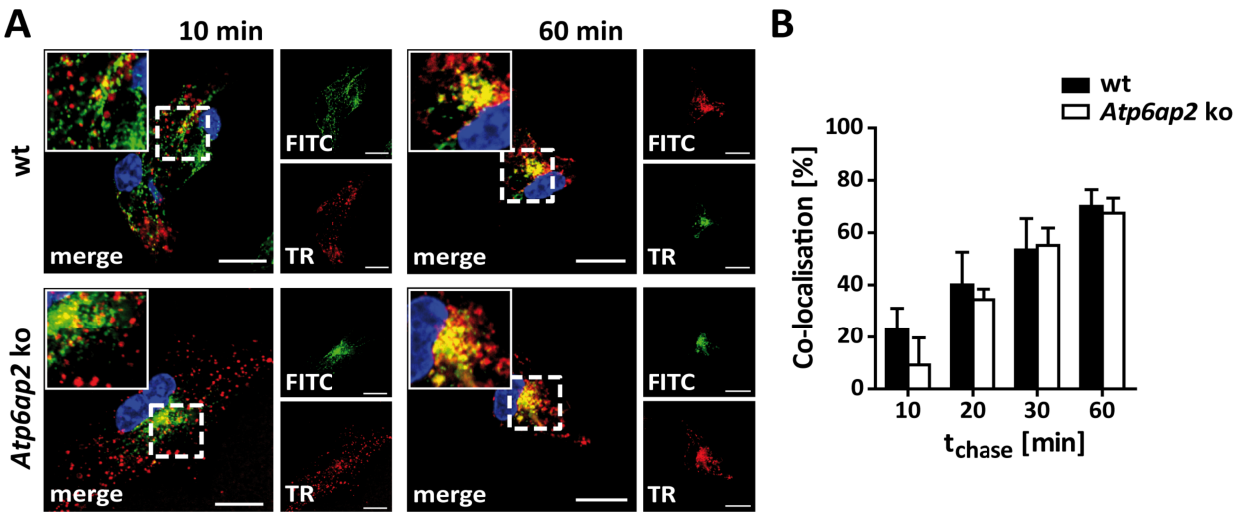

Figure 3.19: Comparable rates of vesicle fusion in presence or absence of ATP6AP2.

(A) Lysosomes of wild-type (wt) and *Atp6ap2* knockout (ko) macrophages were loaded with dextran-FITC (FITC, 10 kDa) overnight and the compound cleared of early compartments during a three hours chase period. To investigate fusion processes, dextran-Texas Red® (TR, 70 kDa) was applied for 30 minutes and the subsequent transport to pre-labelled compartments tracked by fluorescence microscopy for further 60 minutes. Nuclei are visualised by DAPI staining. Insets show magnified regions of interest. Scale bars = 10 µm. (B) Co-localisation between both dextran derivatives was plotted as Pearson´s correlation coefficients in dependence on the incubation period following dextran-Texas Red® uptake. Shown are mean coefficients ± standard error from three independent macrophages preparations per genotype.

After ten minutes in the presence of the high molecular weight dextran, Texas Red® fluorescence was visible at the periphery of all cells and only partially overlapped with the

signals of the pre-loaded low molecular weight dextran-FITC. However, upon longer incubation up to 60 minutes, both fluorescence signals showed a complete overlap in wild-type and *Atp6ap2* knockout macrophages. The rate of co-localisation between Texas Red® and FITC was expressed using the Pearson´s correlation coefficient for the different time points, which revealed a comparable increase from 10 % to 70 % independent of the ATP6AP2 expression (Fig. 3.19B). This suggested similar fusion kinetics in both genotypes as well as functional kiss and run size selection.

Taken together the analyses of phagosome maturation and vesicle fusion conducted in this thesis and in co-operation with the groups from Bonn and Oslo, all made it very unlikely that the physical presence of the V-ATPase complex exerts a role in the fusion between phagosomes and lysosomes.

3.2.7. Vesicle fusion in *Atp6ap2 LysM-Cre* conditional knockout macrophages

To validate the results generated with peritoneal macrophages of *Atp6ap2 Mx1-Cre* conditional knockout mice, an *Atp6ap2 LysM-Cre* conditional knockout mouse model was established to reproduce phagosome-lysosome fusion in the absence of ATP6AP2 and under conditions of reduced V-ATPase expression. The *LysM-Cre* transgene describes an insertion of the coding region for the Cre recombinase into the lysozyme 2 gene locus. This system targets cells of the myeloid cell lineage, including macrophages, without the requirement for an additional induction (Clausen *et al.*, 1999). The breeding strategy matched that of the initial *Atp6ap2 Mx1-Cre* mouse line as described in chapters 2.6.2 and 3.2.1. Animals with floxed *Atp6ap2* but negative for the *LysM-Cre* transgene were termed wild-type controls and mice bearing both, the floxed *Atp6ap2* loci and the *LysM-Cre* transgene were called *LysM* conditional knockout animals. Thioglycollate treatment three days prior to sacrificing of the animals for experimental analysis was used to elucidate peritoneal macrophages in wild-type controls and *Atp6ap2 LysM* conditional knockout mice.

3.2.7.1 Atp6ap2 LysM *conditional knockout macrophages show lysosomal acidification*

The deletion of *Atp6ap2* in peritoneal macrophages isolated from *LysM* conditional knockout animals was characterised at the level of protein expression using immunoblot analysis (Fig. 3.20A). Similar to the results obtained with macrophages from *Mx1-Cre* transgenic

knockout mice, full length and CTF of ATP6AP2 were almost absent in the lysates of *Atp6ap2 LysM* conditional knockout cells when compared to the wild-type lysates. Accordingly, the V-ATPase V_0 subunits a3 was present at only 5 % - 13 % of the wild-type protein level. Furthermore, the V_0 subunits c (38 %), d1 (21 %) and a1 (28 %) were reduced in the samples without ATP6AP2 expression and these lysates showed a slight decrease in the V_0 a2 signal as well. Like in the *Mx1-Cre*-mediated knockout model, the V-ATPase V_1 subunit B2 was not affected, showing the same signal intensity in wild-type and ATP6AP2-deficient macrophages. Overall the V-ATPase knockdown generated with the system using *LysM-Cre* seemed to be equivalent to the V-ATPase manipulation carried out in the *Mx1-Cre*-based knockout animals.

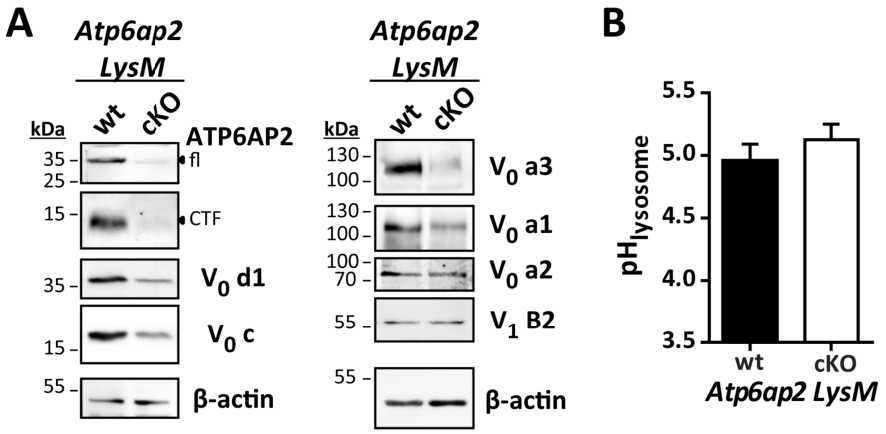

Figure 3.20: Unaltered lysosome pH albeit efficient V-ATPase reduction in Atp6ap2 LysM *conditional knockout macrophages.*

(A) Loss of ATP6AP2 and concomitant reduction of the indicated V-ATPase subunits was examined by immunoblot analyses of lysates from *Atp6ap2 LysM* conditional knockout (cKO) macrophages in comparison to wild-type cells. Full length (fl) and C-terminal fragments (CTF) of ATP6AP2 are indicated by arrowheads. Probing for β-actin was used to control for equal protein loading. (B) The lysosome pH of wild-type and ATP6AP2-depleted peritoneal macrophages was measured utilising dextran-Oregon Green® 514 based on the generation and non-linear regression of an *in situ* calibration curve. Extrapolated values of five individual macrophages isolations per genotype were used to calculate a mean lysosome pH and standard errors.

Although again, the V_0 sector of the V-ATPase was present at significantly reduced levels, the lysosome pH in macrophages of *Atp6ap2 LysM* conditional knockout mice (5.13 ± 0.25) appeared unchanged in comparison to wild-type macrophages (4.96 ± 0.26) as measured by dextran-Oregon Green® 514 fluorescence (Fig. 3.20B). This might reflect a minor difference in the *Atp6ap2* knockout efficiency between the *loxP/ Cre* systems utilising the *Mx1* or the *LysM* promoter, respectively.

3.2.7.2 *Phagosomes of* Atp6ap2 LysM *conditional knockout macrophages acquire LAMP-2*

In order to verify the previously observed independence of fusion of the V-ATPase complex, the analysis of phagosome maturation as in 3.2.5 was continued using this second V-ATPase knockdown mouse model. Consequently, peritoneal macrophages isolated from wild-type and *Atp6ap2 LysM* conditional knockout animals were incubated with murine IgG-opsonised latex beads for 15 minutes and the maturation of the latex bead-containing phagosomes analysed after one additional hour in the absence of external beads by confocal fluorescence microscopy (Fig. 3.21). An immunostaining against LAMP-2 was performed to correlate the localisation of the internalised latex beads with lysosomes. Macrophages derived from both genotypes showed the typical halo of LAMP-2 fluorescence signals around their phagocytosed latex beads, indicating a completed phagosome maturation and matching the data generated with the *Mx1-Cre* ATP6AP2-deficient macrophages.

Altogether, a promoting function for the V_0 sector of the V-ATPase in phagosome-lysosome fusion could not be supported in two independent murine V-ATPase knockdown models, thereby questioning the conservation of this function in different species as it was reported before (Hiesinger *et al.*, 2005; Liegeois *et al.*, 2006; Sun-Wada *et al.*, 2006; Peri and Nusslein-Volhard, 2008; Di Giovanni *et al.*, 2010; Strasser *et al.*, 2011; Poea-Guyon *et al.*, 2013; Wang *et al.*, 2014).

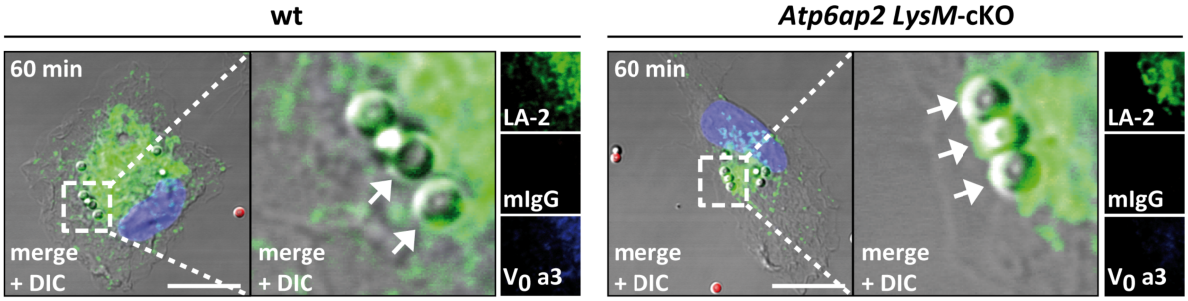

Figure 3.21: Atp6ap2 LysM *conditional knockout macrophages display phagolysosome formation.*

Wild-type (wt) and *Atp6ap2 LysM* conditional knockout (cKO) macrophages were subjected to murine IgG-opsonised latex beads (MOI = 8) for 15 minutes, the bead excess was washed away and phagosome maturation was allowed to progress for 60 minutes. Extracellular beads were then labelled with murine IgG-detecting antibodies (mIgG), and samples were fixed and immunostained for the lysosomal protein LAMP-2 (LA-2). Additional probing was used to reveal V_0 subunit a3 expression in both genotypes. Merge images include DAPI-decorated nuclei and the DIC channel. Latex beads surrounded by a LAMP-2 halo as indicative for completed phagosome maturation are highlighted by arrows. Scale bars = 10 µm.

3.3. The autophagic pathway in the absence of ATP6AP2

Up to that point, murine V-ATPases seemed dispensable for vesicle fusion along the endocytic and phagocytic axes. Yet, these events comprise only a fraction of the cellular processes that rely on the mixing of two compartments. Another pathway that is linked to the V-ATPase complex, and which is founded on sequential fusion steps, is autophagy. Autophagy aims to degrade the cell´s own constituents, *e.g.* proteins and small compartments in order to refresh the supply of nutrients and free amino acids (Mizushima and Komatsu, 2011). For this purpose, a newly formed autophagosome has to acquire degradative properties through the mixture with late endosomes and lysosomes. While these fusion events are discussed to depend on the presence of V-ATPase, the regulation of autophagy is also influenced by the proton pumping complex, since it is involved in the sensing of accessible amino acids and the subsequent signalling to the mechanistic target of rapamycin complex 1 (mTORC1, (Zoncu *et al.*, 2011)). A high abundance of amino acids yields an activation of mTORC1, which then blocks the initiation of autophagy and hence acts as a switch between catabolism and anabolism. Therefore, the impact of the reduced V-ATPase expression level on autophagy and mTORC1 was analysed in *Atp6ap2* conditional knockout mice as described in the following section.

3.3.1. Dysregulation of autophagy in *Atp6ap2* conditional knockout liver

The liver represents the site for multiple metabolic processes, such as fatty acid synthesis and the storage and mobilisation of glycogen multimers (Czaja *et al.*, 2013). Therefore, the liver bears a high basal rate of autophagy (Czaja *et al.*, 2013) and is suited to study the self-degradative process in dependence on the V-ATPase expression level. The general characterisation of the *Atp6ap2* conditional knockout and the *Mx1-Cre* reporter mice (3.2.1) revealed that this tissue was also targeted in *Mx1-Cre*-based knockout systems. Thus, the liver of *Atp6ap2* conditional knockout animals was chosen as the appropriate platform to peruse autophagy and the mTORC1 signalling.

The efficiency of *Atp6ap2* deletion and its ensuing effect on V-ATPase expression in liver was assessed using immunoblot analyses (Fig. 3.22A). The full length form and the CTF of ATP6AP2 were clearly reduced in total liver lysates of *Atp6ap2* conditional knockout mice when compared to the wild-type controls. However, both forms of the protein remained detectable, implying that the interferon α-induced knockout did not target the liver in all its components. The analysis of the V-ATPase V_0 subunits revealed an up to 80 % reduction of V_0 subunit a3 and

as much as 68 % less V_0 subunit a1 in the ATP6AP2-depleted samples. The V_0 subunit d1 showed as low as 33 % of the wild-type expression rate and V_0 subunit c went down to 40 %. To clarify, which cell species were effectively targeted in the *Atp6ap2* conditional knockout liver, the *Mx1-Cre* reporter mice were analysed by confocal fluorescence microscopy. An EYFP fluorescence was visible in hepatocytes and Kupffer cells but not in endothelial cells on liver sections of these mice (Fig. 3.22B).

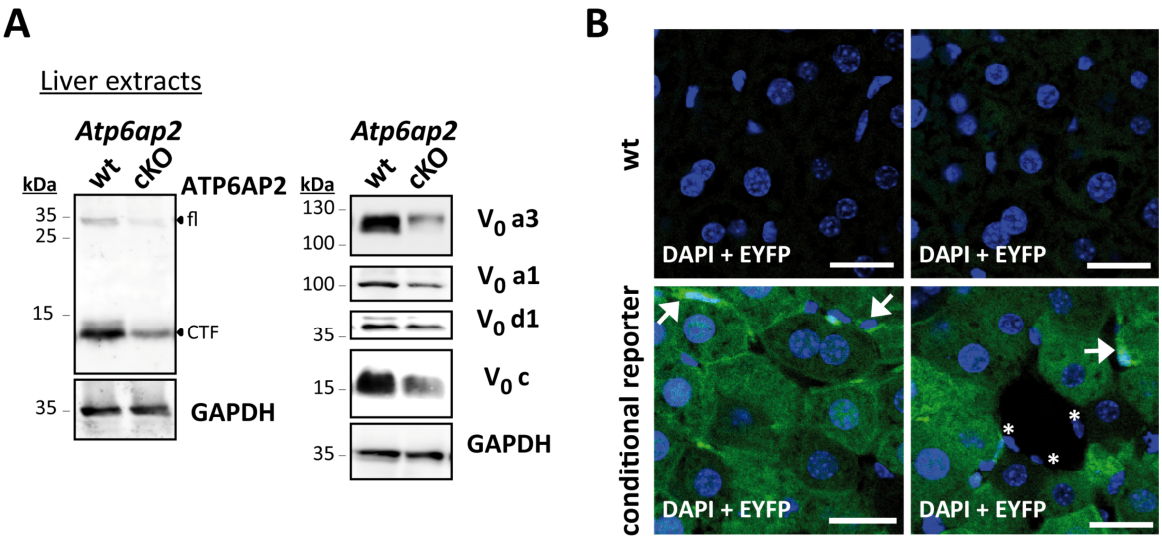

Figure 3.22: Livers of Atp6ap2 *conditional knockout mice harbour targeted and non-targeted cell populations.*

(A) ATP6AP2 expression was analysed by immunoblotting of wild-type (wt) and *Atp6ap2* conditional knockout (cKO) liver extracts. Full length (fl) and C-terminal fragments (CTF) of ATP6AP2 are highlighted by arrowheads. Denoted V-ATPase subunits were assessed in addition. Detection of GAPDH was used as a loading control. (B) *Mx1-Cre*-induced EYFP production was visualised in PFA-fixed liver sections of wild-type and conditional reporter animals. While the main population of liver consists of hepatocytes, liver-resident Kupffer and endothelial cells are indicated by arrows or asterisks, respectively. DAPI incorporation was utilised to reflect nuclei. Scale bars = 20 µm.

The deficiency of ATP6AP2 caused a significant increase in liver size and liver weight in comparison to the wild-type controls (Fig. 3.23A, B). Hematoxylin and eosin staining of cryo-sectioned liver slices revealed a concomitant increase in the size of the *Atp6ap2* knockout hepatocytes (Fig. 3.23C).

This morphological difference between wild-type and *Atp6ap2* conditional knockout liver was defined at an ultra-structural level using electron microscopy in co-operation with *Prof. Dr. Renate Lüllmann-Rauch (Institute of Anatomy, University of Kiel)*. Upon depletion of ATP6AP2 and the associated reduction in the presence of V-ATPase complexes, hepatocytes accumulated densely packed vesicles that contained material of variable electron density (Fig. 3.24).

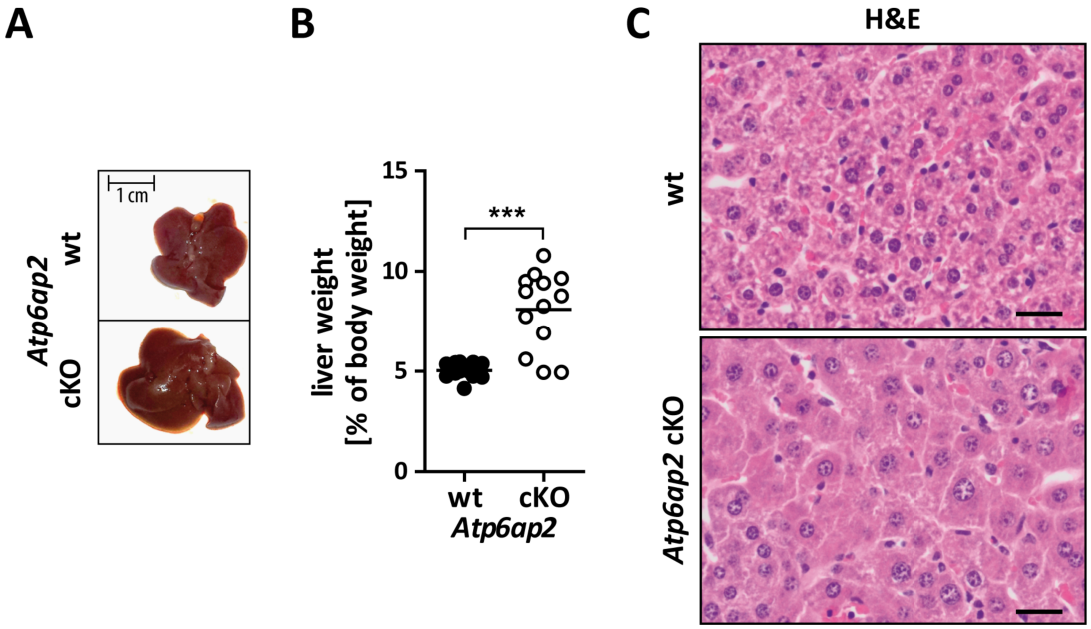

Figure 3.23: Hepatocyte- and Kupffer cell-specific depletion of ATP6AP2 results in hepatomegaly.

(A) Liver morphology of wild-type control (wt) versus *Atp6ap2* conditional knockout (cKO) mice. (B) Livers of 13 animals per genotype were weighed and the liver masses plotted in relation to the total body weights (***, $P < 0.001$ according to an unpaired, two-tailed Student´s t test). (C) Hematoxylin and eosin (H&E) staining was applied on cry-sectioned liver slices of wild-type and ATP6AP2-deficient background to visualise the molecular structure of the tissue. Scale bars = 25 µm

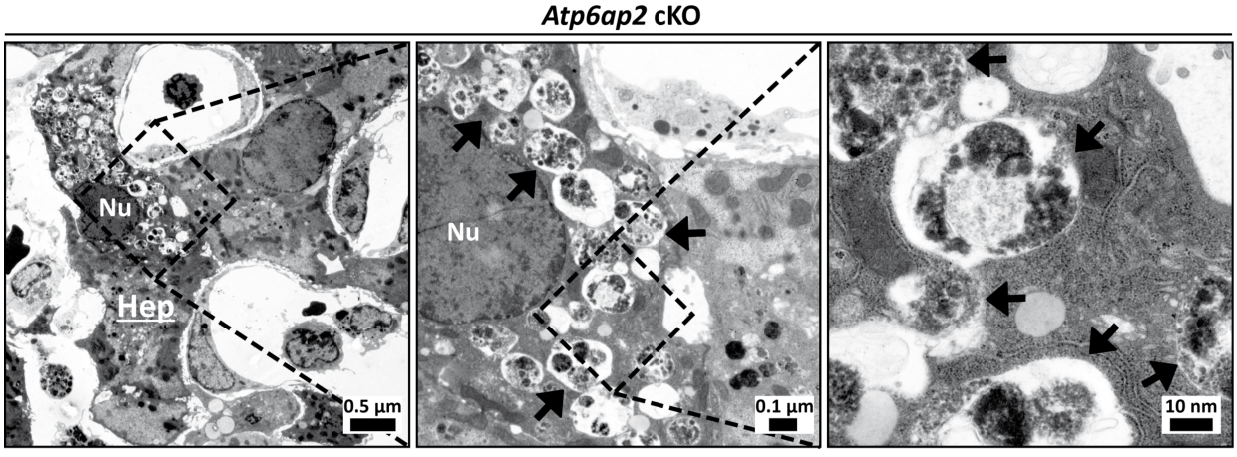

Figure 3.24: Accumulation of vesicular structures in Atp6ap2 *knockout hepatocytes.*

Electron micrographs (courtesy of *Prof. Dr. Renate Lüllmann-Rauch*) generated from glutaraldehyde-fixed liver samples and displaying the liver ultra-structure in *Atp6ap2* conditional knockout (cKO) mice. An abnormal hepatocyte (Hep) and its nucleus (Nu) are marked. Accumulating vesicles are indicated by arrows. From the left to the right panel, characteristic sections are resolved with increasing magnification.

The vesicle appearance suggested an autophagosomal origin, and at least a partial degradative activity was indicated by the dark, electron dense constituents. Whether these vesicles belonged to the autophagic pathway was examined by immunofluorescence staining of liver sections generated from both genotypes (Fig. 3.25A).

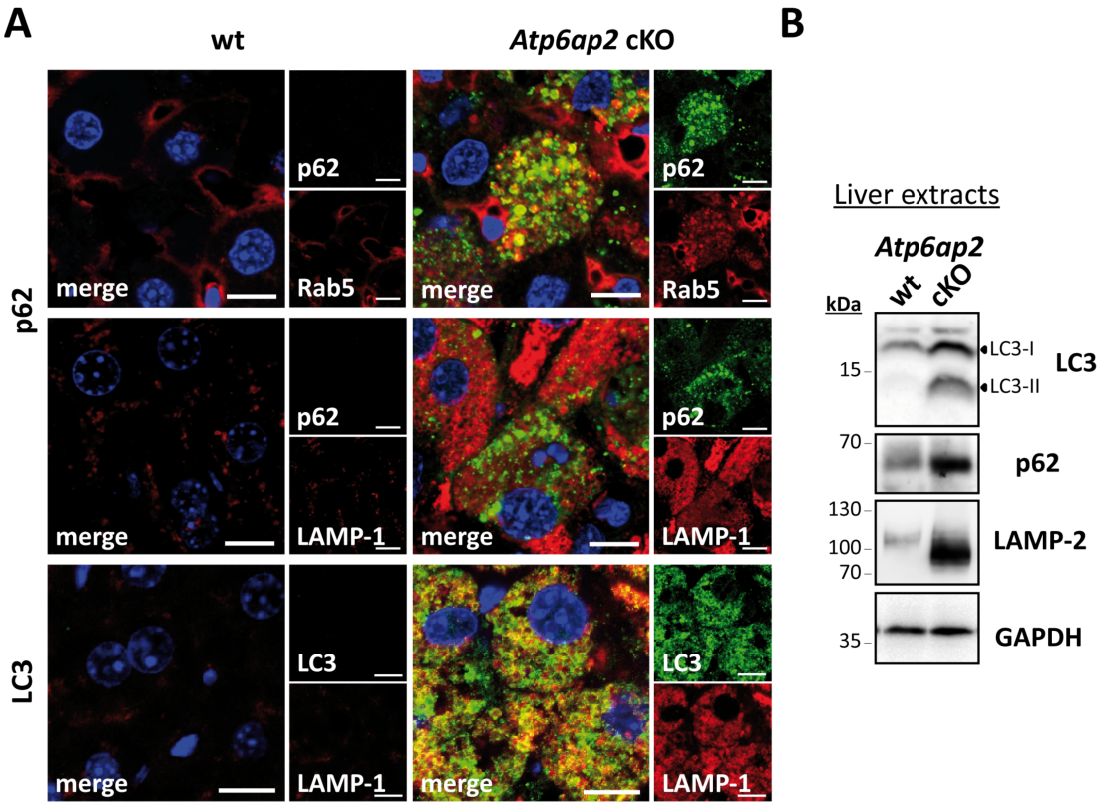

Figure 3.25: Deprivation of ATP6AP2 induces an increased abundance of endocytic and autophagic marker proteins.

(A) Indirect immunofluorescence labelling of the autophagy- and proteasome-related proteins LC3 and p62 on liver cryo-sections of wild-type (wt) and *Atp6ap2* conditional knockout (cKO) animals. Probing for LAMP-1 and Rab5 was performed to visualise components of the endocytic pathway that are prone to fuse with autophagosomes. Scale bars = 20 µm. (B) The occurrence of LC3, p62 and LAMP-2 was studied for both genotypes by utilising immunoblot analysis of whole liver extracts. Unconjugated LC3-I and conjugated LC3-II are indicated by arrowheads. GAPDH served as a loading control.

Indeed, the microtubule-associated protein 1A/ 1B-light chain 3 (LC3), which is actively recruited to the membrane of developing autophagosomes (Kabeya *et al.*, 2000), gave an increased signal in liver samples lacking ATP6AP2 in hepatocytes and macrophages. The same was observed for sequestome 1/ p62, an ubiquitin-binding protein that acts as an adaptor

between ubiquitinated autophagic cargo and LC3 (Bjorkoy *et al.*, 2005; Pankiv *et al.*, 2007; Lamark *et al.*, 2009). Interestingly, LC3 and p62 are regularly degraded at the stage of autolysosomes, and the decline of clearance may be an indication for an affected autophagosome maturation in the liver of *Atp6ap2* conditional knockout animals. At the same time, the small GTPase Rab5, as a marker protein for early endosomes, showed a strong staining in the knockout tissues, which was less prominent in sections from wild-type animals. The same signal increase was also observed for LAMP-1 positive lysosomes on ATP6AP2-depleted liver slices. In the co-staining, p62 signals localised mainly to compartments marked by Rab5 and not by LAMP-1. In contrast, LC3 signals displayed a considerable co-localisation with the lysosomal LAMP-1. Because autophagy is also tightly linked to the proteasome, the proteasomal regulator ubiquitin was further analysed by immunofluorescence staining and revealed plenty of ubiquitin-ligated proteins in the *Atp6ap2* knockout hepatocytes (data not shown). Hence, the proteasomal clearance might be impaired upon loss of ATP6AP2, too.

The observed disparities in the abundance of autophagic and endolysosomal proteins were further characterised by immunoblot analyses (Fig. 3.25B). Probing for LC3 confirmed its activation for autophagy in ATP6AP2-depleted liver lysates, since the conjugate of LC3 to phosphatidylethanolamine (LC3-II) was clearly detectable. The ratio of LC3-II to the unconjugated LC3-I is a measure for autophagy initiation and was increased 5-fold upon loss of ATP6AP2. The level of p62 was found to be twice as high in lysates of *Atp6ap2* conditional knockout liver when compared to wild-type controls and LAMP-2 signals increased to 11-fold.

Altogether, the deletion of *Atp6ap2* triggered a drastic morphological change in hepatocytes that reflected alterations in the vesicle composition and the autophagic pathway of these cells. The cause for this development could be a complex mixture of primary and secondary events as well as of intracellularly or extracellularly initiated signalling cascades.

Three conceivable reasons for the vesicle accumulation were analysed in the following segments: an impairment in lysosome acidification and subsequent proteolytic degradation, a defect in autolysosome formation due to a necessity of the V-ATPase complex for vesicle fusion and a dysregulation of mTORC1 signalling.

3.3.2. Isolated ATP6AP2-deficient hepatocytes contain proteolytically active compartments

Previous reports support a deficiency of lysosome acidification as the cause for a similar autophagy-related phenotype in *Atp6ap2* conditional knockout models for cardiomyocytes and podocytes (Kinouchi *et al.*, 2010; Oshima *et al.*, 2011; Riediger *et al.*, 2011). Hence the proton pumping function of the V-ATPase was assessed in ATP6AP2-depleted hepatocytes by LysoTracker® Red staining.

Hepatocytes were isolated from animals of wild-type or *Atp6ap2* conditional knockout origin five days after the last poly (I:C) application for the knockout induction. However, the yield of isolated cells was reduced by almost 90 % in knockout animals as compared to the wild-type controls, indicating that the *Atp6ap2* knockout cells exhibited a compromised ability to survive the isolation procedure. Wild-type and the remaining 10 % of isolated ATP6AP2-depleted hepatocytes were then incubated in the presence of the acidotropic dye LysoTracker® Red and analysed by confocal microscopy (Fig. 3.26A).

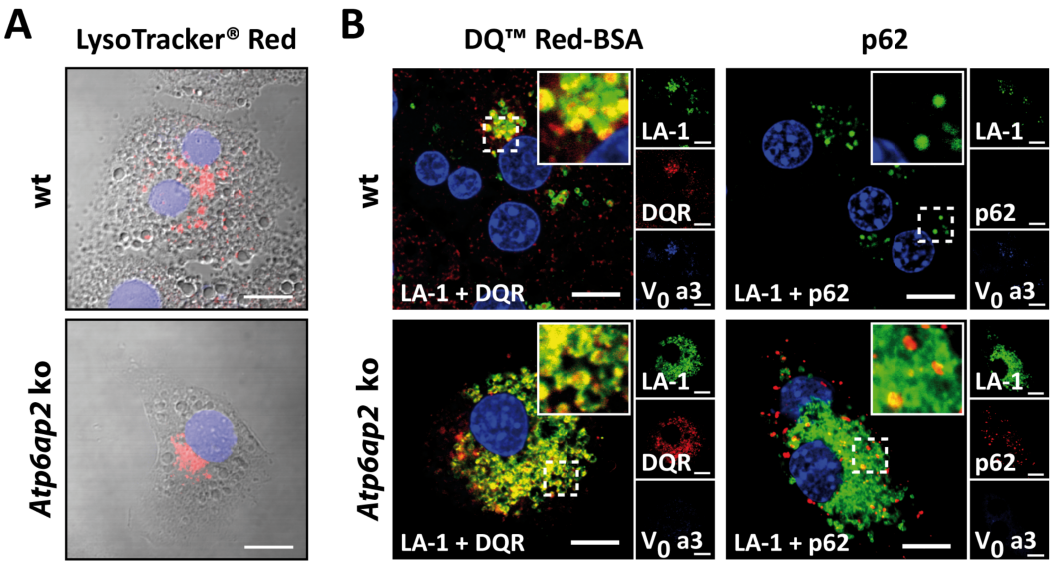

Figure 3.26: ATP6AP2 seems dispensable for lysosome acidification and function in cultured hepatocytes.

Analysis of isolated, primary hepatocytes prepared at day five after *Atp6ap2* knockout induction. (**A**) Acidic compartments of wild-type (wt) and *Atp6ap2* knockout (ko) cells were revealed by LysoTracker® Red staining. Hepatocytes were post-fixed and incubated with DAPI to dye nuclei. (**B**) Fluorescence microscopic analysis of either DQ™ Red-BSA (DQR) dequenching within proteolytically active compartments (left panel) or immunolabelled p62 (right panel). Lysosomes are visualised by a LAMP-1 immunostaining. The V_0 subunit a3 was assessed to verify a loss of ATP6AP2 in *Atp6ap2* knockout populations. Magnified regions of interest are shown in insets. Scale bars = 10 µm. Experiments were conducted in collaboration with *Sönke Rudnik (University of Kiel).*

Both hepatocyte populations were positive for LysoTracker® Red staining, reflecting the presence of acidic compartments regardless of the expression of ATP6AP2. However, when *Atp6ap2* knockout hepatocytes occasionally displayed a lack of LysoTracker® Red signals, these cells seemed to be in a stage of progressing apoptosis (data not shown). Strikingly, while most of the wild-type hepatocytes shared a common binucleated appearance, the majority of *Atp6ap2* knockout hepatocytes harboured only one nucleus. This might imply either a shift to mononucleated hepatocytes under V-ATPase knockdown conditions or a lower susceptibility of these mononucleated cells during the isolation procedure.

The LysoTracker®-positive hepatocyte population of the V-ATPase knockdown cells was then analysed in regard to its lysosomal proteolysis and the activity compared to that of wild-type cells. Therefore, the uptake and dequenching of DQ™ Red-BSA was examined by fluorescence microscopy (Fig. 3.26B). The degradation of BSA was taking place in both genotypes since a fluorescence signal was observable in wild-type and *Atp6ap2* knockout hepatocytes and this fluorescence co-localised with the lysosome-denoting LAMP-2 staining. The loss of ATP6AP2 was visualised through the reduction of the V-ATPase complex by staining for the V_0 subunit a3. Interestingly, *Atp6ap2* knockout hepatocytes that featured degradative, acidic compartments still showed an accumulation of LAMP1 as well as an accumulation of p62 (Fig. 3.26B).

Together these results made the complete loss of acidification and concomitant obstruction of lysosomal protein degradation an unlikely cause for the drastic phenotype seen in the ATP6AP2-depleted liver. However, the experiments provided here are not sufficient to detect small changes in the lysosome pH or the proteolytic activity that might induce the observed accumulation of vesicle.

3.3.3. Intracellular fusion proceeds in hepatocytes that lack ATP6AP2

Until recently, a defect in the fusion between autophagosomes and lysosomes has been linked to an alkalisation of lysosomes (Yamamoto *et al.*, 1998; Kawai *et al.*, 2007). New findings challenged this view by disclosure of an uncoupling of autolysosome formation and the proton pumping function of the V-ATPase in *drosophila melanogaster* (Mauvezin *et al.*, 2015). In addition, evidence for proceeding autophagosome-lysosome fusion upon depletion of the V-ATPase was provided.

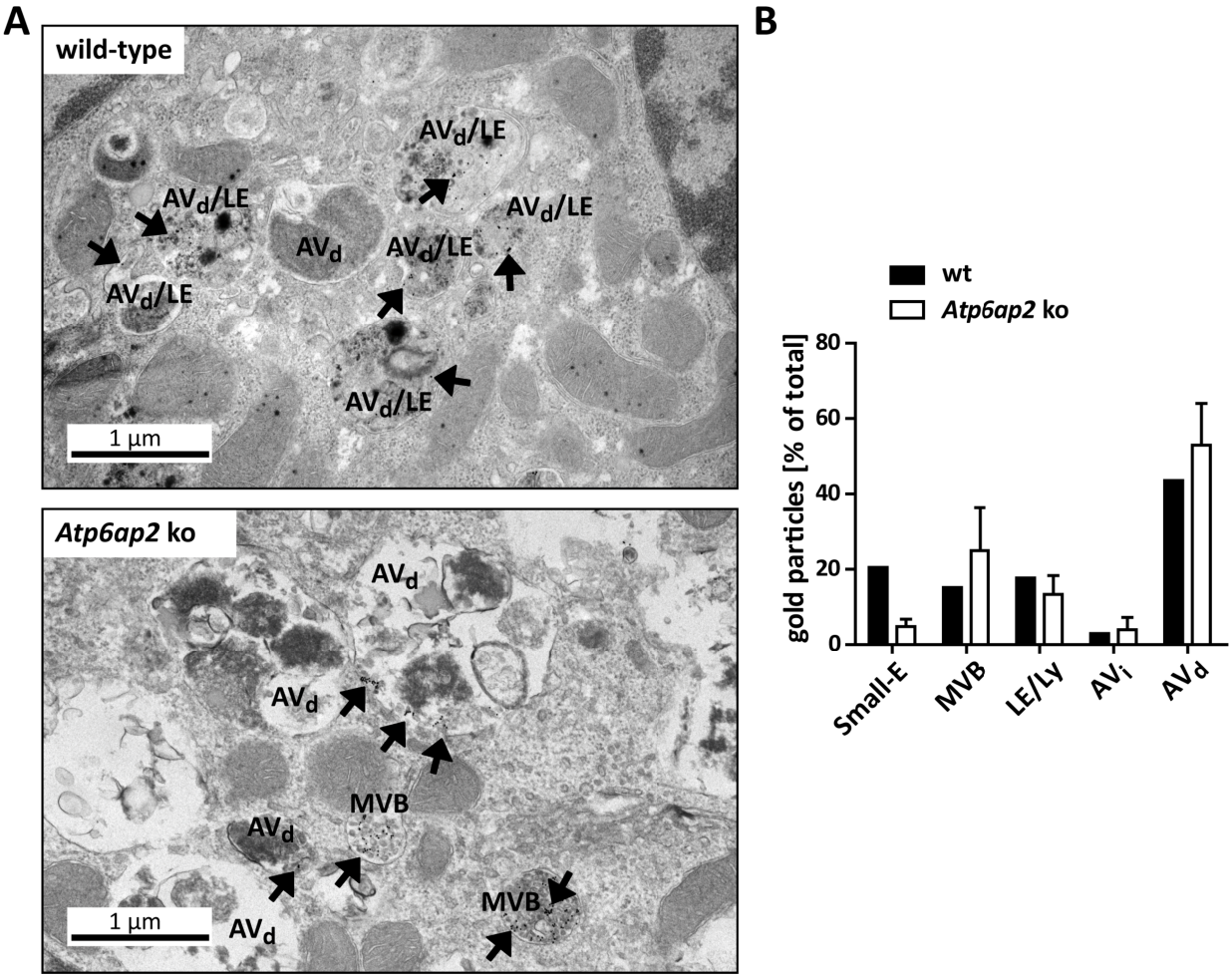

Figure 3.27: Extracellular BSA-gold reaches autolysosomes independent of the ATP6AP2 expression.

(A) Primary hepatocytes of wild-type (wt) or *Atp6ap2* knockout (ko) background were incubated with BSA-gold (10 nm, OD = 5) for one hour, followed by a two hours incubation period in the absence of the tracer. Glutaraldehyde-fixed cells were processed and analysed in electron microscopy in co-operation with *Prof. Dr. Eeva-Liisa Eskelinen (University of Helsinki)*. Shown are representative micrographs and arrows indicating gold depositions within multi-vesicular bodies (MVB), late endosomes (LE) and degradative autophagic vacuoles (AV_d). (B) At least 1300 gold particles were counted for each individual preparation of one wild-type and two knockout hepatocyte populations and assigned to groups summarising small endosomes (Small-E), multi-vesicular bodies (MVB), late endosomes/ lysosomes (LE/Ly) and immature (AV_i) or degradative (AV_d) autophagic vacuoles. Mean values ± standard deviation are depicted for *Atp6ap2* knockout hepatocytes.

Whether these results are applicable to autolysosome formation in murine hepatocytes, should be determined via the endocytic uptake and intracellular delivery of BSA-gold. Thus, wild-type and *Atp6ap2* knockout hepatocytes were cultured in the presence of BSA complexed with 10 nm gold particles (OD = 5) for one hour to label their endocytic system. Following an additional two hours incubation in the absence of BSA-gold, autophagic structures and specifically autolysosomes should have acquired gold particles due to a continuous vesicle

fusion. Hence, the intracellular distribution of BSA-gold was assessed by electron microscopy (Fig. 3.27A) performed by *Prof. Dr. Eeva-Liisa Eskelinen (Department of Biosciences, University of Helsinki)*. According to their morphology, the observed vesicle populations were grouped into small endosomes, multi-vesicular bodies, late endosomes/ lysosomes and immature or degradative autophagic vacuoles, and the distribution of BSA-gold was determined for at least 1300 gold particles per sample (Fig. 3.27B). Gold signals were found throughout the endocytic system in both genotypes, eventually reflecting a slight shift from gold particles within small endosomes to a pronounced localisation in multivesicular bodies in the *Atp6ap2* knockout samples. Nevertheless, mature autophagosomes contained 43 % of the gold particles in wild-type and 53 % of BSA-gold in ATP6AP2-depleted hepatocytes, implying a successful delivery of the tracer to these compartments independent of the ATP6AP2 expression. Immature autophagic vacuoles that did not undergo fusion yet, displayed only smaller numbers of gold particles.

Because BSA-gold reached the degradative autophagic vacuoles also in the absence of ATP6A2, a defective autophagosome-lysosome fusion seemed unlikely in these cells.

3.3.4. *Atp6ap2* conditional knockout liver bears contrary mTORC1 regulation

Autophagy and lysosomal biogenesis are negatively regulated by the mTOR complex 1 (Dunlop and Tee, 2014). Consequently, a malfunction in the mTORC1 regulatory network could be a potential trigger for the expansion of endocytic and autophagic structures in ATP6AP2-depleted hepatocytes. Under conditions of starvation, mTORC1 is inactivated and can no longer support cell cycle and growth promoting processes. It is also no longer inhibiting the autophagy-initiating unc-51-like kinase-1 (ULK1) so that in turn autophagosomes will form within the cell (Ganley *et al.*, 2009; Hosokawa *et al.*, 2009; Jung *et al.*, 2009). The mTORC1 further blocks the nuclear translocation of the transcription factor EB (TFEB). Inhibition of mTORC1 relieves this effect and lysosomal gene transcription is triggered (Martina *et al.*, 2012; Roczniak-Ferguson *et al.*, 2012; Settembre *et al.*, 2012). Since the activation of mTORC1 via amino acids is supposed to rely on the presence of the V-ATPase (Zoncu *et al.*, 2011) and the consequences of an mTORC1 inactivation would mimic the observed phenotype, the role of mTORC1 signalling was addressed in wild-type and *Atp6ap2* conditional knockout liver.

3.3.4.1 *Differential activity of mTORC1 downstream targets in ATP6AP2-deprived liver*

As a first read-out for mTORC1 activity, the TFEB mediated transcriptional activation was characterised, as indicated by the mRNA expression of established TFEB target genes. In this regard, total RNA of whole liver samples was examined utilising qPCR (Fig. 3.28). Liver depleted for ATP6AP2 contained significantly more mRNA coding for three of the five analysed TFEB targets. The mRNA for the lysosomal protein β-hexosaminidase was found at 180 % of the wild-type expression level. Furthermore, the increase in the amount of mRNA translating for the V-ATPase V_0 subunit d1 was equivalent to 160 %, that of the p62 mRNA to 150 % in ATP6AP2-depleted liver. However, the levels of mRNA encoding LAMP-1 and the lysosomal chloride channel CLCN7 were not significantly different between wild-type and *Atp6ap2* knockout liver. Control genes that were not regulated by TFEB but still related to autophagy displayed decreased mRNA expression upon loss of ATP6AP2, presumably reflecting a compensatory regulation towards the prolonged course of self-digestion. The contrary modulation of autophagy-related genes could point to an impairment in the mTORC1 activation.

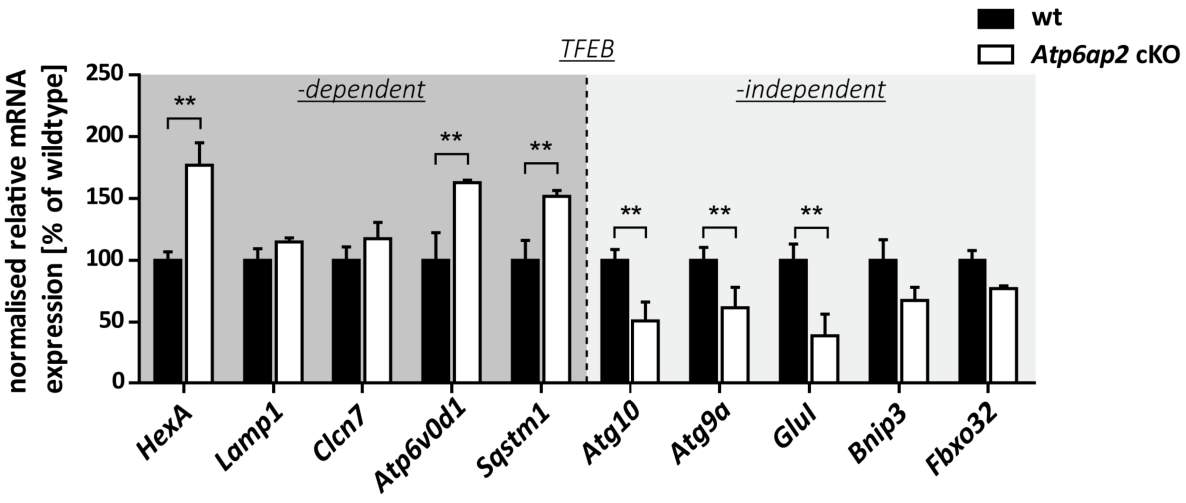

Figure 3.28: TFEB-dependent and -independent autophagy-related genes show opposing regulation in Atp6ap2 *knockout liver.*

Transcription of the indicated TFEB-regulated genes, driving lysosomal biogenesis and autophagy (left panel) was analysed by qPCR using cDNA generated from total liver RNA extracts of wild-type (wt) and *Atp6ap2* conditional knockout (cKO) mice. Autophagic genes that are not activated by TFEB (right panel) were used to assess a further promotion of autophagy. Messenger RNA expression rates were normalised to the expression of the most stable housekeeping genes (*Hprt1*, *Actb*, *Tuba1a*) and related to the wild-type expression level. Bars display means ± standard error of six independent RNA extractions per genotype (**, $P < 0.01$ according to an unpaired, two-tailed Student´s t test between genotypes).

To gain insight into the kinase activity of the mTORC1 key component mTOR, immunoblot analyses of whole liver lysates were performed (Fig. 3.29). These experiments detected an increased phosphorylation of the 70 kDa ribosomal protein S6 kinase (p70S6K), a known mTORC1 downstream target (Magnuson *et al.*, 2012), in the ATP6AP2-depleted tissue. Furthermore the V-ATPase knockdown liver samples revealed an elevated phosphorylation and thereby inactivation of the proline-rich Akt1 substrate 1 (PRAS40), which acts as an inhibitory component of mTORC1 (Sancak *et al.*, 2007; Vander Haar *et al.*, 2007; Wang *et al.*, 2007). Strikingly, this indicated a heightened activity of mTORC1 upon knockout of *Atp6ap2,* which seemed to be in contrast to the concurrent appearance of autophagy and the qPCR results concerning TFEB activity.

A prerequisite for the activation of mTORC1 is its recruitment to the lysosomal surface via the Ragulator complex and the Ras-related GTP-binding proteins RagA to RagD (Sancak *et al.*, 2007). This translocation involves the sensing of the amino acid supply, mediated by the sodium-coupled neutral amino acid transporter 9, shortly SLC38A9 and the V-ATPase complex (Jewell *et al.*, 2015; Rebsamen *et al.*, 2015; Wang *et al.*, 2015). Therefore, the distribution of mTORC1 within isolated hepatocytes of wild-type or *Atp6ap2* conditional knockout origin was traced in an indirect immunofluorescence staining in collaboration with *Sönke Rudnik (University of Kiel)*.

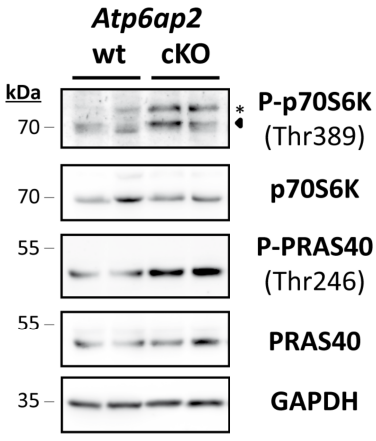

Figure 3.29: ATP6AP2-depleted liver shows increased phosphorylation of mTORC1 downstream targets.

Immunoblot analyses of wild-type and *Atp6ap2* conditional knockout (cKO) liver lysates. Phosphorylation of the mTORC1 downstream targets p70S6K (P- at Thr389) and PRAS40 (P- at Thr246) was assessed by specific antibodies recognising phosphorylated and total proteins. Probing for GAPDH was included to control for an equal protein loading. Unspecific antibody binding is marked by asterisk.

A co-localisation between the signals for mTOR as a representative of the mTOR complex 1 and the signals for the lysosome (LAMP-2) was detectable in wild-type cells, thereby suggesting a lysosomal localisation of mTORC1 (Fig. 3.30A). The accumulation of vesicles in the *Atp6ap2* knockout hepatocytes aggravated the visualisation of the correct mTORC1 localisation. MTOR displayed a diffuser signal in these cells that, if at all, only partially localised to lysosomes. Similarly, a staining of the V-ATPase V_0 subunit a3 was achieved in both genotypes, but the signal intensity was significantly weaker in the V-ATPase knockdown cells when compared to wild-type hepatocytes. Furthermore, the staining did not match a characteristic vesicular pattern in *Atp6ap2* knockout hepatocytes, questioning the functionality of this hemichannel forming V-ATPase subunit.

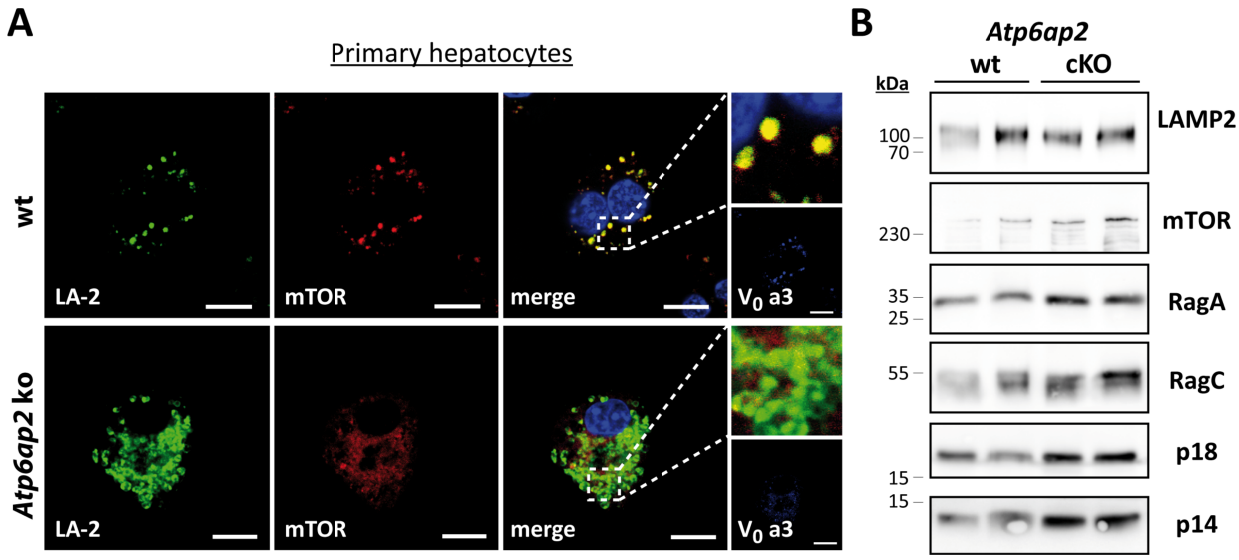

Figure 3.30: Localisation of mTORC1 in ATP6AP2-depleted liver cells.

(A) Fixed, primary hepatocytes were immunolabelled against mTOR to assess the mTORC1 localisation in wild-type (wt) and *Atp6ap2* knockout (ko) cells by confocal fluorescence microscopy. DAPI and LAMP-2 (LA-2) co-staining represents nuclei and lysosomes, respectively. The *Atp6ap2* knockout efficiency was visualised by probing for the V_0 subunit a3. Insets display regions of interest with higher magnification. Scale bars = 10 µm. (B) Wild-type and *Atp6ap2* conditonal knockout (cKO) mice were sacrificed to isolate tritosomes that were lysed and subsequently subjected to immunoblotting against LAMP-2 and the indicated components of the mTORC1 recruiting machinery.

Since immunofluorescence microscopy did not yield a clear evidence for the mTORC1 localisation in the ATP6AP2-depleted hepatocytes, lysosomes of both genotypes were isolated and subsequently tested for an association of mTORC1 in immunoblot analysis. Thus, wild-type and *Atp6ap2* conditional knockout mice were treated with Tyloxapol, which became

incorporated into hepatic lysosomes during three days in housing and enabled the purification of these organelles in a sucrose density gradient (Wattiaux *et al.*, 1963; Leighton *et al.*, 1968). Tyloxapol-enriched lysosomes were hereafter referred to as tritosomes. An equal protein load of wild-type and ATP6AP2-deficient tritosomes showed comparable levels of LAMP-2 in immunoblot analyses, enabling the usage of LAMP-2 as a loading control for normalisation (Fig. 3.30B). Surprisingly, probing for mTOR yielded stronger signals in the *Atp6ap2* knockout tritosomes as compared to the wild-type controls. Furthermore, the mTORC1 recruiting proteins RagA and RagC as well as the Ragulator components p18 (LAMTOR1) and p14 (LAMTOR2) displayed a clear increase in ATP6AP2-deficient samples. An augmented existence of the adaptor molecules between mTORC1 and the lysosome on this V-ATPase knockdown tritosomes could suggest a heightened mTORC1 recruitment.

In total, the proceeding operation of TFEB indicated an inactive mTORC1 in ATP6AP2-deficient hepatocytes, whereas the phosphorylation status of the mTORC1 downstream target p70S6K and the mTORC1 effector PRAS40, both suggested the opposite.

3.3.4.2 Disturbed mTORC1 activation in ATP6AP2-deficient MEFs

Apart from the lysosomal localisation of mTORC1, the activation of the complex via amino acids should be addressed in conditions of a reduced V-ATPase expression. Unfortunately, this was not practicable in isolated, primary hepatocytes, since the number of cells captured by the isolation protocol was not sufficient to serve the demand of the experimental setup.

Accordingly, MEF cells that permanently lack ATP6AP2 were generated and used for the analysis of amino acid-mediated mTORC1 induction. Therefore, mouse embryos with floxed *Atp6ap2* loci were sacrificed at day E13.5 and utilised as a source for fibroblast culture. The genotypes of the resulting MEF lines #4- #7 were analysed by PCR based on genomic DNA (Fig. 3.31A).

An amplification product of 591 bp was found with DNA of MEFs #5 and #6 when primers surrounding exon 2 of *Atp6ap2* were applied. The amplicon corresponded to the floxed form of this allele. Conclusively, these two MEF lines were of homo- or hemizygous floxed origin. The wild-type allele (394 bp PCR product) was detected in the fibroblast lines #4 and #7. No heterozygous fibroblast lines could be found. Since *Atp6ap2* is passed via an X-linked inheritance, the sex of the fibroblast lines was determined in a second PCR to detect the male specific sequence *Sry* (Lambert *et al.*, 2000). An amplification product was visible in samples

from MEF lines #4 and #7. Collectively, this revealed that MEF lines #4 and #7 harboured the *Atp6ap2*$^{+/Y}$ alleles and the fibroblast lines #5 to #6 had an *Atp6ap2*$^{flox/flox}$ genotype.

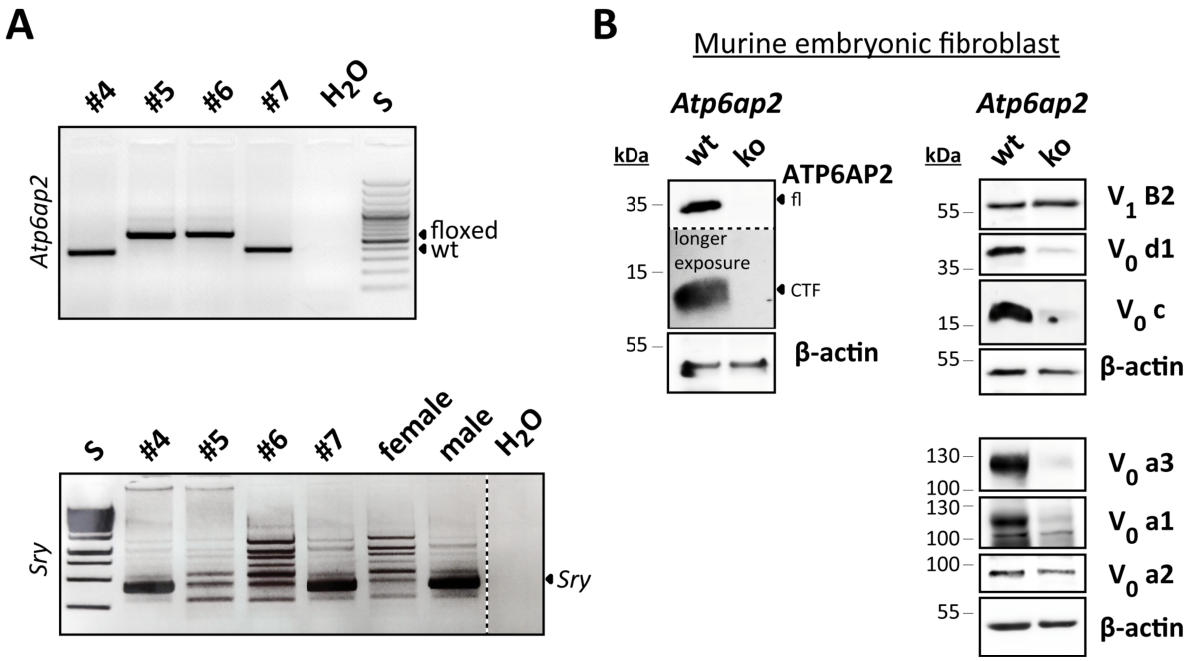

Figure 3.31: Generation and characterisation of ATP6AP2-deficient MEF lines.

(**A**) Genomic DNA of the MEF lines #4 to #7 was analysed by PCR to detect wild-type (wt) and floxed *Atp6ap2* alleles (upper panel) and the male specific sequence (*Sry*, lower panel). The expected amplicons are indicated by arrowheads at the agarose gel showing the separated PCR products. The length of the amplification product was correlated to a standard ladder (S). A water-based PCR (H_2O) served as negative control, genomic DNA of female and male mice was used to specify the *Sry* signal. (**B**) Immunoblot analyses of ATP6AP2 and the indicated V-ATPase subunits using cell lysates of the Cre recombinase expressing MEF lines #7A (wild-type) and #6A (*Atp6ap2* knockout). Full length (fl) and C-terminal fragments (CTF) of ATP6AP2 are highlighted. B-actin was probed to control for an equal protein load.

All four lineages were immortalised with the SV40 large T antigen and stably transfected with a combination of pCAG-Cre:GFP/ pGK-hyg to achieve the expression of the Cre recombinase. Hereafter, they were referred to as wild-type (#4B, #7A) and *Atp6ap2* knockout (#5A, #6A) MEFs. The following studies were performed using the lineages #7A and #6A, only.

Immunoblot analysis of ATP6AP2 and V-ATPase subunit expression in wild-type and *Atp6ap2* knockout MEFs verified that a deletion in *Atp6ap2* could be obtained, since the full length and the CTF signals of ATP6AP2 were absent in the knockout lysates (Fig. 3.31B). As seen in ATP6AP2-depleted macrophages and in liver (3.2.2, 3.3.1), the concentration of the detected V_0 subunits a1 to a3, d1 and c dropped significantly upon loss of ATP6AP2, while the

V_1 subunit B2 remained unaffected. With a reduction of V_0 subunit a3 to as low as 2 % and V_0 subunit c down to 10 % of the wild-type level, the V-ATPase knockdown generated in *Atp6ap2* knockout MEFs was the most effective of the investigated systems.

Still, these ATP6AP2-deficient cells displayed a clear LysoTracker® Red staining (data not shown) and the lysosome pH of 4.86 ± 0.14 measured via dextran-Oregon Green® 514 was comparable to that of wild-type MEFs (pH 5.14 ± 0.15, Fig. 3.32A).

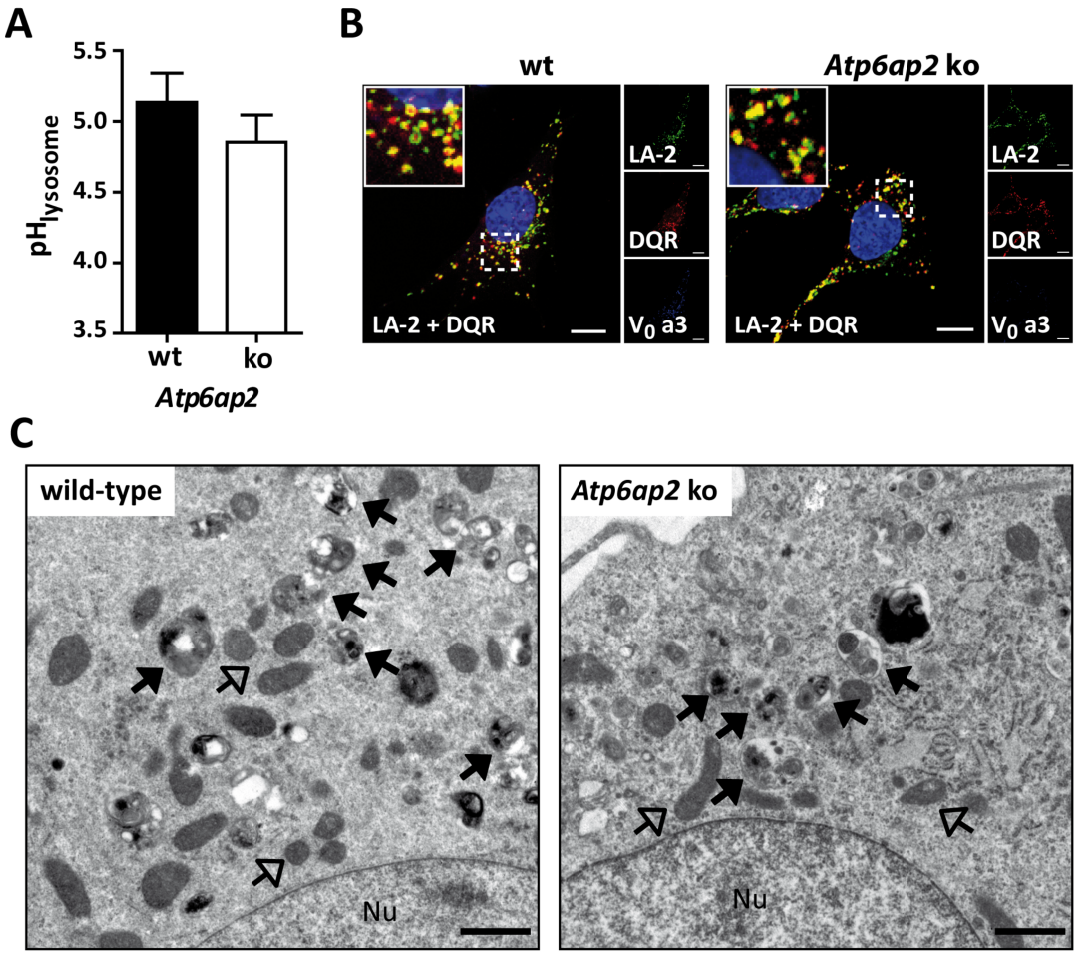

Figure 3.32: Atp6ap2 *knockout MEF display functional lysosomes and lack any vesicle accumulation.*

(A) Mean lysosome pH of wild-type (wt) and *Atp6ap2* knockout (ko) MEFs ± standard deviation, measured ratiometrically with dextran-Oregon Green® 514 in two independent experiments. (B) Lysosomal proteolysis and concomitant dequenching of DQ™ Red-BSA in fixed cells of both genotypic origins was analysed by confocal fluorescence microscopy. Immunolabelling for LAMP-2 (LA-2) and the V_0 subunit a3 was performed to assess lysosomes and the differential V-ATPase expression, respectively. Merge images include DAPI-stained nuclei and insets with magnified regions of interest. Scale bars = 10 µm. (C) Transmission electron micrographs of glutaraldehyde-fixed MEFs with and without ATP6AP2 expression generated by *Prof. Dr. Renate Lüllmann-Rauch (University of Kiel)*. Late endosomes/ lysosomes (closed arrows), mitochondria (open arrows) and nuclei (Nu) are indicated. Scale bars = 1 µm.

Furthermore, the dequenching of DQ™ Red-BSA took place in the lysosomes of both genotypes, indicating ongoing proteolysis within these compartments, which was independent of the presence of ATP6AP2 (Fig. 3.32B). Moreover, the specific activity of β-hexosaminidase and the maturation of cathepsin D and L remained inconspicuous (data not shown).

Overall, the ATP6AP2-depleted MEFs revealed no obvious phenotypic disparities and although an extensive knockdown of the V-ATPase complex was proven, they contained degradative, acidic lysosomes.

Unlike the *Atp6ap2* knockout hepatocytes, MEFs deficient for ATP6AP2 showed no accumulation of autophagic and lysosomal structures in electron micrographs (Fig. 3.32C). In addition, the increase in the ratio of LC3-II to LC3-I and the elevated p62 turnover upon combined amino acid and serum withdrawal were comparable between wild-type and ATP6AP2-deficient MEFs (Master´s thesis S. Rudnik, 2014). This raised the question, whether mTORC1 signalling was affected at all in the V-ATPase knockdown fibroblasts.

Preliminary work conducted in these fibroblast lines indicated an interaction between the V-ATPase and the mTORC1 recruiting Ragulator complex by the successful endogenous co-precipiation of the V_0 subunits c and d1 with p18/ LAMTOR 1 in wild-type MEFs (Master´s thesis S. Rudnik, 2014). However, upon the deletion of *Atp6ap2,* this co-precipitation was not detectable anymore, pointing to a disruption in the cross-talk between the V-ATPase and mTORC1. As a consequence, the ability of amino acids to elucidate mTORC1 activity in priorly starved cells was examined in wild-type and *Atp6ap2* knockout MEFs. Fibroblasts of both genotypes were incubated in Earle´s balanced salt solution (EBSS) for one hour to silence mTORC1 signalling, and a reactivation of the complex was stimulated thereafter by providing amino acids (DMEM) for up to two hours. Immunoblotting was applied to detect phosphorylated and total p70S6K as well as phosphorylated and total PRAS40 as a measure for mTORC1 induction (Fig. 3.33A, B).

The activity determining phosphorylation at threonin 389 of p70S6K was present in the untreated wild-type and *Atp6ap2* knockout cells. However, this phosphorylation was slightly decreased under conditions of a reduced V-ATPase expression. Upon starvation, both cell lines lost the p70S6K phosphate modification, providing evidence for an mTORC1 inactivation. Following additional 60 minutes in the presence of amino acids, wild-type cells partially recovered their initial p70S6K phosphorylation status and also showed a further increase to up

to 40 % of the steady state value within 120 minutes (Fig. 3.33B). This regeneration could be blocked by parallel incubation in the presence of amino acids and the specific mTOR inhibitor Torin 1 (250 nM). In contrast, MEFs lacking ATP6AP2 showed a much slower phosphorylation of p70S6K in response to amino acid stimulation and reached only 26 % of their initial phosphorylation ratio during 120 minutes (Fig. 3.33B).

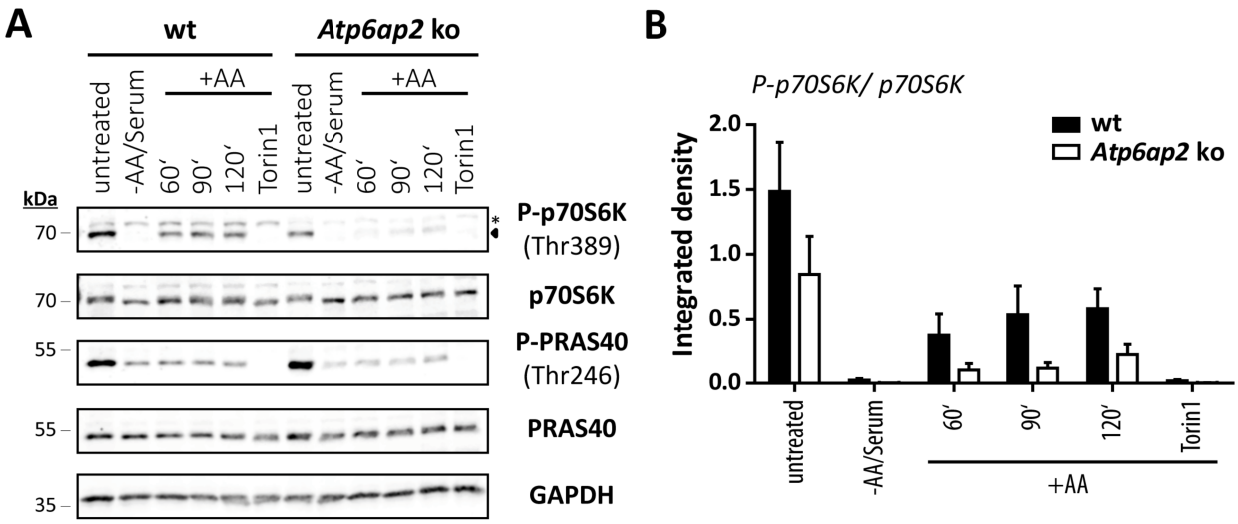

Figure 3.33: Amino acid-mediated mTORC1 activation is disturbed in the absence of ATP6AP2.

Wild-type (wt) and *Atp6ap2* knockout (ko) MEFs were either left in media containing amino acids and serum or cultivated in EBSS in the absence of these components for one hour. Following the nutrient-withdrawal, reapplication of amino acids was used to activate mTORC1 by incubation in DMEM for the indicated time periods. Treatment with Torin 1 (250 nM) during starvation and two hours in the presence of amino acids served as negative control. (A) Immunoblot analysis showing phosphorylated (Thr389, P-) and total p70S6K as well as phosphorylated (Thr246) and total PRAS40. GAPDH was used to control for equal protein loading. (B) Quantification of P-p70S6K to p70S6K ratios as acquired in (A) representing three independent experiments as mean integrated densities ± standard errors.

Next to that, the phosphate addition at threonin 246 of PRAS40 was visible in wild-type and *Atp6ap2* knockout MEFs under conditions of normal nutrition and also decreased upon nutrient withdrawal. The addition of amino acids could not trigger an elevation in the phospho-PRAS40 to PRAS40 ratio in either genotype, which suited the described activation of this mTORC1 regulatory axis specifically through receptor tyrosine kinases and the protein kinase B/ Akt (Sancak *et al.*, 2007). These findings implied an impairment in the activation of mTORC1 via amino acids and the action of SLC38A9, the V-ATPase and Ragulator under conditions of ATP6AP2-deficiency and consequential reduction in V-ATPase levels.

4. DISCUSSION

The membrane-integral sector of V-ATPases promotes vesicle fusion. Although several studies provided evidence supporting this fact, the role of the proton pump in membrane fusion is still controversially discussed (summarised in Vavassori and Mayer, 2014; Cotter *et al.*, 2015). In the course of this thesis, the fusogenic potential of V-ATPases was analysed using genetic and pharmacological approaches in murine fibroblasts and macrophages. To dissect between proton pumping-dependent and proton pumping-independent influences, the activity of the complex and its assembly state were targeted in separate approaches and analysed individually for their importance in vesicle processing. In addition, the function of V-ATPases was assessed with respect to its participation in autophagosome maturation and autophagic degradation as well as in the regulation of autophagy via the mTORC1 signalling cascade.

4.1. The V-ATPase V_0 subunit a3 in proton pumping and vesicle fusion along endocytic uptake pathways

As a first approach, the V_0 subunit a3 was analysed for its contribution to endocytic vesicle fusion events. This V-ATPase subunit is predominantly found on lysosomes (Toyomura *et al.*, 2003; Sun-Wada *et al.*, 2009), which represent the terminal fusion partner of all endocytic uptake pathways. In addition, the V_0 subunit a3 is actively recruited to developing phagosomes (Sun-Wada *et al.*, 2009), bringing phagosome-lysosome fusion into the focus of attention. A3-deficient professional phagocytes, *e.g.* macrophages, would have been the preferred cell type to address phagosome maturation. Although there is a natural mutation in the mouse gene coding for subunit a3 (*Tcirg1*^{oc}), homozygously affected animals suffer from severe osteopetrosis and die within six weeks of age (Scimeca *et al.*, 2000). Due to the dramatic phenotype, isolation of primary macrophages from a3 mutant mice was limited by dense bones and a reduced live span. To be still able to exploit the benefits of this naturally occurring deletion mutation, mouse embryonic fibroblast (MEF) lineages were generated from wild-type and a3-mutated animals. These fibroblasts were utilised to assess both, V-ATPase activity and vesicle fusion in the absence of the V_0 subunit a3.

4.1.1. Potential importance of V_0 subunit a3 for V-ATPase complex function

The genotypes of the newly generated wild-type and a3-deficient MEF lines were confirmed by PCR and immunoblotting. Surprisingly, in spite of the proven genetic deletion, *a3*$^{-/-}$ MEFs expressed mRNA coding for subunit a3. Nevertheless, the excised sequence of *Tcirg1* included its translation initiation site, which is needed for efficient protein synthesis. Consequently, subunit a3 was not detectable at the protein level in immunoblot analyses of *a3*$^{-/-}$ cells. The antigenic peptide used to generate the utilised a3 antibody is located in a distal, C-terminal domain of the protein (Lange *et al.*, 2006). Therefore, the antibody would have recognised any in frame translations of the subunit a3 that might be translated with the aid of downstream ATG codons as alternative initiation sites. Since this was not the case, the expression of a functional, but truncated V_0 subunit a3 is highly unlikely. Alternatively, the translation of the shortened a3 mRNA could have resulted in an unstable product that was prone to rapid turnover by degradation.

A loss of subunit a3 is further supported by the transcriptional up-regulation of the a subunit isoform 1 that was also prominent at the level of protein expression. The two a isoforms 1 and 3 share a high degree of sequence similarity, while their cytoplasmic domains differ more frequently (Fig. 4.1). The proton pumping activity of the V-ATPase complex mostly relies on the conserved transmembranous protein domains. Thus, an up-regulation of subunit a1 might compensate for the loss of subunit a3 in the function of proton translocation. Partial compensation between the subunit a isoforms 1 and 3 has already been discussed for proton pumping in osteoclasts (Nyman and Vaananen, 2010). Latex bead-containing phagolysosomes isolated from osteoclasts contained both, subunit a1 and a3. Compensation between the two isoforms would explain the normal lysosomal acidification as well as the existence of residual bone resorption activity upon single knockout of the V_0 subunit a3 (Taranta *et al.*, 2003; Blair *et al.*, 2004; Del Fattore *et al.*, 2006). This seems to be an evolutionary conserved mechanism, since already the yeast a subunit homologues Vph1p and Stv1p can substitute for each other to form functional V-ATPase complexes (Manolson *et al.*, 1994). In the wild-type and a3-mutant fibroblasts, other a isoforms and subunits assessed by PCR and immunoblotting showed an unaltered expression pattern.

In agreement with a possible compensation by the V_0 subunit a1, the complete knockout of subunit a3 was not sufficient to interfere with the steady-state lysosome pH in fibroblasts.

Lysosomal acidification was moreover comparably sensitive to bafilomycin A1 or nigericin treatment in wild-type and *a3*$^{-/-}$ MEFs. These results suggest a similar operating efficiency of the proton pumps in both genotypes or more explicitly a complex functionality that is independent of the incorporated subunit a isoform.

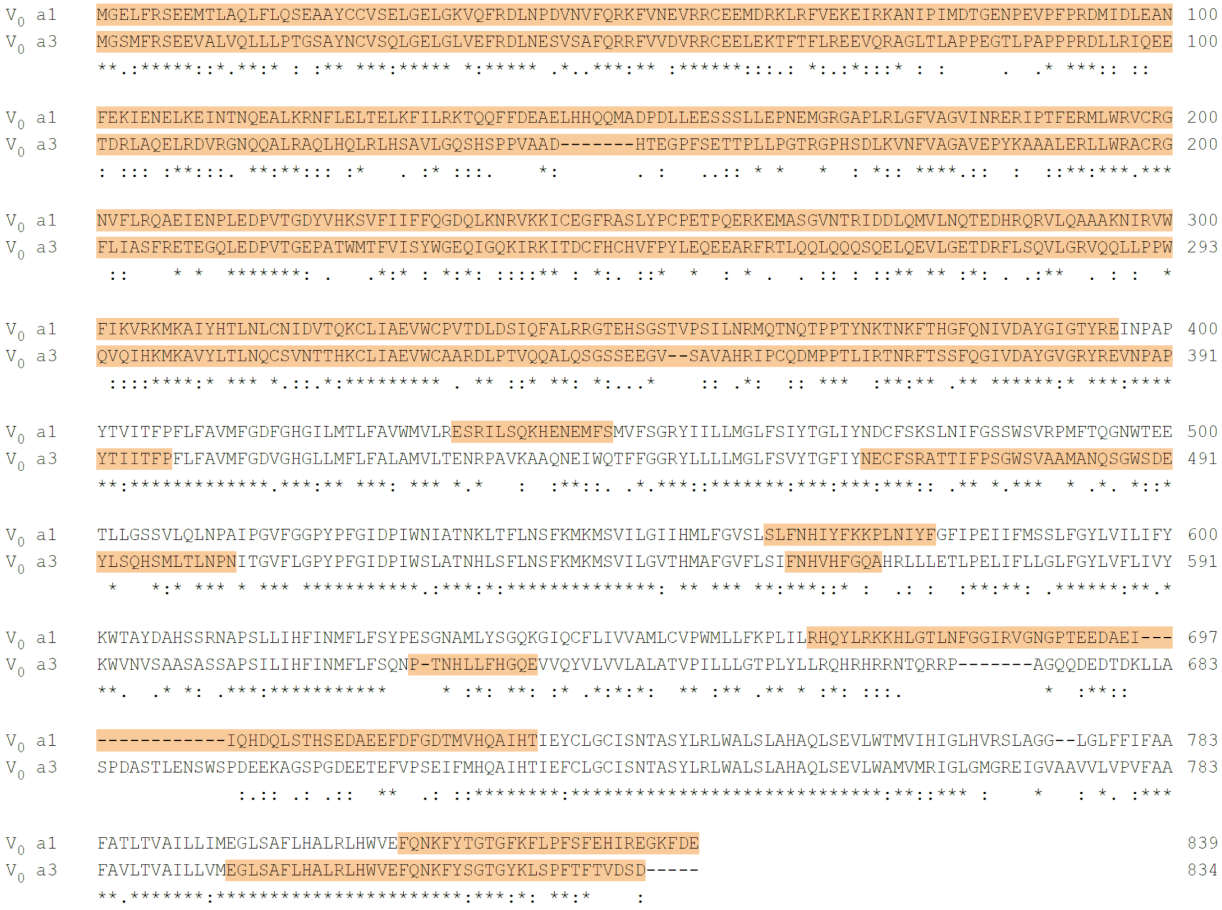

Figure 4.1: Sequence alignment of V_0 subunits a1 and a3.

Alignment of amino acid sequences of V-ATPase V_0 subunit a1 (UniprotKB: Q9Z1G4-1) and V_0 subunit a3 (UniprotKB: Q9JHF5-1) performed with Clustal Omega. Conserved residues (*), conservative (:) and semi-conservative (.) exchanges are denoted. Cytoplasmic domains as assigned by sequence analysis are coloured in orange.

Further supporting the normal lysosome acidification, the activity of lysosomal enzymes and the proteolytic degradation of the self-quenched DQ™ Red-BSA were not affected by the loss of subunit a3. In addition, fibroblasts lacking the V_0 subunit a3 exhibited efficient proteolytic processing of the lysosomal cathepsins D and L. This is consistent with the earlier analyses using osteoclasts (Blair *et al.*, 2004; Del Fattore *et al.*, 2006; Nyman and Vaananen, 2010) and with more recent studies in macrophages that feature a genetic deletion of exon 14 to exon 20 of the V_0 subunit a3 and displayed regular cathepsin maturation (Sun-Wada *et al.*, 2009).

Surprisingly, the V_0 a3-deficient macrophages analysed by Sun-Wada *et al.* failed to acidify newly generated phagosomes and showed a significant drop in bacterial killing when compared to wild-type macrophages. Such deficits imply that some functions of the V-ATPase might be solely mediated through the V_0 subunit a3. However, a comparable phenotype was not observed in the a3-deficient fibroblasts analysed in the present work. MEFs lacking the V_0 subunit a3 displayed LysoTracker® Red acquisition to latex bead-containing phagosomes with similar kinetics as wild-type cells (data not shown). Therefore phagosome acidification was independent of the genotype in the examined fibroblasts. Nevertheless, a comparison between the analysis in macrophages (Sun-Wada *et al.*, 2009) and the analysis in fibroblasts is complicated by the fact that different a3 mutation were analysed in two distinct cell systems. Although both analyses seem to contradict each-other on the first sight, the different influence of V_0 a3 might reflect a cell type-specific effect.

4.1.2. Characteristics of endocytic and phagosomal fusion processes in the absence of V-ATPase V_0 subunit a3

Since acidification and lysosome function were normal in the V_0 subunit a3-deficient MEFs, further analyses were undisturbed by severe lysosomal phenotypes. This enabled a focused study of proton pumping-independent activities of the V_0 subunit a3.

Previous reports already indicate that not all functions of the V_0 subunit a can be compensated by other a isoforms. Often, knockout of a single V-ATPase V_0 a isoform is accompanied by specific diseases. Disruption of V_0 subunit a3 causes severe osteopetrosis due to decreased bone resorption activity (Marks *et al.*, 1985; Scimeca *et al.*, 2000). Mutated versions of the subunits a2 and a4 are associated with deficits in Golgi-resident protein glycosylation or renal tubular acidosis, respectively (Smith *et al.*, 2000; Kornak *et al.*, 2008). A common feature of these phenotypes is the missing delivery of V-ATPases to distinct compartments or the plasma membrane of specialised cells. Therefore, the V_0 subunit a could be important in determining the intracellular localisation of the whole V-ATPase complex. In agreement with this, the subunit isoforms a1 to a4 show tissue- and compartment-specific expression pattern. The targeting information might reside within the less conserved cytoplasmic N-terminus of the protein (Fig. 4.1). For the yeast V_0 subunit a homologue, this N-terminal domain was already identified as a regulator for V-ATPase trafficking and it further defines the complex coupling efficiencies (Kawasaki-Nishi *et al.*, 2001a).

The high amino acid variance of the N-terminus is also present in other cytoplasmic regions of subunit a (Fig. 4.1). These individual protein domains might facilitate further subunit-specific functions. The cytoplasmic faces of the neuronal V_0 subunit a1 interact with the Q-SNARE syntaxin and the Ca^{2+} binder calmodulin (Hiesinger *et al.*, 2005; Zhang *et al.*, 2008; Wang *et al.*, 2014). Both, syntaxin and calmodulin are essential regulators in the mixing of lipid bilayers. Interference with the calmodulin binding site of subunit a1 by mutagenesis resulted in a clear decrease in spontaneous neurotransmitter secretion (Wang *et al.*, 2014). Based on these findings, the V_0 subunit a1 promotes fusion during vesicle exocytosis.

Whether the cytoplasmic domains of the lysosomal V_0 subunit a3 promote a similar positive influence on membrane fusion was analysed in the a3-deficient fibroblasts. Initial experiments showed that cathepsins reached the lysosomes of *a3*$^{-/-}$ MEFs. This hints to an efficient vesicle trafficking from the ER to the lysosome, independent of the V_0 a3 expression. Furthermore, the compounds dextran-Texas Red® and DQ™ Red-BSA, both were taken up by *a3*$^{-/-}$ fibroblasts and localised to lysosomal compartments after the applied chase periods. In conclusion, vesicle trafficking along the endocytic route displayed no impairment in MEFs that lacked the V_0 subunit a3. This suggests normal vesicle fusion between early endosomes, late endosomes and lysosomes in these cells. However, this does not exclude a role in other cellular fusion processes, *e.g.* phagosome-lysosome fusion, as compensation might occur compartment-specific.

To address the mixing of phagosomes with lysosomes, human Fcγ receptor IIa (hFcγRIIa)-expressing wild-type and a3-deficient MEFs were used for latex bead uptake assays. The FcγRIIa facilitates phagocytosis of IgG-opsonised particles, *e.g.* erythrocytes (Tuijnman *et al.*, 1992). Its expression in fibroblasts led to a significant increase in the uptake efficiency of human IgG-opsonised latex beads (data not shown). Phagosome-lysosome fusion was examined in these MEF lines by monitoring latex bead-containing phagosomes with indirect immunofluorescence labelling of early and late endocytic marker proteins. Following receptor-mediated uptake of the latex beads, early markers (EEA1) were recruited to the phagosomes. In the course of phagosome maturation, these early endocytic proteins were successively replaced with late markers (LAMP-2). A quantitative evaluation revealed similar maturation kinetics, *i.e.* marker replacement over time, in wild-type and a3-deficient MEFs. Thus, phagosome maturation occurred normally in the *a3*$^{-/-}$ cells and the V_0 subunit a3 is dispensable

for phagosome-lysosome fusion in fibroblasts. In agreement with this finding, the a3-mutant macrophages analysed by Sun-Wada *et al.* showed normal phagosomal transition from early to late marker proteins, culminating in the acquisition of LAMP2 (Sun-Wada *et al.*, 2009).

To unravel the individual roles of single a subunit isoforms in future studies, mutational analyses might be an alternative to the actual protein knockout. Calmodulin- and SNARE-binding sites that have been found in subunit a1 might be altered but still present in other a isoforms, such as the V_0 subunit a3. Chimeric a subunits that contain mixed N-terminal domains of different a isoforms might help to identify potential binding sites. Site-directed mutagenesis of these sequences should interfere with membrane fusion as it was shown for disruption of the calmodulin binding site of subunit a1 in *Drosophila melanogaster* (Wang *et al.*, 2014).

4.1.3. Impact of luminal acidification and the V-ATPase´s association state on phagosome-lysosome fusion

The proposed physical involvement of the V-ATPase complex in membrane fusion was challenged in a recent report by Coonrod *et al.*. In this study, V-ATPase-mediated acidification of the yeast vacuole was shown to be the critical factor in promoting membrane fusion (Coonrod *et al.*, 2013). A link between both, proton translocation by the V-ATPase and the physical presence of the complex has been found in membrane fusion during exocytic neurotransmitter release from chromaffin cells (Poea-Guyon *et al.*, 2013; Morel and Poea-Guyon, 2015).

The exocytosis of secretory granules from chromaffin cells is one of the most thoroughly studied fusion events (reviewed in Morel and Poea-Guyon, 2015). It was proposed that a low luminal pH of secretory granules is critical for their exocytosis from PC12 cells (Poea-Guyon *et al.*, 2013). However, exocytosis was not generally inhibited by increased intragranular pH. Treatment with the ionophore nigericin alkalised the secretory granules and efficiently blocked the exocytic neurotransmitter release. In contrast, alkalisation using bafilomycin A1 did not interfere with fusion between the granules and the plasma membrane (Poea-Guyon *et al.*, 2013). The difference between both inhibitory components is their mode of operation and the subsequent effect on the V-ATPase´s association state (Fig. 4.2). Nigericin dissipates luminal acidification by exporting protons against an influx of potassium ions. As a consequence, increased association and compensatory activation of the V-ATPase complex are observed. Bafilomycin A1, on the other hand, directly interacts with the V_0 sector of V-ATPases, which favours the dissociation into free V_0 and V_1 sectors (Bowman *et al.*, 2006; Poea-Guyon *et al.*,

2013; Wang and Hiesinger, 2013; Morel and Poea-Guyon, 2015). Therefore, bafilomycin A1 increases the availability of free V_0 sectors, which are proposed to propagate membrane fusion (Vavassori and Mayer, 2014; Cotter *et al.*, 2015). During neurotransmitter loading, the lumen of secretory granules is continuously acidified, which similarly leads to increasing dissociation of the V-ATPase complex (Morel, 2003; Poea-Guyon *et al.*, 2013). Hence, a low luminal pH of secretory granules is critical for their exocytosis as it yields free V_0 sectors to promote fusion with the plasma membrane.

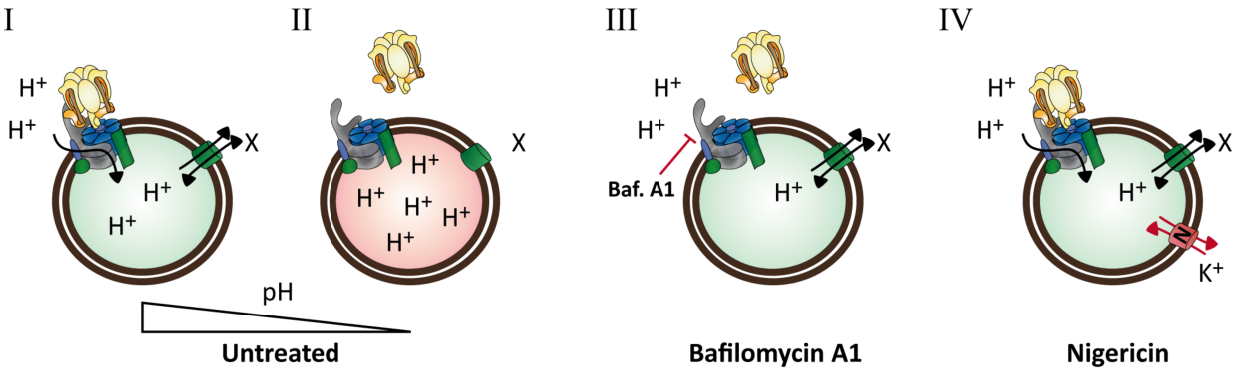

Figure 4.2: Potential influence of luminal pH and pharmaceuticals on V-ATPase assembly.

(I) Upon assembly, V-ATPases mediate proton translocation into the vesicle lumen. Yellow to brown colouring denotes V_1 sector affiliation, whereas blue and grey subunits belong to sector V_0. Accessory subunits are depicted in green. Solute channels transport other cations and anions (X) by utilising the established proton gradient. (II) Acidic vesicular pH leads to V_0-V_1 dissociation. (III) Upon incubation with bafilomycin A1, the compound binds to the V_0 subunits a and c and interferes with complex assembly and function. (IV) Nigericin (N) integrates into the vesicle membrane and mediates H^+/ K^+ exchange. This triggers compensatory activity of V-ATPases and leads to increased V_0-V_1 association.

Whether phagosome-lysosome fusion in fibroblasts is similarly dependent on the V-ATPase´s association state and the luminal pH, was examined in FcγRIIa-expressing wild-type and a3-deficient MEFs. During latex bead-containing phagosome maturation in fibroblasts, the available free V_0 sectors were increased by treatment with bafilomycin A1 or decreased through application of nigericin, respectively. In addition, the luminal pH of phagosomes and lysosomes was elevated under both conditions.

In wild-type and *a3*$^{-/-}$ MEFs, the pharmaceuticals showed no apparent effect on phagolysosome development, *i.e.* the acquisition kinetics of early and late endocytic marker proteins to the maturing phagosomes. In conclusion, the fusion of phagosomes with endocytic compartments was not affected by an altered quantity of accessible V_0 sectors. Therefore, the dissociation of

V-ATPases is not required for phagosome maturation in fibroblasts. This is in contrast to the regulation of granule secretion from chromaffin cells (Poea-Guyon *et al.*, 2013; Morel and Poea-Guyon, 2015). In additional studies on the influence of free V_0 sectors on phagosome maturation, application of saliphenylhalamide A did not alter *in cellulo* and *in vitro* fusion of RAW264.7 lysosomes with phagosomes (Kissing *et al.*, 2015). Saliphenylhalamide A is another potent inhibitor of V-ATPase function that locks V_1 and V_0 sectors together and concomitantly reduces free V_0 sectors. Moreover, bafilomycin A1 had no effect on the maturation of heat-killed *Rhodococcus equi*-containing phagosomes in J774.E macrophages (Kissing *et al.*, 2015). These data suggest differential requirements for fusion along the phagocytic pathway in fibroblasts and macrophages and the exocytic pathway in chromaffin cells. Since all developing phagosomes need to acquire proteolytic activity through fusion with late endocytic compartments, a discrimination between phagosome populations by pH might be dispensable.

Both, bafilomycin A1 and nigericin elevated the luminal pH of phagosomes and endocytic compartments in wild-type and a3-deficient cells. Therefore, a low vesicular pH as such was no prerequisite for fusion in the phagocytic pathway. This is in contrast to the recent study by Coonrod *et al.* concerning vacuole fusion in yeast (Coonrod *et al.*, 2013) and earlier analysis on yeast *trans*-SNARE complex formation (Ungermann *et al.*, 1999), which both depend on a low luminal vacuole pH. These results imply that the importance of vacuole acidification for membrane fusion is not conserved across species.

Considered as a whole, vesicle fusion in the endocytic and phagocytic pathways of fibroblasts was unaffected by increased luminal pH of the fusion partners. Moreover, pharmacological modulation of the V-ATPase´s association state had no influence on the fusion kinetics during phagosome maturation. The dissociation of the V-ATPase complex into free V_1 and V_0 sectors appears to be dispensable under the applied experimental conditions.

4.2. The role of ATP6AP2 and the V-ATPase V_0 sector as mediators of vesicle fusion

Neither the knockout of the V_0 subunit a3 nor a pharmacologically altered availability of free V_0 sectors affected membrane fusion along the endocytic and phagocytic pathways in fibroblasts. For further analyses of V-ATPase functions in fusion processes, the protein level of the membrane-integral V_0 sector was reduced in a genetic approach. The gene encoding the V-ATPase accessory protein 2/ ATP6AP2 was disrupted in mice using an inducible *Cre-LoxP*

recombination system. Since ATP6AP2 harbours a chaperone function for V-ATPase V_0 sector assembly (Kinouchi *et al.*, 2010; Oshima *et al.*, 2011; Riediger *et al.*, 2011), the single knockout of this protein is sufficient to diminish the concentration of the different V_0 subunits. The impact of such reduced V_0 sector levels on phagosome-lysosome fusion as well as on the endocytic route was assessed in primary macrophages from wild-type and conditional *Atp6ap2* knockout animals.

4.2.1. ATP6AP2 is a chaperone for V-ATPase complex assembly

In the course of this thesis, an *Atp6ap2* conditional knockout (cKO) mouse line was established that utilises the Cre recombinase under the control of an *Mx1* promotor. Stimulation with synthetic double-stranded RNA activates the *Mx1* promotor site within all interferon α-sensitive cells (Kuhn *et al.*, 1995). To trace targeted cell populations, *Rosa26-EYFP Mx1-Cre* reporter mice were generated. Upon induction, a prominent Cre recombinase activity was present in various tissues of the conditional reporter animals. Stimulation of the *Mx1* promotor in *Atp6ap2* conditional knockout mice decreased the protein level of ATP6AP2 in the same tissues. The most prominent reduction of ATP6AP2 was observed in liver and lymph nodes.

ATP6AP2 is proteolytically cleaved by furin and/ or ADAM19 (Cousin *et al.*, 2009; Yoshikawa *et al.*, 2011). Following the treatment with poly (I:C), both, the full length ATP6AP2 and its C-terminal fragment (CTF) were reduced in interferon α-sensitive tissues of *Atp6ap2* cKO animals. The decrease of the ATP6AP2 CTF was much stronger than the decrease of full length ATP6AP2. However, it could be shown that the ATP6AP2-mediated assembly of V-ATPases occurs before the proteolytic processing of the accessory subunit (Kinouchi *et al.*, 2013). Therefore, the reduction of full length ATP6AP2 should reflect the actual impairment in V-ATPase V_0 sector assembly.

Residual amounts of ATP6AP2 could be found in all tissues analysed by immunoblotting. These most likely reflect non-targeted cell populations. Immunofluorescene staining of tissue sections from conditional reporter mice confirmed this assumption for the different liver cell clusters.

For the analysis of phagosome-lysosome fusion under conditions of reduced V_0 sector concentrations, professional phagocytes were chosen as a suitable cell system. Thus, macrophages were examined in more detail for the efficiency of ATP6AP2 depletion and its effects on the level of V_0 sector subunits. In all macrophage populations that were analysed –

hepatic Kupffer cells, bone-marrow derived macrophages (data not shown), splenic and peritoneal macrophages – the fraction of Cre recombinase-positive cells was almost 100 % upon *Mx1* promotor stimulation. In peritoneal macrophages of *Atp6ap2* conditional knockout mice, immunoblot analyses showed a complete loss of ATP6AP2 full length protein and both, the N-terminal and C-terminal fragments. Comparable to the knockout of *Atp6ap2* in cardiomyocytes and podocytes (Kinouchi *et al.*, 2010; Oshima *et al.*, 2011; Riediger *et al.*, 2011), the protein levels of the analysed V_0 subunits were decreased in the absence of ATP6AP2. In contrast, there was no visible depletion of the V_1 subunit B2 in *Atp6ap2* knockout macrophages.

So far, the mode of V-ATPase assembly is not completely solved. The differential influence of ATP6AP2 on V_0 and V_1 subunits suggests that the sectors are assembled individually before they associate with each other to form the functional V-ATPase complex (Kinouchi *et al.*, 2013). While the assembly of V_0 sectors depends on ATP6AP2, V_1 sectors are built up also in the absence of this accessory subunit. However, next to fully assembled V_0 and V_1 sectors, also incomplete complexes containing a mixture of V_0 and V_1 subunits were observed in yeast (Kane *et al.*, 1999; Nishi and Forgac, 2002; Malkus *et al.*, 2004). Since there is no homologue for ATP6AP2 in yeast, the assembly pattern of the complex might not be evolutionary conserved.

It could be shown that ATP6AP2 affects V-ATPase assembly only post-transcriptionally, since the mRNA levels of all analysed V-ATPase subunits remained comparable between wild-type and *Atp6ap2* knockout macrophages. Also, there was no feedback loop that would compensate for a decreased V-ATPase assembly by elevated subunit expression. Overall, it could be demonstrated that ATP6AP2 essentially contributes to V-ATPase V_0 sector biogenesis in macrophages.

4.2.2. Influence of reduced V-ATPase V_0 sector concentration on lysosome function

A decreased concentration of whole V_0 sectors presumably affects the functionality of intracellular processes and compartments in ATP6AP2-deficient macrophages. Indeed, the loss of ATP6AP2 in podocytes, cardiomyocytes and fibroblasts was accompanied by an impairment in V-ATPase-mediated proton pumping (Kinouchi *et al.*, 2010; Oshima *et al.*, 2011; Riediger *et al.*, 2011; Kinouchi *et al.*, 2013). As a consequence, cellular processes that rely on an acidic luminal pH, *e.g*. lysosomal protein degradation, were hampered in these cells. Whether a similar phenotype was present in *Atp6ap2* knockout macrophages was analysed in this work.

LysoTracker Red® staining of acidic cell compartments did not reveal a difference between wild-type and ATP6AP2-deficient macrophages. The steady-state lysosome pH was only mildly elevated in *Atp6ap2* knockout cells. This implies that luminal acidification *per se* was not affected by a decreased concentration of V-ATPase V_0 sectors. However, low dosages of the V-ATPase inhibitor bafilomycin A1 were more effective in the macrophages lacking ATP6AP2 than in wild-type controls. Since bafilomycin A1 directly interacts with the V_0 sector of V-ATPases, this suggests a reduction in V-ATPase function upon loss of ATP6AP2.

In line with the still acidic pH of late endocytic compartments, lysosomal hydrolases of *Atp6ap2* knockout macrophages showed an undisturbed activity *in vitro*. Similarly, the abscence of ATP6AP2 did not affect the degradation of the self-quenched DQ™ Red-BSA or the lysosomal processing of the cathepsins D and L. Collectively, these data provide evidence for largely unaltered lysosome functions in the ATP6AP2-deficient macrophages.

The presence of vesicular acidification as well as the normal degradation in lysosomes of *Atp6ap2* knockout macrophages are both in contrast to the results obtained in cardiomyocytes, podocytes and fibroblasts (Kinouchi *et al.*, 2010; Oshima *et al.*, 2011; Riediger *et al.*, 2011; Kinouchi *et al.*, 2013). Furthermore, an accumulation of autophagic structures that was seen in cardiomyocytes and podocytes devoid of ATP6AP2, was not prominent in the *Atp6ap2* knockout macrophages (data not shown). It can be assumed that the reduction of V_0 sectors is less stringent in ATP6AP2-deficient macrophages than in the other systems. The higher number of residual V-ATPase complexes might be sufficient to enable vesicular acidification and support a normal autophagic flux in the *Atp6ap2* knockout macrophages.

Overall, these findings imply that also markedly reduced levels of V-ATPases are capable of maintaining the luminal pH homeostasis. It remains to be clarified, which other physiological roles are performed by the additional V-ATPase complexes that are expressed under wild-type conditions. One additional, proton pumping-independent function might be the proposed propagation of membrane fusion.

4.2.3. Vesicle fusion in the absence of ATP6AP2 and V-ATPase V_0 sectors

Distinct subunits of the V-ATPase V_0 sector have previously been implicated in membrane fusion events along the endocytic and the exocytic pathways (Vavassori and Mayer, 2014; Cotter *et al.*, 2015). The knockout of *Atp6ap2* decreased the level of all of these complex members in a

single genetic approach. Using ATP6AP2-deficient macrophages, fusion processes along multiple vesicle trafficking axes were analysed for their dependency on the presence of V-ATPase V_0 sectors.

The intracellular distribution of cathepsin D was utilised to evaluate membrane fusion in the course of protein sorting. Following biosynthesis at the endoplasmic reticulum, the protease is sorted via the Golgi apparatus to the lysosomes. In immunofluorescence analyses, cathepsin D was mainly found in lysosomes of both, wild-type and ATP6AP2-deficient macrophages. This suggests efficient vesicle fusion along the route of cathepsin D transport. In conclusion, the loss of ATP6AP2 did not affect membrane fusion between the sorting organelles and typical carrier compartments, *e.g.* clathrin-coated vesicles.

Furthermore, the influence of a V-ATPase V_0 sector depletion on fusion events along the endocytic route was examined in macrophages. Following the uptake of dextran-Texas Red® and DQ™ Red-BSA by endocytosis, the compounds were delivered to late endosomes/ lysosomes of wild-type and *Atp6ap2* knockout cells. Hence, the decreased level of V-ATPase V_0 sectors in ATP6AP2-deficient macrophages did not interfere with endosomal processing and the fusion between early and late endocytic compartments.

Overall, many intracellular fusion events proceeded in the absence of ATP6AP2. However, organelles such as carrier vesicles, the Golgi apparatus and early endosomes feature a low expression of V-ATPase complexes. Therefore, vesicle fusion between these compartments might not necessarily be affected by a reduction in V-ATPase V_0 sector levels.

In wild-type phagocytes, V-ATPases are highly enriched in the membrane of lysosomes and maturing phagosomes. This allows the efficient proteolytic degradation by lysosomal hydrolases and protects the cell from pathogenic organisms. Therefore, the fusion between phagosomes and lysosomes might be most sensitive to a reduced availability of V-ATPase V_0 sectors. However, despite the knockout of *Atp6ap2*, latex bead-containing phagosomes acquired the lysosomal marker LAMP-2 during phagosome maturation. This indicates ongoing phagosome-lysosome fusion in the ATP6AP2-deficient macrophages.

To validate this finding, a second, independent *Atp6ap2* knockout mouse line was established that expresses the Cre recombinase under the control of a *LysM* promotor. In *Atp6ap2 LysM-Cre* conditional knockout macrophages, LAMP-2 acquisition to maturing latex bead-containing phagosomes was similar to wild-type cells and to *Atp6ap2 Mx1-Cre* conditional

knockout macrophages. Collectively, these data suggest that ATP6AP2 and the presence of V-ATPase V_0 sectors are dispensable for phagosome-lysosome fusion.

To further assess the delivery of lysosomal contents to maturing phagosomes at an ultra-structural level, electron microscopy was performed in collaboration with the groups of *Prof. Dr. Albert Haas (Institute for Cell Biology, University of Bonn)* and *Prof. Dr. Gareth Griffiths (Department of Biosciences, University of Oslo)* (Fig. 4.3). Pre-loaded nano particles were delivered from lysosomes to latex bead-containing phagosomes in wild-type and *Atp6ap2* knockout macrophages (Kissing *et al.*, 2015). Intriguingly, macrophages lacking ATP6AP2 acquired more lysosomal nano particles per phagosome than the respective wild-type controls. This argues for a higher rate of content exchange between phagosomes and lysosomes in the *Atp6ap2* knockout macrophages. Elevated rates of full fusion as well as an increased occurrence of kiss and run fusion could explain this observation. The deposits of nano particles that were found in phagosomes of ATP6AP2-deficient cells were mainly restricted to small areas, which indicated kiss and run fusion as the mainly responsible process.

As transient mode of membrane fusion, kiss and run processes were initially characterised during vesicle exocytosis at neuromuscular junctions. In the frog, the temporarily formed fusion pores were at least 20 nm in diameter (Heuser and Reese, 1981). A similar sized fusion pore in murine macrophages would suffice to transfer the 10 nm nano particles utilised for electron microscopy. Sequential kiss and run fusion could moreover account for the differential delivery of low and high molecular weight molecules during phagosome maturation (Wang and Goren, 1987; Berthiaume *et al.*, 1995; Desjardins *et al.*, 1997). It remains to be addressed, in how far the decrease in V-ATPase V_0 sector levels propagates kiss and run fusion. Since V-ATPases are bulky protein complexes, a reduction in steric hindrance between phagosomes and lysosomes might support fusion of both organelles with each other. However, this would imply that the presence of V-ATPase V_0 sectors is no prerequisite for membrane fusion itself.

Because kiss and run fusion also contributes to the distribution of endocytic cargo (Berthiaume *et al.*, 1995; Bright *et al.*, 2005), the uptake and transport of dextran-Texas Red® (70 kDa) to lysosomal structures was compared between wild-type and ATP6AP2-deficient macrophages. Similar to the nano particles used for electron microscopy, dextran of 70 kDa has a hydrodynamic diameter of approximately 10 nm (Choi *et al.*, 2010). No kinetic differences were observed for lysosomal dextran-Texas Red® acquisition between the two genotypes. This

suggests that dextran-Texas Red® is transferred from endosomes to lysosomes with a similar efficiency in wild-type and ATP6AP2-deficient macrophages. Hence, kiss and run fusion between endosomes and lysosomes was not increased in *Atp6ap2* knockout macrophages.

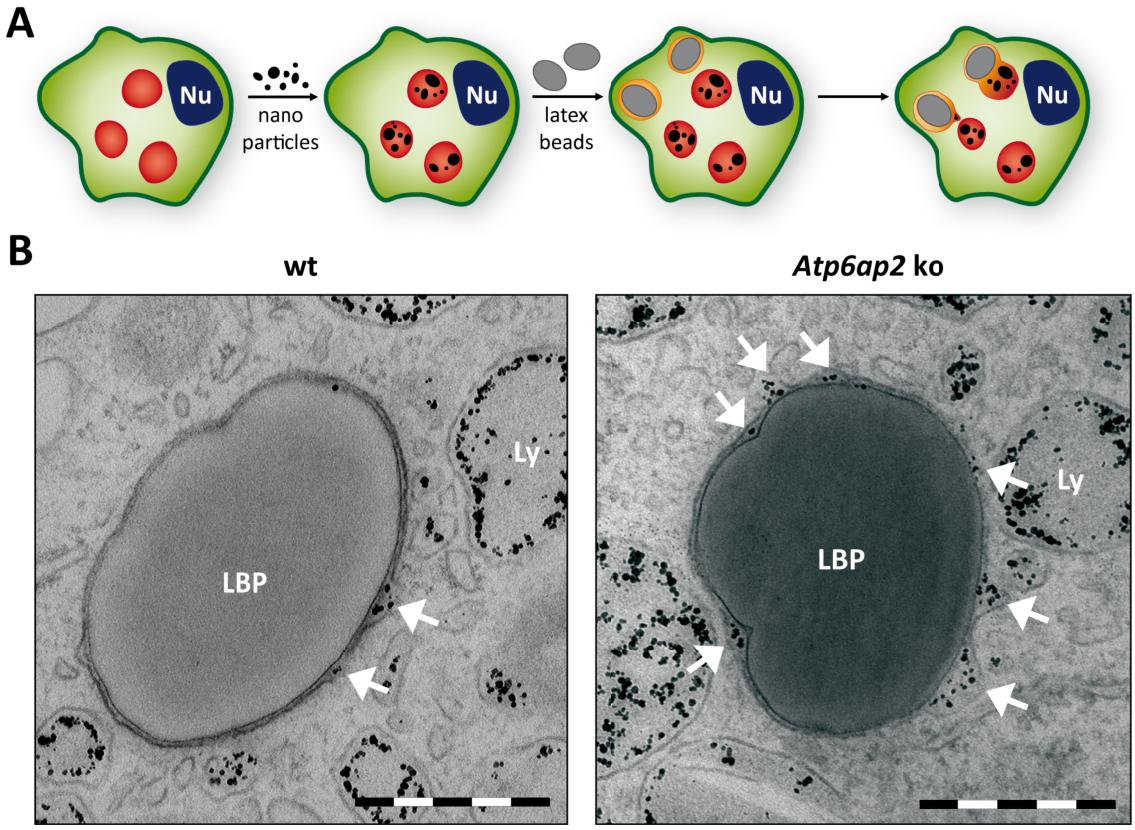

Figure 4.3: Enhanced phagosome-lysosome fusion in Atp6ap2 *knockout macrophages.*

(A) Experimental design to assess fusion between latex bead-containing phagosomes (orange) and lysosomes (red) in bone marrow-derived macrophages. Nuclei (Nu) are depicted in blue. Lysosomes were pulse-chase labelled with ferrous nano particles before cells were fed with latex beads for 10 minutes. (B) Following further two hours of phagosome maturation, samples were processed for electron microscopy. Representative micrographs show latex bead-containing phagosomes (LBP) of wild-type (wt) and *Atp6ap2* knockout (ko) macrophages with deposits of nano particles (arrows). Ly, lysosome. Scale bars = 500 nm. Experiments were conducted and evaluated by *Christina Hermsen (University of Bonn)* and *Urska Repnik (University of Oslo).* Taken from (Kissing *et al.*, 2015).

Taken together, kiss and run processes during phagosome maturation and endosomal processing were not uniformly affected by the loss of ATP6AP2. This could hint to distinct modes of regulation for both processes. Next to kiss and run fusion, also full fusion between lysosomes and endosomes could contribute to the distribution of dextran-Texas Red® upon endocytosis. Therefore, full fusion between endocytic compartments should be further addressed in the *Atp6ap2* knockout macrophages. Particles with diameters exceeding 20 nm

cannot be transferred via kiss and run fusion and are suitable for future analyses of full fusion during phagosome and endosome maturation.

Overall, the lack of an apparent fusion defect in the *Atp6ap2*-deleted macrophages contradicts the multiple reports on V-ATPase-mediated fusion processes. In zebrafish, phagocytosis of apopotic bodies by microglial cells depends on the presence of the V-ATPase V_0 subunit a1 (Peri and Nusslein-Volhard, 2008). Although this process is comparable to the maturation of latex bead-containing phagosomes, a promoting influence of the V-ATPase in phagosome-lysosome fusion was not supported in peritoneal macrophages. Variations in the cell type and the phagocytic cargo could explain the divergent results between this work and the study by Peri and Nusslein-Volhard.

Additional reports argue against a substantial participation of the V-ATPase in vesicle fusion. Reconstitution of membrane fusion from purified yeast vacuoles succeeded in the absence of the V-ATPase complex (Stroupe *et al.*, 2009). Similarly, mammalian fusion processes between early endosomal compartments required Rab GTPases and SNAREs for effective reconstitution, whereas the V-ATPase was dispensable (Ohya *et al.*, 2009). These two *in vitro* studies would be in agreement with the data obtain during this thesis. Therefore, the V-ATPase complex might not be generally required for the process of membrane fusion. The participation of V-ATPases could rather be limited to distinct, specialised vesicle fusion events.

4.3. Importance of ATP6AP2 and the V-ATPase in the autophagic flux

In the process of autophagy, cellular constituents are sequestered into autophagosomes and degraded following the maturation of this newly formed compartment (McEwan and Dikic, 2011). The efficient flow of autophagy requires the activity of V-ATPases at several important stages (Fig. 4.4). A low luminal pH of autophagosomes is a prerequisite for a proteolytically active milieu and is established with the aid of the V-ATPase complex. The maturation of autophagosomes further relies on a number of vesicle fusion processes that are possibly influenced by the V-ATPase (Yamamoto *et al.*, 1998; Kawai *et al.*, 2007). In addition, the proton pumping complex is involved in the regulation of autophagy via the mTOR complex 1. A high abundance of lysosomal amino acid is sensed by V-ATPases in a yet unclear mechanism. This triggers the activation of mTORC1 through a direct interaction with the mTORC1-recruiting Ragulator complex (Zoncu *et al.*, 2011; Zhang *et al.*, 2014; Jewell *et al.*, 2015; Wang *et al.*,

2015). Subsequently the unc-like kinase (ULK) complex is inhibited by mTORC1 (Ganley *et al.*, 2009; Hosokawa *et al.*, 2009; Jung *et al.*, 2009), which interferes with the initiation of autophagy. Because of these multiple connections between the V-ATPase and autophagy, the importance of V-ATPases for the functionality of this pathway was evaluated in the *Atp6ap2* conditional knockout model.

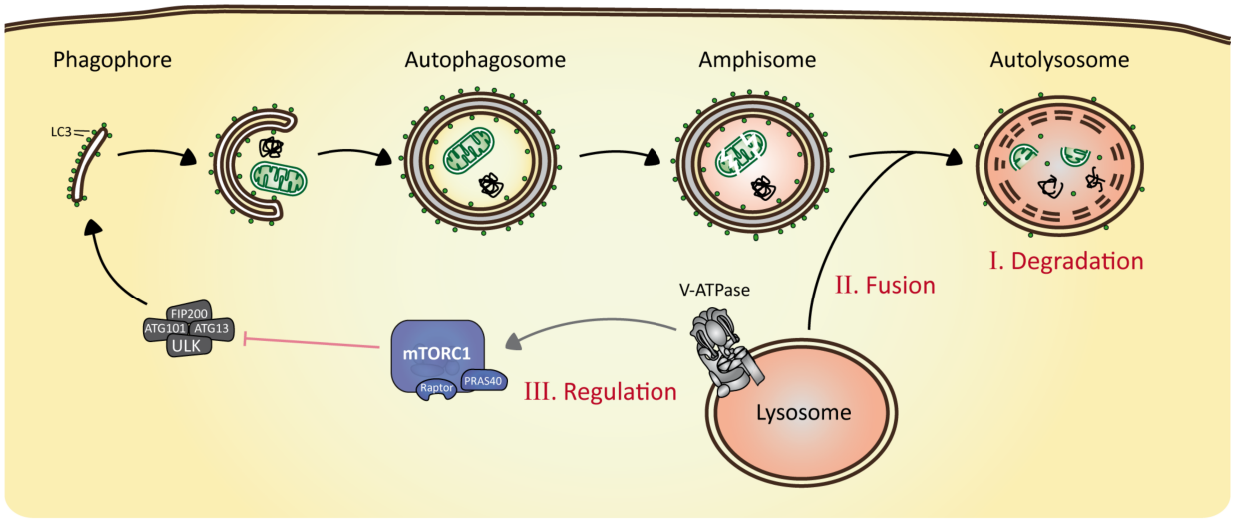

Figure 4.4: Three functions of the V-ATPase complex in autophagosome maturation.

V-ATPases affect the development of degradative autophagosomes at distinct steps. (I) Proteolytic processing in autolysosomes depends on a low luminal pH that requires the proton pumping activity of V-ATPases. (II) Fusion between autophagosomes/ amphisomes and lysosomes relies on the V-ATPase complex. (III) Initiation of autophagy is mediated by the ULK complex consisting of ULK1 or 2, ATG13, ATG101 and FIP200. The ULK complex is inhibited by the V-ATPase via activation of the mTOR complex 1 (mTORC1).

4.3.1. Knockout of *Atp6ap2* elucidates vesicle accumulation in hepatocytes

The liver is a central organ that contributes to essential metabolic functions. Many of these processes, *e.g.* the synthesis and storage of metabolites, are realised in the major cell population of the liver, the hepatocytes. In addition, these cells are responsible for the breakdown of storage material and the subsequent secretion of usable molecules (Czaja *et al.*, 2013). Therefore, hepatocytes feature an augmented appearance of autophagy, which was exploited for the analysis of this process under conditions of reduced V-ATPase V_0 sector levels.

In the *Atp6ap2* conditional knockout system, the liver was most sensitive to an induction of the *Mx1-Cre* transgene. Using *Rosa26-EYFP Mx1-Cre* reporter animals, Cre-mediated recombination

was detectable in hepatocytes and Kupffer cells, whereas endothelial cells showed no Cre recombinase activity. Accordingly, whole liver lysates of *Atp6ap2* conditional knockout animals displayed a clear decrease in the protein level of ATP6AP2. This depletion of ATP6AP2 was associated with diminished protein levels of various V-ATPase V_0 subunits and led to a significant increase in liver size and weight.

On the cellular level, *Atp6ap2* knockout hepatocytes were enlarged and displayed an accumulation of endocytic (Rab5- and LAMP-1-positive) as well as autophagic (p62- and LC3-positive) compartments. Interestingly, co-localisation was observed between LC3 and LAMP-1, but not between the autophagic adaptor protein p62 and the lysosomal marker. This hints to a dysfunction in autophagosome maturation. Earlier analyses of tissue specific *Atp6ap2* knockout mice revealed similar alterations in the ATP6AP2-depleted cells. Upon loss of *Atp6ap2* in cardiomyocytes and podocytes, these cells exhibited an increased vacuolisation (Kinouchi *et al.*, 2010; Oshima *et al.*, 2011; Riediger *et al.*, 2011). However, the autophagosomes of *Atp6ap2* conditional knockout hepatocytes contained partially degraded material as observed by electron microscopy. Therefore, a complete block in autophagic processing is not obvious in the ATP6AP2-depleted hepatocytes.

Pathological situations in distinct tissues and especially the liver are often associated with a malfunction of the Wnt signalling pathway (Thompson and Monga, 2007). In recent years, this signalling cascade has also been brought in connection with ATP6AP2 and the V-ATPase complex (Cruciat *et al.*, 2010; Hermle *et al.*, 2010; Bernhard *et al.*, 2012). However, the accumulation of vesicles in *Atp6ap2* knockout podocytes was seemingly unrelated to Wnt signalling, since a podocyte-specific knockout of the central Wnt effector β-catenin did not yield a comparable phenotype (Dai *et al.*, 2009; Oshima *et al.*, 2011; Riediger *et al.*, 2011). Judging by the similarity of the observations in ATP6AP2-deficient podocytes and hepatocytes, the transformation of *Atp6ap2* conditional knockout liver might also be Wnt-independent. In support of a negligible Wnt influence, initial experiments analysing the expression of the Wnt downstream targets *CycD1* and *Axin2* (Sethi and Vidal-Puig, 2008) revealed no apparent difference between wild-type and ATP6AP2-depleted liver. Other functions of ATP6AP2 and the V-ATPase complex were thus examined as a possible origin of the endocytic and autophagic dysfunction in *Atp6ap2* conditional knockout liver.

4.3.2. Characterisation of functional lysosomes in hepatocytes lacking ATP6AP2

In the terminal phase of autophagy, the autophagic cargo is degraded within autolysosomes. To support an optimal activity of the responsible hydrolases, these late organelles require an acidic luminal pH that is generated by the V-ATPase complex. In ATP6AP2-deficient podocytes and cardiomyocytes, a defect in vesicle acidification impaired the proteolytically active milieu of degradative vesicles and induced their accumulation (Kinouchi *et al.*, 2010; Oshima *et al.*, 2011; Riediger *et al.*, 2011). Whether a similar block in lysosomal and autolysosomal degradation caused the accumulation of the ubiquitin-binding protein p62 and its interaction partner LC3-II in *Atp6ap2* conditional knockout liver was analysed in hepatocytes.

Both, wild-type and ATP6AP2-depleted hepatocytes displayed acidic organelles in fluorescence analyses using LysoTracker Red® staining. Therefore, the reduced levels of the V-ATPase V_0 sector in *Atp6ap2* knockout cells did not interfere with vesicular acidification. It is of note that small changes in the luminal pH were not detectable with the applied LysoTracker® Red staining and might have gone unnoticed. However, following endocytosis of DQ™ Red-BSA, the compound was efficiently hydrolysed in LAMP-1-positive lysosomes of wild-type and ATP6AP2-deficient hepatocytes. Therefore, the proven vesicular acidification in *Atp6ap2* knockout cells sufficed to facilitate lysosomal protein degradation.

Kinetics of this degradation process have not yet been analysed in ATP6AP2-deficient hepatocytes. Over an extended period, small disparities in the degradation efficiency could add up to the accumulation of degradation prone proteins in ATP6AP2-depleted liver. Therefore, the rate of lysosomal protein degradation should be examined in future experiments, *e.g.* in an analysis of long-lived protein degradation upon incorporation of [^{14}C]-valine.

Due to the low yield of ATP6AP2-deficient cells during the hepatocyte isolation procedure, conclusions from the *in cellulo* experiments to the *in vivo* situation in liver have to be drawn carefully. The non-isolable population of *Atp6ap2* knockout hepatocytes might reflect extensively damaged cells of the ATP6AP2-depleted liver.

Overall, the obtained *Atp6ap2* knockout hepatocytes displayed proteolytically active lysosomes but still accumulated p62 and LAMP-1. This suggests that a defect in luminal acidification and consequentially in vesicular degradation is not the initial trigger of the vesicle accumulation in ATP6AP2-depleted liver. Further analyses focussing on vesicle acidification and lysosome function in total liver could help to strengthen this assumption.

4.3.3. Autophagic vesicle fusion under conditions of reduced V-ATPase V_0 sector levels

In the course of autophagosome maturation, autophagic vesicles experience a number of membrane fusion events. Decreased levels of the V-ATPase complex might interfere with these processes, which could explain the accumulation of autophagic organelles in ATP6AP2-deficient hepatocytes. A proton pumping-independent influence of V-ATPases could have caused the increased vacuolisation in these cells. This would be in agreement with previously characterised fusion processes that depend on the presence of the V-ATPases complex (Vavassori and Mayer, 2014; Cotter *et al.*, 2015).

Vesicle fusion during autophagosome maturation was assessed by electron microscopy using BSA-gold as an endocytic tracer. In wild-type and ATP6AP2-deficient hepatocytes, BSA-gold was taken up and delivered to autophagosomes of all maturation stages. Although hepatocytes lacking ATP6AP2 showed an accumulation of endocytic and autophagic organelles, the distribution of BSA-gold was comparable between both genotypes. Thus, fusion between endocytic and autophagic compartments was not generally impaired by the loss of ATP6AP2 and the subsequent reduction in V-ATPase V_0 sector levels.

However, the vesicles that were categorised as degradative autophagic vacuoles in electron micrographs could represent both, autolysosomes and amphisomes. A delivery of BSA-gold to amphisomes does not require contact between autophagosomes and lysosomes and could mask a block in autolysosome generation. Arguing against this hypothesis, LC3 and LAMP-1 displayed a clear co-localisation in immunofluorescence analyses of ATP6AP2-depleted liver sections. This indicates an efficient delivery of autophagic cargo to autolysosomes. Furthermore, immunogold-labelling of LAMP-2 in electron microscopy illustrates the autolysosomal identity of the BSA-gold-containing autophagic vacuoles in *Atp6ap2* knockout hepatocytes (data not shown). Therefore, the immunofluorescence and the immunogold analysis, both indicate functional autophagosome-lysosome fusion under conditions of reduced V-ATPase V_0 sector expression. In accordance with these findings, a recent study by Mauvezin *et al.* revealed continuous autolysosome generation in the absence of functional V-ATPase complexes (Mauvezin *et al.*, 2015).

Taken together, the loss of ATP6AP2 did not interfere with membrane fusion along the autophagic pathway in hepatocytes. Therefore, a disruption in autophagosome maturation is

most likely not the cause for the cellular pathology in ATP6AP2-depleted liver. Similar to the analysis of vesicle acidification in *Atp6ap2* knockout hepatocytes, kinetic differences in membrane fusion cannot be excluded and could contribute to the observed phenotype. Therefore, the fusion kinetics of autophagosome maturation should be examined in future assays.

4.3.4. Regulation of autophagy by mTORC1 and the V-ATPase complex

Neither protein clearance in endosomes nor vesicle fusion were clearly impaired in the *Atp6ap2* knockout hepatocytes. Therefore, the regulation of autophagy came into the focus of attention. The switch between cell growth and autophagy is mediated by the mTOR complex 1. Active mTORC1 inhibits the progression of autophagy at several instances. It phosphorylates and thereby inactivates the ULK complex, which represents a crucial component in autophagy initiation (Ganley *et al.*, 2009; Hosokawa *et al.*, 2009; Jung *et al.*, 2009). Furthermore, the promotion of autophagic and lysosomal gene expression is attenuated by mTORC1 through phosphorylation of the transcription factor EB (TFEB) (Palmieri *et al.*, 2011; Settembre *et al.*, 2011; Martina *et al.*, 2012; Roczniak-Ferguson *et al.*, 2012; Settembre *et al.*, 2012).

In line with its central position in metabolic regulation, the activation of mTORC1 depends on multiple input signals. Extracellularly initiated signalling cascades, e.g. the PI3K/ Akt pathway provide one stimulus for mTORC1 activity. In addition, the supply of lysosomal amino acids is sensed with the aid of the V-ATPase complex and further triggers the activation of mTORC1 (Zoncu *et al.*, 2011; Jewell *et al.*, 2015; Wang *et al.*, 2015).

4.3.4.1 Activation state of mTORC1 in ATP6AP2-depleted liver

In ATP6AP2-deficient hepatocytes, the reduction of V-ATPase V_0 sectors could impair the activation of mTORC1 leading to the increased occurrence of autophagy. Accordingly, the activity of mTORC1 was determined in ATP6AP2-depleted liver with respect to mTORC1 downstream targets and the subcellular localisation of the complex.

Three of five analysed TFEB-regulated genes displayed an increased transcription level in *Atp6ap2* conditional knockout liver. This could correlate with a reduced phosphorylation of the transcription factor by mTORC1, which would favour the nuclear localisation of TFEB. However, our experiments revealed no difference in the ratio of phosphorylated (cytoplasmic) and non-phosphorylated (nuclear) TFEB between wild-type and ATP6AP2-depleted liver (data not

shown). Instead, the overall protein level of TFEB was increased in *Atp6ap2* conditional knockout livers, which similarly causes an augmented transcription of TFEB target genes.

Interestingly, the transcription of mRNA coding for LAMP-1 is regulated by TFEB but was not significantly increased in *Atp6ap2* conditional knockout liver and hepatocytes. This is in contrast to the much higher protein level of LAMP-1 that was present in these samples. Additional post-transcriptional factors might influence the accumulation of autophagic and endocytic proteins. In this context, reduced kinetics of lysosomal degradation could explain the accumulation of the analysed proteins in ATP6AP2-deficient cells. It is of note that TFEB-independent autophagy-related genes showed significantly decreased transcription levels in ATP6AP2-depleted liver. This may be explained by a compensatory mechanism to rescue the vesicle and protein accumulation and provide better cell survival. However, the transcriptional regulation was not sufficient to restore wild-type levels of vesicle populations in *Atp6ap2* conditional knockout livers.

The V-ATPase complex promotes the lysosomal recruitment of mTORC1 (Zoncu *et al.*, 2011), which is a prerequisite for activation of the kinase mTOR by lysosome-resident Rheb (Saucedo *et al.*, 2003; Stocker *et al.*, 2003; Long *et al.*, 2005). Therefore, the subcellular localisation of mTOR was determined. Unfortunately, immunofluorescence analyses in *Atp6ap2* knockout hepatocytes were aggravated by the accumulation of LAMP-positive structures and a low anti-mTOR antibody performance. Hence, isolated liver lysosomes (tritosomes) were examined by immunoblotting. Surprisingly, this revealed an elevated lysosomal presence of mTOR upon depletion of ATP6AP2. In addition, components of the mTORC1 recruiting machinery were more abundant on tritosomes of *Atp6ap2* conditional knockout livers.

The elevated lysosomal presence of mTOR in ATP6AP2-depleted liver hints to an increased stimulation of the mTORC1. In support of this finding, enhanced mTORC1 activity was indicated by the prominent phosphorylation of p70S6K and PRAS40 in *Atp6ap2* conditional knockout liver(Master´s thesis S. Rudnik, 2014). However, an active mTORC1 in ATP6AP2-depleted liver contradicts the accumulation of endocytic and autophagic vacuoles in this tissue. Apart from mTORC1, growth factor-mediated PI3K- and Akt signalling could be responsible for the observed phosphorylation of p70S6K and PRAS40 (Dufner and Thomas, 1999; Sancak *et al.*, 2007). Therefore, the results concerning mTORC1 activity in *Atp6ap2* conditional knockout liver should be evaluated with caution.

Overall, the accumulation of autophagic and endocytic vacuoles in *Atp6ap2* conditional knockout liver is presumably unrelated to a lack of mTORC1 activity. An interplay between different intracellular pathways might determine the rate of mTORC1 signalling in this tissue. In addition, the extracellular stimulation of mTORC1 and PI3K/ Akt signalling could be influenced by other interferon α-sensitive cell populations that secrete *e.g.* insulin and growth factors.

4.3.4.2 Role of the V-ATPase complex in mTORC1 regulation in fibroblasts

The phenotype of ATP6AP2-deficient hepatocytes complicates an evaluation of the relationship between mTORC1 signalling and the presence of the V-ATPase complex. To minimise the influence of secondary effects by additionally targeted cell populations, immortalised *Atp6ap2* knockout MEF lines were used.

Fibroblasts lacking ATP6AP2 displayed a significant drop in V-ATPase V_0 sector subunits that impaired neither the lysosomal pH nor lysosome functions. Importantly, *Atp6ap2* knockout MEFs displayed no vacuolisation comparable to the phenotype that was observed in ATP6AP2-depleted liver. Therefore, the cultivated fibroblast lineages allowed to focus on the link between the V-ATPase and the activation of mTORC1.

In *Atp6ap2* knockout fibroblasts the response of mTORC1 to amino acid stimulation was drastically reduced. In line with this finding, recent studies revealed an impaired mTORC1 activation in HEK 293 cells and fibroblasts depleted for the V-ATPase V_0 subunit c (Zoncu *et al.*, 2011; Jewell *et al.*, 2015). Overall, this confirms a requirement for the V-ATPase complex to signal the abundance of amino acids to mTORC1.

It is of note that the stimulation of mTORC1 by amino acids was not completely abolished in ATP6AP2-deficient fibroblasts. This might be due to residual V-ATPase complexes or the activation of mTORC1 by additional pathways (Fig. 1.6). The presence of cytoplasmic leucine can induce mTORC1 activity via sestrin 2 and a subsequent inhibition of the Gator complex (Chantranupong *et al.*, 2014; Wolfson *et al.*, 2015). Similarly, cytoplasmic arginine alleviates the inhibitory effect of TSC2 on the lysosomal mTORC1 activator Rheb (Carroll *et al.*, 2016). Thereby, both amino acids could stimulate mTORC1 independent of the V-ATPase complex.

Glucose that was present in the reactivation medium also affects the activity of mTORC1. High levels of the sugar modulate the activation of the mTORC1-recruiting Rag GTPases.

Furthermore, glucose indirectly stimulates the PI3K-/ Akt signalling cascade that activates mTORC1 (Mahimainathan *et al.*, 2006; Efeyan *et al.*, 2013). However, the addition of DMEM as reactivation medium could not initiate the Akt-dependent phosphorylation of PRAS40. This argues against a substantial influence of glucose on the Akt pathway.

Surprisingly, the loss of ATP6AP2 had no marked impact on the steady-state phosphorylation of mTORC1 downstream targets in fibroblasts. It remains open, which regulatory pathways compensate for the decreased response of mTORC1 to amino acid stimulation in these cells. Comparable to ATP6AP2-depleted liver, an increased activation of the PI3K/ Akt pathway by insulin and growth factors could provide a possible explanation. In this respect, a heightened sensitivity of ATP6AP2-deficient MEFs to insulin is indicated (data not shown). In follow-up studies, the influence of V-ATPases on extracellularly activated signalling pathways will be examined in more detail.

Taken together, the experiments using *Atp6ap2* knockout fibroblasts confirmed the necessity of the V-ATPase for the activation of mTORC1 by amino acids. However, additional factors, such as insulin signalling, stimulate mTORC1 also in the absence of the V-ATPase and help to maintain an unaltered steady-state activity of mTORC1 signalling.

4.4. Conclusions

In the present thesis, intracellular fusion events along the endocytic and autophagic pathways proceeded under conditions of reduced V-ATPase expression levels. Neither inhibition of the proton-pumping activity nor a reduction of accessible free V_0 sectors led to an altered rate of phagosomal fusion.

Overall, these data do not support a model for membrane fusion that involves a V-ATPase-mediated fusion pore. The alternative model, the SNARE-dependent formation of a fusion pore is favoured as a likely intermediate of membrane fusion. Other proposed components of the fusion machinery, *e.g.* members of the HOPS tethering complex, represent interesting targets that could be analysed in regard to membrane fusion in future projects.

In general, vesicle fusion is involved in many different processes within a cell that feature distinct regulatory mechanisms. Previous reports showed that V-ATPases are required for granule secretion from neuronal cells (Hiesinger *et al.*, 2005; Di Giovanni *et al.*, 2010; Poea-Guyon *et al.*, 2013; Wang *et al.*, 2014). It will be of interest to further evaluate the influence of

the proton pump on exocytosis. This could clarify, whether the reported V-ATPase-dependent fusion events represent exceptional fusion steps rather than a general mechanism.

In the framework of this thesis, the influence of the V-ATPase complex on the amino acid-dependent activation of mTORC1 confirmed another role of the proton pump in fibroblasts. Yet, the molecular mechanism of this function remains unclear. The activity of the V-ATPase is required for efficient mTORC1 activation (Zoncu *et al.*, 2011; Wang *et al.*, 2015). Thus, the V-ATPase-mediated enrichment of luminal protons might be a prerequisite to transport amino acids across the lysosomal membrane. Direct interactions have been demonstrated between the V-ATPase and members of the mTORC1 recruiting Ragulator complex as well as between the V-ATPase and the amino acid transporter SLC38A9 (Zoncu *et al.*, 2011; Wang *et al.*, 2015). This could indicate a cross-talk between these complexes by conformational changes to promote the lysosomal recruitment of mTORC1 in the presence of amino acids.

Interestingly, in liver depleted for ATP6AP2, the reduction of V-ATPase V_0 sectors induced an accumulation of autophagic and endocytic vesicles, while mTORC1 signalling remained active. Whether a dysregulation of mTORC1 and/ or kinetic defects in lysosomal protein clearance and vesicle fusions are reasons for the vacuolisation in ATP6AP2-depleted hepatocytes is still unclear. To further address the activity of the mTORC1 in *Atp6ap2* conditional knockout liver, extracellular input signals and subsequently activated kinase cascades, such as the PI3K pathway, will be analysed in more detail.

In addition to the progression of mTORC1 signalling, it will be exciting to study other cellular functions and structures that are influenced by the V-ATPase in ATP6AP2-depleted liver. Distinct V_1 subunits interact with filamentous actin (Lee *et al.*, 1999; Chen *et al.*, 2004; Beaulieu *et al.*, 2005; Vitavska *et al.*, 2005). An influence of reduced V-ATPase expression levels on the integrity of the cytoskeleton might be conceivable. Altered cytoskeleton dynamics may provide an additional explanation for the vesicle accumulation in the ATP6AP2-deficient hepatocytes.

5. REFERENCES

Advani, A., Kelly, D.J., Cox, A.J., White, K.E., Advani, S.L., Thai, K., Connelly, K.A., Yuen, D., Trogadis, J., Herzenberg, A.M., *et al.* (2009). The (Pro)renin receptor: site-specific and functional linkage to the vacuolar H+-ATPase in the kidney. Hypertension *54*, 261-269.

Alvarez de Toledo, G., Fernandez-Chacon, R., and Fernandez, J.M. (1993). Release of secretory products during transient vesicle fusion. Nature *363*, 554-558.

Antonin, W., Holroyd, C., Tikkanen, R., Honing, S., and Jahn, R. (2000). The R-SNARE endobrevin/VAMP-8 mediates homotypic fusion of early endosomes and late endosomes. Mol Biol Cell *11*, 3289-3298.

Bainton, D.F. (1981). The discovery of lysosomes. J Cell Biol *91*, 66s-76s.

Balderhaar, H.J., Lachmann, J., Yavavli, E., Brocker, C., Lurick, A., and Ungermann, C. (2013). The CORVET complex promotes tethering and fusion of Rab5/Vps21-positive membranes. Proc Natl Acad Sci U S A *110*, 3823-3828.

Bar-Peled, L., and Sabatini, D.M. (2014). Regulation of mTORC1 by amino acids. Trends Cell Biol *24*, 400-406.

Bayer, M.J., Reese, C., Buhler, S., Peters, C., and Mayer, A. (2003). Vacuole membrane fusion: V0 functions after trans-SNARE pairing and is coupled to the Ca2+-releasing channel. J Cell Biol *162*, 211-222.

Beaulieu, V., Da Silva, N., Pastor-Soler, N., Brown, C.R., Smith, P.J., Brown, D., and Breton, S. (2005). Modulation of the actin cytoskeleton via gelsolin regulates vacuolar H+-ATPase recycling. J Biol Chem *280*, 8452-8463.

Benlekbir, S., Bueler, S.A., and Rubinstein, J.L. (2012). Structure of the vacuolar-type ATPase from Saccharomyces cerevisiae at 11-A resolution. Nat Struct Mol Biol *19*, 1356-1362.

Bernhard, S.M., Seidel, K., Schmitz, J., Klare, S., Kirsch, S., Schrezenmeier, E., Zaade, D., Meyborg, H., Goldin-Lang, P., Stawowy, P., *et al.* (2012). The (pro)renin receptor ((P)RR) can act as a repressor of Wnt signalling. Biochem Pharmacol *84*, 1643-1650.

Berthiaume, E.P., Medina, C., and Swanson, J.A. (1995). Molecular size-fractionation during endocytosis in macrophages. J Cell Biol *129*, 989-998.

Bjorkoy, G., Lamark, T., Brech, A., Outzen, H., Perander, M., Overvatn, A., Stenmark, H., and Johansen, T. (2005). p62/SQSTM1 forms protein aggregates degraded by autophagy and has a protective effect on huntingtin-induced cell death. J Cell Biol *171*, 603-614.

Blair, H.C., Borysenko, C.W., Villa, A., Schlesinger, P.H., Kalla, S.E., Yaroslavskiy, B.B., Garcia-Palacios, V., Oakley, J.I., and Orchard, P.J. (2004). In vitro differentiation of CD14 cells from osteopetrotic subjects: contrasting phenotypes with TCIRG1, CLCN7, and attachment defects. J Bone Miner Res *19*, 1329-1338.

Bock, J.B., Matern, H.T., Peden, A.A., and Scheller, R.H. (2001). A genomic perspective on membrane compartment organization. Nature *409*, 839-841.

Bond, S., and Forgac, M. (2008). The Ras/cAMP/protein kinase A pathway regulates glucose-dependent assembly of the vacuolar (H+)-ATPase in yeast. J Biol Chem *283*, 36513-36521.

Bowman, B.J., McCall, M.E., Baertsch, R., and Bowman, E.J. (2006). A model for the proteolipid ring and bafilomycin/concanamycin-binding site in the vacuolar ATPase of Neurospora crassa. J Biol Chem *281*, 31885-31893.

Bright, N.A., Gratian, M.J., and Luzio, J.P. (2005). Endocytic delivery to lysosomes mediated by concurrent fusion and kissing events in living cells. Curr Biol *15*, 360-365.

Brown, E.J., Albers, M.W., Shin, T.B., Ichikawa, K., Keith, C.T., Lane, W.S., and Schreiber, S.L. (1994). A mammalian protein targeted by G1-arresting rapamycin-receptor complex. Nature *369*, 756-758.

Brown, E.J., Beal, P.A., Keith, C.T., Chen, J., Shin, T.B., and Schreiber, S.L. (1995). Control of p70 s6 kinase by kinase activity of FRAP in vivo. Nature *377*, 441-446.

Brubaker, S.W., Bonham, K.S., Zanoni, I., and Kagan, J.C. (2015). Innate immune pattern recognition: a cell biological perspective. Annu Rev Immunol *33*, 257-290.

Brugarolas, J.B., Vazquez, F., Reddy, A., Sellers, W.R., and Kaelin, W.G., Jr. (2003). TSC2 regulates VEGF through mTOR-dependent and-independent pathways. Cancer Cell *4*, 147-158.

Brunn, G.J., Hudson, C.C., Sekulic, A., Williams, J.M., Hosoi, H., Houghton, P.J., Lawrence, J.C., Jr., and Abraham, R.T. (1997). Phosphorylation of the translational repressor PHAS-I by the mammalian target of rapamycin. Science *277*, 99-101.

Bryant, C.E., Orr, S., Ferguson, B., Symmons, M.F., Boyle, J.P., and Monie, T.P. (2015). International Union of Basic and Clinical Pharmacology. XCVI. Pattern recognition receptors in health and disease. Pharmacol Rev *67*, 462-504.

Burckle, C., and Bader, M. (2006). Prorenin and its ancient receptor. Hypertension *48*, 549-551.

Burnett, P.E., Barrow, R.K., Cohen, N.A., Snyder, S.H., and Sabatini, D.M. (1998). RAFT1 phosphorylation of the translational regulators p70 S6 kinase and 4E-BP1. Proc Natl Acad Sci U S A *95*, 1432-1437.

Cabrera, M., Arlt, H., Epp, N., Lachmann, J., Griffith, J., Perz, A., Reggiori, F., and Ungermann, C. (2013). Functional separation of endosomal fusion factors and the class C core vacuole/endosome tethering (CORVET) complex in endosome biogenesis. J Biol Chem *288*, 5166-5175.

Capecci, J., and Forgac, M. (2013). The function of vacuolar ATPase (V-ATPase) a subunit isoforms in invasiveness of MCF10a and MCF10CA1a human breast cancer cells. J Biol Chem *288*, 32731-32741.

Carroll, B., Maetzel, D., Maddocks, O.D., Otten, G., Ratcliff, M., Smith, G.R., Dunlop, E.A., Passos, J.F., Davies, O.R., Jaenisch, R.*, et al.* (2016). Control of TSC2-Rheb signaling axis by arginine regulates mTORC1 activity. Elife *5*.

Ceccarelli, B., Hurlbut, W.P., and Mauro, A. (1973). Turnover of transmitter and synaptic vesicles at the frog neuromuscular junction. J Cell Biol *57*, 499-524.

Chantranupong, L., Wolfson, R.L., Orozco, J.M., Saxton, R.A., Scaria, S.M., Bar-Peled, L., Spooner, E., Isasa, M., Gygi, S.P., and Sabatini, D.M. (2014). The Sestrins interact with GATOR2 to negatively regulate the amino-acid-sensing pathway upstream of mTORC1. Cell Rep *9*, 1-8.

Chen, S.H., Bubb, M.R., Yarmola, E.G., Zuo, J., Jiang, J., Lee, B.S., Lu, M., Gluck, S.L., Hurst, I.R., and Holliday, L.S. (2004). Vacuolar H+-ATPase binding to microfilaments: regulation in response to phosphatidylinositol 3-kinase activity and detailed characterization of the actin-binding site in subunit B. J Biol Chem *279*, 7988-7998.

Choi, J.J., Wang, S., Tung, Y.S., Morrison, B., 3rd, and Konofagou, E.E. (2010). Molecules of various pharmacologically-relevant sizes can cross the ultrasound-induced blood-brain barrier opening in vivo. Ultrasound Med Biol *36*, 58-67.

Christoforidis, S., McBride, H.M., Burgoyne, R.D., and Zerial, M. (1999). The Rab5 effector EEA1 is a core component of endosome docking. Nature *397*, 621-625.

Clare, D.K., Orlova, E.V., Finbow, M.A., Harrison, M.A., Findlay, J.B., and Saibil, H.R. (2006). An expanded and flexible form of the vacuolar ATPase membrane sector. Structure *14*, 1149-1156.

Clausen, B.E., Burkhardt, C., Reith, W., Renkawitz, R., and Forster, I. (1999). Conditional gene targeting in macrophages and granulocytes using LysMcre mice. Transgenic Res *8*, 265-277.

Collins, K.M., Thorngren, N.L., Fratti, R.A., and Wickner, W.T. (2005). Sec17p and HOPS, in distinct SNARE complexes, mediate SNARE complex disruption or assembly for fusion. EMBO J *24*, 1775-1786.

Coonrod, E.M., Graham, L.A., Carpp, L.N., Carr, T.M., Stirrat, L., Bowers, K., Bryant, N.J., and Stevens, T.H. (2013). Homotypic vacuole fusion in yeast requires organelle acidification and not the V-ATPase membrane domain. Dev Cell *27*, 462-468.

Cotter, K., Stransky, L., McGuire, C., and Forgac, M. (2015). Recent Insights into the Structure, Regulation, and Function of the V-ATPases. Trends Biochem Sci *40*, 611-622.

Cousin, C., Bracquart, D., Contrepas, A., Corvol, P., Muller, L., and Nguyen, G. (2009). Soluble form of the (pro)renin receptor generated by intracellular cleavage by furin is secreted in plasma. Hypertension *53*, 1077-1082.

Cruciat, C.M., Ohkawara, B., Acebron, S.P., Karaulanov, E., Reinhard, C., Ingelfinger, D., Boutros, M., and Niehrs, C. (2010). Requirement of prorenin receptor and vacuolar H+-ATPase-mediated acidification for Wnt signaling. Science *327*, 459-463.

Cunningham, J.T., Rodgers, J.T., Arlow, D.H., Vazquez, F., Mootha, V.K., and Puigserver, P. (2007). mTOR controls mitochondrial oxidative function through a YY1-PGC-1alpha transcriptional complex. Nature *450*, 736-740.

Czaja, M.J., Ding, W.X., Donohue, T.M., Jr., Friedman, S.L., Kim, J.S., Komatsu, M., Lemasters, J.J., Lemoine, A., Lin, J.D., Ou, J.H.*, et al.* (2013). Functions of autophagy in normal and diseased liver. Autophagy *9*, 1131-1158.

Dai, C., Stolz, D.B., Kiss, L.P., Monga, S.P., Holzman, L.B., and Liu, Y. (2009). Wnt/beta-catenin signaling promotes podocyte dysfunction and albuminuria. J Am Soc Nephrol *20*, 1997-2008.

Del Fattore, A., Peruzzi, B., Rucci, N., Recchia, I., Cappariello, A., Longo, M., Fortunati, D., Ballanti, P., Iacobini, M., Luciani, M.*, et al.* (2006). Clinical, genetic, and cellular analysis of 49 osteopetrotic patients: implications for diagnosis and treatment. J Med Genet *43*, 315-325.

Desjardins, M. (1995). Biogenesis of phagolysosomes: the 'kiss and run' hypothesis. Trends Cell Biol *5*, 183-186.

Desjardins, M., Huber, L.A., Parton, R.G., and Griffiths, G. (1994). Biogenesis of phagolysosomes proceeds through a sequential series of interactions with the endocytic apparatus. J Cell Biol *124*, 677-688.

Desjardins, M., Nzala, N.N., Corsini, R., and Rondeau, C. (1997). Maturation of phagosomes is accompanied by changes in their fusion properties and size-selective acquisition of solute materials from endosomes. J Cell Sci *110 (Pt 18)*, 2303-2314.

Di Giovanni, J., Boudkkazi, S., Mochida, S., Bialowas, A., Samari, N., Leveque, C., Youssouf, F., Brechet, A., Iborra, C., Maulet, Y.*, et al.* (2010). V-ATPase membrane sector associates with synaptobrevin to modulate neurotransmitter release. Neuron *67*, 268-279.

Diab, H., Ohira, M., Liu, M., Cobb, E., and Kane, P.M. (2009). Subunit interactions and requirements for inhibition of the yeast V1-ATPase. J Biol Chem *284*, 13316-13325.

Dibble, C.C., Elis, W., Menon, S., Qin, W., Klekota, J., Asara, J.M., Finan, P.M., Kwiatkowski, D.J., Murphy, L.O., and Manning, B.D. (2012). TBC1D7 is a third subunit of the TSC1-TSC2 complex upstream of mTORC1. Mol Cell *47*, 535-546.

Dibble, C.C., and Manning, B.D. (2013). Signal integration by mTORC1 coordinates nutrient input with biosynthetic output. Nat Cell Biol *15*, 555-564.

Downey, G.P., Botelho, R.J., Butler, J.R., Moltyaner, Y., Chien, P., Schreiber, A.D., and Grinstein, S. (1999). Phagosomal maturation, acidification, and inhibition of bacterial growth in nonphagocytic cells transfected with FcgammaRIIA receptors. J Biol Chem *274*, 28436-28444.

Duclos, S., Diez, R., Garin, J., Papadopoulou, B., Descoteaux, A., Stenmark, H., and Desjardins, M. (2000). Rab5 regulates the kiss and run fusion between phagosomes and endosomes and the acquisition of phagosome leishmanicidal properties in RAW 264.7 macrophages. J Cell Sci *113 Pt 19*, 3531-3541.

Dufner, A., and Thomas, G. (1999). Ribosomal S6 kinase signaling and the control of translation. Exp Cell Res *253*, 100-109.

Dunlop, E.A., and Tee, A.R. (2014). mTOR and autophagy: a dynamic relationship governed by nutrients and energy. Semin Cell Dev Biol *36*, 121-129.

Duve, C.D., Pressman, B.C., Gianetto, R., Wattiaux, R., and Appelmans, F. (1955). Tissue Fractionation Studies .6. Intracellular Distribution Patterns of Enzymes in Rat-Liver Tissue. Biochemical Journal *60*, 604-617.

Duvel, K., Yecies, J.L., Menon, S., Raman, P., Lipovsky, A.I., Souza, A.L., Triantafellow, E., Ma, Q., Gorski, R., Cleaver, S., *et al.* (2010). Activation of a metabolic gene regulatory network downstream of mTOR complex 1. Mol Cell *39*, 171-183.

Efeyan, A., Zoncu, R., Chang, S., Gumper, I., Snitkin, H., Wolfson, R.L., Kirak, O., Sabatini, D.D., and Sabatini, D.M. (2013). Regulation of mTORC1 by the Rag GTPases is necessary for neonatal autophagy and survival. Nature *493*, 679-683.

Eskelinen, E.L., Tanaka, Y., and Saftig, P. (2003). At the acidic edge: emerging functions for lysosomal membrane proteins. Trends Cell Biol *13*, 137-145.

Fasshauer, D., Sutton, R.B., Brunger, A.T., and Jahn, R. (1998). Conserved structural features of the synaptic fusion complex: SNARE proteins reclassified as Q- and R-SNAREs. Proc Natl Acad Sci U S A *95*, 15781-15786.

Feng, H., Cheng, T., Pavlos, N.J., Yip, K.H., Carrello, A., Seeber, R., Eidne, K., Zheng, M.H., and Xu, J. (2008). Cytoplasmic terminus of vacuolar type proton pump accessory subunit Ac45 is required for

proper interaction with V(0) domain subunits and efficient osteoclastic bone resorption. J Biol Chem *283*, 13194-13204.

Fernandez, J.M., Neher, E., and Gomperts, B.D. (1984). Capacitance measurements reveal stepwise fusion events in degranulating mast cells. Nature *312*, 453-455.

Fesce, R., Grohovaz, F., Valtorta, F., and Meldolesi, J. (1994). Neurotransmitter release: fusion or 'kiss-and-run'? Trends Cell Biol *4*, 1-4.

Fethiere, J., Venzke, D., Diepholz, M., Seybert, A., Geerlof, A., Gentzel, M., Wilm, M., and Bottcher, B. (2004). Building the stator of the yeast vacuolar-ATPase: specific interaction between subunits E and G. J Biol Chem *279*, 40670-40676.

Forgac, M. (1999). Structure and properties of the vacuolar (H+)-ATPases. J Biol Chem *274*, 12951-12954.

Forgac, M. (2007). Vacuolar ATPases: rotary proton pumps in physiology and pathophysiology. Nat Rev Mol Cell Biol *8*, 917-929.

Fukuda, M. (1991). Lysosomal membrane glycoproteins. Structure, biosynthesis, and intracellular trafficking. J Biol Chem *266*, 21327-21330.

Ganley, I.G., Lam du, H., Wang, J., Ding, X., Chen, S., and Jiang, X. (2009). ULK1.ATG13.FIP200 complex mediates mTOR signaling and is essential for autophagy. J Biol Chem *284*, 12297-12305.

Gautreau, A., Oguievetskaia, K., and Ungermann, C. (2014). Function and regulation of the endosomal fusion and fission machineries. Cold Spring Harb Perspect Biol *6*.

Getlawi, F., Laslop, A., Schagger, H., Ludwig, J., Haywood, J., and Apps, D. (1996). Chromaffin granule membrane glycoprotein IV is identical with Ac45, a membrane-integral subunit of the granule's H(+)-ATPase. Neurosci Lett *219*, 13-16.

Gieselmann, V., Hasilik, A., and von Figura, K. (1985). Processing of human cathepsin D in lysosomes in vitro. J Biol Chem *260*, 3215-3220.

Giraudo, C.G., Hu, C., You, D., Slovic, A.M., Mosharov, E.V., Sulzer, D., Melia, T.J., and Rothman, J.E. (2005). SNAREs can promote complete fusion and hemifusion as alternative outcomes. J Cell Biol *170*, 249-260.

Gu, F., and Gruenberg, J. (2000). ARF1 regulates pH-dependent COP functions in the early endocytic pathway. J Biol Chem *275*, 8154-8160.

Guinea, R., and Carrasco, L. (1995). Requirement for vacuolar proton-ATPase activity during entry of influenza virus into cells. J Virol *69*, 2306-2312.

Han, X., Bushweller, J.H., Cafiso, D.S., and Tamm, L.K. (2001). Membrane structure and fusion-triggering

conformational change of the fusion domain from influenza hemagglutinin. Nat Struct Biol *8*, 715-720.

Hansen, C.G., and Nichols, B.J. (2009). Molecular mechanisms of clathrin-independent endocytosis. J Cell Sci *122*, 1713-1721.

Hara, K., Yonezawa, K., Kozlowski, M.T., Sugimoto, T., Andrabi, K., Weng, Q.P., Kasuga, M., Nishimoto, I., and Avruch, J. (1997). Regulation of eIF-4E BP1 phosphorylation by mTOR. J Biol Chem *272*, 26457-26463.

Hayashi, H., Shitara, M., and Yamasaki, F. (1982). The origin of lipid accumulated in liver lysosomes after administration of triton WR-1339. J Biochem *92*, 1585-1590.

Henne, W.M., Stenmark, H., and Emr, S.D. (2013). Molecular mechanisms of the membrane sculpting ESCRT pathway. Cold Spring Harb Perspect Biol *5*.

Hermle, T., Saltukoglu, D., Grunewald, J., Walz, G., and Simons, M. (2010). Regulation of Frizzled-dependent planar polarity signaling by a V-ATPase subunit. Curr Biol *20*, 1269-1276.

Heuser, J.E., and Reese, T.S. (1973). Evidence for recycling of synaptic vesicle membrane during transmitter release at the frog neuromuscular junction. J Cell Biol *57*, 315-344.

Heuser, J.E., and Reese, T.S. (1981). Structural changes after transmitter release at the frog neuromuscular junction. J Cell Biol *88*, 564-580.

Hickey, C.M., and Wickner, W. (2010). HOPS initiates vacuole docking by tethering membranes before trans-SNARE complex assembly. Mol Biol Cell *21*, 2297-2305.

Hiesinger, P.R., Fayyazuddin, A., Mehta, S.Q., Rosenmund, T., Schulze, K.L., Zhai, R.G., Verstreken, P., Cao, Y., Zhou, Y., Kunz, J., *et al.* (2005). The v-ATPase V0 subunit a1 is required for a late step in synaptic vesicle exocytosis in Drosophila. Cell *121*, 607-620.

Hirata, R., Graham, L.A., Takatsuki, A., Stevens, T.H., and Anraku, Y. (1997). VMA11 and VMA16 encode second and third proteolipid subunits of the Saccharomyces cerevisiae vacuolar membrane H+-ATPase. J Biol Chem *272*, 4795-4803.

Holroyd, C., Kistner, U., Annaert, W., and Jahn, R. (1999). Fusion of endosomes involved in synaptic vesicle recycling. Mol Biol Cell *10*, 3035-3044.

Holthuis, J.C., Jansen, E.J., Schoonderwoert, V.T., Burbach, J.P., and Martens, G.J. (1999). Biosynthesis of the vacuolar H+-ATPase accessory subunit Ac45 in Xenopus pituitary. Eur J Biochem *262*, 484-491.

Hosokawa, N., Hara, T., Kaizuka, T., Kishi, C., Takamura, A., Miura, Y., Iemura, S., Natsume, T., Takehana, K., Yamada, N.*, et al.* (2009). Nutrient-dependent mTORC1 association with the ULK1-Atg13-FIP200 complex required for autophagy. Mol Biol Cell *20*, 1981-1991.

Hudson, C.C., Liu, M., Chiang, G.G., Otterness, D.M., Loomis, D.C., Kaper, F., Giaccia, A.J., and Abraham, R.T. (2002). Regulation of hypoxia-inducible factor 1alpha expression and function by the mammalian target of rapamycin. Mol Cell Biol *22*, 7004-7014.

Huotari, J., and Helenius, A. (2011). Endosome maturation. EMBO J *30*, 3481-3500.

Hurtado-Lorenzo, A., Skinner, M., El Annan, J., Futai, M., Sun-Wada, G.H., Bourgoin, S., Casanova, J., Wildeman, A., Bechoua, S., Ausiello, D.A.*, et al.* (2006). V-ATPase interacts with ARNO and Arf6 in early endosomes and regulates the protein degradative pathway. Nat Cell Biol *8*, 124-136.

Imamura, H., Nakano, M., Noji, H., Muneyuki, E., Ohkuma, S., Yoshida, M., and Yokoyama, K. (2003). Evidence for rotation of V1-ATPase. Proc Natl Acad Sci U S A *100*, 2312-2315.

Inoki, K., Li, Y., Xu, T., and Guan, K.L. (2003). Rheb GTPase is a direct target of TSC2 GAP activity and regulates mTOR signaling. Genes Dev *17*, 1829-1834.

Inoki, K., Li, Y., Zhu, T., Wu, J., and Guan, K.L. (2002). TSC2 is phosphorylated and inhibited by Akt and suppresses mTOR signalling. Nat Cell Biol *4*, 648-657.

Inoue, T., and Forgac, M. (2005). Cysteine-mediated cross-linking indicates that subunit C of the V-ATPase is in close proximity to subunits E and G of the V1 domain and subunit a of the V0 domain. J Biol Chem *280*, 27896-27903.

Ishidoh, K., Saido, T.C., Kawashima, S., Hirose, M., Watanabe, S., Sato, N., and Kominami, E. (1998). Multiple processing of procathepsin L to cathepsin L in vivo. Biochem Biophys Res Commun *252*, 202-207.

Iwata, M., Imamura, H., Stambouli, E., Ikeda, C., Tamakoshi, M., Nagata, K., Makyio, H., Hankamer, B., Barber, J., Yoshida, M.*, et al.* (2004). Crystal structure of a central stalk subunit C and reversible association/dissociation of vacuole-type ATPase. Proc Natl Acad Sci U S A *101*, 59-64.

Jahn, R., and Scheller, R.H. (2006). SNAREs--engines for membrane fusion. Nat Rev Mol Cell Biol *7*, 631-643.

Jahreiss, L., Menzies, F.M., and Rubinsztein, D.C. (2008). The itinerary of autophagosomes: from peripheral formation to kiss-and-run fusion with lysosomes. Traffic *9*, 574-587.

Jansen, E.J., Hafmans, T.G., and Martens, G.J. (2010). V-ATPase-mediated granular acidification is regulated by the V-ATPase accessory subunit Ac45 in POMC-producing cells. Mol Biol Cell *21*, 3330-3339.

Jansen, E.J., Scheenen, W.J., Hafmans, T.G., and Martens, G.J. (2008). Accessory subunit Ac45 controls the V-ATPase in the regulated secretory pathway. Biochim Biophys Acta *1783*, 2301-2310.

Jefferies, K.C., and Forgac, M. (2008). Subunit H of the vacuolar (H+) ATPase inhibits ATP hydrolysis by the free V1 domain by interaction with the rotary subunit F. J Biol Chem *283*, 4512-4519.

Jewell, J.L., Kim, Y.C., Russell, R.C., Yu, F.X., Park, H.W., Plouffe, S.W., Tagliabracci, V.S., and Guan, K.L. (2015). Metabolism. Differential regulation of mTORC1 by leucine and glutamine. Science *347*, 194-198.

Jung, C.H., Jun, C.B., Ro, S.H., Kim, Y.M., Otto, N.M., Cao, J., Kundu, M., and Kim, D.H. (2009). ULK-Atg13-FIP200 complexes mediate mTOR signaling to the autophagy machinery. Mol Biol Cell *20*, 1992-2003.

Jung, J., Genau, H.M., and Behrends, C. (2015). Amino Acid-Dependent mTORC1 Regulation by the Lysosomal Membrane Protein SLC38A9. Mol Cell Biol *35*, 2479-2494.

Kabeya, Y., Mizushima, N., Ueno, T., Yamamoto, A., Kirisako, T., Noda, T., Kominami, E., Ohsumi, Y., and Yoshimori, T. (2000). LC3, a mammalian homologue of yeast Apg8p, is localized in autophagosome membranes after processing. EMBO J *19*, 5720-5728.

Kabeya, Y., Mizushima, N., Yamamoto, A., Oshitani-Okamoto, S., Ohsumi, Y., and Yoshimori, T. (2004). LC3, GABARAP and GATE16 localize to autophagosomal membrane depending on form-II formation. J Cell Sci *117*, 2805-2812.

Kane, P.M. (1995). Disassembly and reassembly of the yeast vacuolar H(+)-ATPase in vivo. J Biol Chem *270*, 17025-17032.

Kane, P.M., Tarsio, M., and Liu, J. (1999). Early steps in assembly of the yeast vacuolar H+-ATPase. J Biol Chem *274*, 17275-17283.

Kantidakis, T., Ramsbottom, B.A., Birch, J.L., Dowding, S.N., and White, R.J. (2010). mTOR associates with TFIIIC, is found at tRNA and 5S rRNA genes, and targets their repressor Maf1. Proc Natl Acad Sci U S A *107*, 11823-11828.

Karet, F.E., Finberg, K.E., Nelson, R.D., Nayir, A., Mocan, H., Sanjad, S.A., Rodriguez-Soriano, J., Santos, F., Cremers, C.W., Di Pietro, A., *et al.* (1999). Mutations in the gene encoding B1 subunit of H+-ATPase cause renal tubular acidosis with sensorineural deafness. Nat Genet *21*, 84-90.

Kawai, A., Uchiyama, H., Takano, S., Nakamura, N., and Ohkuma, S. (2007). Autophagosome-lysosome fusion depends on the pH in acidic compartments in CHO cells. Autophagy *3*, 154-157.

Kawasaki-Nishi, S., Bowers, K., Nishi, T., Forgac, M., and Stevens, T.H. (2001a). The amino-terminal domain of the vacuolar proton-translocating ATPase a subunit controls targeting and in vivo dissociation,

and the carboxyl-terminal domain affects coupling of proton transport and ATP hydrolysis. J Biol Chem *276*, 47411-47420.

Kawasaki-Nishi, S., Nishi, T., and Forgac, M. (2001b). Arg-735 of the 100-kDa subunit a of the yeast V-ATPase is essential for proton translocation. Proc Natl Acad Sci U S A *98*, 12397-12402.

Kawasaki-Nishi, S., Nishi, T., and Forgac, M. (2001c). Yeast V-ATPase complexes containing different isoforms of the 100-kDa a-subunit differ in coupling efficiency and in vivo dissociation. J Biol Chem *276*, 17941-17948.

Kawasaki-Nishi, S., Nishi, T., and Forgac, M. (2003). Interacting helical surfaces of the transmembrane segments of subunits a and c' of the yeast V-ATPase defined by disulfide-mediated cross-linking. J Biol Chem *278*, 41908-41913.

Kim, B.Y., Kramer, H., Yamamoto, A., Kominami, E., Kohsaka, S., and Akazawa, C. (2001). Molecular characterization of mammalian homologues of class C Vps proteins that interact with syntaxin-7. J Biol Chem *276*, 29393-29402.

Kim, J.E., and Chen, J. (2004). regulation of peroxisome proliferator-activated receptor-gamma activity by mammalian target of rapamycin and amino acids in adipogenesis. Diabetes *53*, 2748-2756.

Kinouchi, K., Ichihara, A., Sano, M., Sun-Wada, G.H., Wada, Y., Kurauchi-Mito, A., Bokuda, K., Narita, T., Oshima, Y., Sakoda, M.*, et al.* (2010). The (pro)renin receptor/ATP6AP2 is essential for vacuolar H+-ATPase assembly in murine cardiomyocytes. Circ Res *107*, 30-34.

Kinouchi, K., Ichihara, A., Sano, M., Sun-Wada, G.H., Wada, Y., Ochi, H., Fukuda, T., Bokuda, K., Kurosawa, H., Yoshida, N.*, et al.* (2013). The role of individual domains and the significance of shedding of ATP6AP2/(pro)renin receptor in vacuolar H(+)-ATPase biogenesis. PLoS One *8*, e78603.

Kissing, S., Hermsen, C., Repnik, U., Nesset, C.K., von Bargen, K., Griffiths, G., Ichihara, A., Lee, B.S., Schwake, M., De Brabander, J.*, et al.* (2015). Vacuolar ATPase in phagosome-lysosome fusion. J Biol Chem *290*, 14166-14180.

Kobia, F., Duchi, S., Deflorian, G., and Vaccari, T. (2014). Pharmacologic inhibition of vacuolar H+ ATPase reduces physiologic and oncogenic Notch signaling. Mol Oncol *8*, 207-220.

Koren, I., Reem, E., and Kimchi, A. (2010). DAP1, a novel substrate of mTOR, negatively regulates autophagy. Curr Biol *20*, 1093-1098.

Kornak, U., Reynders, E., Dimopoulou, A., van Reeuwijk, J., Fischer, B., Rajab, A., Budde, B., Nurnberg, P., Foulquier, F., Lefeber, D.*, et al.* (2008). Impaired glycosylation and cutis laxa caused by mutations in the vesicular H+-ATPase subunit ATP6V0A2. Nat Genet *40*, 32-34.

Koyanagi, M., Asahara, S., Matsuda, T., Hashimoto, N., Shigeyama, Y., Shibutani, Y., Kanno, A., Fuchita, M., Mikami, T., Hosooka, T., *et al.* (2011). Ablation of TSC2 enhances insulin secretion by increasing the number of mitochondria through activation of mTORC1. PLoS One *6*, e23238.

Kramer, L., and Ungermann, C. (2011). HOPS drives vacuole fusion by binding the vacuolar SNARE complex and the Vam7 PX domain via two distinct sites. Mol Biol Cell *22*, 2601-2611.

Krop, M., Lu, X., Danser, A.H., and Meima, M.E. (2013). The (pro)renin receptor. A decade of research: what have we learned? Pflugers Arch *465*, 87-97.

Kuhn, R., Schwenk, F., Aguet, M., and Rajewsky, K. (1995). Inducible gene targeting in mice. Science *269*, 1427-1429.

Laemmli, U.K. (1970). Cleavage of structural proteins during the assembly of the head of bacteriophage T4. Nature *227*, 680-685.

Lamark, T., Kirkin, V., Dikic, I., and Johansen, T. (2009). NBR1 and p62 as cargo receptors for selective autophagy of ubiquitinated targets. Cell Cycle *8*, 1986-1990.

Lambert, J.F., Benoit, B.O., Colvin, G.A., Carlson, J., Delville, Y., and Quesenberry, P.J. (2000). Quick sex determination of mouse fetuses. J Neurosci Methods *95*, 127-132.

Lange, P.F., Wartosch, L., Jentsch, T.J., and Fuhrmann, J.C. (2006). ClC-7 requires Ostm1 as a beta-subunit to support bone resorption and lysosomal function. Nature *440*, 220-223.

Laplante, M., and Sabatini, D.M. (2012). mTOR signaling in growth control and disease. Cell *149*, 274-293.

Laughner, E., Taghavi, P., Chiles, K., Mahon, P.C., and Semenza, G.L. (2001). HER2 (neu) signaling increases the rate of hypoxia-inducible factor 1alpha (HIF-1alpha) synthesis: novel mechanism for HIF-1-mediated vascular endothelial growth factor expression. Mol Cell Biol *21*, 3995-4004.

Lee, B.S., Gluck, S.L., and Holliday, L.S. (1999). Interaction between vacuolar H(+)-ATPase and microfilaments during osteoclast activation. J Biol Chem *274*, 29164-29171.

Leighton, F., Poole, B., Beaufay, H., Baudhuin, P., Coffey, J.W., Fowler, S., and De Duve, C. (1968). The large-scale separation of peroxisomes, mitochondria, and lysosomes from the livers of rats injected with triton WR-1339. Improved isolation procedures, automated analysis, biochemical and morphological properties of fractions. J Cell Biol *37*, 482-513.

Li, S., Brown, M.S., and Goldstein, J.L. (2010). Bifurcation of insulin signaling pathway in rat liver: mTORC1 required for stimulation of lipogenesis, but not inhibition of gluconeogenesis. Proc Natl Acad Sci U S A *107*, 3441-3446.

Liberman, R., Bond, S., Shainheit, M.G., Stadecker, M.J., and Forgac, M. (2014). Regulated assembly of vacuolar ATPase is increased during cluster disruption-induced maturation of dendritic cells through a phosphatidylinositol 3-kinase/mTOR-dependent pathway. J Biol Chem *289*, 1355-1363.

Liegeois, S., Benedetto, A., Garnier, J.M., Schwab, Y., and Labouesse, M. (2006). The V0-ATPase mediates apical secretion of exosomes containing Hedgehog-related proteins in Caenorhabditis elegans. J Cell Biol *173*, 949-961.

Lin, X., Yang, T., Wang, S., Wang, Z., Yun, Y., Sun, L., Zhou, Y., Xu, X., Akazawa, C., Hong, W., *et al.* (2014). RILP interacts with HOPS complex via VPS41 subunit to regulate endocytic trafficking. Sci Rep *4*, 7282.

Liou, W., Geuze, H.J., Geelen, M.J., and Slot, J.W. (1997). The autophagic and endocytic pathways converge at the nascent autophagic vacuoles. J Cell Biol *136*, 61-70.

Lobingier, B.T., and Merz, A.J. (2012). Sec1/Munc18 protein Vps33 binds to SNARE domains and the quaternary SNARE complex. Mol Biol Cell *23*, 4611-4622.

Long, X., Lin, Y., Ortiz-Vega, S., Yonezawa, K., and Avruch, J. (2005). Rheb binds and regulates the mTOR kinase. Curr Biol *15*, 702-713.

Lubke, T., Lobel, P., and Sleat, D.E. (2009). Proteomics of the lysosome. Biochim Biophys Acta *1793*, 625-635.

Luzio, J.P., Poupon, V., Lindsay, M.R., Mullock, B.M., Piper, R.C., and Pryor, P.R. (2003). Membrane dynamics and the biogenesis of lysosomes. Mol Membr Biol *20*, 141-154.

Magnuson, B., Ekim, B., and Fingar, D.C. (2012). Regulation and function of ribosomal protein S6 kinase (S6K) within mTOR signalling networks. Biochem J *441*, 1-21.

Mahimainathan, L., Das, F., Venkatesan, B., and Choudhury, G.G. (2006). Mesangial cell hypertrophy by high glucose is mediated by downregulation of the tumor suppressor PTEN. Diabetes *55*, 2115-2125.

Malkus, P., Graham, L.A., Stevens, T.H., and Schekman, R. (2004). Role of Vma21p in assembly and transport of the yeast vacuolar ATPase. Mol Biol Cell *15*, 5075-5091.

Manolson, M.F., Wu, B., Proteau, D., Taillon, B.E., Roberts, B.T., Hoyt, M.A., and Jones, E.W. (1994). STV1 gene encodes functional homologue of 95-kDa yeast vacuolar H(+)-ATPase subunit Vph1p. J Biol Chem *269*, 14064-14074.

Manolson, M.F., Yu, H., Chen, W., Yao, Y., Li, K., Lees, R.L., and Heersche, J.N. (2003). The a3 isoform of the 100-kDa V-ATPase subunit is highly but differentially expressed in large (>or=10 nuclei) and small (<or= nuclei) osteoclasts. J Biol Chem *278*, 49271-49278.

Marjuki, H., Gornitzky, A., Marathe, B.M., Ilyushina, N.A., Aldridge, J.R., Desai, G., Webby, R.J., and Webster, R.G. (2011). Influenza A virus-induced early activation of ERK and PI3K mediates V-ATPase-dependent intracellular pH change required for fusion. Cell Microbiol *13*, 587-601.

Marks, S.C., Jr., Seifert, M.F., and Lane, P.W. (1985). Osteosclerosis, a recessive skeletal mutation on chromosome 19 in the mouse. J Hered *76*, 171-176.

Martina, J.A., Chen, Y., Gucek, M., and Puertollano, R. (2012). MTORC1 functions as a transcriptional regulator of autophagy by preventing nuclear transport of TFEB. Autophagy *8*, 903-914.

Martinez-Zaguilan, R., Lynch, R.M., Martinez, G.M., and Gillies, R.J. (1993). Vacuolar-type H(+)-ATPases are functionally expressed in plasma membranes of human tumor cells. Am J Physiol *265*, C1015-1029.

Mauvezin, C., Nagy, P., Juhasz, G., and Neufeld, T.P. (2015). Autophagosome-lysosome fusion is independent of V-ATPase-mediated acidification. Nat Commun *6*, 7007.

Maxfield, F.R., and Yamashiro, D.J. (1987). Endosome acidification and the pathways of receptor-mediated endocytosis. Adv Exp Med Biol *225*, 189-198.

Mayer, A., Wickner, W., and Haas, A. (1996). Sec18p (NSF)-driven release of Sec17p (alpha-SNAP) can precede docking and fusion of yeast vacuoles. Cell *85*, 83-94.

Mayer, C., Zhao, J., Yuan, X., and Grummt, I. (2004). mTOR-dependent activation of the transcription factor TIF-IA links rRNA synthesis to nutrient availability. Genes Dev *18*, 423-434.

Mayorga, L.S., Bertini, F., and Stahl, P.D. (1991). Fusion of newly formed phagosomes with endosomes in intact cells and in a cell-free system. J Biol Chem *266*, 6511-6517.

McEwan, D.G., and Dikic, I. (2011). The Three Musketeers of Autophagy: phosphorylation, ubiquitylation and acetylation. Trends Cell Biol *21*, 195-201.

Meister, M., Tomasovic, A., Banning, A., and Tikkanen, R. (2013). Mitogen-Activated Protein (MAP) Kinase Scaffolding Proteins: A Recount. Int J Mol Sci *14*, 4854-4884.

Meredith, M.J. (1988). Rat hepatocytes prepared without collagenase: prolonged retention of differentiated characteristics in culture. Cell Biol Toxicol *4*, 405-425.

Methot, D., and Reudelhuber, T.L. (2001). Knockout of renin-angiotensin system genes: effects on vascular development. Curr Hypertens Rep *3*, 68-73.

Miller, R.L., Zhang, P., Smith, M., Beaulieu, V., Paunescu, T.G., Brown, D., Breton, S., and Nelson, R.D. (2005). V-ATPase B1-subunit promoter drives expression of EGFP in intercalated cells of kidney, clear cells of epididymis and airway cells of lung in transgenic mice. Am J Physiol Cell Physiol *288*, C1134-1144.

Miller, S.E., Collins, B.M., McCoy, A.J., Robinson, M.S., and Owen, D.J. (2007). A SNARE-adaptor interaction is a new mode of cargo recognition in clathrin-coated vesicles. Nature *450*, 570-574.

Mizushima, N., and Komatsu, M. (2011). Autophagy: renovation of cells and tissues. Cell *147*, 728-741.

Montecucco, C., Schiavo, G., and Pantano, S. (2005). SNARE complexes and neuroexocytosis: how many, how close? Trends Biochem Sci *30*, 367-372.

Morel, N. (2003). Neurotransmitter release: the dark side of the vacuolar-H+ATPase. Biol Cell *95*, 453-457.

Morel, N., Dedieu, J.C., and Philippe, J.M. (2003). Specific sorting of the a1 isoform of the V-H+ATPase a subunit to nerve terminals where it associates with both synaptic vesicles and the presynaptic plasma membrane. J Cell Sci *116*, 4751-4762.

Morel, N., and Poea-Guyon, S. (2015). The membrane domain of vacuolar H(+)ATPase: a crucial player in neurotransmitter exocytotic release. Cell Mol Life Sci *72*, 2561-2573.

Mullock, B.M., Smith, C.W., Ihrke, G., Bright, N.A., Lindsay, M., Parkinson, E.J., Brooks, D.A., Parton, R.G., James, D.E., Luzio, J.P.*, et al.* (2000). Syntaxin 7 is localized to late endosome compartments, associates with Vamp 8, and Is required for late endosome-lysosome fusion. Mol Biol Cell *11*, 3137-3153.

Nelson, R.D., Guo, X.L., Masood, K., Brown, D., Kalkbrenner, M., and Gluck, S. (1992). Selectively amplified expression of an isoform of the vacuolar H(+)-ATPase 56-kilodalton subunit in renal intercalated cells. Proc Natl Acad Sci U S A *89*, 3541-3545.

Nguyen, G., Delarue, F., Burckle, C., Bouzhir, L., Giller, T., and Sraer, J.D. (2002). Pivotal role of the renin/prorenin receptor in angiotensin II production and cellular responses to renin. J Clin Invest *109*, 1417-1427.

Nielsen, E., Christoforidis, S., Uttenweiler-Joseph, S., Miaczynska, M., Dewitte, F., Wilm, M., Hoflack, B., and Zerial, M. (2000). Rabenosyn-5, a novel Rab5 effector, is complexed with hVPS45 and recruited to endosomes through a FYVE finger domain. J Cell Biol *151*, 601-612.

Nishi, T., and Forgac, M. (2002). The vacuolar (H+)-ATPases--nature's most versatile proton pumps. Nat Rev Mol Cell Biol *3*, 94-103.

Noumi, T., Beltran, C., Nelson, H., and Nelson, N. (1991). Mutational analysis of yeast vacuolar H(+)-ATPase. Proc Natl Acad Sci U S A *88*, 1938-1942.

Nyman, J.K., and Vaananen, H.K. (2010). A rationale for osteoclast selectivity of inhibiting the lysosomal V-ATPase a3 isoform. Calcif Tissue Int *87*, 273-283.

Ohkuma, S., and Poole, B. (1978). Fluorescence probe measurement of the intralysosomal pH in living cells and the perturbation of pH by various agents. Proc Natl Acad Sci U S A *75*, 3327-3331.

Ohya, T., Miaczynska, M., Coskun, U., Lommer, B., Runge, A., Drechsel, D., Kalaidzidis, Y., and Zerial, M. (2009). Reconstitution of Rab- and SNARE-dependent membrane fusion by synthetic endosomes. Nature *459*, 1091-1097.

Oka, T., Toyomura, T., Honjo, K., Wada, Y., and Futai, M. (2001). Four subunit a isoforms of Caenorhabditis elegans vacuolar H+-ATPase. Cell-specific expression during development. J Biol Chem *276*, 33079-33085.

Onel, S.F., Rust, M.B., Jacob, R., and Renkawitz-Pohl, R. (2014). Tethering membrane fusion: common and different players in myoblasts and at the synapse. J Neurogenet *28*, 302-315.

Oshima, Y., Kinouchi, K., Ichihara, A., Sakoda, M., Kurauchi-Mito, A., Bokuda, K., Narita, T., Kurosawa, H., Sun-Wada, G.H., Wada, Y., *et al.* (2011). Prorenin receptor is essential for normal podocyte structure and function. J Am Soc Nephrol *22*, 2203-2212.

Palmieri, M., Impey, S., Kang, H., di Ronza, A., Pelz, C., Sardiello, M., and Ballabio, A. (2011). Characterization of the CLEAR network reveals an integrated control of cellular clearance pathways. Hum Mol Genet *20*, 3852-3866.

Pankiv, S., Clausen, T.H., Lamark, T., Brech, A., Bruun, J.A., Outzen, H., Overvatn, A., Bjorkoy, G., and Johansen, T. (2007). p62/SQSTM1 binds directly to Atg8/LC3 to facilitate degradation of ubiquitinated protein aggregates by autophagy. J Biol Chem *282*, 24131-24145.

Parra, K.J., and Kane, P.M. (1998). Reversible association between the V1 and V0 domains of yeast vacuolar H+-ATPase is an unconventional glucose-induced effect. Mol Cell Biol *18*, 7064-7074.

Parra, K.J., Keenan, K.L., and Kane, P.M. (2000). The H subunit (Vma13p) of the yeast V-ATPase inhibits the ATPase activity of cytosolic V1 complexes. J Biol Chem *275*, 21761-21767.

Peplowska, K., Markgraf, D.F., Ostrowicz, C.W., Bange, G., and Ungermann, C. (2007). The CORVET tethering complex interacts with the yeast Rab5 homolog Vps21 and is involved in endo-lysosomal biogenesis. Dev Cell *12*, 739-750.

Peri, F., and Nusslein-Volhard, C. (2008). Live imaging of neuronal degradation by microglia reveals a role for v0-ATPase a1 in phagosomal fusion in vivo. Cell *133*, 916-927.

Peters, C., Bayer, M.J., Buhler, S., Andersen, J.S., Mann, M., and Mayer, A. (2001). Trans-complex formation by proteolipid channels in the terminal phase of membrane fusion. Nature *409*, 581-588.

Peters, C., and Mayer, A. (1998). Ca2+/calmodulin signals the completion of docking and triggers a late step of vacuole fusion. Nature *396*, 575-580.

Peterson, T.R., Sengupta, S.S., Harris, T.E., Carmack, A.E., Kang, S.A., Balderas, E., Guertin, D.A., Madden, K.L., Carpenter, A.E., Finck, B.N., *et al.* (2011). mTOR complex 1 regulates lipin 1 localization to control the SREBP pathway. Cell *146*, 408-420.

Pfeffer, S.R. (1999). Transport-vesicle targeting: tethers before SNAREs. Nat Cell Biol *1*, E17-22.

Plemel, R.L., Lobingier, B.T., Brett, C.L., Angers, C.G., Nickerson, D.P., Paulsel, A., Sprague, D., and Merz, A.J. (2011). Subunit organization and Rab interactions of Vps-C protein complexes that control endolysosomal membrane traffic. Mol Biol Cell *22*, 1353-1363.

Poea-Guyon, S., Ammar, M.R., Erard, M., Amar, M., Moreau, A.W., Fossier, P., Gleize, V., Vitale, N., and Morel, N. (2013). The V-ATPase membrane domain is a sensor of granular pH that controls the exocytotic machinery. J Cell Biol *203*, 283-298.

Pols, M.S., ten Brink, C., Gosavi, P., Oorschot, V., and Klumperman, J. (2013). The HOPS proteins hVps41 and hVps39 are required for homotypic and heterotypic late endosome fusion. Traffic *14*, 219-232.

Porstmann, T., Santos, C.R., Griffiths, B., Cully, M., Wu, M., Leevers, S., Griffiths, J.R., Chung, Y.L., and Schulze, A. (2008). SREBP activity is regulated by mTORC1 and contributes to Akt-dependent cell growth. Cell Metab *8*, 224-236.

Pryor, P.R., Mullock, B.M., Bright, N.A., Gray, S.R., and Luzio, J.P. (2000). The role of intraorganellar Ca(2+) in late endosome-lysosome heterotypic fusion and in the reformation of lysosomes from hybrid organelles. J Cell Biol *149*, 1053-1062.

Pryor, P.R., Mullock, B.M., Bright, N.A., Lindsay, M.R., Gray, S.R., Richardson, S.C., Stewart, A., James, D.E., Piper, R.C., and Luzio, J.P. (2004). Combinatorial SNARE complexes with VAMP7 or VAMP8 define different late endocytic fusion events. EMBO Rep *5*, 590-595.

Rebsamen, M., Pochini, L., Stasyk, T., de Araujo, M.E., Galluccio, M., Kandasamy, R.K., Snijder, B., Fauster, A., Rudashevskaya, E.L., Bruckner, M., *et al.* (2015). SLC38A9 is a component of the lysosomal amino acid sensing machinery that controls mTORC1. Nature *519*, 477-481.

Reese, C., Heise, F., and Mayer, A. (2005). Trans-SNARE pairing can precede a hemifusion intermediate in intracellular membrane fusion. Nature *436*, 410-414.

Richardson, S.C., Winistorfer, S.C., Poupon, V., Luzio, J.P., and Piper, R.C. (2004). Mammalian late vacuole protein sorting orthologues participate in early endosomal fusion and interact with the cytoskeleton. Mol Biol Cell *15*, 1197-1210.

Riediger, F., Quack, I., Qadri, F., Hartleben, B., Park, J.K., Potthoff, S.A., Sohn, D., Sihn, G., Rousselle, A., Fokuhl, V.*, et al.* (2011). Prorenin receptor is essential for podocyte autophagy and survival. J Am Soc Nephrol *22*, 2193-2202.

Roczniak-Ferguson, A., Petit, C.S., Froehlich, F., Qian, S., Ky, J., Angarola, B., Walther, T.C., and Ferguson, S.M. (2012). The transcription factor TFEB links mTORC1 signaling to transcriptional control of lysosome homeostasis. Sci Signal *5*, ra42.

Roth, W., Deussing, J., Botchkarev, V.A., Pauly-Evers, M., Saftig, P., Hafner, A., Schmidt, P., Schmahl, W., Scherer, J., Anton-Lamprecht, I.*, et al.* (2000). Cathepsin L deficiency as molecular defect of furless: hyperproliferation of keratinocytes and pertubation of hair follicle cycling. FASEB J *14*, 2075-2086.

Rudnik, S. (2014). Rolle der vesikulären H+-ATPase in Endozytose und Autophagy, *Master´s thesis*.

Sabatini, D.M., Erdjument-Bromage, H., Lui, M., Tempst, P., and Snyder, S.H. (1994). RAFT1: a mammalian protein that binds to FKBP12 in a rapamycin-dependent fashion and is homologous to yeast TORs. Cell *78*, 35-43.

Sabers, C.J., Martin, M.M., Brunn, G.J., Williams, J.M., Dumont, F.J., Wiederrecht, G., and Abraham, R.T. (1995). Isolation of a protein target of the FKBP12-rapamycin complex in mammalian cells. J Biol Chem *270*, 815-822.

Saftig, P., Hetman, M., Schmahl, W., Weber, K., Heine, L., Mossmann, H., Koster, A., Hess, B., Evers, M., von Figura, K.*, et al.* (1995). Mice deficient for the lysosomal proteinase cathepsin D exhibit progressive atrophy of the intestinal mucosa and profound destruction of lymphoid cells. EMBO J *14*, 3599-3608.

Sancak, Y., Thoreen, C.C., Peterson, T.R., Lindquist, R.A., Kang, S.A., Spooner, E., Carr, S.A., and Sabatini, D.M. (2007). PRAS40 is an insulin-regulated inhibitor of the mTORC1 protein kinase. Mol Cell *25*, 903-915.

Sardiello, M., Palmieri, M., di Ronza, A., Medina, D.L., Valenza, M., Gennarino, V.A., Di Malta, C., Donaudy, F., Embrione, V., Polishchuk, R.S.*, et al.* (2009). A gene network regulating lysosomal biogenesis and function. Science *325*, 473-477.

Saucedo, L.J., Gao, X., Chiarelli, D.A., Li, L., Pan, D., and Edgar, B.A. (2003). Rheb promotes cell growth as a component of the insulin/TOR signalling network. Nat Cell Biol *5*, 566-571.

Sautin, Y.Y., Lu, M., Gaugler, A., Zhang, L., and Gluck, S.L. (2005). Phosphatidylinositol 3-kinase-mediated effects of glucose on vacuolar H+-ATPase assembly, translocation, and acidification of intracellular compartments in renal epithelial cells. Mol Cell Biol *25*, 575-589.

Schoonderwoert, V.T., Jansen, E.J., and Martens, G.J. (2002). The fate of newly synthesized V-ATPase accessory subunit Ac45 in the secretory pathway. Eur J Biochem *269*, 1844-1853.

Schoonderwoert, V.T., and Martens, G.J. (2002). Targeted disruption of the mouse gene encoding the V-ATPase accessory subunit Ac45. Mol Membr Biol *19*, 67-71.

Schwake, M., Schroder, B., and Saftig, P. (2013). Lysosomal membrane proteins and their central role in physiology. Traffic *14*, 739-748.

Scimeca, J.C., Franchi, A., Trojani, C., Parrinello, H., Grosgeorge, J., Robert, C., Jaillon, O., Poirier, C., Gaudray, P., and Carle, G.F. (2000). The gene encoding the mouse homologue of the human osteoclast-specific 116-kDa V-ATPase subunit bears a deletion in osteosclerotic (oc/oc) mutants. Bone *26*, 207-213.

Seals, D.F., Eitzen, G., Margolis, N., Wickner, W.T., and Price, A. (2000). A Ypt/Rab effector complex containing the Sec1 homolog Vps33p is required for homotypic vacuole fusion. Proc Natl Acad Sci U S A *97*, 9402-9407.

Seol, J.H., Shevchenko, A., and Deshaies, R.J. (2001). Skp1 forms multiple protein complexes, including RAVE, a regulator of V-ATPase assembly. Nat Cell Biol *3*, 384-391.

Sethi, J.K., and Vidal-Puig, A.J. (2008). Wnt signalling at the crossroads of nutritional regulation. Biochem J *416*, e11-13.

Settembre, C., Di Malta, C., Polito, V.A., Garcia Arencibia, M., Vetrini, F., Erdin, S., Erdin, S.U., Huynh, T., Medina, D., Colella, P.*, et al.* (2011). TFEB links autophagy to lysosomal biogenesis. Science *332*, 1429-1433.

Settembre, C., Zoncu, R., Medina, D.L., Vetrini, F., Erdin, S., Huynh, T., Ferron, M., Karsenty, G., Vellard, M.C., Facchinetti, V.*, et al.* (2012). A lysosome-to-nucleus signalling mechanism senses and regulates the lysosome via mTOR and TFEB. EMBO J *31*, 1095-1108.

Shor, B., Wu, J., Shakey, Q., Toral-Barza, L., Shi, C., Follettie, M., and Yu, K. (2010). Requirement of the mTOR kinase for the regulation of Maf1 phosphorylation and control of RNA polymerase III-dependent transcription in cancer cells. J Biol Chem *285*, 15380-15392.

Sihn, G., Rousselle, A., Vilianovitch, L., Burckle, C., and Bader, M. (2010). Physiology of the (pro)renin receptor: Wnt of change? Kidney Int *78*, 246-256.

Simonsen, A., Lippe, R., Christoforidis, S., Gaullier, J.M., Brech, A., Callaghan, J., Toh, B.H., Murphy, C., Zerial, M., and Stenmark, H. (1998). EEA1 links PI(3)K function to Rab5 regulation of endosome fusion. Nature *394*, 494-498.

Smardon, A.M., and Kane, P.M. (2007). RAVE is essential for the efficient assembly of the C subunit with the vacuolar H(+)-ATPase. J Biol Chem *282*, 26185-26194.

Smardon, A.M., Tarsio, M., and Kane, P.M. (2002). The RAVE complex is essential for stable assembly of the yeast V-ATPase. J Biol Chem *277*, 13831-13839.

Smith, A.N., Skaug, J., Choate, K.A., Nayir, A., Bakkaloglu, A., Ozen, S., Hulton, S.A., Sanjad, S.A., Al-Sabban, E.A., Lifton, R.P., *et al.* (2000). Mutations in ATP6N1B, encoding a new kidney vacuolar proton pump 116-kD subunit, cause recessive distal renal tubular acidosis with preserved hearing. Nat Genet *26*, 71-75.

Sollner, T., Bennett, M.K., Whiteheart, S.W., Scheller, R.H., and Rothman, J.E. (1993). A protein assembly-disassembly pathway in vitro that may correspond to sequential steps of synaptic vesicle docking, activation, and fusion. Cell *75*, 409-418.

Srinivas, S., Watanabe, T., Lin, C.S., William, C.M., Tanabe, Y., Jessell, T.M., and Costantini, F. (2001). Cre reporter strains produced by targeted insertion of EYFP and ECFP into the ROSA26 locus. BMC Dev Biol *1*, 4.

Stocker, H., Radimerski, T., Schindelholz, B., Wittwer, F., Belawat, P., Daram, P., Breuer, S., Thomas, G., and Hafen, E. (2003). Rheb is an essential regulator of S6K in controlling cell growth in Drosophila. Nat Cell Biol *5*, 559-565.

Storrie, B., and Desjardins, M. (1996). The biogenesis of lysosomes: is it a kiss and run, continuous fusion and fission process? Bioessays *18*, 895-903.

Strasser, B., Iwaszkiewicz, J., Michielin, O., and Mayer, A. (2011). The V-ATPase proteolipid cylinder promotes the lipid-mixing stage of SNARE-dependent fusion of yeast vacuoles. EMBO J *30*, 4126-4141.

Stroupe, C., Hickey, C.M., Mima, J., Burfeind, A.S., and Wickner, W. (2009). Minimal membrane docking requirements revealed by reconstitution of Rab GTPase-dependent membrane fusion from purified components. Proc Natl Acad Sci U S A *106*, 17626-17633.

Sudhof, T.C., and Rizo, J. (2011). Synaptic vesicle exocytosis. Cold Spring Harb Perspect Biol *3*.

Sun-Wada, G., Murata, Y., Yamamoto, A., Kanazawa, H., Wada, Y., and Futai, M. (2000). Acidic endomembrane organelles are required for mouse postimplantation development. Dev Biol *228*, 315-325.

Sun-Wada, G.H., Tabata, H., Kawamura, N., Aoyama, M., and Wada, Y. (2009). Direct recruitment of H+-ATPase from lysosomes for phagosomal acidification. J Cell Sci *122*, 2504-2513.

Sun-Wada, G.H., Toyomura, T., Murata, Y., Yamamoto, A., Futai, M., and Wada, Y. (2006). The a3 isoform of V-ATPase regulates insulin secretion from pancreatic beta-cells. J Cell Sci *119*, 4531-4540.

Supek, F., Supekova, L., Mandiyan, S., Pan, Y.C., Nelson, H., and Nelson, N. (1994). A novel accessory subunit for vacuolar H(+)-ATPase from chromaffin granules. J Biol Chem *269*, 24102-24106.

Sutton, B.J., and Gould, H.J. (1993). The human IgE network. Nature *366*, 421-428.

Swanson, J.A., and Watts, C. (1995). Macropinocytosis. Trends Cell Biol *5*, 424-428.

Tabata, H., Kawamura, N., Sun-Wada, G.H., and Wada, Y. (2008). Vacuolar-type H(+)-ATPase with the a3 isoform is the proton pump on premature melanosomes. Cell Tissue Res *332*, 447-460.

Tanida, I. (2011). Autophagosome formation and molecular mechanism of autophagy. Antioxid Redox Signal *14*, 2201-2214.

Taranta, A., Migliaccio, S., Recchia, I., Caniglia, M., Luciani, M., De Rossi, G., Dionisi-Vici, C., Pinto, R.M., Francalanci, P., Boldrini, R., *et al.* (2003). Genotype-phenotype relationship in human ATP6i-dependent autosomal recessive osteopetrosis. Am J Pathol *162*, 57-68.

Tee, A.R., and Blenis, J. (2005). mTOR, translational control and human disease. Semin Cell Dev Biol *16*, 29-37.

Tee, A.R., Manning, B.D., Roux, P.P., Cantley, L.C., and Blenis, J. (2003). Tuberous sclerosis complex gene products, Tuberin and Hamartin, control mTOR signaling by acting as a GTPase-activating protein complex toward Rheb. Curr Biol *13*, 1259-1268.

Thompson, M.D., and Monga, S.P. (2007). WNT/beta-catenin signaling in liver health and disease. Hepatology *45*, 1298-1305.

Toei, M., Saum, R., and Forgac, M. (2010). Regulation and isoform function of the V-ATPases. Biochemistry *49*, 4715-4723.

Toei, M., Toei, S., and Forgac, M. (2011). Definition of membrane topology and identification of residues important for transport in subunit a of the vacuolar ATPase. J Biol Chem *286*, 35176-35186.

Tong, J., Yan, X., and Yu, L. (2010). The late stage of autophagy: cellular events and molecular regulation. Protein Cell *1*, 907-915.

Toyomura, T., Murata, Y., Yamamoto, A., Oka, T., Sun-Wada, G.H., Wada, Y., and Futai, M. (2003). From lysosomes to the plasma membrane: localization of vacuolar-type H+ -ATPase with the a3 isoform during osteoclast differentiation. J Biol Chem *278*, 22023-22030.

Trombetta, E.S., Ebersold, M., Garrett, W., Pypaert, M., and Mellman, I. (2003). Activation of lysosomal function during dendritic cell maturation. Science *299*, 1400-1403.

Tuijnman, W.B., Capel, P.J., and van de Winkel, J.G. (1992). Human low-affinity IgG receptor Fc gamma RIIa (CD32) introduced into mouse fibroblasts mediates phagocytosis of sensitized erythrocytes. Blood *79*, 1651-1656.

Ungermann, C., Wickner, W., and Xu, Z. (1999). Vacuole acidification is required for trans-SNARE pairing, LMA1 release, and homotypic fusion. Proc Natl Acad Sci U S A *96*, 11194-11199.

Unkeless, J.C., Scigliano, E., and Freedman, V.H. (1988). Structure and function of human and murine receptors for IgG. Annu Rev Immunol *6*, 251-281.

Vaccari, T., Duchi, S., Cortese, K., Tacchetti, C., and Bilder, D. (2010). The vacuolar ATPase is required for physiological as well as pathological activation of the Notch receptor. Development *137*, 1825-1832.

van de Winkel, J.G., and Anderson, C.L. (1991). Biology of human immunoglobulin G Fc receptors. J Leukoc Biol *49*, 511-524.

van der Kant, R., Fish, A., Janssen, L., Janssen, H., Krom, S., Ho, N., Brummelkamp, T., Carette, J., Rocha, N., and Neefjes, J. (2013). Late endosomal transport and tethering are coupled processes controlled by RILP and the cholesterol sensor ORP1L. J Cell Sci *126*, 3462-3474.

Vander Haar, E., Lee, S.I., Bandhakavi, S., Griffin, T.J., and Kim, D.H. (2007). Insulin signalling to mTOR mediated by the Akt/PKB substrate PRAS40. Nat Cell Biol *9*, 316-323.

Vavassori, S., and Mayer, A. (2014). A new life for an old pump: V-ATPase and neurotransmitter release. J Cell Biol *205*, 7-9.

Vitavska, O., Merzendorfer, H., and Wieczorek, H. (2005). The V-ATPase subunit C binds to polymeric F-actin as well as to monomeric G-actin and induces cross-linking of actin filaments. J Biol Chem *280*, 1070-1076.

Voss, M., Vitavska, O., Walz, B., Wieczorek, H., and Baumann, O. (2007). Stimulus-induced phosphorylation of vacuolar H(+)-ATPase by protein kinase A. J Biol Chem *282*, 33735-33742.

Wang, D., Epstein, D., Khalaf, O., Srinivasan, S., Williamson, W.R., Fayyazuddin, A., Quiocho, F.A., and Hiesinger, P.R. (2014). Ca2+-Calmodulin regulates SNARE assembly and spontaneous neurotransmitter release via v-ATPase subunit V0a1. J Cell Biol *205*, 21-31.

Wang, D., and Hiesinger, P.R. (2013). The vesicular ATPase: a missing link between acidification and exocytosis. J Cell Biol *203*, 171-173.

Wang, L., Harris, T.E., Roth, R.A., and Lawrence, J.C., Jr. (2007). PRAS40 regulates mTORC1 kinase activity by functioning as a direct inhibitor of substrate binding. J Biol Chem *282*, 20036-20044.

Wang, S., Tsun, Z.Y., Wolfson, R.L., Shen, K., Wyant, G.A., Plovanich, M.E., Yuan, E.D., Jones, T.D., Chantranupong, L., Comb, W., *et al.* (2015). Metabolism. Lysosomal amino acid transporter SLC38A9 signals arginine sufficiency to mTORC1. Science *347*, 188-194.

Wang, Y., Inoue, T., and Forgac, M. (2004). TM2 but not TM4 of subunit c'' interacts with TM7 of subunit a of the yeast V-ATPase as defined by disulfide-mediated cross-linking. J Biol Chem *279*, 44628-44638.

Wang, Y.L., and Goren, M.B. (1987). Differential and sequential delivery of fluorescent lysosomal probes into phagosomes in mouse peritoneal macrophages. J Cell Biol *104*, 1749-1754.

Ward, D.M., Pevsner, J., Scullion, M.A., Vaughn, M., and Kaplan, J. (2000). Syntaxin 7 and VAMP-7 are soluble N-ethylmaleimide-sensitive factor attachment protein receptors required for late endosome-lysosome and homotypic lysosome fusion in alveolar macrophages. Mol Biol Cell *11*, 2327-2333.

Wattiaux, R., Wibo, M., and Baudhuin, P. (1963). [Effect of the injection of Triton WR 1339 on the hepatic lysosomes of the rat]. Arch Int Physiol Biochim *71*, 140-142.

Wilkens, S., Vasilyeva, E., and Forgac, M. (1999). Structure of the vacuolar ATPase by electron microscopy. J Biol Chem *274*, 31804-31810.

Wirawan, E., Vanden Berghe, T., Lippens, S., Agostinis, P., and Vandenabeele, P. (2012). Autophagy: for better or for worse. Cell Res *22*, 43-61.

Wolfson, R.L., Chantranupong, L., Saxton, R.A., Shen, K., Scaria, S.M., Cantor, J.R., and Sabatini, D.M. (2015). Sestrin2 is a leucine sensor for the mTORC1 pathway. Science.

Wurmser, A.E., Sato, T.K., and Emr, S.D. (2000). New component of the vacuolar class C-Vps complex couples nucleotide exchange on the Ypt7 GTPase to SNARE-dependent docking and fusion. J Cell Biol *151*, 551-562.

Xu, T., and Forgac, M. (2001). Microtubules are involved in glucose-dependent dissociation of the yeast vacuolar [H+]-ATPase in vivo. J Biol Chem *276*, 24855-24861.

Xu, Y., Zhang, F., Su, Z., McNew, J.A., and Shin, Y.K. (2005). Hemifusion in SNARE-mediated membrane fusion. Nat Struct Mol Biol *12*, 417-422.

Yamamoto, A., Tagawa, Y., Yoshimori, T., Moriyama, Y., Masaki, R., and Tashiro, Y. (1998). Bafilomycin A1 prevents maturation of autophagic vacuoles by inhibiting fusion between autophagosomes and lysosomes in rat hepatoma cell line, H-4-II-E cells. Cell Struct Funct *23*, 33-42.

Yan, Y., Denef, N., and Schupbach, T. (2009). The vacuolar proton pump, V-ATPase, is required for notch signaling and endosomal trafficking in Drosophila. Dev Cell *17*, 387-402.

Yang, D.Q., Feng, S., Chen, W., Zhao, H., Paulson, C., and Li, Y.P. (2012). V-ATPase subunit ATP6AP1 (Ac45) regulates osteoclast differentiation, extracellular acidification, lysosomal trafficking, and protease exocytosis in osteoclast-mediated bone resorption. J Bone Miner Res *27*, 1695-1707.

Yla-Anttila, P., Vihinen, H., Jokitalo, E., and Eskelinen, E.L. (2009). Monitoring autophagy by electron microscopy in Mammalian cells. Methods Enzymol *452*, 143-164.

Yoshikawa, A., Aizaki, Y., Kusano, K., Kishi, F., Susumu, T., Iida, S., Ishiura, S., Nishimura, S., Shichiri, M., and Senbonmatsu, T. (2011). The (pro)renin receptor is cleaved by ADAM19 in the Golgi leading to its secretion into extracellular space. Hypertens Res *34*, 599-605.

Zachos, C., Blanz, J., Saftig, P., and Schwake, M. (2012). A critical histidine residue within LIMP-2 mediates pH sensitive binding to its ligand beta-glucocerebrosidase. Traffic *13*, 1113-1123.

Zaidi, N., Maurer, A., Nieke, S., and Kalbacher, H. (2008). Cathepsin D: a cellular roadmap. Biochem Biophys Res Commun *376*, 5-9.

Zhang, C.S., Jiang, B., Li, M., Zhu, M., Peng, Y., Zhang, Y.L., Wu, Y.Q., Li, T.Y., Liang, Y., Lu, Z., *et al.* (2014). The lysosomal v-ATPase-Ragulator complex is a common activator for AMPK and mTORC1, acting as a switch between catabolism and anabolism. Cell Metab *20*, 526-540.

Zhang, H.H., Huang, J., Duvel, K., Boback, B., Wu, S., Squillace, R.M., Wu, C.L., and Manning, B.D. (2009). Insulin stimulates adipogenesis through the Akt-TSC2-mTORC1 pathway. PLoS One *4*, e6189.

Zhang, W., Wang, D., Volk, E., Bellen, H.J., Hiesinger, P.R., and Quiocho, F.A. (2008). V-ATPase V0 sector subunit a1 in neurons is a target of calmodulin. J Biol Chem *283*, 294-300.

Zhao, J., Benlekbir, S., and Rubinstein, J.L. (2015). Electron cryomicroscopy observation of rotational states in a eukaryotic V-ATPase. Nature *521*, 241-245.

Zick, M., and Wickner, W. (2013). The tethering complex HOPS catalyzes assembly of the soluble SNARE Vam7 into fusogenic trans-SNARE complexes. Mol Biol Cell *24*, 3746-3753.

Zoncu, R., Bar-Peled, L., Efeyan, A., Wang, S., Sancak, Y., and Sabatini, D.M. (2011). mTORC1 senses lysosomal amino acids through an inside-out mechanism that requires the vacuolar H(+)-ATPase. Science *334*, 678-683.

6. List of tables and figures

List of tables

List of figures

7. DECLARATION

I herewith declare that, apart from the supervisor's guidance, I have prepared the present thesis autonomously and in accordance with the Rules of Good Scientific Practice of the German Research Foundation. All ideas and concepts that were taken either directly or indirectly from other sources are indicated as such.

This thesis has not been submitted partially or wholly as part of a doctoral degree to another examining body.

Parts of this work have been published in the following article:

Kissing, S.*, Hermsen, C.*, Repnik, U., Nesset, C.K., von Bargen, K., Griffiths, G., Ichihara, A., Lee, B.S., Schwake, M., De Brabander, J., Haas, A. and Saftig, P. (2015) Vacuolar ATPase in phagosome-lysosome fusion. J Biol Chem *290*, 14166-14180.

* authors contributed equally

In addition, parts of this thesis are processed in a manuscript in preparation for scientific publication:

Kissing, S.*, Rudnik, S.*, Damme, M., Lüllmann-Rauch, R., Ichihara, A., Kornak, U., Eskelinen, E.L., Jabs, S., Heeren, J., De Brabander, J., Haas, A. and Saftig, P.

Disruption of the v-H^+-ATPase complex in liver causes mTORC1-independent accumulation of autophagosomes

* authors contributed equally

Kiel, March 2016 Sandra Kissing

8. Curriculum Vitae

Eckenerplatz 12
24159 Kiel

Sandra Kissing

Born April, 27th 1987 in Halle (Saale)

Nationality: german

Education

since 10/2011	**Phd studies** as a member of the *SPP 1580:* Priority Programme 'Intracellular Compartments as Places of Pathogen-Host-Interaction' Working group of Prof. Dr. Paul Saftig Department of Biochemistry, University Kiel Title: *The influence of V-type H^+-ATPases on vesicle fusion processes*
10/2010 – 07/2011	**Diploma thesis** Max Planck Research Unit for Enzymology of Protein Folding Halle (Saale) Title: *Neuroprotektive und neuroregenerative Eigenschaften von Liganden der FK506-bindenden Protein und deren Mechanismus*
10/2006 – 07/2011	**Diploma studies** in Biochemistry Martin-Luther-University Halle-Wittenberg, Halle (Saale)
09/1999 – 07/2006	Abitur Goethe-Gymnasium, Weißenfels

Practical Experiences

05/2013	DFG Course on Electron Microscopy, University Oslo, Norway
06/2015 – 07/2015	SPP1580 Workshop on Phagosome Membrane Biology Research Center Borstel

9. PUBLICATIONS AND SCIENTIFIC PARTICIPATION

Publications

Linnert, M., Haupt, K., Lin, Y.J., **Kissing, S.**, Paschke, A.K., Fischer, G., Weiwad, M. and Lücke, C. (2012) NMR assignments of the FKBP-type PPIase domain of the human aryl-hydrocarbon receptor-interacting protein (AIP). Biomol NMR Assign *6,* 209-212

Kraft, S., Jouvin, M.H., Kulkarni, N., **Kissing, S.**, Morgan, E.S., Dvorak, A.M., Schröder, B., Saftig, P. and Kinet, J.P. (2013) The tetraspanin CD63 is required for efficient IgE-mediated mast cell degranulation and anaphylaxis. J Immunol *191*, 2871-2878

Grimm, C., Holdt, L.M., Chen, C.C., Hassan, S., Müller, C., Jörs, S., Cuny, H., **Kissing, S.**, Schröder, B., Butz, E., Northoff, B., Castonguay, J., Luber, C.A., Moser, M., Spahn, S., Lüllmann-Rauch, R., Fendel, C., Klugbauer, N., Griesbeck, O., Haas, A., Mann, M., Bracher, F., Teupser, D., Saftig, P., Biel, M. and Wahl-Schott, C. (2014) High susceptibility to fatty liver disease in two-pore channel 2-deficient mice. Nat Commun *5*, 4699.

Kissing, S.*, Hermsen, C.*, Repnik, U., Nesset, C.K., von Bargen, K., Griffiths, G., Ichihara, A., Lee, B.S., Schwake, M., De Brabander, J., Haas, A. and Saftig, P. (2015) Vacuolar ATPase in phagosome-lysosome fusion. J Biol Chem *290*, 14166-14180.

Presentations

09/2013 – 10/2013	International Conference on Intracellular Niches of Pathogens Glashütten, Germany (oral and poster presentation, award for best student talk)
01/2014	Embo Workshop on Protein and Lipid Function in Secretion and Endocytosis, Goldegg am See, Austria (poster presentation)
09/2014	3rd International Symposium on Protein Trafficking in Health and Disease, Hamburg, Germany (oral and poster presentation)
10/2015	20th Workshop of the European Study Group on Lysosomal Diseases Pozzuoli, Italy (selected oral presentation)

10. ACKNOWLEDGEMENT

An dieser Stelle möchte ich all diejenigen erwähnen, die das Entstehen dieser Arbeit erst ermöglicht haben.

Mein Dank gilt Herrn Prof. Dr. Paul Saftig für die Möglichkeit, diese Promotion in seiner Arbeitsgruppe durchführen zu können, für die wissenschaftliche Betreuung während der letzten 4 ½ Jahre, sowie die konstruktiven Diskussionen und Ratschläge.

Ich danke Herrn Prof. Dr. Axel Scheidig für die Übernahme des Zweitgutachtens dieser Arbeit.

Ganz besonders möchte ich mich bei Christina Hermsen und Prof. Dr. Albert Haas für die gemeinsame Arbeit an diesem Projekt im Rahmen des SPP1580 bedanken. Unsere zahlreichen, munteren Treffen lieferten stets neue und interessante Einblicke in die Welt der Fusion.

Auch bei Dr. Urska Repnik und Prof. Dr. Gareth Griffiths möchte ich mich für die Zusammenarbeit und eine einzigartige Woche voller Elektronenmikroskopie herzlich bedanken.

Darüber hinaus danke ich Dagmar Niemeier, Prof. Dr. Renate Lüllmann-Rauch und Prof. Dr. Eeva-Liisa Eskelinen für die Vielzahl weiterer elektronenmikroskopischer Analysen.

Ich danke den Mitgliedern des GRK1459 für die Aufnahme als assoziiertes Mitglied und speziell Prof. Dr. Jörg Heeren und Sandra Ehret für den warmen Empfang in ihrer Gruppe.

Den Mitarbeitern des Viktor-Hensen-Hauses, allen voran Andrea Henke, danke ich für die kompetente Haltung und Pflege unserer Mauslinien.

Nicht zu vergessen, möchte ich mich bei meinen alltäglichen Begleitern innerhalb und außerhalb des Labors ganz besonders herzlich für die schöne Zeit bedanken. Lisa, Sönke, Basti, Torben, Ann-Christine, Kristin, Maike, Sebastian, Marlies und Anne – mit euch schmeckte jeder Kaffee einfach besser, hatte ich musikalischen Input von Einhörnern bis zu Cocktailbars, und einfach immer einen guten Grund zum Lachen! Auf den Kreuzotter!

Lieber Sönke, danke für deine Unterstützung von der Masterarbeit an, für jeden roten Pandabär und dafür, dass du mir vor allem in der Endphase dieser Arbeit den Rücken freigehalten hast!

Schließlich gilt mein Dank meinem Freund Sebastian, der auch diesen Weg in Höhen und Tiefen mit mir zusammen gegangen ist, sowie meiner Familie, die stets geduldig hinter mir stand.

Ich danke Euch von Herzen!